TÉCNICO LISBOA

In-Band Full-Duplex Architectures for Future 5G Multi-Hop Networks

João Francisco Aragão Aboim de Sande e Lemos

Thesis to obtain the Master of Science Degree in

Electrical and Computer Engineering

Supervisors: Prof. António José Castelo Branco Rodrigues
Prof. Francisco António Taveira Branco Nunes Monteiro

Examination Committee

Chairperson: Prof. José Eduardo Charters Ribeiro da Cunha Sanguino
Supervisor: Prof. Francisco António Taveira Branco Nunes Monteiro
Member of the Committee: Prof. Mário Alexandre Teles de Figueiredo

November 2015

To my father

”It is generally not possible for radios to receive and transmit on the same frequency band because of the interference that results.”

Andrea Goldsmith, Wireless Communications [1]

Acknowledgments

Firstly, my deep gratitude goes to Professor Francisco A. Monteiro for the supervision and guidance given during this thesis. For his contagious passion about science, which inspired me through all the research done in these last months. For the many hours spent in his office. For all his help in my first steps towards a research career, by trusting me to guide this work and by giving me the opportunity to interact with prestigious scientists. For the conferences and meetings we attended together, which contributed to my growth as a young researcher. For the various lunches where we discussed insightful ideas for the heading of the work. For his true commitment to the academic life.

Special thanks to my supervisor Professor António Rodrigues for his unceasing support, solving every bureaucratic problem I had during the course of the work. For asking the right technical questions in a practical perspective, and for letting me find the answers. For motivating me in the hard moments and for encouraging me in the good ones. Professor Rodrigues has provided me with all the necessary means to conduct the research presented here and has always given me wise advice, helping me along my academic path, not only in *Instituto Superior Técnico* but also in the year I spent at KTH Royal Institute of Technology pursuing a Dual Master degree in Wireless Communications.

I am grateful to the Portuguese *Fundação para a Ciência e a Tecnologia* for funding our work, through the prestigious research center *Instituto de Telecomunicações*, where I have been a research scholar within the project L-DimM-NetCod: Large-Dimensional MIMO Physical Layer Network Coding.

I would like to express my heartfelt thanks to Professor João Xavier, without whom part of this work would not be possible. For all his availability to help solve some problems I faced, despite not having any responsibility for this thesis. Professor Xavier has always had a moment in his busy academic life to discuss some of the work hereafter presented and has shown great flexibility in co-authoring papers with us, for which I am deeply grateful and honored.

A special word goes to my colleague and friend Francisco Rosário, with whom I have carried out many projects in these recent years, and who has always pushed me to pursue higher and higher goals. For all the knowledge I gained working with him, for his direct and underlying contributions to this thesis, and for co-authoring a paper with me. Further, I would like to thank Ivo Sousa for the peer review he did on this work, mainly in the paper we co-author, and for all the encouragement he gave me. Finally, thanks to my friend Jonathan Munro for his small but important contribution.

Thanks to my colleagues with whom I have shared the progress of my work and have accompanied me during this period of our lives. Especially those in room 4.14, namely João Pereira, Manel Faria and João Crisóstomo Costa. Thanks to Paulo Barata, head of my workplace, who was always ready to solve my computer related technical problems and improve the performance of my machine to bear the heavy simulations done. Also, I would like to thank Professor José Sanguino for kindly lent me the Satellite Laboratory, such that I could finish this thesis.

Last but not least, I would like to heartily thank my close friends that encouraged and motivated me during this time, as well as my family, specially my parents, for the constant support and love. Despite not having contributed to this work, they all gave me the necessary strength to conclude it.

Abstract

With regard to the forthcoming requirements for mobile services in 5G networks, several new technologies have recently become the focus of leading-edge research. One of those is in-band full-duplex communications. The idea is to simply employ the same frequency band to simultaneously transmit and receive information, allowing more spectrally efficient communications when compared to the traditional half-duplex or out-of-band full-duplex counterparts. By breaking a long-held assumption in wireless communications, in-band full-duplex may double the throughput or reduce by half the allocated bandwidth in future transmissions. Nevertheless, the self-inflected interference, that naturally arises, poses the major problem to the use of this technique, enhanced when in presence of system impairments. Therefore, this thesis aims to study self-interference suppression methods, in multi-hop relaying environments, and proposes different systems where it may contribute the most, focusing solely on the digital domain. Particularly, digital spatial suppression filters are studied, as well as feedback adaptive filtering is proposed for relay systems with multiple-input multiple-out (MIMO) antennas. Furthermore, the orthogonal properties of large-scale arrays are resorted to, such that an extra level of mitigation is achieved. In this case, the relay system energy efficiency is maximized by finding the optimal transmit powers, while maintaining a certain individual link quality. Finally, physical layer network coding (PLNC) is combined with bidirectional in-band full-duplex relaying, reducing the allocated resources down to the same of machine-to-machine communication. For this scenario, the effect of massive MIMO is likewise addressed, and an algorithm that maximizes the system total achievable rate is derived.

Keywords: 5G, in-band full-duplex, massive MIMO, physical layer network coding, multi-hop communications, optimal power allocation.

Resumo

Recentemente, tendo em consideração os requisitos das comunicações móveis em redes 5G, têm vindo a ser desenvolvidas novas tecnologias. Uma destas tecnologias é *in-band full-duplex*, que consiste em transmitir e receber sem fios sinais na mesma banda de frequências e em simultâneo, permitindo um aumento da eficiência espectral quando comparada com as transmissões *half-duplex*. Este conceito, que vem quebrar uma ideia pré-estabelecida, permitirá duplicar o débito binário ou reduzir para metade a banda utilizada nas transmissões. No entanto, a interferência gerada pelo próprio transmissor é neste momento o maior problema no uso desta tecnologia. Dessa forma, esta tese visa estudar técnicas de supressão da auto-interferência, em redes com múltiplos repetidores e numa perspetiva de processamento digital, propondo sistemas onde estas técnicas podem ser preponderantes. Nomeadamente, é estudado o uso de filtros espaciais de supressão, assim como é proposta a utilização de filtragem adaptativa em repetidores com múltiplas antenas. Faz-se uso também das propriedades de sistemas com elevado número de antenas de forma a que seja possível aumentar o ganho na supressão desta interferência. Neste caso, a eficiência energética é maximizada através da escolha das potências a transmitir, mantendo o nível de qualidade exigido pelas ligações. Finalmente, é integrada codificação da camada física de rede em comunicação *in-band full-duplex* bidirecional, reduzindo o número de recursos necessários neste cenário para o mesmo que comunicações ponto-a-ponto. O efeito da utilização de um número elevado de antenas é também estudado, assim como é proposto um algoritmo que maximiza a capacidade do sistema.

Palavras-chave: 5G, *in-band full-duplex*, MIMO maciço, codificação da camada física de rede, comunicação com múltiplos saltos, alocação ótima de potência.

Contents

List of Figures

List of Tables

Chapter 1

Introduction

The constant demand for higher rates and lower latencies has already driven the scientific community and industry to pursue a new generation of mobile communications. Simply known as the fifth generation (5G), and with expected release date in 2020, telecommunications are about to go through a deep change in their foundations. One of those central changes is the long-held, but now obsolete, assumption that radios can only simultaneously transmit and receive in different frequency bands on the same channel. Thus, the concept of in-band full-duplex communication, i.e., simultaneously employing the same frequency band to transmit and receive data in wireless nodes, will certainly incorporate this new generation, providing a leap forward in terms of spectral usage efficiency. Moreover, when integrated under a physical layer network perspective or when combined with the rise in the number of antennas at base stations, its gains are beyond those expected few years ago.

This first chapter presents the main objective of this thesis and the reasons that motivated the work on in-band full-duplex communications. An historical overview of telecommunications, the current cutting-edge research and how this thesis may contribute to the progress of future 5G communications are also assessed. In addition, the document organization and academic contributions are mentioned.

1.1 Historical Overview

In recent decades, the topic of mobile communication has been a subject of interest to the research and industry communities. Several different technologies were studied so that a standard system could be implemented, allowing wireless communications to be a reality today. In the last 20 years, different major market requirements have appeared, pushing the telecommunication industry to develop new solutions. Firstly, the need for wireless real-time voice communication boosted the first generation (1G) of analog cellular transmissions. Then, short message service (SMS) was incorporated in a digital system that led to the second mobile generation (2G), the first to use a digital transmission. Due to the popularity of laptops and wireless local access networks (WLAN), wireless data connectivity became an hot topic and with it the third generation (3G) emerged. Currently, the fourth generation (4G) of wireless connectivity has been derived from the need for faster links, aiming to provide higher bandwidth access anywhere.

Currently, the fifth generation (5G) is in a research stage where several methods and techniques are being explored, aiming to be among the wireless connectivity technologies used in 2020. For that reason, this thesis aims to study the problems rising from in-band full-duplex systems and develop some new considerations to make them a reality in the next wireless generation of communications.

1.2 Motivation

The demand of data exchanged in future wireless networks will certainly pose new challenges to the industry, and particularly to research and development (R&D) departments, requiring a shift of paradigm when compared to that observed today. Exponential growth is expected in cellular data traffic and a thousand fold increase upon the current mobile data volume, in the next 10 years [2]. This demand for broadband cellular access, mainly for video applications, is driving the conceptualization of future radio mobile networks. The pursuit for the next generation of cellular communications has already started, boosted by European research organizations and projects such as 5GPP [3], 5GNOW [4] and METIS [5], but also by the academia and industry all over the world. The main target is to create a standard communication protocol capable of solving expected application requirements in 2020. Among them are the recently popular topic of the Internet of Things (IoT), involving machine-type communication, the gigabit wireless connectivity (giving the same experience as in a wired connection), the concept of tactile Internet (real-time applications requiring latency of 1 ms) and many others [6]. As defined by the METIS European project [2, 7], the future architecture should support:

- Mobile traffic volume 1000 times higher;
- Support 10 to 100 times more devices connected;
- Increase of up to 100 times throughput capacity;
- 5 times reduced latency.

Several different radio technologies are currently being studied and developed in order to achieve the above mentioned specifications. For example, in [8] the five major technologies that are believed to potentially fulfill 5G needs are pointed out:

Device-centric architectures: Changing the interaction between the base-station and the users, exploiting new control and data flows;

Millimeter waves: Moving towards higher frequencies, due to the spectrum scarcity at the current used carrier frequencies;

Massive MIMO: Using various antennas for multiplexing data for users at the same time instant and focusing energy in the user direction;

Smarter devices: Taking advantage of the device capability of processing information;

Machine-to-machine communication: Supporting a massive number of devices connected to the network, and allowing low data rate and very low latency applications.

As mentioned above, one of the possible future technologies is so-called device-centric architectures. The downlink-uplink paradigm between user and a base station in a mobile cell has necessarily to be replaced by a more cooperative network approach. Smarter communication systems are emerging, such as Cooperative multipoint (CoMP) or new more efficient relaying techniques, that will certainly increase the connection throughput of links by exploiting high spectrally efficient transmissions. Advanced full-duplex relaying techniques for multi-hop communication, but also for short-range communication, are believed to asymptotically double the spectral efficiency in radio communication systems and wireless networks, making it an attractive technology to achieve 5G demands.

The idea of re-using the same spectral band to transmit and receive information at the same time, therefore operating in in-band full-duplex mode, theoretically doubles the link capacity when compared with the half-duplex mode. As a consequence, the current telecommunication concepts of frequency-division duplexing (FDD) and time-division duplexing (TDD) become obsolete, with the appearance of this new idea of any-division duplexing (ADD) and eliminating the long-held paradigm of any type of digital communication so far used. However, once frequency and time resources are used simultaneously, self-interference cancellation techniques have to be applied in order to isolate the desired signal from the interfering one [9]. Another important aspect for 5G that full-duplex may solve is spectrum management, by means of duplicating the available current spectrum (commonly known as spectrum virtualization). The possibility to enable almost instantaneous retransmissions for network connections, i.e., with no need to wait for a time slot or for the attribution of frequency bands, can also be viewed as an advantage. Combining this new concept of in-band full-duplex with the state-of-the-art ideas coming from physical layer network coding (PLNC) and large/massive multiple-input multiple-output (MIMO), the performance of multi-hop networks may be drastically improved, allowing each relay to serve more and more users with higher requirements.

This technology can actually be implemented in current wireless networks. The main target of full-duplex technique is to enhance link capacity for future 5G, although there are some systems that would benefit from it with some slight modifications. Table 1.1 shows some different applications of in-band full-duplex to the industry beyond mobile communications and the process of technology implementation and standard adoption in modern and forthcoming networks.

No standards modification:	**5G Adoption:**	**Beyond 5G Cellular:**
Self backhaul for small cells	In-band full-duplex for 5G	Ad hoc mesh networks
Full-duplex microwave backhaul	5G spectrum virtualization	Military radio jammers
Adaptive duplexers for mobiles		Multi-channel Wi-Fi AP

Table 1.1: Full-duplex current and future possible applications (adapted from [9]).

1.3 Problem Statement

In this thesis, in-band full-duplex exchange of information under a MIMO and under a physical wireless network perspective is assessed. The main objective is to study and propose some techniques

for in-band full-duplex systems, that take tools from current state-of-the-art technologies described in Chapter 2. Self-interference mitigation methods, relaying techniques, physical layer networking and the use of massive antennas are further studied and proposed to integrate in-band full-duplex systems. This work focuses mainly on the theoretical side of telecommunications, always assuming transmissions in the digital baseband domain. A simulation framework is then developed to evaluate and confirm the performance of the proposed systems.

1.4 Key Innovations of this Thesis

The work developed during this thesis contains several contributions to the academic community. Mainly, in Chapter 4, a relay model that operates in full-duplex mode is characterized, self-interference suppression filters are studied for imperfect state information, and adaptive filtering for combating the self-interference in frequency-selective channels is proposed. In Chapter 5, massive MIMO full-duplex relaying is introduced for slow and fast fading channels, where the relay and user optimal power allocation that guarantees a certain communication quality is obtained. Finally, in Chapter 6, bidirectional communication through a relay is shown to be possible by using only one time slot, taking advantage of physical layer coding. Further, the power distribution that maximizes the system throughput is also obtained.

The contributions of this work may be summarized by the already produced and ongoing papers:

- A research combining the in-band full-duplex transmission in a relay station with the use of a massive number of antennas. A communication link is established between several pairs through the relay system. This relay incorporates self-interference suppression filters, as well as detector and precoder filters, whose performance is evaluated at the relay and at the destinations with BER curves. Further, an optimization problem is solved that ensures a minimum quality link for the pairs, while minimizing the total energy spent. Accepted, presented and published:

  [10] João S. Lemos, Francisco Rosário, Francisco A. Monteiro, João Xavier, and António Rodrigues. "Massive MIMO Full-Duplex Relaying with Optimal Power Allocation for Independent Multipairs". *In IEEE 16th Workshop on Signal Processing Advances in Wireless Communications (SPAWC)*, pages 306–310, Stockholm, Sweden, July 2015.

- The use of adaptive filters, namely the Recursive Least Squares (RLS) algorithm, is proposed in order to effectively cancel the power of the residual self-interference terms. This filter is derived for MIMO frequency-selective channels with OFDM transmissions. The filter performance is then evaluated by its convergence time and by the BER at the relay. Accepted for publication:

  [11] João S. Lemos, Francisco A. Monteiro, Ivo Sousa, and António Rodrigues. "Full-Duplex Relaying in MIMO-OFDM Frequency-Selective Channels with Optimal Adaptive Filtering". *Accepted in IEEE 3rd Global Conference on Signal and Information Processing (GlobalSIP)*, Orlando, FL, USA, December 2015.

- A paper where in-band full-duplex is combined with PLNC, allowing the bidirectional exchange of information through a relay in only one time slot. This proposed system is further evaluated and its sum rate derived. Based on that, an algorithm to achieve the maximum possible sum rate is proposed, by setting different powers to the terminals and to the relay. In preparation for submission:

  [12] João S. Lemos, Francisco A. Monteiro, João Xavier and António Rodrigues. "Sum Rate Maximization for Full-Duplex Bidirectional Relaying with Physical Layer Network Coding". *In preparation for submission*, 2015.

- The orthogonal properties of massive MIMO relaying are combined with PLNC, allowing an increase in the amount of information exchanged and also canceling the inherent interference in these systems. Lattice Network Coding is used for such effect, where it is shown how the increase in the number of relay antennas affects the proposed system performance. In preparation for submission:

  [13] João S. Lemos, Francisco A. Monteiro, and António Rodrigues. "On the Massive MIMO Effect in Practical Physical Layer Network Coding Systems". *In preparation for submission*, 2015.

1.5 Outline

This document reflects the work done in this Master's project and is presented to obtain the Master of Science degree in Electrical and Computer Engineering. Therefore, the document organization is as follows:

Chapter 2 presents an overview of the state-of-the-art papers published in the last five years and builds a theoretical foundation upon which the research work is based;

Chapter 3 contains the concepts of spatial-time communication, commonly known as MIMO, that form the preliminary knowledge required to understand the full-duplex proposed systems;

Chapter 4 describes the problem of in-band full-duplex relaying and proposes new approaches to improve this technique, using spatial filtering suppression and feedback adaptive cancellation;

Chapter 5 exploits the properties of massive MIMO transmissions in order to increase the level of self-interference suppression at a relay station;

Chapter 6 proposes a new network approach to communication that combines PLNC and in-band full-duplex transmissions to reduce the number of channel uses for exchange of information. The effect of massive MIMO is also explored;

Chapter 7 briefly refers to and comments on the results obtained in this Master's thesis and suggests possible future research headings within the topic here discussed.

Chapter 2

In-Band Full-Duplex in Context

The main idea of in-band full-duplex architectures is to use the same time and spectral resources to exchange information. Contrary to current systems that operate in half-duplex mode (unidirectional communication) or in out-of-band full-duplex mode (time or frequency division multiple access schemes), this novel approach enables a terminal to operate simultaneously over the same frequency band, doubling the spectral efficiency of a system. When doing so, the problem of self-interference arises. Self-interference consists of a perturbation of the transmitted signal caused at the receiving antenna of the same terminal. Thus, a terminal can cause interference to itself when transmitting a signal in the same frequency band of the signal it is also trying to listen to. Take a femto-cell of a mobile system as an example: the power difference between these two signals is about 40 dB, while the receiver noise floor is around -100 dBm. Imagine that a 0 dBm power signal is transmitted. The received power at a 15 cm away antenna is about -40 dBm, hence if 60 dB of self-interference is removed, the signal is theoretically decodable. Furthermore, it is intuitive that once a transmitted signal is perfectly known at the transmitter, the self-interference can be totally suppressed. However, several non-linearities in the radio frequency (RF) chain and errors in the channel estimations may severely harm the filtering processes. Note that this value is quite high and therefore the problem is not trivial [14, 15]. For those reasons, not so many years ago, the telecommunication community thought that radio equipment could not receive and transmit on the same frequency band. However, the demand for faster data link streams and for reduced spectrum allocation encouraged the study of in-band full-duplex communication in the last 4-5 years, which makes it a novel idea with a huge potential to integrate future technologies. As it will be shown further, in order to suppress 60 dB of self-interference, in-band full-duplex needs to cover a broad research area, involving telecommunications fields such as antenna theory, propagation modeling, radio frequency circuits, information theory, analogue signal processing, digital signal processing, networking, etc [16].

Usually, the process of canceling the self-interference is divided into three different stages or domains. Firstly, in terms of wireless propagation, there is the possibility of combining techniques such as antenna directionality, cross-polarization or transmit beamforming. In this case, the desired signal may also be affected by these methods, which motivates the introduction of analog circuit domain techniques.

The latter consists of subtracting a copy of the transmitted signal from the received one, adjusted with a proper gain, phase and delay, usually performed by RF circuits. Although the applications of the mentioned methods can achieve the required power-to-interference-plus-noise level to reliably communicate in test sets [14], when taking into account real environment effects it is usually not enough. In order to deal with the channel variations in such scenarios, digital domain filters are employed, allowing a necessary heavy signal processing. Moreover, this domain allows the use of techniques such as optimal power allocation, adaptive filtering, adaptive beamforming, etc., to further improve the mitigation of self-interference. Thus, an in-band full-duplex terminal needs to incorporate the processing stages represented in Fig. 2.1.

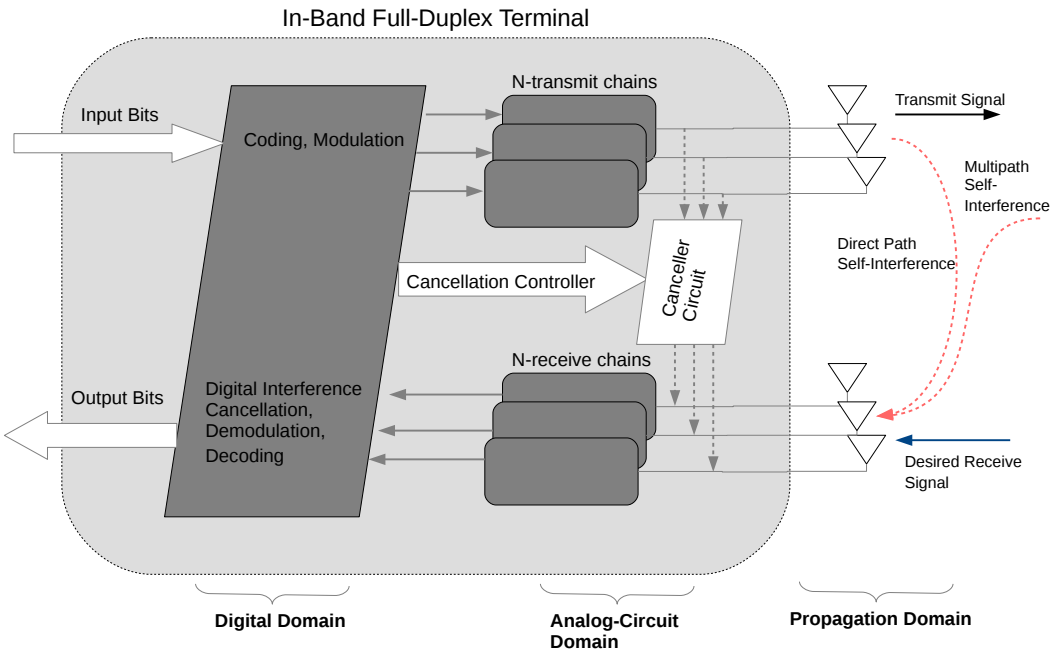

Figure 2.1: Block representation of a possible in-band full-duplex terminal with the three mentioned domains for self-interference mitigation detailed.

In this chapter an overview is given of the in-band full-duplex systems developed in the last 4 years, especially in academic work, as well as the engineering fields needed to design such systems [17]. The research challenges within the topic explored in this thesis are also presented. Moreover, the contextualization of this work within the topic area is carried out.

2.1 Propagation Domain

The first approach to mitigate self-interference was based solely on propagation properties of electromagnetic waves. The need to connect terminals that are too far to establish reliable communication brought about the idea of using relay stations. In order to increase the coverage of networks, relays can operate within the same bandwidth and act as passive amplifiers by receiving and retransmitting an amplified version of the desired signal, known in literature as amplify-and-forward (AF). Therefore,

wireless propagation insulation techniques were developed, aiming for separation of the receiving side from the transmitting side of the terminal. This procedure consists of the first stage of self-interference suppression, and it is essential to reduce the signal power so that its range fits in the downstream receiver hardware RF band. There are two different schemes of propagation techniques, based on the design of antennas, as Fig 2.2 shows.

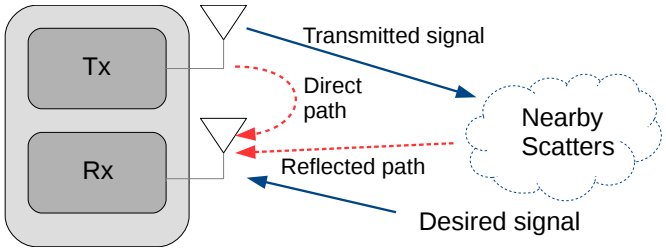

(a) Separated-antenna design.

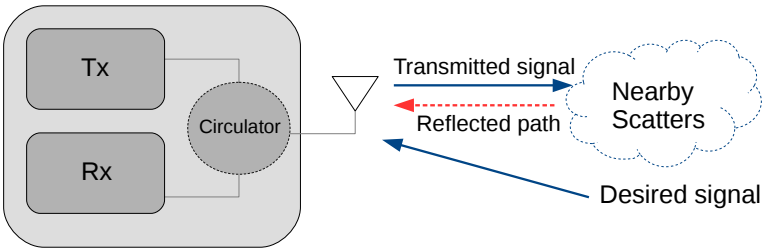

(b) Shared-antenna design.

Figure 2.2: Different possibilities to mitigate self-interference using wave propagation properties.

The first, separated-antenna design, consists of using different antennas to transmit and receive, as shown in Fig. 2.2(a). Using this procedure, it is then possible to suppress interference by path loss attenuation, increasing the antennas distance to further increase the attenuation or by placing absorptive material between them [18, 19, 20, 21]. However, this approach is limited by the terminal design that today plays a serious and important part in commercial products. Cross-polarization solutions are also interesting possibilities to insulate antennas and enhance the interference suppression [19, 21], for example, by transmitting in vertical polarization and by receiving in horizontal polarization. Another possibility is to exploit the antenna radiation pattern, carefully placing the receive antennas in radiation null points of the transmit antenna array [19, 22, 23]. The second one, shared-antenna design, in Fig. 2.2(b), consists of using the same antenna to transmit and receive. This is possible by means of a circulator, a circuit that routes the signals from the transmit chain to the antenna and from the antenna to the receive chain [24, 25]. In the case of a relay station, it is common to place antennas back-to-back, i.e., arraying antennas together that connect each relay end. Furthermore one can apply techniques such as wavetraps [26], which extend the relay isolation by connecting short circuit resonant transmission lines, such as band-gap structures [27]. These materials have high surface impedance and for that reason

attenuate the wave propagation. Also, one may use slots on the ground plane [28], which consist of internal dual band diversity antennas with dual frequency notched resonators to enhance electromagnetic attenuation.

The problem of both of the designs described above is sensitivity to environment conditions. For a rich scattering channel, the self-interference is composed of multiple copies of the transmitted signal, which may vary rapidly in time. It is possible that the desired signal is also deteriorated by applying these propagation methods, since they are blind to the carried information, i.e., the desired signal may also be attenuated by the propagation methods along with the self-interference component. Therefore, it is necessary to track these variations in the channels as described in the following sections.

2.2 Analog Radio Circuits

Analog circuit mitigation techniques are performed to increase attenuation on the self-interference signal and used as the second suppression stage of in-band full-duplex architectures. These circuits are placed before the analog-to-digital converter (ADC) and act either over the baseband or broadband analog received signal. The main idea is to track the propagation effect of the interfering signal and by means of electronic processing in the analog domain subtract it from the received signal. Moreover, it is also possible to tap the transmitted signal in the digital domain, apply the interference channel effect by means of gain and phase adjustment, and convert it back to the analog domain so that one can subtract it from the received signal [15, 18].

As in the propagation domain, some analog circuits are not able to track channel variations in multiple scatter conditions. These so called channel-unaware circuits are focused only on suppressing the interference direct path [15, 18, 19]. However, analog processing development has brought channel-aware circuits, that are capable of tracking channel variations and, therefore, more effectively cancel self-interference [23, 24]. Both consist of a delay tapped line with amplitude and phase correction. For the first case, the circuit is calibrated once and before its operation stage. For the second case, it is possible to continuously adjust those values in order to track channel variations.

As is known from the literature, cellular channels are commonly frequency-selective, due to multipath received copies of the desired signal at the receiver. For most current systems, it is essential to have this channel property in order to exploit spatial diversity, for example. Thus, analog circuits, even if channel-aware, cannot completely cancel out the self-interference multipath components. For that reason, a stage of digital signal processing is used so that the remaining self-interference, usually referred to as residual component, is further suppressed, thus, allowing reliable in-band full-duplex communication.

2.3 Digital Signal Processing

Digital signal processing techniques cancel out the self-interference by applying complex and heavy signal processing, in the digital domain (after the system ADC). As they work in the digital domain, sophisticated filtering techniques are applied without great effort (especially with the recent appearance

of powerful digital signal processing boards). However, this stage is only possible if the other two described above are successfully implemented, since the ADC dynamic range may limit the amount of interference allowed [29]. In literature, it is usually said that digital signal processing is done over the residual self-interference and acts as fine signal filtering.

Unlike its propagation and analog counterpart, there is not a standard set of techniques used in digital domain. This research field is developing in a grate pace, and a considerable amount of papers have been published in recent years proposing new perspectives and ways of dealing with the interference problem. The most important in this stage is to model the channel chain from the transmitter digital-to-analog converter (DAC) to the receiver ADC, so that filtering is effectively applied. It is then possible to perform beamforming [30], optimal power gain control and allocation, antenna selection [29, 31, 32, 33], null-space projections and minimum mean square error (MMSE) filters [34], joint decoding [33], etc.

2.4 State-of-the-Art Systems

In this section, fully operational in-band full-duplex systems are presented, as well as already simulated and published methods to achieve full-duplex communication, mainly through a relay station. The purpose is to briefly show state-of-the-art implementations of in-band full-duplex systems, some of them further explored in the work presented, and also to contextualize this thesis among the academic work previously presented.

2.4.1 Radio Terminals

During the last few years, several in-band full-duplex terminals have been developed in academia, mainly at Stanford University and Rice University. These research groups were primarily focused on the real system implementation, rather than studying digital signal processing techniques. Some of their work consists of important characterization and modeling of the interference, and is detailed bellow.

One of the first methods proposed to reduce self-interference is to use antenna separation along with analog circuit interference cancellation and some digital signal processing. Melissa Duarte and Ashutosh Sabharwal, from Rice University, showed theoretically that full-duplex systems with these characteristics are possible to implement with off-the-shelf radios and can overcome the rates achieved by half-duplex systems [18]. They also focused on characterizing the wireless full-duplex system with antenna analog cancellation and digital cancellation [15], as well as studying propagation techniques to further reduce self-interference as directional diversity [22]. Most of the work to characterize and implement operational full-duplex systems came from Melissa Duarte's PhD work at Rice University [35].

The research group from Stanford University published their first paper in 2010 [23]. They implemented an antenna cancellation scheme, consisting of a combination of proper antenna placing (in the propagation domain) followed by interference cancellation in the analog domain and digital interference cancellation. Two transmitting antennas separated from one receiving antenna by half wavelength are proposed, so that they interfere destructively making the receiving antenna hear a weaker inter-

ference (exploiting the phase offset). However, this method may have problems related to bandwidth constraints, since it creates a frequency-selective channel (perfect cancellation is only achieved at the carrier frequency) and with far distance power distribution, by perturbing the antenna radiation pattern. Notwithstanding, the paper argues that combining this with analog interference cancellation and digital interference cancellation can make in-band full-duplex possible. In another work [36], it is argued that using a $N \times N$ MIMO system can theoretically increase by N the system throughput (by MIMO single valued decomposition precoding), whereas the use of full-duplex just duplicates it, and therefore the obtained gain using full-duplex may be fallacious. The use of a balun (balance-unbalance, similar to a ciculator) circuit in the propagation domain is then proposed, which makes it possible to use the same antenna for transmitting and receiving. This component creates a perfect inverted copy of the transmit signal that is then subtracted (signal inversion), providing an additional 40-50 dB attenuation. A digital interference cancellation using channel estimation is afterwards applied to remove the residual and remaining self-interference. However, this approach requires delay lines with high resolution and a strong attenuation after the balun circuit, which cannot be implemented in practice with the required quality.

Very recently, an in-band full-duplex system for Wi-Fi radios was presented by a Stanford University research group [24]. The same antenna is used both to transmit and receive in this proposal, equipped with a circulator circuit. They likewise propose novel self-interference circuits and algorithms that achieve the 100 dB required attenuation on Wi-Fi standard. Firstly, an analog cancellation circuit based on parallel fixed lines of varying delays recreates the channel effect and gives a 60 dB attenuation on the self-interference signal. Secondly, a digital cancellation processing is used to clean out the remaining interference. The signal linear component is estimated with a maximum likelihood (ML) method, giving an extra 50 dB attenuation, which is followed by a non-linear residual component estimate. This paper represents an important cornerstone on full-duplex radio systems, although the radios used are still too large to incorporate current practical terminals. It is worth mentioning that some members of this Stanford research group created a startup in full-duplex radio solutions (url: *http://kumunetworks.com*), which was fully operational at the date this thesis was written.

2.4.2 Communication via Relay Stations

A promising area for future networks is the use of wireless relay stations in order to suppress shadowing effect, broadening network coverage and enhancing its maximum throughput, especially for future long-range millimeter wave communication [2]. Considering radio networks are increasing exponentially, relays may be used to shorten distances between users. Originally, relays were considered to operate in half-duplex mode, using two different channel resources for transmission and reception. This mode incurs a spectral inefficiency, since it uses two channel resources for exchanging the same message. For that reason, in-band full-duplex relays have been studied in recent years, so that spectral efficiency may be increased. Of course, self-interference mitigation techniques described above need to be applied so that the loopback interference is mitigated at the relay. Fig. 2.3 shows an in-band full-duplex relay serving in a two-hop communication between several sources and destinations.

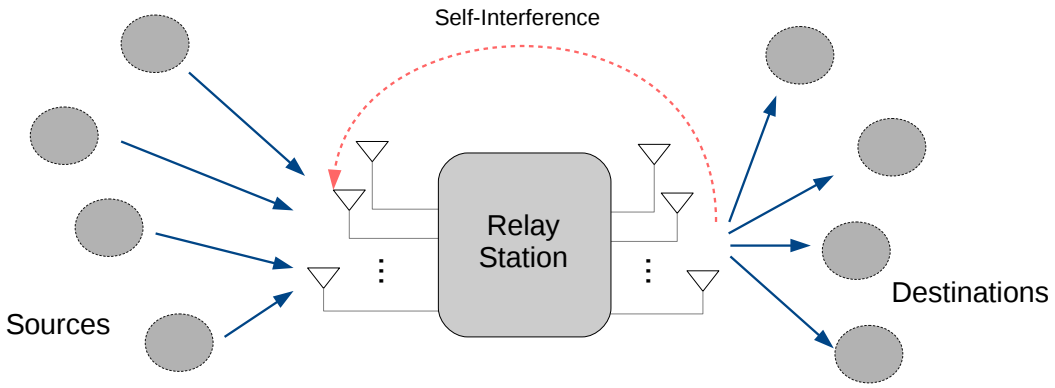

Figure 2.3: Full-duplex relay station representation with the self-interference problem highlighted.

The capacity trade-off in this approach was for the first time studied by Taneli Riihonen, Stefan Werner, and Risto Wichman [37], from Aalto and Tampere Universities, who were mainly focused on the signal processing and assumed a certain attenuation for the propagation and analog domain. They first propose an AF method (also with a relay gain control scheme [38]) within only the propagation domain and state that it is better to allow some degradation of the signal-to-noise ratio (SNR) using in-band full-duplex rather than to have the spectral inefficiency of the half-duplex mode. In [39], the same authors present a paper based on MIMO transmission links with loopback interference suppression decode-and-forward (DF) scheme, which means that the relay fully regenerates the digital signal. They assume channel state information (CSI) at the relay and use a zero forcing (ZF) approach, called null-space projection (NSP), or an MMSE estimation to filter the input and output of the relay. However, the channel erroneous estimations and the deviation of the transmitted signal from the original, caused by RF impairments, may give rise to errors that rapidly deteriorate its performance. Also, one can take into account the ratio between the useful signal power and the self-interference power when designing the filter and try to maximize it at the relay reception and transmission as in [40]. The optimal relay input and output filter may be chosen based on the direction of the interference signal but also based on the useful signal, by numerical optimization. The performance of this method is shown to slightly improve the one in [39].

A comparison between the advantages of using in-band full-duplex transmissions and half-duplex transmissions is described in [41]. The analysis is with respect to both instantaneous and long-term achievable rate by each mode, considering any relay protocol and any self-interference cancellation scheme. The authors derive the achievable rate expressions for the full-duplex AF and DF modes, half-duplex mode, and direct transmission, employing the optimal relay transmission power that maximizes each mode capacity. Then, a hybrid relay that selects the mode with higher capacity is introduced, by showing a threshold in terms of signal-to-interference-plus-noise ratio (SINR) to switch between them, and, therefore, mitigate the interference effect in the overall relaying system.

In [34], more advanced suppression techniques are explored. The authors use basic RF techniques such as antenna separation and analog cancellation combined with spatial suppression schemes (taking advantage of the MIMO extra degrees of freedom). Independent, separated and joint filter design are

proposed by the authors. Antenna selection for complex fading channels is presented as a generalized antenna subset selection for the binary channel. Then, it is further developed to eigenbeam selection based on the singular value decomposition. This method generally suffers from residual loopback interference even if there are no channel state estimation errors. Null-space suppression is presented as a method that can completely eliminate loopback interference when perfect CSI is considered and there are sufficient dimensions, i.e., there are enough antennas to project the interference. Therefore, filter design is accomplished such that a relay may transmit and receive in different subspaces. A MMSE filter is likewise proposed in order to minimize the distortion and attenuate the loopback interference, while preserving the desired signal path through the relay. Finally, a combination between interference cancellation and spatial suppression is presented. However, the main drawback of these schemes is that they are very sensitive to estimation errors in the loopback MIMO channel, which is considered as residual interference and treated as an additive perturbation. When channel estimations become large, the performance of the system deteriorates quickly with the interference power.

The relay transmit power is optimized in [42], with respect to the end-to-end (e2e) system sum rate. The authors assume that a beamforming filter for interference suppression is applied and show that under peak power constraints there is an optimal relay transmit power. This method allows to point the residual interference in the direction of the least ”harmful” dimension. Moreover, they deduce the relay optimal power closed form expression for the single-input single-output (SISO) case and compare the results with the half-duplex counterpart.

Another different approach is to use time-domain cancellation instead of filtering suppression, since it requires less degrees of freedom. Time-domain cancellation subtracts an estimation of the interference from the receive signal, while suppression, as already stated, takes advantage of MIMO systems to perform filtering and ensures orthogonality between the desired signal and interference. In [43], these two methods are compared. The authors evaluate a bidirectional stream of communication when null-space projection is performed and when time-domain cancellation with the same degrees of freedom is used. The methods are compared based on the achievable rates, and they conclude that time-domain cancellation may have better achievable rate regions for the channel model used. Also, they observe that antenna imbalance, i.e., having more antennas to transmit than receive or vice-versa, can improve suppression methods. More recently, other approaches have been published as in [44]. The authors propose an adaptive filter, based on a gradient descent algorithm to mitigate the self-interference in a DF single frequency relay. The system also uses linear beamforming to forward the symbols from one end to another. By applying the feedback adaptive filter, the authors show perfect self-interference cancellation under certain filter conditions, even when imperfect channel estimations are assumed. Moreover, it is also proved by Lyapunov function analysis that the proposed algorithm converges independently from the initial point if a proper step size is chosen.

In [45], the authors explore an advanced combination of propagation, analog and digital domain cancellation techniques for a in-band full-duplex relay station, where real implementation system specifications are taken into consideration. They propose the design of loops on the ground plane, based on near-field wave simulation via finite elements theory. The idea is to create electromagnetic fields

that help to cancel the waves transmitted by the relay. They also propose a non-linear self-interference cancellation method, arguing that linear filters may distort the signal introducing non-linearities and deteriorating the full-duplex system performance. The non-linearities are modelled by polynomials, where each coefficient is estimated with a linear least square method.

2.5 Researched Areas

Finally, state-of-the-art work on the areas of investigation that were incorporated in the study and development of interference mitigation schemes are briefly addressed.

2.5.1 Large/Massive MIMO

A recent emerging approach to further mitigate the interference present in a communication system, mainly in an in-band full-duplex relay station, is to employ large/massive arrays. Massive MIMO is considered to be an emerging technology that can upscale the attractiveness of MIMO, reducing noise, fading and interference, therefore enhancing the average system throughput. The theory of MIMO has provided new breakthrough performances in transmit beamforming, spatial multiplexing, space division multiple access and interference alignment, being present today in several cellular standards. The Massive MIMO transmission techniques are expected to further improve these performances in future wireless networks [46, 47].

Therefore, focusing on the interference alignment and cancellation provided by large antenna array systems, the study of the achievable performance in such systems has recently been conducted. In [48], the capacity of a relay station employing massive antennas that serve several multipairs is analyzed . The authors show that, by assuming an infinite number of antennas available at the relay, the interference between users can be made negligible when performing ZF or maximum-ratio combining/maximum ratio transmission (MRC/MRT) equalization, thus, attaining the capacity limit associated with the system there evaluated. In [49], the same system is considered, where different power-scaling schemes are employed to evaluated the limits and benefits of interference suppression. In [50], the spectral efficiency and power-scaling laws are derived when in presence of imperfect CSI, where simulation results are in accord with the theoretical results.

There is also the possibility of employing massive MIMO arrays in order to cope with the self-interference present in in-band full-duplex terminals. The orthogonality property present in large scale channels allows a better level of mitigation in the self-interference component. In [51], it is proven that massive MIMO renders more resilience in terms of inter-pair interference (ISI), while also mitigation the self-interference effect. The authors proposed a ZF precoding and an extended regularized channel inversion that is proven to exploit and combine the advantages of massive MIMO systems and in-band full-duplex transmissions. In [43], a study of full-duplex terminals with large dimensions employing suppression techniques and cancellation techniques is carried out. The number of antennas required to cancel the interference in the terminal is compared against the estimation level error in the channel

self-interference matrix, while the authors deduce the achievable rates in such scenarios.

Combining massive MIMO with in-band full-duplex relay station may provide outstanding results. In [31], a multipair DF full-duplex relay that combines massive antenna array techniques is presented to mitigate the self-interference borne by the relay. Those authors propose a method where the relay station receives pilots to estimate the loopback channel and then processes the signal using ZF or MRC/MRT detection and precoding. The multipair users are seen as a distributed multiple-input transmitting to the multiple-output relay. Thus, a linear ZF or MRC detection algorithm decodes the received signal. Since linear decoders can perform as well as non-linear ones with large arrays [52], the outgoing signal is precoded with a corresponding ZF or MRT, and forwarded. When the relay input and output antennas tend to infinity, the authors show that the loopback interference becomes orthogonal with the desired signal, perfectly canceling its undesired effect. Moreover, an optimization of the power allocation is developed, where the system energy efficiency (EE) is maximized, only subject to a given spectral efficiency and peak power. Nevertheless, their results assume perfect CSI for the large-scale fading components of the channels, and for that reason interference will always be present, albeit, with a low power component.

2.5.2 Physical Layer Network Coding

The interference in wireless networks is considered a central problem, due to the natural properties of the wireless medium, and is always avoided when possible to allow proper communication of all nodes in the network. This issue is considered to be a major challenge in multi-user cellular networks. Therefore, simultaneous transmissions are treated carefully, so that the interference between users is strictly avoided. This procedure of regarding interference as an harmful effect has been contributing to the limitation of the capacity of commercial networks. Mainly, the allocation of resources available, for example at a base station, is distributed among the users, guaranteeing that interference is brought to zero. Wireless networks usually employ scheduling algorithms of time and frequency resources to achieve the aforementioned goal. However, with a proper understanding of the characteristics of the interference, these resources may be more efficiently used, thus, enlarging the amount of information exchanged in wireless networks. For that reason, interference may be seen as nothing more than the superposition or sum of delayed and attenuated versions of the user's transmitted signals. Thus, this perceptive seeks to decode the interference, rather then avoid it.

The concept of physical layer network coding (PLNC) is among such techniques. This novel away of processing interference was inspired by the principle of network coding [53] along with the additive properties of wireless channels. The idea is that functions of user's messages are propagated in the intermediate nodes of the network, instead of the messages themselves. As mentioned, PLNC takes this procedure to the physical layer, i.e., it used the channel itself to help perform a linear combination of messages that are then broadcast. With a sufficient number of these combinations of messages, it is possible to obtain back all the messages and reuse the previous resources to avoid interference, enhancing the capacity of networks. The conceptualization of PLNC seems to be developed independently

by some research groups: Zhang, Liew and Lam [54]; Popovski and Yomo [55]; and Nazer and Gatspar [56]. Since the beginning of wireless networks, interference from users that transmit at the same time has been avoided or reduced. PLNC proposes a revolutionary method: interference can actually improve average throughput of a channel if treated properly [57]. By doing so, it is assumed that a relay node must somehow understand its output signals and the receivers should be able to isolate the information addressed to it. Thus, the concept of PLNC relies on a physical level modulation/demodulation techniques at the relay that allows the interference to enhance the system performance. The implementation of PLNC relies on a network code, which is specified by a codeword length and a defined sum operation over the same code. As it is designed for a physical level, a one-to-one modulation mapping should map the information in the available codewords to symbols that are then transmitted to the channel. This transmitted information then arrives at some intermediate node summed with the information from other nodes. Since these intermediate nodes are usually assumed to employ some non-linear detection, a many-to-one demodulation mapping is performed, such that the transmitted information is decoded. For example, consider the simplest case of two-way relay channel (TWRC), where most research has been done [58]. Consider also four codewords are used, which are pulse amplitude modulated with the set $\{-3, -1, 1, 3\}$. To correctly decode information in an additive white Gaussian noise channel (AWGN), a demodulation mapping for the set $\{-6, -4, -2, 0, 2, 4, 6\}$ would be necessary to estimate some function of the transmitted data (for example the binary XOR function, $\hat{\mathbf{u}} = f(\mathbf{w1} \oplus \mathbf{w2} \oplus \mathbf{e})$). This procedure would reduce the number of time slots used for bidirectional information flow from 4 to 2. In the first time slot (the multiple access phase), both ends transmit simultaneously, providing the relay with a noisy version of each codeword. In the second time slot (the broadcast phase), the relay broadcasts the decoded information to the ends, that can then extract their desired information. Due to its simplicity, PLNC has received enormous attention since 2010. A large number of strategies for PLNC have been proposed, especially for the TWRC, that are described in the following paragraphs.

As described in section 2.4.1, the most basic idea is to forward the information that arrives at a relay by only applying a gain. This procedure is known as analog network coding (ANC) and is the most basic form of PLNC. The relay acts as a passive element, while the end nodes use the knowledge of their own messages to decode the desired information. This idea was firstly implemented in [59], and further studied in [60, 61, 62]. However, the amount of noise introduced in intermediate nodes of a network limits the performance of such systems, even when channel coding is employed. Therefore, the DF strategy is resorted to enhance the performance of those systems. In this case, the intermediate nodes decode each codeword of the transmitted nodes and perform a linear function that is forwarded through the network. This idea is proposed in [55, 63, 64], where the bitwise XOR function is used to forward information with typical pulse amplitude modulation (PAM) as the physical mapping. In those works it is shown that under high SINR it is possible to approach the channel capacity. Nevertheless, this procedure involves the detection of each individual received codeword, which is not necessary since only a function of them is forwarded to the network. Therefore, the concept of denoise-and-forward (DeF) has appeared. This idea is based on a many-to-one map that directly maps the received information to the desired function to be forward. For example, in a TWRC the received symbols are directly mapped to a

constellation that is formed based on the combination of the transmitted constellations. This constellation is isomorphic to the network linear code and, thus, the network code is embedded into the symbols of the constructed constellation. In [65, 66] the authors study the performance of this scheme. Firstly, a generalized XOR function is used and also a non-conventional quadrature amplitude modulation (QAM), in order to optimize the information flow. Spatial diversity techniques are used to enhance the system performance. Moreover, a comparison between the linear function XOR and the addition over the finites function is compared based on the symbol and bit error rate (BER) for different PAM schemes. Furthermore, these works present per-symbol coding instead of per-message coding. In order to enhance the performance of TWRC with per-message coding and to generalize it to multi-user networks, a new concept was introduced, as follows.

The concept of compute-and-forward (CP) was initially proposed by Nazer and Gastpar in [67]. The TWRC is generalized to a Gaussian multiple access channel (MAC) where each node transmits a symbol from a multi-dimension lattice. The idea is to explore the group property that any integer combination of a lattice point is always a point of that lattice. Therefore, the intermediate nodes try to create a network code that approximates the received information to a integer combination of points in the used lattice. The performance of CP is based on the effective noise, which is created due to the difference between the integer code and the real or complex nature of the channel. Nazer and Gastpar have shown that the computation rate of this protocol for one-hop networks gets very close to the Shanon channel capacity [68], when there exists an infinite sequence of ”good” lattice codes, described in [69]. The idea of CP is exemplified in Fig. 6.3 for the TWRC. Firstly, each node maps its message onto a point in the lattice code and sends it through the channel. The lattice code is constructed based on the intersection of a fine lattice fundamental region with a coarse lattice. This called nested lattices codes are usually generated from channel correction codes, as convolutional codes or low-density parity-check codes (LDPC) [70, 71]. Then, the intermediate node receives the sum of the signals and quantizes it onto the fine lattice to obtain an approximation of the sum of messages, which is forwarded through the network or back to the nodes.

The CP can also be extended to MIMO, where each node of the network may employ more than one antenna, as in [72]. Significant performance gains in the rate analysis by the use of multiple antennas are shown. Also, it is possible to improve the performance of CP by resorting to well-established methods in wireless communication, such as successive decoding of information [73].

The step forward in terms of communications is to combine PLNC with in-band full-duplex transmissions. As already mentioned, initially the exchange of information in a TWRC was done in four time slots. Network coding reduced this number to only three slots. The physical network coding further improved the exchange of information to two time slots. By incorporating the techniques of full-duplex communication and PLNC, only one time slot may be used for bidirectional relaying streams of information. This could be the major step towards finding solutions to meet the requirements of future networks. Few works on combining in-band full-duplex and PLNC have been presented. Gan Zheng has proposed a system for the TWRC [74], where the relay and the users have multiple antennas. An ANC to forward information with a ZF constrain at the relay is proposed there, in order to attenuate the problem of self-

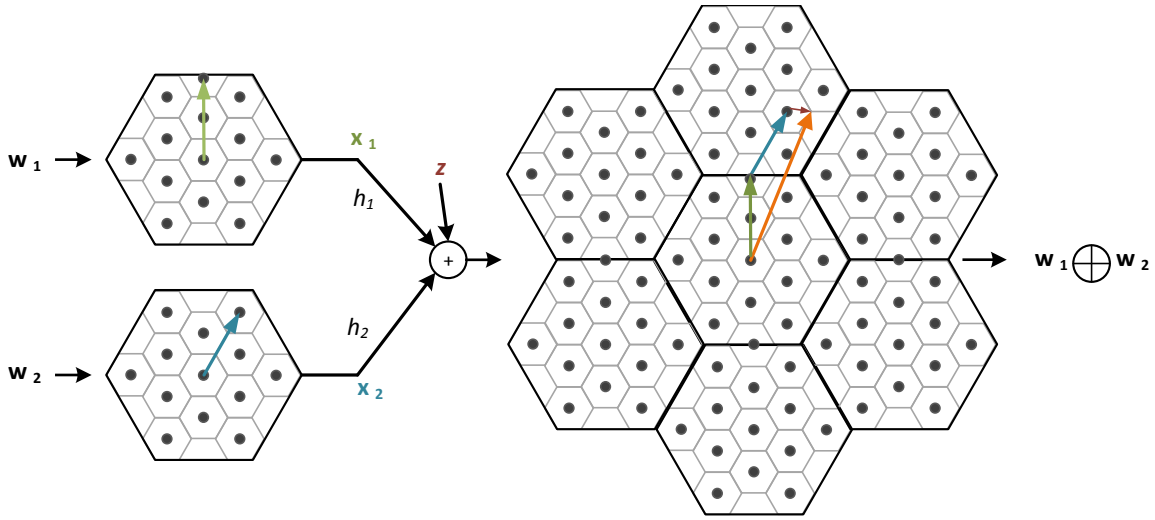

Figure 2.4: Compute-and-forward transmission over a nested lattice code for the two-way relay channel (figure adapted from [57]).

interference. Moreover, the author presents power control to optimize the system rates. Semiha Tedik and Gunes Karabulut Kurt have presented a system that utilizes DF relaying based on ML estimation of the XOR function for binary pulse shift keying (BPSK) [75]. The self-interference from full-duplex transmissions at the nodes and at the relay are canceled with antenna separation at a propagation level and with time-domain cancellation at a digital level.

2.6 Thesis Contextualization

As demonstrated above, in order to establish reliable full-duplex communication, it is necessary to address a broad domain of communication theory and engineering concepts. The combination of RF circuits, system design, digital signal processing, relaying and networking is needed so that fully in-band full-duplex systems may be a reality in the future of wireless communications. All the above-mentioned areas are in major development and several problems are still to be solved. This thesis focuses on the digital signal processing domain for in-band full-duplex relaying in symbol coded networks. The main objective of this work is to propose and study some in-band full-duplex systems that use state-of-the-art improved techniques and employ methods from the mentioned recent signal processing areas.

Chapter 3

MIMO Communications

For discussion of the in-band full-duplex problem it is essential to understand multiple-input multiple-output (MIMO) communications, a field that has been well developed in the last 15 years. Thus, the MIMO theory is briefly explained in this chapter. This study is based on some of the most influential textbooks on the topic [76, 77, 78, 79, 80, 81]. Most of the studied and implemented techniques in this chapter are further employed in the implementation and simulation of in-band full-duplex relay systems in the chapters that follow.

3.1 MIMO Concept

MIMO transmissions have provided the tools to design faster and more reliable systems for wireless communications networks. The idea is to exploit the space diversity introduced by using multiple antennas, in order to increase user capacity. Using a MIMO channel for communication provides several data streams sent simultaneously, called spatial multiplexing, where information is beamformed to serve different users. The key concept is to take advantage of the multiple scattered uncorrelated signals that arrive via different paths at the receiver to extract the information under transmission.

3.1.1 MIMO Channel

The MIMO channel is almost always modelled as a narrowband channel where the channel coefficients are complex scalars. M_T antennas transmit a symbol at each time slot n to M_R receive antennas as shown in Fig. 3.1.

Each stream from the transmit antenna i to the receive antenna j experiences a complex channel coefficient $h_{ji}(n)$. Therefore, the received signal at the receive antenna j is given by a sum of sent symbols multiplied by the correspondent channel, $y_j(k) = \sum_{i=1}^{M_T} h_{ji}(n)x_i(n) + n_j(n)$, where $x_i(n)$, $y_i(n)$ are random processes and $n_j(n)$ is a zero mean complex circular symmetric (ZMCCS) Gaussian random

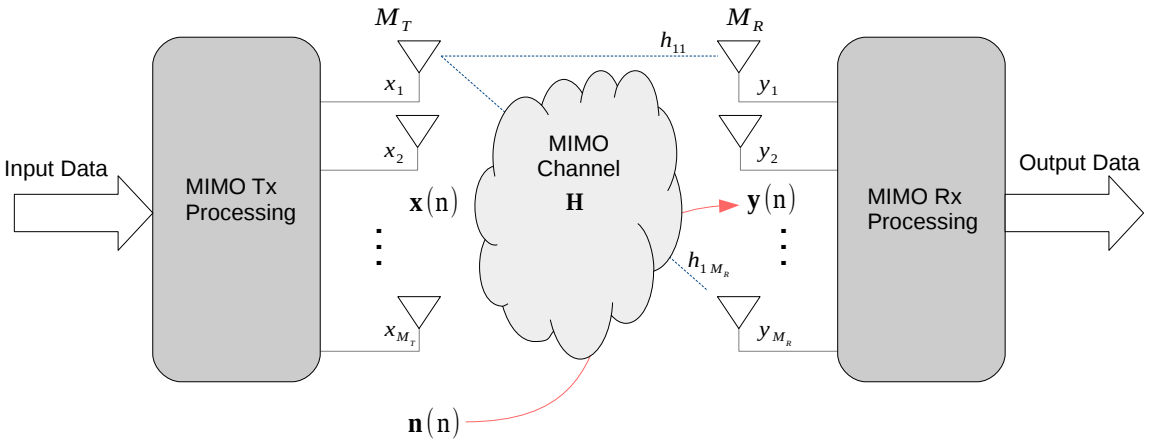

Figure 3.1: MIMO Channel.

variable with zero mean and σ_n^2 variance (for $n \in \mathbb{N}$). By defining the vectors

$$\begin{aligned} \mathbf{x}(n) &= [x_1(n), ..., x_{M_T}(n)]^T, \\ \mathbf{y}(n) &= [y_1(n), ..., y_{M_R}(n)]^T, \\ \mathbf{n}(n) &= [n_1(n), ..., n_{M_R}(n)]^T, \end{aligned} \tag{3.1}$$

it is then possible to create a representation for the MIMO channel with the channel matrix $\mathbf{H}(n)$, usually used in the literature, with entries given by

$$\mathbf{H}(n) = \begin{bmatrix} h_{11}(n) & \cdots & h_{1M_T}(n) \\ \vdots & \ddots & \vdots \\ h_{M_R1}(n) & \cdots & h_{M_RM_T}(n) \end{bmatrix}, \tag{3.2}$$

and, therefore, the time-discrete MIMO input-output relation is as follows

$$\mathbf{y}(n) = \mathbf{H}(n)\mathbf{x}(n) + \mathbf{n}(n) \tag{3.3}$$

The coefficients in matrix $\mathbf{H}$ can be either known (time-invariant channel), remain constant over many block transmissions (slow fading channel) or change several times over a transmission block (fast fading channel). The knowledge of the channel coefficients is usually called channel state information (CSI), and may be instantaneous if the transmitter and/or the receiver knows its value. Also, it is common that the system only knows an erroneous estimation of the MIMO matrix, usually denoted as imperfect channel estimation. When designing and testing MIMO systems, another possibility is to assume that only the channel distribution is known. Nevertheless, the CSI is estimated using pilot sequences, with traditional estimators, studied in deep in the last 20 years, but adapted to the MIMO case. At the limit, each $h_{ji}(n)$ is estimated individually and feedback properties and channel reciprocity can be assumed to obtain $h_{ij}(n)$.

3.1.2 MIMO Capacity

In order to understand the theoretically achievable capacity of a MIMO channel, it is more intuitive to start by understanding the special cases of MIMO, as detailed in [77] and stated in table 3.1.

	SISO	SIMO	MISO	MIMO
M_T	$=1$	$=1$	>1	>1
M_R	$=1$	>1	$=1$	>1

Table 3.1: Special cases of MIMO.

Due to the purpose of this work, only the MIMO case is looked at, but the special cases of MIMO are easily derived from the theory built for it in most cases. Therefore, consider the case where the channel is time-invariant and there is full CSI (at both transmitter and receiver). It is possible to create a set of independent parallel channels by singular value decomposition, where $\mathbf{H} = \mathbf{U}\mathbf{\Lambda}\mathbf{V}^H$. The matrix $\mathbf{\Lambda}$ is a diagonal matrix containing the singular values of $\mathbf{H}$ and representing the gain of the parallel channels. By a pre and postcoding, it is possible to derive an orthogonal equivalent channel, given by $\tilde{\mathbf{y}} = \mathbf{\Lambda}\tilde{\mathbf{x}} + \tilde{\mathbf{n}}$, where $\tilde{\mathbf{x}} = \mathbf{V}^H\mathbf{x}$, $\tilde{\mathbf{y}} = \mathbf{U}^H\mathbf{y}$ and $\tilde{\mathbf{n}} = \mathbf{U}^H\mathbf{n}$. The scattered MIMO channel is by this process transformed into $\min\{M_T, M_R\}$ parallel channels. The capacity of this MIMO system then becomes the sum capacity of each individual channel and is computed in bits/s/Hz as

$$C_{MIMO}^{TI} = \sum_{k=1}^{\min\{M_R, M_T\}} \log_2\left(1 + P_k^O \gamma_k\right), \tag{3.4}$$

where the optimal power P_k^O is obtained by the water filling solution (optimization of the sum capacity with a total power constraint [79]) and $\gamma_k = \frac{\lambda_k^2}{\sigma_n^2}$ is the signal-to-noise ratio (SNR) of parallel channel k (note that the transformation does not change the total system power).

Considering now the fast fading channel, $\mathbf{H}(n)$ becomes the realization of a fading channel process, usually assumed to be stationary and ergodic. In this case, it is possible to adapt the transmission to the distribution of the channel coefficients. The covariance matrix of transmitted signals $\mathbf{R_{xx}} = \mathbb{E}\{\mathbf{x}\mathbf{x}^H\}$, is taken into consideration, giving an achievable rate of $\log_2 \det(\mathbf{I} + \mathbf{H}\mathbf{R_{xx}}\mathbf{H}^H/\sigma_n^2)$. The ergodic capacity is therefore the average of the maximum achievable rate over the fading channels, assuming a transmission peak power of $\bar{\mathbf{P}}$ for example, and given by equation (3.5)

$$C_{MIMO}^{FF} = \max_{\mathbf{R_{xx}}\ s.t.\ \mathrm{tr}(\mathbf{R_{xx}}) \leq \bar{\mathbf{P}}} \mathbb{E}\Big\{ \log_2 \det\left(\mathbf{I} + \frac{1}{\sigma_n^2}\mathbf{H}\mathbf{R_{xx}}\mathbf{H}^H\right)\Big\}. \tag{3.5}$$

The most common example in the literature is to model the channel with the famous Rayleigh distribution, where both real, $\mathcal{R}\{h_{ji}(n)\}$, and imaginary, $\mathcal{I}\{h_{ji}(n)\}$, part of $h_{ji}(k)$ are drawn from a normal distribution. In that case, $\mathbf{R_{xx}} = \frac{\bar{P}}{M_T}\mathbf{I}$, where $\bar{P}$ is the mean power of the transmitted sequence, and the rate in equation (3.6) is obtained.

$$C_{MIMO}^{FF,Rayleigh} = \mathbb{E}\Big\{ \log_2 \det\left(\mathbf{I} + \frac{\bar{P}}{M_T\sigma_n^2}\mathbf{H}\mathbf{H}^H\right)\Big\}. \tag{3.6}$$

Finally, the slow fading channel is analyzed. The channel realization spreads over a block of data that

is much smaller than the channel coherence time. Thus, the channel matrix becomes approximately a constant, $\mathbf{H}$. In order to characterize this channel, the outage probability is introduced, since the channel can be in deep fading during a block of code and for that reason there is no averaging effect, as in the previous case. The outage probability is then defined as the amount of time the actual transmission rate is under a certain predefined rate, R_0 (chosen for a specific application for example), as in

$$p_{out}^{SF}(R_0) = \mathbb{P}\{R \leq R_0\}. \tag{3.7}$$

In the case of slow fading Rayleigh channel, the outage probability is defined as in equation (3.8)

$$p_{out}^{SF,Rayleigh}(R_0) = \mathbb{P}\Big\{ \log_2 \det \big(\mathbf{I} + \frac{\bar{P}}{M_T \sigma_n^2} \mathbf{H}\mathbf{H}^H\big) < R_0 \Big\}. \tag{3.8}$$

However, the log-normal distribution is often used to characterize channel slow fading effects. Moreover, both fast and slow fading may be present in a real transmission.

3.1.3 MIMO Performance Gains

Two different indicators may be introduced in order to evaluate the gain of using space-time communication. These indicators are compared to the single link scenario.

The **multiplexing gain** is the number of independent streams transmitted simultaneously and given by

$$\lim_{\mathsf{SNR}\to\infty} C(\mathsf{SNR})/\log_2(\mathsf{SNR}),$$

where $\mathsf{SNR} = \bar{P}/\sigma_n^2$. For the fast fading channel in rich scattering conditions it is equal to $\min\{M_T, M_R\}$.

The **diversity order** is defined for fast fading channels as the increasing rate of the error probability with the SNR, and is defined by

$$-\lim_{\mathsf{SNR}\to\infty} \log_2 p_{error}(\mathsf{SNR})/\log_2(\mathsf{SNR}),$$

where $\mathsf{SNR} = \bar{P}/\sigma_n^2$. It measures the number of resolvable paths over fast fading effect that the detector can average out. Note that the diversity gain corresponds to the modulo of the slope of the BER curves when plotted versus the SNR [81].

3.2 MIMO Detection Techniques

The previous section presented information theory based aspects of MIMO. The design and implementation of the transmitter and the receiver of a MIMO real system is here studied. These detection algorithms provide the background for implementing techniques that are able to suppress the self-interference present in in-band full-duplex architectures. In the following, it is assumed that all detection filters are followed by a symbol-wise quantizer, $\mathrm{Q}(\cdot)$.

3.2.1 Maximum Likelihood

The maximum likelihood (ML) detector, as in other schemes, consists on an exhaustive search over all the possible symbol realizations. The objective is to choose the closest vector in the constellation of possible points to the transmitted vector, as in equation (3.9).

$$\mathbf{s_{ML}} = \arg\min_{\mathbf{z}\in\mathcal{C}} \parallel \mathbf{y} - \mathbf{Hz} \parallel^2, \tag{3.9}$$

where $\mathcal{C}$ is the set of all possible input vectors. It can be shown that this detector is optimal, i.e., it gets the maximum M_R value for spacial diversity [78]. Nevertheless, the algorithm complexity is $\mathcal{O}(m^{M_T})$, i.e., it increases exponentially with M_T, and where the base *m* is the number of possible symbols (drawn from a modulation with dimension size m).

3.2.2 Matched Filter

The matched filter (MF) is the most basic linear family detector (of the form $\hat{\mathbf{x}} = \mathbf{W}^H\mathbf{y}$). It is very simple to implement, however, the MF is only optimal when parallel channels are present (diagonal $\mathbf{H}$ matrix). The expression consists of basic channel equalization, which does not fully suppress the interference in general (since usually $\mathbf{h_k^H h_i} \neq \delta(i-k)$).

$$\mathbf{s_{MF}} = \mathbf{H}^H\mathbf{y} = \mathbf{H}^H\mathbf{Hx} + \mathbf{H}^H\mathbf{n}. \tag{3.10}$$

Equation (3.10) shows the filter output, which provides a SNR of

$$\text{SNR}(k) = \frac{P_{x_k} \parallel \mathbf{h_k} \parallel^2}{(\sum_{i\neq k} \|\mathbf{h_k^H h_i}\|^2 / \parallel \mathbf{h_k} \parallel^2) + \sigma_n^2},$$

and has a complexity of $\mathcal{O}(M_T^2 M_R)$, which corresponds to the multiplication of the channel matrix [81].

3.2.3 Zero Forcing

The zero forcing (ZF) filter is designed in opposition to the MF, aiming to completely eliminate the stream's interference. The channel inverse $\mathbf{H}^{-1}$ is intuitively the solution, however it would require a square $\mathbf{H}$. Generalizing the filter expression, the Moore-Penrose pseudo-inverse is used and is given by $(\mathbf{H}^H\mathbf{H})^{-1}\mathbf{H}^H$. Although, if $\mathbf{H}$ is not full column rank, the ZF is not applicable since there is insufficient streams to decode the number of transmitted symbols or, in a geometric perspective, there is no null space to project each stream interference.

$$\mathbf{s_{ZF}} = \mathbf{H}^\dagger\mathbf{y} = (\mathbf{H}^H\mathbf{H})^{-1}\mathbf{H}^H\mathbf{y} = \mathbf{x} + (\mathbf{H}^H\mathbf{H})^{-1}\mathbf{H}^H\mathbf{n}. \tag{3.11}$$

As can be seen in equation (3.11), the interference is suppressed (projection of the desired stream onto the interference null space), but in this process the noise is not taken into consideration and, therefore,

its power is enhanced. The signal-to-noise ratio in each stream is SNR$(k) = P_{x_k}/\sigma_n^2[(\mathbf{H}^H\mathbf{H})^{-1}]_{kk}$, and the complexity of the algorithm corresponds to $\mathcal{O}(\min\{M_T, M_R\}^3)$ [78].

3.2.4 Minimum Mean Square Error

The minimum mean square error (MMSE) filter is introduced so that the average square error is minimized, which also takes into consideration the noise power present in each data stream. The idea is to solve $\min_{\mathbf{W}} \mathbb{E}\{(\mathbf{x} - \mathbf{W}^H\mathbf{y})^2\}$ in order to derive the filter expression, which can be obtained as in (3.12) .

$$\mathbf{s_{MMSE}} = (\mathbf{H}^H\mathbf{H} + \frac{\sigma_n^2}{P_x}\mathbf{I})^{-1}\mathbf{H}^H\mathbf{H}\mathbf{y}. \tag{3.12}$$

It is possible to deduce that the SNR$(k) = P_{x_k}/\sigma_n^2[(\mathbf{H}^H\mathbf{H} + \frac{\sigma_n^2}{P_{x_k}}\mathbf{I})^{-1}]_{kk}$ and that the method has complexity of the same order of the ZF filter [79].

3.2.5 Successive Interference Cancellation Receiver

Successive interference cancellation receivers are a family of MIMO detectors that decode one stream at a time, firstly intruded in [82] as V-BLAST architecture (from Bell Labs). The main idea is to use iterative decoding where only one stream is decoded at each step, while the rest is considered interference. After having been decoded, the stream is then removed from the total received signal. This procedure is successively done until there are no more streams to decode (detection layer-by-layer). Equation (3.13) shows the procedure idea, where L_k stands for the k^{th} received stream [81].

$$\begin{aligned} \mathbf{y}_{L_k} &= \mathbf{h}_k x_k + \sum_{i=k+1}^{M_T} \mathbf{h}_i x_i + \mathbf{n}; \\ \mathbf{y}_{L_{k+1}} &= \mathbf{y}_{L_k} - \mathbf{h}_k \hat{x}_k. \end{aligned} \tag{3.13}$$

At each layer detection, the stream can be decoded by employing a linear detector as described in the previous sections. However, this method suffers from error propagation through its layers that can perturb the overall performance. Thus, finding the optimal order for decoding that minimizes the bit error rate (BER) becomes crucial, but at the same time unfeasible when the number of antennas increases. Thus, ordered successive interference cancellation (OSIC) detectors are used when the streams are decoded from the highest post-processing SNR to the lowest. This detector is close to optimal, i.e., approaches the full capacity for fast fading channels. The complexity of this detector has also the same order of the ZF detector, i.e., it varies cubically with the number of antennas [83].

3.2.6 Lattice Reduction Aided

In the literature, the most comprehensive way of looking at MIMO detection makes use of the lattice theory. The goal is to detect a vector with optimal performance, thus, achieving the maximum multiplexing gain, and with reduced complexity that could be used in a real-time system. This new mathematical

framework has provided the tools to further study MIMO systems and has created more advanced detectors. The previous detectors briefly referred to in the previous sections can also be explained under the lattice theory. In this and the next section two lattice based algorithms are presented.

Consequently, one can define a lattice as an infinite discrete subgroup of $\mathbb{R}^n$

$$\mathbf{\Lambda} = \left\{ \mathbf{y} \in \mathbb{R}^n : \mathbf{y} = \sum_{i=1}^{M_T} \mathbf{h}_i x_i, x_i \in \mathbb{Z}, \mathbf{h}_i \in \mathbb{R}^n \right\}. \tag{3.14}$$

A lattice is then seen as an infinite set of points of integer combinations of the basis channel matrix $\mathbf{H}$. The fundamental region of a lattice is defined by $\mathcal{F}(\mathbf{H}) = \{\mathbf{Hx}, 0 \leq x_i \leq 1\}$ (more detailed lattice theory in [84]).

Lattice Reduction Aided methods are based on the idea that two basis matrices can generate the same lattice, but they may have different fundamental regions (it may vary in area and vector's orthogonality). As shown in [85], using shorter vector bases that are close to orthogonal can effectively improve the detection method by maximizing the coverage of the detector region compared to the Voronoi cell of the transmitted vector [80]. Before employing the detectors described in the previous subsections, it is possible to reduce the channel matrix $\mathbf{H}$ in a pre-processing stage, aiming the performance enhancement of the linear detectors. The LLL algorithm, proposed by the authors Lenstra, Lenstra and Lovász, and named after them, was first introduced for real channels and then adapted to complex ones [86]. When considering complex channels a transformation of the complex constellation to a lattice is also necessary. Algorithm 1 shows the complex lattice reduction (CLR) receiver stages with the complex LLL (CLLL) method:

Algorithm 1 Complex Lattice Reduction

a) Convert Complex constellation to lattice problem (for QAM constellation):
$\mathbf{y_L} = 0.5(\mathbf{y} + \mathbf{H}(\mathbf{1} \cdot (1 + j)))$

b) Lattice Basis reduction:
$(\mathbf{H_{red}}, \mathbf{M})) = \text{CLLL}(\mathbf{H})$

c) Detection with linear based filter:
$\mathbf{s_{CLR}} = \text{detect}(\mathbf{H_{red}}, \mathbf{y_L})$

d) Shift-back and obtain the estimated vector:
$\hat{\mathbf{x}} = 2\mathbf{M}\mathrm{Q}_\Lambda(\mathbf{s_{CLR}}) - \mathbf{1} \cdot (1 + j)$

where $\mathbf{1}$ is a column vector of ones, $\mathbf{M}$ is a unimodular matrix (square matrix with integer entries and $\det(\mathbf{M}) = \pm 1$) and Q_Λ is the function that outputs the closest lattice point. The complexity of the algorithm is shown in [86] as $\mathcal{O}(n^4 \log(n))$, where $n = \min\{M_T, M_R\}$.

3.2.7 Sphere Decoder

The state-of-the-art detection technique for MIMO systems is called sphere decoding and is an exact method in terms that it can achieve the same performance of the ML detector, but with an on average much lower complexity. The main idea behind this detector relies on advanced lattice theory, where it is

possible to decompose the given lattice and the received vector in a rigid rotation matrix, for which the closest vector problem simplifies. The equivalent lattice obtained has the property that it is possible to set a norm of any lattice point composed by independent contributions. In order to find the closest vector to the received one a tree based search is performed using the referred norm and by comparing it to an upper bound. If the norm upper bound is properly chosen, the ML solution is always found [80].

The complexity of the algorithm is measured by the number of tree nodes that are needed to visit, and it is on average given by $\mathcal{O}(m^{\alpha M_T})$ with $0 \leq \alpha \leq 1$ [87]. The complexity is exponential, however for low dimensional lattices, sphere decoders (SD) are affordable to used.

3.2.8 Performance Evaluation

The performance of the described detectors (except from the SD) is compared based on the BER plots in Fig. 3.2. Uncoded MIMO in additive white Gaussian noise with $M_T = 4$, $M_R = 4$ and with 4-QAM and 16-QAM modulation schemes is used for this assessment. The channel matrix is assumed to be Rayleigh fading, i.e., each entry of $\mathbf{H}$ is i.i.d. as $\mathcal{CN}(0,1)$, and the noise is distributed as $\mathcal{CN}(0,\sigma_n^2)$. Monte Carlo simulation is used with 10^6 channel realizations. The diversity order may be measured from the slope of the curves.

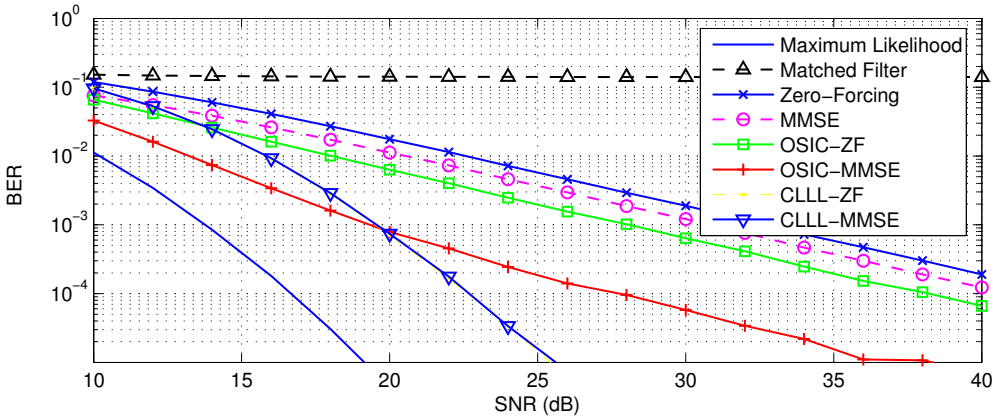

(a) BER of 4x4 MIMO receivers for i.i.d. fast fading channel with 4-QAM

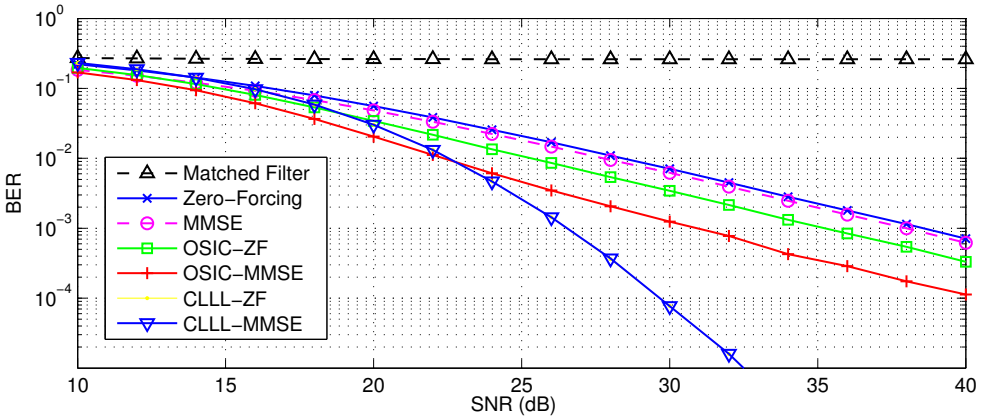

(b) BER of 4x4 MIMO receivers for i.i.d. fast fading channel with 16-QAM

Figure 3.2: BER vs SNR (total SNR $= P_x/\sigma_n^2$) performance of the implemented detectors.

The ML decoder exhibits a diversity order of $d_{\text{ML}} = \min\{M_T, M_R\} = 4$. The ZF and MMSE achieve $d_{\text{ZF,MMSE}} = M_R - M_T + 1 = 1$, however, the MMSE receiver has a gain when compared with the ZF from considering the additive Gaussian noise. The OSIC also achieves a diversity order $d_{\text{OSIC}} = M_R - M_T + 1 = 1$, but with a higher dB gain margin in the BER curve when compared to the ZF and MMSE, respectively. Finally the CLLL has a diversity order of $d_{\text{CLLL}} = M_R = 4$, the same diversity order of the ML detector [88], as previously stated as optimal condition.

3.3 Broadband MIMO

The study of the MIMO channel presented above assumed a frequency-flat channel, represented by $\mathbf{H}$, which only depends on the instantaneous input $\mathbf{x}(n)$ to generate its output $\mathbf{y}(n)$. This procedure is commonly presented in the literature, where it is assumed that each entry of the MIMO channel is a composition of multiple scatters summed at the output to form a complex gain, and which vary faster than the symbol interval, or more specifically, assuming the symbol rate is less than the coherence bandwidth of the channel. Nevertheless, most systems that operate in broadband need to deal with frequency-selective MIMO channels [89, 90], since the previous assumption is no longer valid. Modern wireless applications require faster data rates where the flat fading assumption cannot be assumed, enhancing the study of techniques to overcome this problem. The channel equation for this system representation now becomes

$$\mathbf{y}(n) = \mathbf{H}(z)\mathbf{x}(n) + \mathbf{n}(n), \tag{3.15}$$

where $\mathbf{x}(n) \in \mathbb{C}^{M_T}$ represents the complex symbol vector and $\mathbf{n}(n) \in \mathbb{C}^{M_R}$ the additive noise, for both $n, k \in \mathbb{Z}$. The frequency-selective channel is here represented by its z-transform

$$\mathbf{H}(z) = \sum_{k=0}^{L} \mathbf{H}[k] z^{-k}, \tag{3.16}$$

where z denotes the delay operator, i.e., $z^{-k}\mathbf{x}(n) = \mathbf{x}(n-k)$, while L represents the causal channel order [91]. The MIMO impulse response at instant $n-k$ is $\mathbf{H}[k] \in \mathbb{C}^{M_R \times M_T}$, where quasi-static fading is assumed, i.e., the channel is fixed for a transmission frame and for that reason does not depend on the time instant n.

The main disadvantage of this kind of channel is the inter-symbolic interference (ISI), that spreads out a symbol in time, overlapping its energy to subsequent symbols. It is necessary to cope with both inter-pair interference (IPI) associated with space-time communication and at the same time handle the ISI present in frequency-selective channels.

3.3.1 Exploiting Frequency Selective Channels

One may think that ISI is undesirable in wireless communications, since it degrades the performance of frequency-flat MIMO receivers, as previously studied. However, if treated properly, this phenomenon can provide new degrees of freedom, providing more resolvable paths to decode a symbol. The maximum

number of uncorrelated paths between the transmitter and the receiver is then

$$\begin{cases} M_T M_R & \text{, for flat fading channels,} \\ M_T M_R(L+1) & \text{, for frequency-selective channels.} \end{cases} \tag{3.17}$$

The previous equation shows that frequency-selective channels may actually achieve higher rates than flat channels. This issue has been analysed in [92], where the authors develop a simulation-based method to compute the achievable rate of MIMO systems operating under ISI conditions. The main result to mention is that the rate increases with the selective channel order L. Methods for combating ISI are usually categorized into single carrier techniques or multiple carrier techniques. The first method uses only one carrier frequency to transport information that is filtered, equalized, at the receiver (it can be performed linear or feedback equalizers). The latter, consist of splitting the broadband signal that suffers ISI into several small narrowband signals that only perceive a flat channel. Once this is done, the previously discussed MIMO techniques can be applied to each flat fading block channel. Single carrier systems are computationally more demanding than multiple carrier systems, and for that reason most MIMO transmissions do not employ single carrier systems to mitigate frequency-selective multipath effects. In the next section, the most well-known multiple carrier method to combat ISI is presented.

3.3.2 MIMO OFDM

Orthogonal frequency division multiplexing (OFDM) is a multiple carrier transmission scheme that employs orthogonal waveforms to carry information, and, therefore, is more spectrally efficient when compared to single frequency division schemes. With the development of powerful digital signal processing boards, OFDM has also become computationally efficient, becoming today the most attractive transmission modulation in broadband wireless systems. Originally developed for frequency selective SISO systems, the generalization of OFDM for MIMO systems is straightforward, and for that reason only a brief explanation of the MIMO-OFDM concept is given. Fig. 3.3 displays a simplified OFDM system.

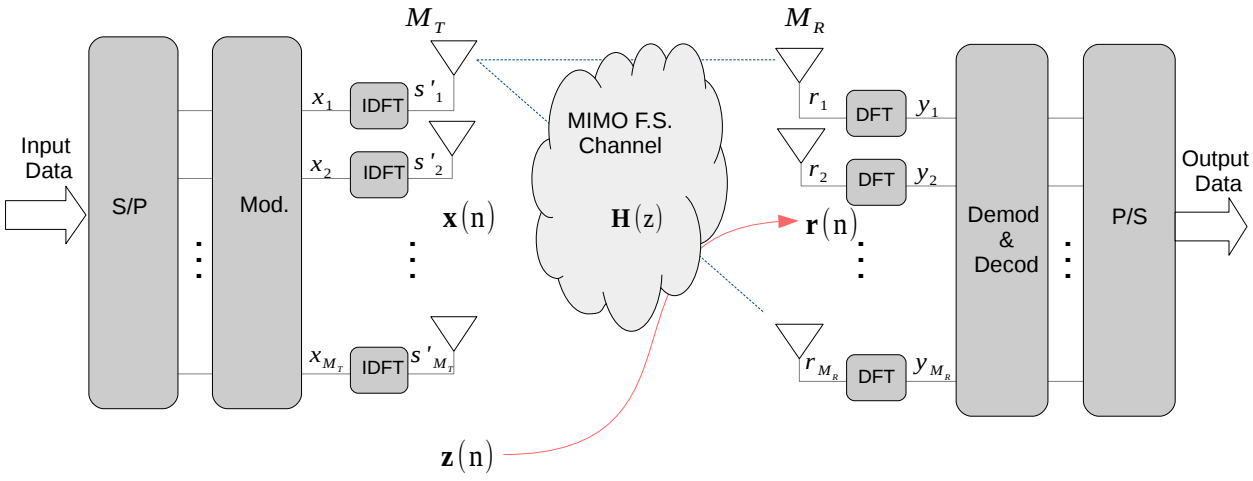

Figure 3.3: System representation of OFDM modulation for a MIMO frequency-selective channel.

The main idea is to use complex exponential orthogonal waveforms to transmit the symbols in each antenna. Equation (3.18) shows the discrete version of the OFDM symbols

$$s'_j(k') = \sum_{n=0}^{N_s-1} x_j(n) e^{j2\pi k' n/N_s}, \tag{3.18}$$

where $j \in \{1, \cdots, M_T\}$ is the index of the j^{th} antenna stream and N_s represents the number of waveforms used, or subcarriers. As one may recognize, $s'_j(k')$ is the inverse discrete Fourier transform (IDFT) of a N_s block of $x(n)$ [91], thus, the receiver applies the inverse procedure, i.e., the discrete Fourier transform (DFT) to obtain back the sequence being transmitted. Note the index k' and n are employed to distinguish between a signal before and after IFDT. A close analysis to the DFT properties shows that it is still necessary to add a guard interval between OFDM sequences, so that they do not suffer from the delay spread introduced by ISI [79]. This guard interval is usually a cyclic prefix that reproduces the last OFDM symbols, and should be sufficiently large so that (in discrete time) it is larger than the channel resolvable multipath effect, i.e., $N_{cp} \geq L$. Therefore, the transmitted sequence of OFDM symbols in each antenna is

$$s_j(k') = \begin{cases} s'_j(k' + N_s - N_{cp}), & k' = 0, ..., N_{cp} - 1 \\ s'_j(k' - N_{cp}), & k' = N_{cp}, ..., N_s + N_{cp} - 1. \end{cases} \tag{3.19}$$

The received sequence, after the frequency-selective channel effect, in receive antenna i at time index k' is given by

$$r_i(k') = \sum_{j=1}^{M_T} \sum_{l=0}^{L} h_{i,j}^{(l)} s_j(k' - l) + z_i(k'),\ n = 0, ..., N_s + N_{cp} - 1, \tag{3.20}$$

where $h_{i,j}^{(l)},\ l = 0, ..., L$ is the channel impulse response and $z_i(k')$ the additive noise at receive antenna i. At this stage, the cyclic prefixed is removed

$$r'_i(k') = \begin{cases} r_i(k'), & k' = 0, ..., N_s - 1 \\ 0, & otherwise. \end{cases} \tag{3.21}$$

The receiver finally performs the DFT of $r'_i(k')$ to obtain

$$\begin{aligned} y_i(n') &= \sum_{k'=0}^{N_s-1} r'_i(k') e^{-j2\pi k' n'/N_s} = \sum_{k'=0}^{N_s-1} r_i(k' + N_{cp}) e^{-j2\pi k' n'/N_s} \\ &= \sum_{k'=0}^{N_s-1} \sum_{j=1}^{M_T} \sum_{l=0}^{L} h_{i,j}^{(l)} s_j(k' + N_{cp} - l) e^{-j2\pi k' n'/N_s} + \sum_{k'=0}^{N_s-1} z_i(k' + N_{cp}) e^{-j2\pi k' n'/N_s} \\ &= \sum_{k'=0}^{N_s-1} \sum_{j=1}^{M_T} \sum_{l=0}^{L} h_{i,j}^{(l)} \Big(\sum_{n=0}^{N_s-1} x_j(n) e^{j2\pi (k'-l) n/N_s} \Big) e^{-j2\pi k' n'/N_s} + Z_i(n') \\ &= \sum_{n=0}^{N_s-1} \sum_{j=1}^{M_T} \sum_{l=0}^{L} h_{i,j}^{(l)} x_j(n) e^{-j2\pi k' l/N_s} \sum_{k'=0}^{N_s-1} e^{-j2\pi k'(n-n')/N_s} + Z_i(n'), \end{aligned} \tag{3.22}$$

where the n' index is used to distinguish the signals' instants at the receiver and at the transmitter, and

$Z_i(n')$ is the DFT of the noise vector. By using the fact that $\sum_{k'=0}^{N_s-1} e^{-j2\pi k'(n-n')/N_s} = N_s\delta(n-n')$, equation (3.22) simplifies as follows

$$\begin{aligned} y_i(n') &= N_s \sum_{j=1}^{M_T} \sum_{l=0}^{L} h_{i,j}^{(l)} x_j(n') e^{-j2\pi k' l/N_s} + Z_i(n') \\ &= N_s \sum_{j=1}^{M_T} x_j(n') \sum_{l=0}^{L} h_{i,j}^{(l)} e^{-j2\pi k' l/N_s} + Z_i(n') \\ &= N_s \sum_{j=1}^{M_T} x_j(n') \mathcal{H}_{i,j}(n') e^{-j2\pi k' l/N_s} + Z_i(n'),\ n' = 0, ..., N_s - 1, \end{aligned} \tag{3.23}$$

where $\mathcal{H}_{i,j}(n') = \sum_{l=0}^{L} h_{i,j}^{(l)} e^{-j2\pi k' l/N_s}$ is the frequency-selective response of the channel between transmitter j and receiver i. This value is a complex constant, which illustrates the fact that the MIMO-OFDM transforms a frequency-selective channel into N_s flat channels. These channels may be expressed in a matrix format as in (3.24)

$$\mathbf{Y}(n') = N_s \boldsymbol{\mathcal{H}}(n') \mathbf{X}(n') + \mathbf{Z}(n'),\ n' = 0, ..., N_s - 1, \tag{3.24}$$

where

$$\mathbf{Y}(n') = [y_1(n'), ..., y_{M_R}(n')]^T,$$

$$\mathbf{X}(n') = [x_1(n'), ..., y_{M_T}(n')]^T,$$

$$\mathbf{Z}(n') = [Z_1(n'), ..., Z_{M_R}(n')]^T$$

and

$$\boldsymbol{\mathcal{H}}(n') = \begin{bmatrix} \mathcal{H}_{1,1}(n') & \cdots & \mathcal{H}_{1,M_T}(n')) \\ \vdots & \ddots & \vdots \\ \mathcal{H}_{M_R,1}(n') & \cdots & \mathcal{H}_{M_R,M_T}(n') \end{bmatrix}.$$

After obtaining the N_s frequency-flat channels, the detectors already studied may be used to eliminate the IPI in each flat channel.

3.3.3 Performance of MIMO OFDM

In order to demonstrate the performance of MIMO-OFDM and analyse the benefits of this technique in comparison with the flat fading channel and with what was done in section 3.2.8, the BER for a frequency-selective MIMO channel with some of the detectors studied in section 3.2 is presented. In this case, MIMO-OFDM modulation in additive white Gaussian noise is used, also with $M_T = 4, M_R = 4$, and with 4-QAM and 16-QAM mapping schemes. The frequency-selective MIMO channel has 4 taps, $L = 3$, and each matrix with entries generated form a i.i.d. $\mathcal{CN}(0, 1)$. The noise is also additive white Gaussian noise with $\mathcal{CN}(0, \sigma_z^2)$. Assume a block transmission with $N_s = 1024$ symbols. The cyclic prefix is chosen to be equal to $N_{cp} = L$. The BER for the ZF, MMSE, OSIC-ZF and CLLL-MMSE are shown in Fig. 3.4.

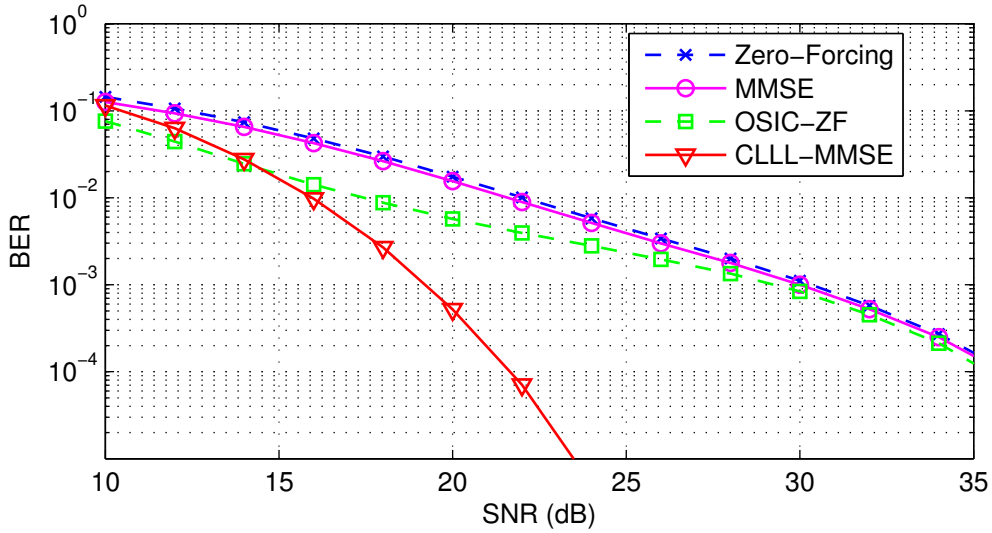

(a) BER of 4x4 MIMO receivers for i.i.d. frequency-selective channel with 4-QAM

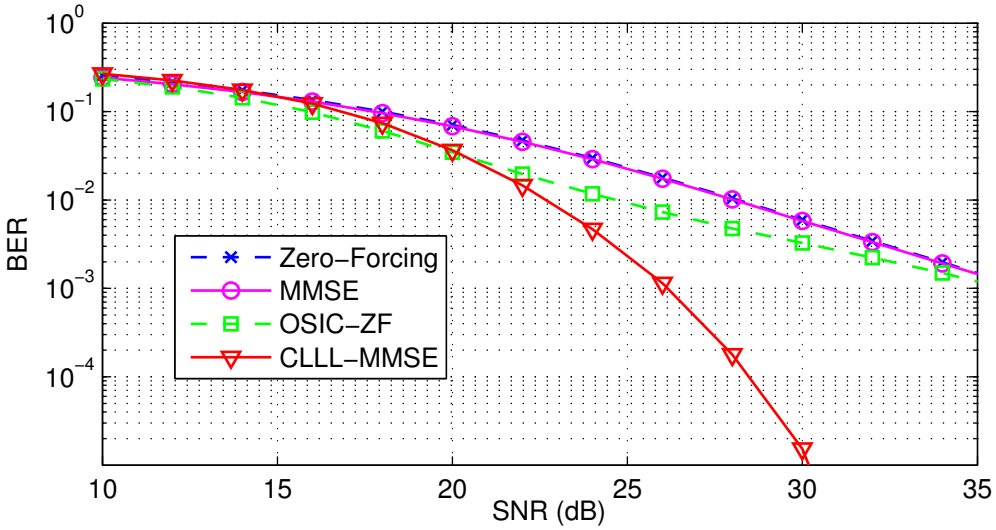

(b) BER of 4x4 MIMO receivers for i.i.d. frequency-selective channel with 16-QAM

Figure 3.4: BER vs SNR (total SNR $= P_x/\sigma_z^2$) performance of the MIMO-OFDM modulation with the studied detectors.

The results show that, as previously predicted, the MIMO-OFDM system can cope with the frequency-selective channel effect. The curves for the simulated detectors show the same slope, maintaining the same diversity order in section 3.2.8, and approximately the same BER values, as one can compare with the results obtained in Fig. 3.2. The OSIC-ZF filter remained with the same properties, having a slight gain in comparison to the ZF and MMSE filters, but with the same diversity order of the latter. This gain tends to vanish as the SNR improves, since the equivalent noise in each of the N_s channels also disappears, attenuating the effect of per-stream decoding. The lattice reduction MMSE filter can also achieve the same diversity as the ML detector, in this case for the frequency-selective channel.

Chapter 4

Self-Interference Mitigation Techniques

A relay station is a key element in a wireless multi-hop network, and is believed to incorporate future communication systems. It may provide a wider coverage, a higher data rate and a lower transmit peak power, which are substantially important for future millimeter wave communication, for example. For that reason, a considerable amount of research has been conducted in relaying techniques, where the integration of multiple-input multiple-output (MIMO) transmissions at the relay appear as a natural solution to avoid the well-known key-hole effect [93]. In this chapter, in-band full-duplex communication are proposed and studied for relay stations. However, these methods can be extended to any type of communication. Thus, a sophisticated digital relay is considered, i.e., a relay that is capable of heavy baseband signal processing, and incorporates multiple antennas (as much as necessary). Since the relay simultaneously uses the same time and frequency resources, the main focus of this chapter is to present and propose self-interference cancellation schemes, which are essential based on previously published work combined with novel techniques here used for the first time. Initially, a model of the relay channel considering the self-interference is presented. Then, two different techniques of spatial suppression are introduced. After that, new feedback cancellation methods are proposed, resorting to adaptive filtering.

4.1 Relay Station Model

The in-band full-duplex relay studied during this chapter is composed of M_R receive antennas and M_T transmit antennas, which provide a two-hop communication between a N_S antenna source and a N_D antenna destination, as Fig. 4.1 shows. The received signal at the relay and at the destination, at instant n, is given by equation (4.1),

$$\begin{aligned} \mathbf{r}(n) =& \mathbf{H_{SR}}\mathbf{x}(n) + \mathbf{H_{LI}}\mathbf{t}(n) + \mathbf{n_R}(n), \\ \mathbf{y}(n) =& \mathbf{H_{RD}}\mathbf{t}(n) + \mathbf{n_D}(n), \end{aligned} \tag{4.1}$$

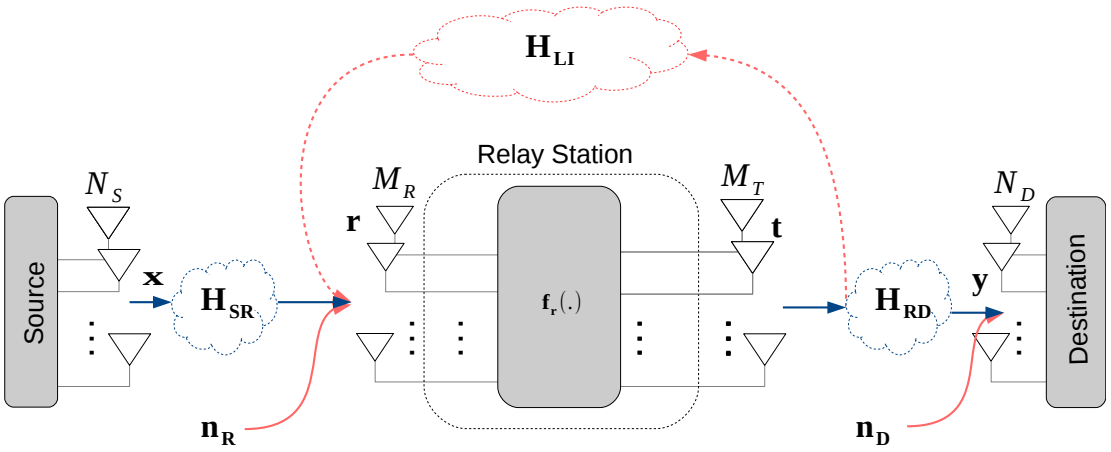

Figure 4.1: System model of an in-band full-duplex relay station.

where it is assumed that $\mathbf{x} \triangleq [x_1(n), \cdots, x_{N_S}(n)]^T$ and $\mathbf{t} = f_r(\mathbf{r}[n-d], \mathbf{r}[n-(d+1)], \cdots) \in \mathbb{C}^{M_T \times 1}$ are the vectors containing the transmitted signals by both source and relay. The matrices $\mathbf{H_{SR}} \in \mathbb{C}^{M_R \times N_S}$ and $\mathbf{H_{RD}} \in \mathbb{C}^{N_D \times M_T}$ are the channel complex matrices from the sources to the relay and from the relay to the destinations, respectively, which assume a MIMO frequency-flat block fading, as in related literature, e.g. [31, 34]. The matrix $\mathbf{H_{LI}} \in \mathbb{C}^{M_R \times M_T}$ represents the loopback residual self-interference effect, which it is assumed only accounts for the remaining interference power, not properly eliminated by the propagation domain or by the self-interference suppression electronic circuits. Note that in the digital domain stage only a residual effect of the self-interference is present, as in this case. The $\mathbf{n_R} \in \mathbb{C}^{M_R \times 1}$ and $\mathbf{n_D} \in \mathbb{C}^{N_D \times 1}$ represents the source-relay and relay-destination additive white Gaussian noise (AWGN), assumed i.i.d. $\mathcal{CN}(0, \sigma_n^2)$. Function $f_r(\cdot)$ represents the relay protocol, where d denotes the integer digital processing delay, necessary for the relay digital operation [48]. This value has to be strictly positive, since it may create problems in the practical implementation of relaying systems [39]. Furthermore, a decode-and-forward (DF) relay protocol is considered during this chapter, i.e., $f_r(\cdot)$ is a function that regenerates the received signal, which is then forwarded to the destination.

In order to suppress the resulting self-interference term, $\mathbf{H_{LI}t}(n)$, the relay needs information from its surroundings, i.e., it needs to know the channel matrices and its own transmitted vector. Thus, it is assumed that the relay employs some estimation methods to acquire them [35]. The principle is simple to describe by knowing $\mathbf{t}$ and $\mathbf{H_{LI}}$, it is possible to completely suppress the self-interference effect at the relay in (4.1). However, the estimation of the channel matrices are usually not performed without errors, as it is well-known in the literature. Therefore, in order to properly model a real system, the following channel estimation noise in the channel matrices is assumed

$$\mathbf{H_{SR}} = \tilde{\mathbf{H}}_{\mathbf{SR}} + \mathcal{E}_{\mathbf{H_{SR}}}, \ \mathbf{H_{RD}} = \tilde{\mathbf{H}}_{\mathbf{RD}} + \mathcal{E}_{\mathbf{H_{RD}}}, \ \mathbf{H_{LI}} = \tilde{\mathbf{H}}_{\mathbf{LI}} + \mathcal{E}_{\mathbf{H_{LI}}}, \tag{4.2}$$

where the first term on the right of each equality is the estimated channel matrix and the second term represents its error when compared to the real value.

Furthermore, although the relay knows exactly the transmitted baseband signal it generates, after the conversion from baseband to broadband the signal present in $\mathbf{t}$ suffers several distortion effects such as frequency offset, AD/DA conversion imperfections, I/Q imbalance, oscillator phase noise, power

amplifier non-linearities etc. [29]. The transmitted signal is often modeled as additive distortion, given by

$$\mathbf{t} = \tilde{\mathbf{t}} + \mathcal{E}_{\mathbf{t}}, \tag{4.3}$$

where $\tilde{\mathbf{t}}$ is now the baseband transmitted vector known at the relay digital signal processing stage, and $\mathcal{E}_{\mathbf{t}}$ accounts for the distortion. The processing stage considered is made in the digital domain and it assumes that the propagation and analog domains have already reduced these effects significantly [34].

4.2 Interference Mitigation with Spatial Filtering Suppression

As already stated, the relay is able to apply MIMO receive filters, as well as MIMO transmit filters (discussed in Chapter 3), so that the residual self-interference is suppressed in the digital domain. To that end, it is assumed that the relay operates in a DF protocol mode, exploiting the degrees of freedom offered by spatial multiplexing in order to eliminate or suppress the self-interference that is generated. The main idea is to create an equivalent relay free of self-interference by projecting the receive and transmit signals onto orthogonal sub-spaces, hence creating the free interference system

$$\begin{aligned} \hat{\mathbf{r}} &= \hat{\mathbf{H}}_{\mathbf{SR}}\mathbf{x} + \hat{\mathbf{n}}_{\mathbf{R}}, \\ \mathbf{y} &= \hat{\mathbf{H}}_{\mathbf{RD}}\hat{\mathbf{t}} + \mathbf{n}_{\mathbf{D}}, \end{aligned} \tag{4.4}$$

where $\hat{\mathbf{r}} \in \mathbb{C}^{\hat{M}_R \times 1}$ and $\hat{\mathbf{t}} \in \mathbb{C}^{\hat{M}_T \times 1}$ are the respective receive and transmit signal vectors, $\hat{\mathbf{H}}_{\mathbf{SR}} \in \mathbb{C}^{\hat{M}_R \times N_S}$ and $\hat{\mathbf{H}}_{\mathbf{RD}} \in \mathbb{C}^{N_D \times \hat{M}_T}$ represent the equivalent interference free MIMO channels and $\hat{\mathbf{n}}_{\mathbf{R}} \in \mathbb{C}^{\hat{M}_R \times 1}$ is the relay equivalent received noise, that accounts for the residual self-interference component after mitigation and the AWGN term. Note that $\hat{M}_R \leq M_R$, $\hat{M}_T \leq M_T$ are the equivalent interference free relay dimensions, i.e., the input and output relay protocol available dimensions, while the remaining dimensions are employed for projecting the interference. Thus, the new equivalent free interference relay only processes a set of $\hat{M}_R$ and $\hat{M}_T$ streams from the total antenna set of M_R and M_T, to transmit and receive information, respectively. Fig. 4.2 depicts in detail a relay that employs this technique, with the suppression filters that are following defined.

Therefore, a receive filter is introduced and represented by $\mathbf{G}_{\mathbf{R}} \in \mathbb{C}^{\hat{M}_R \times M_R}$, and a transmit filter represented by $\mathbf{G}_{\mathbf{T}} \in \mathbb{C}^{M_T \times \hat{M}_T}$. These filters should be designed so that the power of the equivalent noise seen by the equivalent relay is minimized. This term is given by equation (4.5), and includes the residual self-interference components

$$\hat{\mathbf{n}}_{\mathbf{R}} = \hat{\mathbf{H}}_{\mathbf{LI}}\hat{\mathbf{t}} + \mathbf{G}_{\mathbf{R}}\mathbf{H}_{\mathbf{LI}}\mathcal{E}_{\mathbf{t}} + \mathbf{G}_{\mathbf{R}}\mathbf{n}_{\mathbf{R}}, \tag{4.5}$$

where system impairments and imperfect channel estimation terms as introduced above are considered, and where the equivalent self-interference matrix, $\hat{\mathbf{H}}_{\mathbf{LI}}$, is given by

$$\hat{\mathbf{H}}_{\mathbf{LI}} = \mathbf{G}_{\mathbf{R}}\mathbf{H}_{\mathbf{LI}}\mathbf{G}_{\mathbf{T}} = \mathbf{G}_{\mathbf{R}}\tilde{\mathbf{H}}_{\mathbf{LI}}\mathbf{G}_{\mathbf{T}} + \mathbf{G}_{\mathbf{r}}\mathcal{E}_{\mathbf{H}_{\mathbf{LI}}}\mathbf{G}_{\mathbf{T}}. \tag{4.6}$$

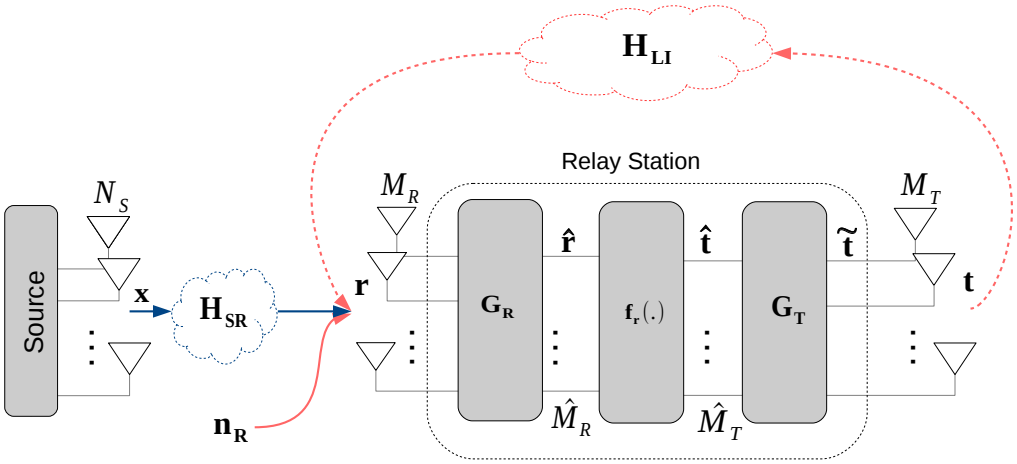

Figure 4.2: Decode-and-forward relay with self-interference spatial suppression.

Thus, considering equation (4.5), the average power of the residual self-interference component present at the defined equivalent relay can be computed as

$$\begin{aligned}
&\mathbb{E}\{(\hat{\mathbf{H}}_{\mathbf{LI}}\hat{\mathbf{t}} + \mathbf{G_R}\mathbf{H_{LI}}\mathcal{E}_{\mathbf{t}})^H(\hat{\mathbf{H}}_{\mathbf{LI}}\hat{\mathbf{t}} + \mathbf{G_r}\mathbf{H_{LI}}\mathcal{E}_{\mathbf{t}})\} = \\
&= \mathbb{E}\{\hat{\mathbf{t}}^H\hat{\mathbf{H}}_{\mathbf{LI}}^H\hat{\mathbf{H}}_{\mathbf{LI}}\hat{\mathbf{t}}\} + \mathbb{E}\{\mathcal{E}_{\mathbf{t}}{}^H\mathbf{H_{LI}}{}^H\mathbf{G_R}{}^H\mathbf{G_R}\mathbf{H_{LI}}\mathcal{E}_{\mathbf{t}}\} \\
&= \mathrm{Tr}\{\hat{\mathbf{H}}_{\mathbf{LI}}\mathbf{R}_{\hat{\mathbf{t}}}\hat{\mathbf{H}}_{\mathbf{LI}}^H\} + \mathrm{Tr}\{\mathbf{H_{LI}}\mathbf{G_r}\mathbf{R}_{\mathcal{E}_{\mathbf{t}}}\mathbf{H_{LI}}{}^H\mathbf{G_R}{}^H\},
\end{aligned} \tag{4.7}$$

where $\mathbf{R}_{\hat{\mathbf{t}}} = \mathbb{E}\{\hat{\mathbf{t}}\hat{\mathbf{t}}^H\}$ is the correlation matrix of the transmitted baseband signal at the relay, $\mathbf{R}_{\mathcal{E}_{\mathbf{t}}} = \mathbb{E}\{\mathcal{E}_{\mathbf{t}}\mathcal{E}_{\mathbf{t}}{}^H\}$ is the correlation matrix of the error associated with transmit impairements at the relay, assumed independent from $\hat{\mathbf{t}}$, and where the last step comes from the algebra property that $\mathbf{a}^H\mathbf{a} = \mathrm{Tr}\{\mathbf{a}\mathbf{a}^H\}$ [94]. $\mathrm{Tr}\{\cdot\}$ represents the trace of a matrix. Therefore, as equation (4.7) suggests, the self-interference effect may be mitigated as long as a proper design of the filters $\mathbf{G_R}$ and $\mathbf{G_T}$ is conducted. This design should provide a self-interference attenuation, however, at the same time it should not interfere with the relay transmit signal that has to reach the destination in order to be correctly decoded.

The design of the filters can be carried out in one of the following manners, as proposed in [34]:

- Independent design: One filter is designed without the knowledge of the other (which can be replaced by $\mathbf{I}$);
- Separated design: One filter is designed given the other filter expression;
- Joint design: The filters are completely designed together.

In the following sections, two different methods to design such filters are addressed.

4.2.1 Suppression with Null-Space Projection

The idea behind null-space projection (NSP) is the selection of a subset of antennas at the relay to receive information, while the remaining antennas are used to project the self-interference (the desired signal at the destinations). Therefore, in order to reduce the power of the self-interference present in the

equivalent interference free system, an optimization problem that tries to minimize the power in equation (4.6) is introduced as follows

$$\min_{\mathbf{G_R},\mathbf{G_T}} \quad \| \mathbf{\hat{H}_{LI}} \|_F^2 = \| \mathbf{G_R H_{LI} G_T} \|_F^2, \tag{4.8}$$

where the self-interference power is measured with the help of the Frobenius norm. However, due to the unknown noise sources introduced by system impairments and imperfect estimation of the self-interference channel, as (4.8) is formulated, it is only possible to mitigate the interference known component, which translates into

$$\min_{\mathbf{G_R},\mathbf{G_T}} \quad \| \mathbf{G_R \tilde{H}_{LI} G_T} \|_F^2 \, . \tag{4.9}$$

Considering a simple solution to the problem that tries to respect the desired signal while dealing with the self-interference, an antenna selection method along with beamforming is employed in the filters definition. The objective is that the relay transmitted signal is not affected by this method, being available at the destination for decoding, and at the same time only the interference is canceled [34]. This procedure may be performed with the help of the singular value decomposition of the known component of the self-interference channel as

$$\mathbf{\tilde{H}_{LI}} = \mathbf{\tilde{U}\tilde{\Sigma}\tilde{V}}^H, \tag{4.10}$$

where $\mathbf{\tilde{\Sigma}}$ is a diagonal matrix containing the singular values of $\mathbf{\tilde{H}_{LI}}$, and $\mathbf{\tilde{U}}$ and $\mathbf{\tilde{V}}$ are the unitary matrix containing the basis vectors associated with it, such that $\mathbf{\tilde{U}}^H\mathbf{\tilde{U}} = \mathbf{I}$ and $\mathbf{\tilde{V}}^H\mathbf{\tilde{V}} = \mathbf{I}$ [79]. Thus, it is possible to define the filters as

$$\begin{aligned} \mathbf{G_R} &= \sqrt{\frac{M_R}{\hat{M}_R}} \mathbf{S_R}^T \mathbf{\tilde{U}}^H, \\ \mathbf{G_T} &= \sqrt{\frac{M_T}{\hat{M}_T}} \mathbf{\tilde{V}} \mathbf{S_T}, \end{aligned} \tag{4.11}$$

where the matrices $\mathbf{S_R}$ and $\mathbf{S_T}$ select the rows and columns of the singular matrices, respectively, performing the antenna selection mentioned above. The coefficients $\sqrt{M_R/\hat{M}_R}$ and $\sqrt{M_T/\hat{M}_T}$ are introduced to normalize the filter matrices so that $\| \mathbf{G_R} \|_F^2 = M_R$ and $\| \mathbf{G_T} \|_F^2 = M_T$.

Therefore, bearing in mind that the objective is to minimize the self-interference power inside the equivalent interference free relay, the selection matrices are jointly designed based on the following optimization problem

$$\min_{\mathbf{S_R},\mathbf{S_T}} \quad \| \mathbf{\hat{H}_{LI}} \|_F^2 = \| \mathbf{G_R \tilde{H}_{LI} G_T} \|_F^2 = \| \sqrt{\frac{M_R}{\hat{M}_R}} \mathbf{S_R}^T \mathbf{\tilde{U}}^H \mathbf{\tilde{U}\tilde{\Sigma}\tilde{V}}^H \sqrt{\frac{M_T}{\hat{M}_T}} \mathbf{\tilde{V}} \mathbf{S_T} \|_F^2$$

$$\min_{\mathbf{S_R},\mathbf{S_T}} \quad \frac{M_R M_T}{\hat{M}_R \hat{M}_T} \| \mathbf{S_R}^T \mathbf{\tilde{\Sigma}} \mathbf{S_T} \|_F^2 \tag{4.12}$$

In order to solve (4.12), for a low number of antennas it is possible to obtain the solution by exhaustive search of the $\binom{M_R}{\hat{M}_R}\binom{M_T}{\hat{M}_T}$ possible combinations. Otherwise, other methods can be employed to reduce the complexity of the problem, however, not in general ensuring the optimal choice.

The target of NSP is to guarantee that all the known interference components are suppressed, i.e., having $\mathbf{G_R}\tilde{\mathbf{H}}_{\mathbf{LI}}\mathbf{G_T} = 0$. This is only possible when setting the equivalent channel dimensions at the relay station as

$$\hat{M}_R + \hat{M}_T + \text{rank}\{\tilde{\mathbf{H}}_{\mathbf{LI}}\} \leq M_R + M_T,$$

i.e., the overall space dimensions where the signals exists is sufficiently large to project the relay receive signal and the signal that the relay transmits (desired at the destinations, but seen as self-interference at the relay) onto orthogonal sub-spaces.

Hence, by setting proper space dimensions, the NSP is able to totally mitigate the known component of the self-interference, however, at a cost of reducing the available relay dimensions and distorting the relay transmitted signal, which may happen under the considered system impairments. Moreover, the unknown self-interference components are not taken in consideration, which form the main limiting factor of this method's performance.

4.2.2 Suppression with MMSE Filtering

In order to avoid the cost of reducing the available dimensions at the relay to forward information and the risk of distorting its transmitted signal, a minimum mean square error (MMSE) filter is here introduced. In this case, the objective is that this filter is capable of both minimizing the distortion inflected at the relay transmit signal $\hat{\mathbf{t}}$ by the employment of spatial filters, and attenuating the self-interference effect, while taking into account the AWGN power, not considered in NSP. Thus, assume there is no reduction in the relay dimensions, i.e., $\hat{M}_R = M_R$ and $\hat{M}_T = M_T$. Defining the error covariance matrix $\mathbf{M}$ of the relay input signal with respect to its desired vector to be detected, i.e., $\mathbf{H_{SR}x}$, according to [95], it is possible to obtain

$$\begin{aligned}\mathbf{M} &= \mathbb{E}\{(\mathbf{H_{SR}x} - \hat{\mathbf{r}})(\mathbf{H_{SR}x} - \hat{\mathbf{r}})^H\} \\ &= (\mathbf{I} - \mathbf{G_R})\mathbf{H_{SR}}\mathbf{R_x}{\mathbf{H_{SR}}}^H(\mathbf{I} - \mathbf{G_R})^H + \mathbf{R}_{\hat{\mathbf{n}}_\mathbf{R}},\end{aligned} \tag{4.13}$$

where

$$\begin{aligned}\mathbf{R_x} &= \mathbb{E}\{\mathbf{x}\mathbf{x}^H\}; \\ \mathbf{R}_{\hat{\mathbf{n}}_\mathbf{R}} &= \mathbb{E}\{\hat{\mathbf{n}}_\mathbf{R}{\hat{\mathbf{n}}_\mathbf{R}}^H\} = \mathbb{E}\{(\hat{\mathbf{H}}_{\mathbf{LI}}\hat{\mathbf{t}} + \mathbf{G_R}\mathbf{H_{LI}}\mathcal{E}_\mathbf{t} + \mathbf{G_R}\mathbf{n_R})(\hat{\mathbf{H}}_{\mathbf{LI}}\hat{\mathbf{t}} + \mathbf{G_R}\mathbf{H_{LI}}\mathcal{E}_\mathbf{t} + \mathbf{G_R}\mathbf{n_R})^H\} \\ &= \mathbf{G_R}(\mathbf{H_{LI}}\mathbf{R_t}{\mathbf{H_{LI}}}^H + \mathbf{R}_{\mathbf{n_R}}){\mathbf{G_R}}^H; \\ \mathbf{R_t} &= \mathbf{R}_{\tilde{\mathbf{t}}} + \mathbf{R}_{\mathcal{E}_\mathbf{t}} = \mathbb{E}(\tilde{\mathbf{t}}\tilde{\mathbf{t}}^H) + \mathbb{E}(\mathcal{E}_\mathbf{t}\mathcal{E}_\mathbf{t}^H) = \mathbf{G_T}\mathbf{R_x}{\mathbf{G_T}}^H + \mathbf{R}_{\mathcal{E}_\mathbf{t}}.\end{aligned}$$

As shown in Chapter 3, the MMSE filter may be obtained by the derivation of matrix $\mathbf{M}$, with respect to one of the filters, while fixing the other. For this specific case, to do so, the relation that a function defined as $f(\mathbf{Z}) = \text{Tr}\{\mathbf{Z}\mathbf{A}_0\mathbf{Z}^H\mathbf{A}_1\}$ has derivative $\frac{d}{d\mathbf{Z}^*}f(\mathbf{Z}) = \mathbf{A}_1\mathbf{Z}\mathbf{A}_0$ is used [96]. Thus, it is possible to find the MMSE filter expression for a full-duplex relay that preserves the transmit signal, suppressing the self-interference and canceling the additive noise simultaneously, by taking $\frac{\partial}{\partial{\mathbf{G_R}}^*}\text{Tr}\{\mathbf{M}\} = \mathbf{0}$ and fixing

$\mathbf{G_T}$, as a separate filter design. Thus

$$\frac{\partial}{\partial \mathbf{G_R}^*}\text{Tr}\{\mathbf{M}\} = \mathbf{G_R}(\tilde{\mathbf{H}}_{\mathbf{LI}}\mathbf{R_t}\tilde{\mathbf{H}}_{\mathbf{LI}}^H + \mathbf{R}_{\mathbf{n_R}}) - (\mathbf{I} - \mathbf{G_R})\tilde{\mathbf{H}}_{\mathbf{SR}}\mathbf{R_x}\tilde{\mathbf{H}}_{\mathbf{SR}}^H = \mathbf{0}, \tag{4.14}$$

which finally gives the receive filter expression as

$$\mathbf{G_R} = \tilde{\mathbf{H}}_{\mathbf{SR}}\mathbf{R_x}\tilde{\mathbf{H}}_{\mathbf{SR}}^H(\tilde{\mathbf{H}}_{\mathbf{SR}}\mathbf{R_x}\tilde{\mathbf{H}}_{\mathbf{SR}}^H + \tilde{\mathbf{H}}_{\mathbf{LI}}\mathbf{R_t}\tilde{\mathbf{H}}_{\mathbf{LI}}^H + \mathbf{R}_{\mathbf{n_R}})^{-1}. \tag{4.15}$$

Note that the filter expression in (4.15) needs to be scaled to ensure that $\| \mathbf{G_R} \|_F^2 = M_R$. Furthermore, the transmit filter can be fixed to the identity matrix, i.e., $\mathbf{G_T} = \mathbf{I}$.

4.2.3 Performance of Spatial Suppression

The performance of the presented self-interference suppression schemes is evaluated in terms of bit error rate (BER), for a typical relay scenario, where the effect of the mentioned system parameters is highlighted.

System Parameters

Consider that the channel matrices $\mathbf{H_{SR}}$ and $\mathbf{H_{RD}}$ are drawn from an i.i.d. Raleigh distribution with normalized power equal to 0 dB, i.e., taken from $\mathcal{CN}(0, 1)$, while the loopback interference has a similar distribution, however, with varying self-interference power as $\mathbf{H_{LI}} \sim \mathcal{CN}(0, \sigma_{LI}^2)$. Note that it is assumed non line-of-site in $\mathbf{H_{SR}}$ and $\mathbf{H_{RD}}$, as in a typical urban cellular environment, and also non line-of-site in $\mathbf{H_{LI}}$, since the propagation techniques and analog circuits have already removed some of the self-interference power [15]. The transmit source and relay signals have normalized powers, i.e., $\mathbb{E}\{\mathbf{x}^H\mathbf{x}\} = 1$ and $\mathbb{E}\{\tilde{\mathbf{t}}^H\tilde{\mathbf{t}}\} = 1$. The system impairments are taken into consideration in the form of the relay transmitted signal noise component, generated as $\mathcal{E}_\mathbf{t} \sim \mathcal{CN}(0, \sigma_\mathbf{t}^2)$. Also, in the form of channel estimation errors present in the matrices $\tilde{\mathbf{H}}_{\mathbf{SR}}$, $\tilde{\mathbf{H}}_{\mathbf{RD}}$ with distribution $\mathcal{E}_{\mathbf{H_{SR,RD}}} \sim \mathcal{CN}(0, \sigma_\mathbf{H}^2)$, and $\tilde{\mathbf{H}}_{\mathbf{LI}}$ with distribution $\mathcal{E}_{\mathbf{H_{LI}}} \sim \mathcal{CN}(0, \sigma_\mathbf{H}^2 \cdot \sigma_{LI}^2)$. Thus, the system performance will be dependent on the unknown components power $\sigma_\mathbf{t}^2$, $\sigma_\mathbf{H}^2$ and σ_{LI}^2. For the transmission itself, consider uncoded MIMO with a 16-QAM and 64-QAM modulations and with a signal-to-noise ratio (SNR), defined by SNR $= P_\mathbf{x}/P_{\mathbf{n_R}} = 10$ dB, i.e., the additive noise at the relay is generated as $\mathbf{n_R}(n) \sim \mathcal{CN}(0, \sigma_{\mathbf{n_R}}^2)$, with $\sigma_{\mathbf{n_R}}^2 = -10$ dB. The relay employs a complex lattice reduction aided zero forcing detector (CLLL-ZF), described in section 3.2.6, for both studied techniques.

The proposed techniques are compared with the case where no filtering is performed, i.e., when setting the filters as $\mathbf{G_R} = \mathbf{G_T} = \mathbf{I}$, commonly known in literature as natural isolation (NI), and also with a half-duplex (HD) similar relay system. For the NSP scheme and for the purpose of simulation, it is assumed that $N_s = M_R = \hat{M}_R = \hat{M}_T = 3,\ M_T = 4$, and that rank$\{\tilde{\mathbf{H}}_{\mathbf{LI}}\} = 1$, which guarantees the necessary condition of having a sufficiently large subspace dimension to project the interference, $\hat{M}_R + \hat{M}_T +$ rank$\{\tilde{\mathbf{H}}_{\mathbf{LI}}\} = M_R + M_T$. For the MMSE filter a symmetric relay is considered, thus, it is assumed that $N_s = M_R = \hat{M}_R = \hat{M}_T = M_T = 3$, and also that rank$\{\tilde{\mathbf{H}}_{\mathbf{LI}}\} = 1$. The self-interference

channel erroneous estimation and the transmitted signal noise effect are considered with typical values, as $\sigma^2_{\mathbf{H}} \in \{10^{-2}, 10^{-3}\}$ and $\sigma^2_{\mathbf{t}} \in \{10^{-2}, 10^{-3}\}$.

BER Curves

Fig. 4.3 shows the gain obtained when using NSP and MMSE in terms of BER, where it is possible to observe the suppression of the self-interference. Firstly, it is worth mentioning that the BER of the suppression schemes NSP and MMSE are not compared in the same figure, since the number of transmit antennas at the relay station, M_T, is not the same. The NSP requires the existence of a transmit null space with the same dimension of the self-interference channel, which is done by introducing one more antenna at the relay transmit side, since for simulation purposes it is considered rank$\{\tilde{\mathbf{H}}_{\mathbf{LI}}\} = 1$. The MMSE can be employed without introducing an extra antenna, therefore reducing the relay station cost. However, the schemes are compared for the same system parameters and their performance can be evaluated together.

NSP: As may be seen in Fig. 4.3(a) and Fig. 4.3(c), the NSP suppression scheme is able to obtain at most a 20 dB margin gain, when compared to the NI curve, i.e., it is possible to transmit in full-duplex relaying mode for about 20 dB of self-interference power more, maintaining the same performance of an HD equivalent relay, while doubling the transmission spectral efficiency. The NSP curves for different values of $(\sigma^2_{\mathbf{H}}, \sigma^2_{\mathbf{t}})$ also show that the main degradation effect is caused by the errors in the estimation of the self-interference channel matrix (comparison between dotted red curve with the dotted orange and brown ones). This matrix is used to perform the spectral decomposition for beam selection, therefore, exposing the NSP performance to errors in the self-interference channel matrix.

MMSE: When employing the MMSE filters, it is no longer possible to maintain the same performance of an equivalent HD relay when the effects of the self-interference start to be considerable, as it may be observed in Fig. 4.3(b) and Fig. 4.3(d). Nevertheless, the MMSE filter is capable of significantly suppress the self-interference, as suggested by the filter expression in equation (4.15). The BER curves for both simulated modulations show a gain of 25 dB when compared to NI, however, only for higher BER values than the HD system. Moreover, the considered channel estimation errors and relay signal transmitted noise effect on the MMSE performance is approximately similar (BER curves similar for the considered $(\sigma^2_{\mathbf{H}}, \sigma^2_{\mathbf{t}})$ pair). This effect is explained by the fact that the MMSE filter expression takes into consideration the mentioned effects power level, thus, being able to combat it.

Finally, on the one hand, the NSP is able to maintain the HD BER for a broad level of unknown interference power, at a cost of introducing extra degrees of freedom by placing more antennas at the relay (which directly depends on rank$\{\tilde{\mathbf{H}}_{\mathbf{LI}}\}$) and being more sensitive to the system impairments. On the other hand, the MMSE filters cannot suppress the interference while maintaining the HD BER values, however, it can achieve a better performance for higher values of BER and can use all the available degrees of freedom for transmitting information. Moreover, the different simulated modulations depict different levels of error floor, i.e., the error associated with the HD relay. The interference mitigation is not affected by this parameter, as expected.

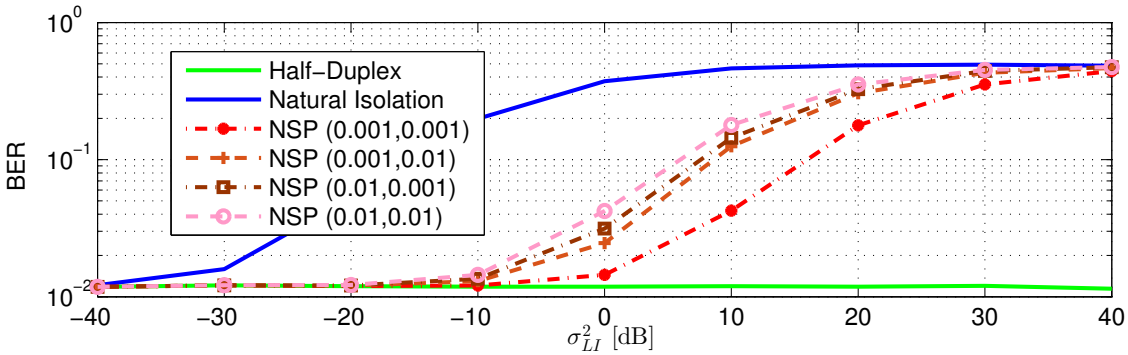

(a) NSP for 16-QAM (pair in the legend: $(\sigma^2_{\mathbf{H}}, \sigma^2_{\mathbf{t}})$).

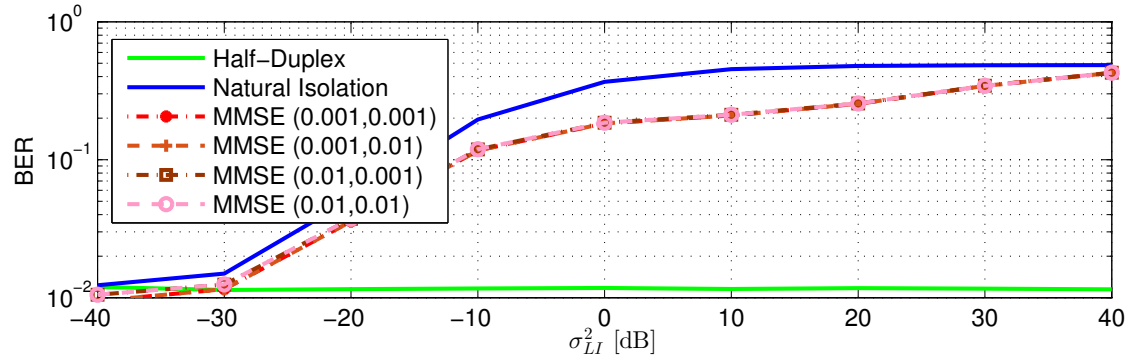

(b) MMSE for 16-QAM (pair in the legend: $(\sigma^2_{\mathbf{H}}, \sigma^2_{\mathbf{t}})$).

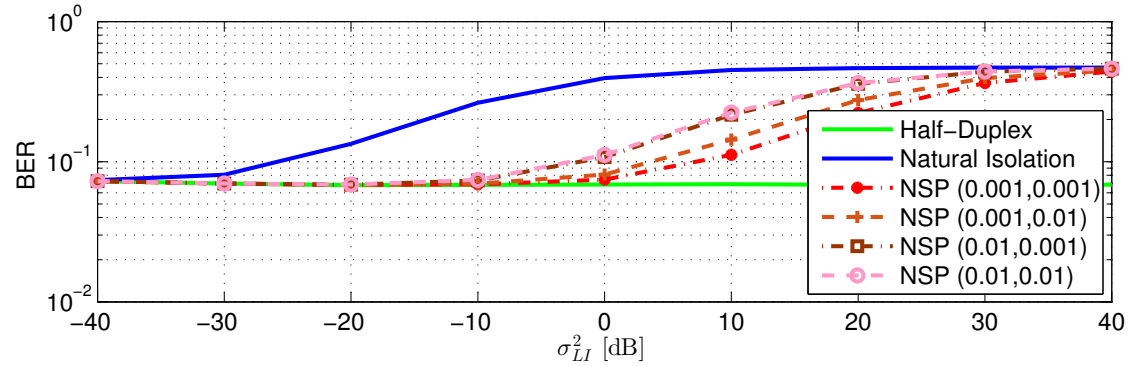

(c) NSP for 64-QAM (pair in the legend: $(\sigma^2_{\mathbf{H}}, \sigma^2_{\mathbf{t}})$).

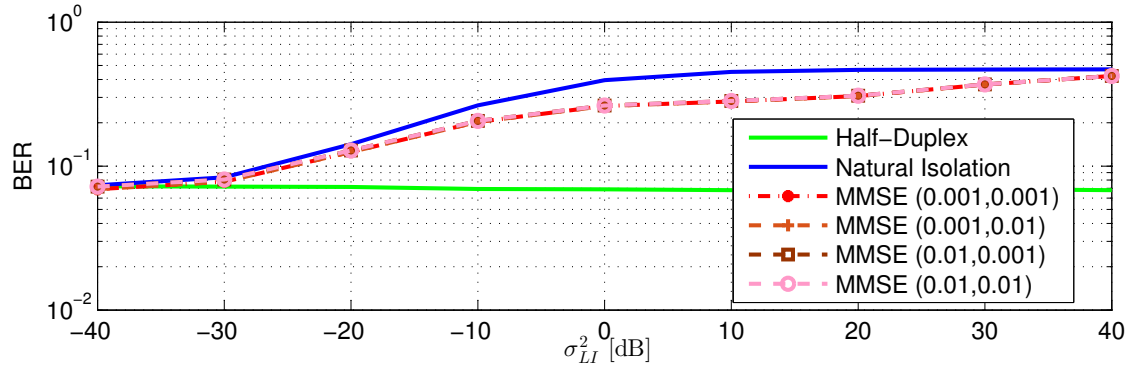

(d) MMSE for 64-QAM (pair in the legend: $(\sigma^2_{\mathbf{H}}, \sigma^2_{\mathbf{t}})$).

Figure 4.3: Comparison of NSP (with $N_s = M_R = \hat{M}_R = \hat{M}_T = 3,\ M_T = 4$), MMSE (with $N_s = M_R = \hat{M}_R = \hat{M}_T = M_T = 3$), with the NI and HD respective equivalent systems for different self-interference power, σ^2_{LI}, and system impairments power $(\sigma^2_{\mathbf{H}}, \sigma^2_{\mathbf{t}})$. The modulation schemes used are 16-QAM and 64-QAM.

4.3 Interference Mitigation with Feedback Cancellation

(The work in this section was accepted for publication in [11])

Besides spatial filtering, another possibility to cancel the self-interference present at a relay is to use feedback cancellation techniques. These techniques are based on the idea that the relay knows the signal it is transmitting and estimates the channel it goes through, or has a good approximation of both at least. Therefore, a replica of the loopback signal arriving at the relay may be subtracted in order to cancel this problem in a feedback fashion. The idea is a kin to what happens in the analog domain interference suppression circuits, however, the need to further suppress the interference in a dynamic way, i.e., capable of tracking channel variations, requires the introduction of this baseband processing. When compared to the previously presented interference suppression with spatial filtering, feedback cancellation does not reduce the input and output dimensions of the relay and does not distort the desired signal at the destinations [44]. Thus, feedback cancellation schemes are proposed and analyzed, focusing on MIMO frequency-selective channels, rarely studied in literature, and also exploring OFDM based transmissions. In order to overcome the channel estimation errors and the transmitted signal noise, presented in the previous section, the use of adaptive methods to estimate the self-interference effect is proposed [97, 98].

4.3.1 Broadband Relay Channel with Feedback Cancellation

The architecture considered in this section is similar to the one demonstrated in section 4.2, however, adapted to MIMO frequency-selective channels with feedback cancellation. These channels are commonly present in broadband communication, where the rate of the transmitted signal is larger than the channel coherence time, thus, creating the inter-symbol interference (ISI) phenomenon. Therefore, the self-interference is now canceled by means of a feedback filter, which subtracts a version of the output transmitted signal to the relay's input. Fig. 4.4 depicts the equivalent discrete-time proposed system.

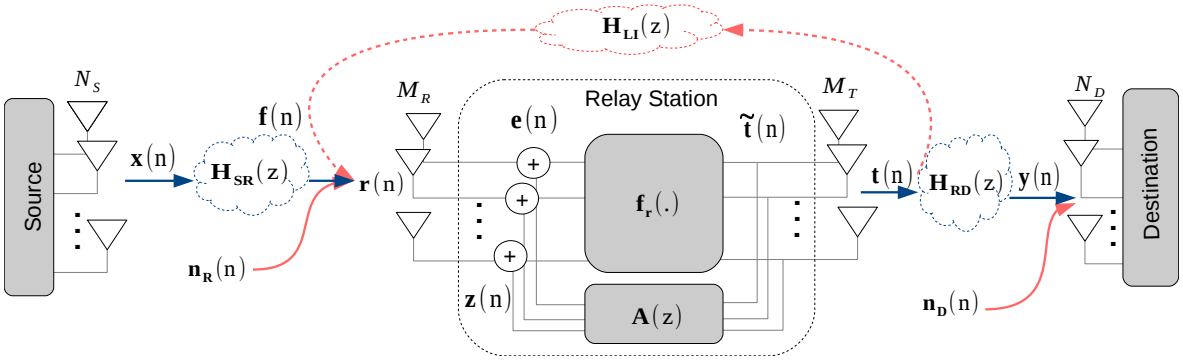

Figure 4.4: System model of a feedback interference canceling relay.

At time instant n, a source signal $\mathbf{x}(n) \in \mathbb{C}^{N_S \times 1}$ is transmitted via a relay station to a destination. The relay station receives a version of that signal, $\mathbf{r}(n) \in \mathbb{C}^{M_R \times 1}$, after being subject to the discussed

frequency-selective channel effects in section 3.3. Then, the relay sends an estimation of the received signal, $\mathbf{t}(n) \in \mathbb{C}^{M_T \times 1}$, which finally reaches the destination as $\mathbf{y}(n) \in \mathbb{C}^{N_D \times 1}$. Equation (4.16) shows the expressions for the relay and destination received signals

$$\begin{aligned} \mathbf{r}(n) =& \mathbf{H_{SR}}(z)\mathbf{x}(n) + \mathbf{H_{LI}}(z)\mathbf{t}(n) + \mathbf{n_R}(n), \\ \mathbf{y}(n) =& \mathbf{H_{RD}}(z)\mathbf{t}(n) + \mathbf{n_D}(n), \end{aligned} \tag{4.16}$$

where now $\mathbf{H_{SR}}(z) \in \mathbb{C}^{M_R \times N_S}$ of order L_{SR}, $\mathbf{H_{RD}}(z) \in \mathbb{C}^{N_D \times M_T}$ of order L_{RD} and $\mathbf{H_{LI}}(z) \in \mathbb{C}^{M_R \times M_T}$ of order L_{LI}, are the z-transform matrices of the source to the relay, relay to the destination and self-interference channels, respectively (see section 3.3 for the frequency-selective channel definition). Again, $\mathbf{n_R}(n)$ and $\mathbf{n_D}(n)$ are the additive white Gaussian noise at the input of the relay station and destination, respectively. The relay DF protocol, $f_r(\cdot)$, is independent of the self-interference cancellation architecture, and regenerates a delayed estimation of the N_S source data streams, $\tilde{\mathbf{t}}(n) = \hat{\mathbf{x}}(n-d) = f_r(\mathbf{e}(n-d), \mathbf{e}(n-d-1), \cdots, \mathbf{e}(n-d-D))$, where d stands for the necessary processing delay and $D+1$ is the length of the employed time-window for detection. In addition, the processing delay is considered strictly positive and sufficiently long [34], so that $\mathbf{x}(n-k)$ and $\mathbf{t}(n-l)$ become uncorrelated, i.e., $\mathbb{E}\{\mathbf{x}(n-k)\mathbf{t}^H(n-l)\} = \mathbf{0}$, for all $k = 0, \cdots, L_{SR}$ and all $l = 0, \cdots, L_{LI}$. The errors in the estimations of the channel matrices are still considered, as well as the error in the transmitted signal after broadband conversion. In this case, it is assumed each channel tap, of the three frequency-selective channels, has an additive estimation error that varies rapidly, as equation (4.17) illustrates.

$$\begin{aligned} \mathbf{H}[k] &= \tilde{\mathbf{H}}[k] + \mathcal{E}_{\mathbf{H}}[k](n), \\ \mathbf{t}(n) &= \tilde{\mathbf{t}}(n) + \mathcal{E}_{\mathbf{t}}(n). \end{aligned} \tag{4.17}$$

As mentioned above, in order to mitigate the self-interference, instead of using spatial filtering, a feedback filter in the time domain is introduced. The main objective is to estimate the loopback channel effect on the relay transmitted signal, i.e., $\mathbf{f}(n) = \mathbf{H_{LI}}(z)\mathbf{t}(n)$, employing a finite impulse response filter (FIR) defined as $\mathbf{A}(z) \in \mathbb{C}^{M_R \times M_T}$, with L_A order. Therefore, the signal $\mathbf{z}(n) = \mathbf{A}(z)\tilde{\mathbf{t}}(n)$ is added inside the relay to the receive signal $\mathbf{r}(n)$, generating $\mathbf{e}(n)$, which is given by

$$\begin{aligned} \mathbf{e}(n) &= \mathbf{r}(n) + \mathbf{A}(z)\tilde{\mathbf{t}}(n), \\ &= \mathbf{H_{SR}}(z)\mathbf{x}(n) + \mathbf{H_{LI}}(z)\mathbf{t}(n) + \mathbf{n_R}(n) + \mathbf{A}(z)\tilde{\mathbf{t}}(n). \end{aligned} \tag{4.18}$$

4.3.2 Conventional Time-Domain Cancellation

Time-domain cancellation (TDC) is the trivial solution to the problem presented above, as it uses a self-interference channel estimation independent of the relay transmission to define the filter's $M_R \times M_T \times (L_A + 1)$ parameters and to perform the cancellation of the self-interference [34]. The feedback filter is then set to

$$\mathbf{A}(z) = -\tilde{\mathbf{H}}_{\mathbf{LI}}(z), \tag{4.19}$$

where the filter order is the same as the channel order, i.e., $L_A = L_{LI}$. However, this procedure is severely harmed by the above mentioned system impairments coming from an independent estimation process, and for that reason the residual interference cannot be totally removed. This technique is dependent on the power of these residual terms, given in the last line of (4.20), which will affect the system performance.

$$\begin{aligned}\mathbf{f}(n)+\mathbf{z}(n) &= \mathbf{H_{LI}}(z)\mathbf{t}(n)+\mathbf{A}(z)\tilde{\mathbf{t}}(n)\\ &= \tilde{\mathbf{H}}_{\mathbf{LI}}(z)\tilde{\mathbf{t}}(n)+\mathcal{E}_{\mathbf{H_{LI}}}(z)\Big(\tilde{\mathbf{t}}(n)+\mathcal{E}_{\mathbf{t}}(n)\Big)+\tilde{\mathbf{H}}_{\mathbf{LI}}(z)\mathcal{E}_{\mathbf{t}}(n)-\tilde{\mathbf{H}}_{\mathbf{LI}}(z)\tilde{\mathbf{t}}(n)\\ &= \sum_{k=0}^{L_{LI}}\mathcal{E}_{\mathbf{H_{LI}}}[k]\Big(\tilde{\mathbf{t}}(n)+\mathcal{E}_{\mathbf{t}}(n)\Big)+\sum_{k=0}^{L_{LI}}\tilde{\mathbf{H}}_{\mathbf{LI}}[k]\mathcal{E}_{\mathbf{t}}(n),\end{aligned} \tag{4.20}$$

In fact, this method is only able to cancel the known term $\tilde{\mathbf{H}}_{\mathbf{LI}}(z)\tilde{\mathbf{t}}(n)$, while the remaining terms present in (4.20) are fed to the relay detector with the desired signal.

This effect is clearly observed when the power spectral density (PSD) of the relay input signal is derived. To that end, the autocorrelation matrix of $\mathbf{e}(n)$ is presented in (4.21), considering $\mathbf{e}(n)$ as a weak stationary process and constant channel matrices for a block interval [91].

$$\begin{aligned}\mathbf{R}_{\mathbf{e},\mathbf{e}}(k) &= \mathbb{E}\{\mathbf{e}(n)\mathbf{e}^H(n-k)\}\\ &= \mathbb{E}\{(\mathbf{H_{SR}}(z)\mathbf{x}(n)+\mathbf{H_{LI}}(z)\mathbf{t}(n)+\mathbf{n_R}(n)+\mathbf{A}(z)\tilde{\mathbf{t}}(n))\\ &\quad\cdot(\mathbf{H_{SR}}(z)\mathbf{x}(n-k)+\mathbf{H_{LI}}(z)\mathbf{t}(n-k)+\mathbf{n_R}(n-k)+\mathbf{A}(z)\tilde{\mathbf{t}}(n-k))^H\}\\ &= \mathbf{H_{SR}}(z)\mathbf{R}_{\mathbf{x},\mathbf{x}}(k){\mathbf{H_{SR}}}^H(z)+\big(\mathbf{H_{LI}}(z)+\mathbf{A}(z)\big)\mathbf{R}_{\tilde{\mathbf{t}},\tilde{\mathbf{t}}}(k)\big({\mathbf{H_{LI}}}^H(z)+\mathbf{A}^H(z)\big)\\ &\quad+\mathbf{H_{LI}}(z)\mathbf{R}_{\mathcal{E}_{\mathbf{t}},\mathcal{E}_{\mathbf{t}}}(k){\mathbf{H_{LI}}}^H(z)+\mathbf{R}_{\mathbf{n_R},\mathbf{n_R}}(k),\end{aligned} \tag{4.21}$$

where $\mathbf{R}_{\mathbf{x},\mathbf{x}}(k)=\mathbb{E}\{\mathbf{x}(n)\mathbf{x}^H(n-k)\}$, $\mathbf{R}_{\tilde{\mathbf{t}},\tilde{\mathbf{t}}}(k)=\mathbb{E}\{\tilde{\mathbf{t}}(n)\tilde{\mathbf{t}}^H(n-k)\}$, $\mathbf{R}_{\mathcal{E}_{\mathbf{t}},\mathcal{E}_{\mathbf{t}}}(k)=\mathbb{E}\{\mathcal{E}_{\mathbf{t}}(n){\mathcal{E}_{\mathbf{t}}}^H(n-k)\}$, and $\mathbf{R}_{\mathbf{n_R},\mathbf{n_R}}(k)=\mathbb{E}\{\mathbf{n_R}(n){\mathbf{n_R}}^H(n-k)\}$ represent the autocorrelation matrices of $\mathbf{x}(n)$, $\tilde{\mathbf{t}}(n)$, $\mathcal{E}_{\mathbf{t}}(n)$, and $\mathbf{n_R}(n)$, respectively. The noise is considered to be AWGN and not correlated with both transmitted signals from the source and from the relay, i.e., $\mathbb{E}\{\mathbf{n_R}(n)\mathbf{t}^H(n-k)\}=\mathbf{0}$ and $\mathbb{E}\{\mathbf{n_R}(n)\mathbf{x}^H(n-k)\}=\mathbf{0}$. Moreover, as mentioned above and very important in these feedback filters, the source transmitted vector and the relay transmitted vector are also uncorrelated, since it is assumed that

$$\mathbb{E}\{(\mathbf{H_{LI}}(z)\mathbf{t}(n))^H\mathbf{H_{SR}}(z)\mathbf{x}(n-k)\}=\mathbb{E}\{\hat{\mathbf{x}}^H(n-d){\mathbf{H_{LI}}}^H(z)\mathbf{H_{SR}}(z)\mathbf{x}(n-k)\}=P_{\mathbf{x}}\delta(k-d),$$

for $k=0,\cdots,L_{SR}$, and since d is considered sufficiently large, i.e., $d\geq L_{SR}$. The PSD of $\mathbf{e}(n)$ follows now by taking the z-transform of the autocorrelation matrix $\mathbf{R}_{\mathbf{e},\mathbf{e}}(k)$, given by

$$\begin{aligned}\mathbf{\Phi}_{\mathbf{e},\mathbf{e}}(z) &= \sum_{k=-\infty}^{+\infty}\mathbf{R}_{\mathbf{e},\mathbf{e}}(k)z^{-k}\\ &= \mathbf{H_{SR}}(z)\mathbf{\Phi}_{\mathbf{x},\mathbf{x}}(z){\mathbf{H_{SR}}}^H(1/z^*)+\big(\mathbf{H_{LI}}(z)+\mathbf{A}(z)\big)\mathbf{\Phi}_{\tilde{\mathbf{t}},\tilde{\mathbf{t}}}(z)\big({\mathbf{H_{LI}}}^H(1/z^*)+\mathbf{A}^H(1/z^*)\big)\\ &\quad+\mathbf{H_{LI}}(z)\mathbf{\Phi}_{\mathcal{E}_{\mathbf{t}},\mathcal{E}_{\mathbf{t}}}(z){\mathbf{H_{LI}}}^H(1/z^*)+\mathbf{\Phi}_{\mathbf{n_R},\mathbf{n_R}}(z)\end{aligned} \tag{4.22}$$

$$
\begin{aligned}
&= \underbrace{\mathbf{H_{SR}}(z)\mathbf{\Phi}_{\mathbf{x},\mathbf{x}}(z){\mathbf{H_{SR}}}^{H}(1/z^*)}_{\text{desired component}} \\
&+ \underbrace{\big(\tilde{\mathbf{H}}_{\mathbf{LI}}(z) + \mathcal{E}_{\mathbf{H_{LI}}}(z) + \mathbf{A}(z)\big)\mathbf{\Phi}_{\tilde{\mathbf{t}},\tilde{\mathbf{t}}}(z)\big(\tilde{\mathbf{H}}_{\mathbf{LI}}(1/z^*) + \mathcal{E}_{\mathbf{H_{LI}}}(1/z^*) + \mathbf{A}(1/z^*)\big)}_{\text{noise level possible to be suppressed}} \\
&+ \underbrace{\big(\tilde{\mathbf{H}}_{\mathbf{LI}}(z) + \mathcal{E}_{\mathbf{H_{LI}}}(z)\big)\mathbf{\Phi}_{\mathcal{E}_\mathbf{t},\mathcal{E}_\mathbf{t}}(z)\big(\tilde{\mathbf{H}}_{\mathbf{LI}}(1/z^*) + \mathcal{E}_{\mathbf{H_{LI}}}(1/z^*)\big) + \mathbf{\Phi}_{\mathbf{n_R},\mathbf{n_R}}(z)}_{\text{residual noise level}},
\end{aligned}
$$

where it was used the z-transform property that $\mathcal{F}\{\mathbf{H}(z)\mathbf{R}_{\mathbf{x},\mathbf{x}}(k)\mathbf{H}^H(z)\} = \mathbf{H}(z)\mathbf{\Phi}_{\mathbf{x},\mathbf{x}}(z)\mathbf{H}^H(1/z^*)$ [91] and where the PSD of $\mathbf{t}(n)$ is given by $\mathbf{\Phi}_{\mathbf{t},\mathbf{t}}(z) = \mathbf{\Phi}_{\tilde{\mathbf{t}},\tilde{\mathbf{t}}}(z) + \mathbf{\Phi}_{\mathcal{E}_\mathbf{t},\mathcal{E}_\mathbf{t}}(z)$.

Thus, as shown above, the design of the feedback filter can be designed so that the noise in the interference channel $\mathbf{H_{LI}}(z)$ is minimized or completely canceled. However, there is always a power component that comes from the noise in the relay transmit signal, impossible to handle using this feedback cancellation technique. In the following sections, adaptive feedback cancellation filters that try to estimate the channel $\mathbf{H_{LI}}(z)$ on the fly, i.e., based on the signals transmitted by the relay and carrying information, are proposed and evaluated. The so-called TDC method presented in this section serves as a model for comparison, since it is assumed that it uses typical values for the channel estimation errors and is independent of the relaying operation (therefore designated as conventional). Nevertheless, the following adaptive feedback filtering is a more complex and interesting form of time-domain cancellation.

4.3.3 Least Mean Square Cancellation

Aiming at improving the relaying system performance, adaptive filtering techniques are proposed. This type of cancellation schemes only makes use of the available signals at the relay, thus, is not dependent on estimations of the channel self-interference matrix and the errors it introduces. Furthermore, adaptive filters are capable of tracking temporal variations of the self-interference channel [98].

As mentioned above, consider only estimators that are based on direct methods, i.e., that are focused on a system identification problem using the observed signals. The target of the relay station is to estimate the self-interference channel by knowing the time delayed transmitted vectors $[\tilde{\mathbf{t}}(n), \tilde{\mathbf{t}}(n-1), \cdots]$, and the received vector it observes, $\mathbf{r}(n)$. Defining $\mathbf{z}(n)$ to be equal to the correction vector the relay performs in its input, i.e., $\mathbf{z}(n) = \mathbf{A}(z)\tilde{\mathbf{t}}(n)$, as in Fig. 4.4. The goal is then to estimate $\mathbf{f}(n)$ as

$$
\mathbf{z}(n) = \hat{\mathbf{f}}(n) = \mathbf{A}(z)\tilde{\mathbf{t}}(n) = \sum_{k=0}^{L_A} \mathbf{A}[k]\tilde{\mathbf{t}}(n-k). \tag{4.23}
$$

To do so, the criterion here employed to determine the filter parameters will consist of the mean square error (MSE), which is simply given by the following expression

$$
\begin{aligned}
MSE(n, \mathbf{A}(z)) &= \mathbb{E}\{\big(\mathbf{f}(n) - \hat{\mathbf{f}}(n)\big)^H\big(\mathbf{f}(n) - \hat{\mathbf{f}}(n)\big)\} \\
&= \mathbb{E}\{\big(\mathbf{f}(n) - \sum_{k=0}^{L_A}\mathbf{A}[k]\tilde{\mathbf{t}}(n-k)\big)^H\big(\mathbf{f}(n) - \sum_{l=0}^{L_A}\mathbf{A}[l]\tilde{\mathbf{t}}(n-l)\big)\},
\end{aligned} \tag{4.24}
$$

and where it may be further developed as a MIMO generalization of the well studied SISO case to take

the form

$$MSE(n,\mathbf{A}(z)) = \mathbb{E}\{\mathbf{f}^H(n)\mathbf{f}(n) - 2\sum_{k=0}^{L_A}\tilde{\mathbf{t}}^H(n-k)\mathbf{A}^H[k]\mathbf{f}(n) + \sum_{k=0}^{L_A}\sum_{l=0}^{L_A}\tilde{\mathbf{t}}^H(n-k)\mathbf{A}^H[k]\mathbf{A}[l]\tilde{\mathbf{t}}(n-l)\}, \tag{4.25}$$

Using the vector relation that $\mathbf{a}^H\mathbf{a} = \mathsf{Tr}\{\mathbf{a}\mathbf{a}^H\}$ [94], and defining the concatenaton matrix of all filter coefficients $\mathbf{A}_\star = \big[\mathbf{A}[0],\cdots,\mathbf{A}[L_A]\big]^T$, equation (4.25) further simplifies to

$$\begin{aligned} MSE(n,\mathbf{A}(z)) =& \mathsf{Tr}\{\mathbb{E}\{\mathbf{f}(n)\mathbf{f}^H(n)\}\} - 2\mathsf{Tr}\{\mathbb{E}\{\sum_{k=0}^{L_A}\mathbf{A}[k]\tilde{\mathbf{t}}(n-k)\mathbf{f}^H(n)\}\} \\ &+ \mathsf{Tr}\{\mathbb{E}\{\sum_{k=0}^{L_A}\sum_{l=0}^{L_A}\mathbf{A}[k]\tilde{\mathbf{t}}(n-k)\tilde{\mathbf{t}}^H(n-l)\mathbf{A}^H[l]\} = \\ =& \mathsf{Tr}\{\mathbb{E}\{\mathbf{f}(n)\mathbf{f}^H(n)\}\} - 2\mathsf{Tr}\Big\{\mathbb{E}\big\{\big[\mathbf{A}[0]|\cdots|\mathbf{A}[L_A]\big]\odot\big[\tilde{\mathbf{t}}(k)|\cdots|\tilde{\mathbf{t}}(k-L_A)\big]\otimes\mathbf{f}^H(n)\big\}\Big\} \\ &+ \mathsf{Tr}\Big\{\mathbb{E}\big\{\big[\mathbf{A}[0]|\cdots|\mathbf{A}[L_A]\big]\odot\big[\tilde{\mathbf{t}}(n)|\cdots|\tilde{\mathbf{t}}(n-L_A)\big]\otimes\big[\tilde{\mathbf{t}}(n)|\cdots|\tilde{\mathbf{t}}(n-L_A)\big]^H\odot\big[\mathbf{A}[0]|\cdots|\mathbf{A}[L_A]\big]^H\big\}\Big\}, \end{aligned} \tag{4.26}$$

where $\odot$ represents the inner product between a composition of sub-matrices and a composition of column sub-vectors, i.e., $\big[\mathbf{H}[0]|\cdots|\mathbf{H}[L]\big]\odot\big[\mathbf{x}(n)|\cdots|\mathbf{x}(n-L)\big] = \sum_{l=0}^{L}\mathbf{H}[l]\mathbf{x}(n-l)$, introduced to generalize the filter SISO definitions for the MIMO case [99]. Further, $\otimes$ represents the Kronecker or the outer product [94]. Defining the following correlation matrices of the signals present in expression (4.24), assuming the involved vectors as weakly stationary processes,

$$\mathbf{\Sigma}_{\tilde{\mathbf{t}},\mathbf{f}} = \mathbb{E}\{[\tilde{\mathbf{t}}(n)\mathbf{f}^H(n),\cdots,[\tilde{\mathbf{t}}(n-L_A)\mathbf{f}^H(n)]\} = [\mathbf{R}_{\tilde{\mathbf{t}},\mathbf{f}}(0),\cdots,\mathbf{R}_{\tilde{\mathbf{t}},\mathbf{f}}(L_A)]^T,$$

$$\mathbf{\Sigma}_{\tilde{\mathbf{t}},\tilde{\mathbf{t}}} = \begin{bmatrix} \mathbb{E}\{\tilde{\mathbf{t}}(n)\hat{\mathbf{t}}^H(n)\} & \cdots & \mathbb{E}\{\tilde{\mathbf{t}}(n)\hat{\mathbf{t}}^H(n-L_A)\} \\ \vdots & \ddots & \vdots \\ \mathbb{E}\{\tilde{\mathbf{t}}(n-L_A)\hat{\mathbf{t}}^H(n)\} & \cdots & \mathbb{E}\{\tilde{\mathbf{t}}(n-L_A)\hat{\mathbf{t}}^H(n-L_A)\} \end{bmatrix} = \begin{bmatrix} \mathbf{R}_{\tilde{\mathbf{t}},\tilde{\mathbf{t}}}(0) & \cdots & \mathbf{R}_{\tilde{\mathbf{t}},\tilde{\mathbf{t}}}(L_A) \\ \vdots & \ddots & \vdots \\ \mathbf{R}_{\tilde{\mathbf{t}},\tilde{\mathbf{t}}}(L_A) & \cdots & \mathbf{R}_{\tilde{\mathbf{t}},\tilde{\mathbf{t}}}(0) \end{bmatrix},$$

equation (4.26) can be rewritten again in the compact form [98]

$$\begin{aligned} MSE(n,\mathbf{A}(z)) &= \mathsf{Tr}\{\mathbf{R}_{\mathbf{f},\mathbf{f}}(0) - 2\,\mathbf{A}_\star^T\mathbf{\Sigma}_{\tilde{\mathbf{t}},\mathbf{f}} + \mathbf{A}_\star^T\mathbf{\Sigma}_{\tilde{\mathbf{t}},\tilde{\mathbf{t}}}\mathbf{A}_\star\}, \\ &= \mathsf{Tr}\{\mathbf{R}_{\mathbf{f},\mathbf{f}}(0) - \mathbf{\Sigma}_{\tilde{\mathbf{t}},\mathbf{f}}^T\mathbf{\Sigma}_{\tilde{\mathbf{t}},\tilde{\mathbf{t}}}^{-1}\mathbf{\Sigma}_{\tilde{\mathbf{t}},\mathbf{f}} + [\mathbf{A}_\star - \mathbf{\Sigma}_{\tilde{\mathbf{t}},\tilde{\mathbf{t}}}^{-1}\mathbf{\Sigma}_{\tilde{\mathbf{t}},\mathbf{f}}]^T\mathbf{\Sigma}_{\tilde{\mathbf{t}},\tilde{\mathbf{t}}}[\mathbf{A}_\star - \mathbf{\Sigma}_{\tilde{\mathbf{t}},\tilde{\mathbf{t}}}^{-1}\mathbf{\Sigma}_{\tilde{\mathbf{t}},\mathbf{f}}]\}. \end{aligned} \tag{4.27}$$

Therefore, it is clear from (4.27) that the optimal filter parameters with respect to minimizing the MSE are given by

$$\mathbf{A}_{\star,Opt.} = \mathbf{\Sigma}_{\tilde{\mathbf{t}},\tilde{\mathbf{t}}}^{-1}\mathbf{\Sigma}_{\tilde{\mathbf{t}},\mathbf{f}}. \tag{4.28}$$

However, this expression of the optimal filter is defined based on the second order moments (correlation matrices) of the involved signals, which have also to be estimated (due to the expected value). To that end, it is resorted to the least mean square algorithm (LMS). The idea is to drop the expectation operator

in $MSE(n, \mathbf{A}(z))$ and compute the instantaneous error instead of the mean error,

$$\widehat{MSE}_{LMS}(n, \mathbf{A}(z)) = \big(\mathbf{f}(n) - \sum_{k=0}^{L_A} \mathbf{A}[k]\tilde{\mathbf{t}}(n-k)\big)^H \big(\mathbf{f}(n) - \sum_{l=0}^{L_A} \mathbf{A}[l]\tilde{\mathbf{t}}(n-l)\big), \tag{4.29}$$

and to use a gradient descent approach to update the filter estimations. Thus, consider the matrix with the column concatenation of the relay transmitted vectors

$$\tilde{\mathbf{T}}(n) = \big[\tilde{\mathbf{t}}(n), \cdots, \tilde{\mathbf{t}}(n-L_A)\big] \in \mathbb{C}^{M_T \times (L_A+1)},$$

and the vector with all the elements in $\tilde{\mathbf{T}}(n)$, given by $\bar{\mathbf{t}}(n) = \text{vect}\{\tilde{\mathbf{T}}(n)\} \in \mathbb{C}^{(L_A+1)M_T \times 1}$. The MSE criterion for the LMS algorithm is then obtained, based on matrix derivation properties [94], in a compact representation as

$$\begin{aligned} \frac{\partial}{\partial \mathbf{A}_\star} \widehat{MSE}_{LMS}(n, \mathbf{A}_\star) &= \frac{\partial}{\partial \mathbf{A}_\star} \big(\mathbf{f}(n) - \sum_{k=0}^{L_A} \mathbf{A}[k]\tilde{\mathbf{t}}(n-k)\big)^H \big(\mathbf{f}(n) - \sum_{l=0}^{L_A} \mathbf{A}[l]\tilde{\mathbf{t}}(n-l)\big) \\ &= -2\big(\mathbf{f}(n) - \mathbf{A}_\star^T \odot \tilde{\mathbf{T}}(n)\big) \otimes \tilde{\mathbf{T}}^H(n). \end{aligned} \tag{4.30}$$

Applying the gradient descent algorithm, it is finally possible to achieve the LMS update rule as

$$\begin{aligned} \hat{\mathbf{A}}_{\star,n+1} &= \hat{\mathbf{A}}_{\star,n} - \frac{\mu}{2} \frac{\partial}{\partial \mathbf{A}_\star} \widehat{MSE}_{LMS}(n, \mathbf{A}_\star) \\ &= \hat{\mathbf{A}}_{\star,n} + \mu\big(\mathbf{f}(n) - \mathbf{A}_\star^T \odot \tilde{\mathbf{T}}(n)\big) \otimes \tilde{\mathbf{T}}^H(n), \end{aligned} \tag{4.31}$$

where μ represents the step size of the gradient descent algorithm [99]. Highlighting each filter tap, the update rule becomes

$$\hat{\mathbf{A}}[k](n+1) = \hat{\mathbf{A}}[k](n) + \mu\big(\mathbf{f}(n) - \sum_{l=0}^{L_A} \hat{\mathbf{A}}[l](n)\tilde{\mathbf{t}}(n-l)\big)\tilde{\mathbf{t}}^H(n-k),\ k = 0, \cdots, L_A. \tag{4.32}$$

The presented LMS algorithm is capable of estimating a parametric model of the self-interference channel, concretely in a z-transform matrix representation. Nevertheless, it was considered that the observed signal is $\mathbf{f}(n)$, which is in fact false. The observed signal is rather $\mathbf{r}(n)$. Thus, to derive a practical filter update rule, it is necessary to compute the correlation between $\mathbf{r}(n)$ and $\tilde{\mathbf{t}}(n)$. Assuming again weak stationary variables, one obtains

$$\begin{aligned} \mathbf{R}_{\mathbf{r},\tilde{\mathbf{t}}}(k) &= \mathbb{E}\{\mathbf{r}(n)\tilde{\mathbf{t}}^H(n-k)\} \\ &= \mathbb{E}\{(\mathbf{H}_{\mathbf{SR}}(z)\mathbf{x}(n) + \mathbf{f}(n) + \mathbf{n}_{\mathbf{R}}(n))\tilde{\mathbf{t}}^H(n-k)\} \\ &= \mathbb{E}\{\mathbf{f}(n)\tilde{\mathbf{t}}^H(n-k)\}\}, \end{aligned} \tag{4.33}$$

where $\mathbb{E}\{\mathbf{x}(n)\tilde{\mathbf{t}}^H(n-k)\} = \mathbf{0}$, for a sufficiently large processing delay, and also $\mathbb{E}\{\mathbf{n}_{\mathbf{R}}(n)\tilde{\mathbf{t}}^H(n-k)\} = \mathbf{0}$ by the definition of Gaussian noise. This result allows to observe $\mathbf{r}(n)$ instead of $\mathbf{f}(n)$, since the correlation matrix in (4.33) is $\mathbf{R}_{\mathbf{r},\tilde{\mathbf{t}}}(k) = \mathbf{R}_{\mathbf{f},\tilde{\mathbf{t}}}(k)$, therefore, not changing the filter convergence properties. The

LMS update rule for each filter tap now becomes

$$\hat{\mathbf{A}}[k](n+1) = \hat{\mathbf{A}}[k](n) + \mu\big(\mathbf{r}(n) - \sum_{l=0}^{L_A} \hat{\mathbf{A}}[l](n)\tilde{\mathbf{t}}(n-l)\big)\tilde{\mathbf{t}}^H(n-k),\ k = 0, \cdots, L_A. \tag{4.34}$$

As may be observed, the filter update rule has slightly changed, however, its structure remains the same. The equivalent noise present in the observed signal $\mathbf{r}(n)$ is now composed of the source and additive noise vectors, which will affect the filter performance, mainly its convergence time. Furthermore, it is worth mentioning that the LMS algorithm costs $\mathcal{O}(M_T \times (L_A+1)^3)$, which come form the multiplication of the filter matrix by the observed vector, for each filter tap.

Brief Analysis of the LMS

The properties of the LMS filter are broadly known in literature [98]. Nevertheless, the main characteristics of the behavior of the filter for this case are here presented. The average system describing the error propagation for the proposed LMS filter (see appendix A.1) is given by

$$\tilde{\mathbf{A}}_{\star,n} = \ \hat{\mathbf{A}}_{\star,n} - \mathbf{A}_{\star,Opt.} \approx \big[\mathbf{I} - \mu\boldsymbol{\Sigma}_{\tilde{\mathbf{t}},\tilde{\mathbf{t}}}\big]\tilde{\mathbf{A}}_{\star,n-1} - \mu\tilde{\mathbf{f}}(n) \otimes \tilde{\mathbf{T}}^H(n), \tag{4.35}$$

where $\mathbf{A}_{\star,Opt.}$ is as in (4.28) and $\tilde{\mathbf{f}}(n) = \mathbf{f}_{Opt.}(n) - \mathbf{r}(n) = \sum_{l=0}^{L_A} \mathbf{A}_{Opt.}[k]\tilde{\mathbf{t}}(n-l) - \mathbf{r}(n)$ is the filter estimation error plus the relay desired signal. Equation (4.35) represents a time-invariant state-space model with a stochastic input, which can be easily evaluated. The stability of the filter depends on the eigenvalues of the system matrix $\mathbf{I} - \mu\boldsymbol{\Sigma}_{\tilde{\mathbf{t}},\tilde{\mathbf{t}}}$. The filter will converge whenever its eigenvalues are strictly inside the unite circle, which happens when $0 < \mu < \frac{2}{\lambda_1}$, where λ_1 is the maximum eigenvalue of $\boldsymbol{\Sigma}_{\tilde{\mathbf{t}},\tilde{\mathbf{t}}}$. As equation (4.35) shows, and under a step size that guarantees convergence, the filter mean error parameter converges to zero, since as an MMSE filter, the asymptotic algorithm error is orthogonal to the observations, i.e., $\mathbb{E}\{\tilde{\mathbf{f}}(n) \otimes \overline{\mathbf{t}}(n)\} = \mathbf{0}$, for $k = 0, \cdots, L_A$.

The mean square error of this filter may also be evaluated. Considering appendix A.2 one can obtain

$$\mathbf{P}(n) = \mathbb{E}\{\tilde{\mathbf{A}}_{\star,n}\tilde{\mathbf{A}}_{\star,n}^H\} = \ \big[\mathbf{I} - \mu\boldsymbol{\Sigma}_{\tilde{\mathbf{t}},\tilde{\mathbf{t}}}\big]\mathbf{P}(n-1)\big[\mathbf{I} - \mu\boldsymbol{\Sigma}_{\tilde{\mathbf{t}},\tilde{\mathbf{t}}}\big]^H + \mu^2\mathbb{E}\{\tilde{\mathbf{f}}^H(n)\tilde{\mathbf{f}}(n)\}\boldsymbol{\Sigma}_{\tilde{\mathbf{t}},\tilde{\mathbf{t}}}, \tag{4.36}$$

which represents a linear time-invariant state space model with $\mathbf{P}(n)$ as state variables. Once again, the above system, converges to a steady state value i.f.f. $0 < \mu < 2/\lambda_1$. The steady state value of the error, $\mathbf{P}$, is obtained by solving the Lyapunov equation

$$\mathbf{P} = \big[\mathbf{I} - \mu\boldsymbol{\Sigma}_{\tilde{\mathbf{t}},\tilde{\mathbf{t}}}\big]\mathbf{P}\big[\mathbf{I} - \mu\boldsymbol{\Sigma}_{\tilde{\mathbf{t}},\tilde{\mathbf{t}}}\big]^H + \mu^2\mathbb{E}\{\tilde{\mathbf{f}}^H(n)\tilde{\mathbf{f}}(n)\}\boldsymbol{\Sigma}_{\tilde{\mathbf{t}},\tilde{\mathbf{t}}}, \tag{4.37}$$

which, based on the spectral decomposition of $\boldsymbol{\Sigma}_{\tilde{\mathbf{t}}\tilde{\mathbf{t}}}$, yields a diagonal matrix solution with entries

$$q_i = \frac{\mu^2\mathbb{E}\{\tilde{\mathbf{f}}^H(n)\tilde{\mathbf{f}}(n)\}}{2 - \mu\lambda_i}, \text{for } i = 1, \cdots, L_A. \tag{4.38}$$

where λ_i, for $i = 1, \cdots, L_A$, are the eigenvalues of $\mathbf{\Sigma}_{\tilde{\mathbf{t}}\tilde{\mathbf{t}}}$. The above result shows for the possible choices of μ that the mean square error of the filter parameters does not converge to zero. However, by choosing an appropriated step size, the error can be made sufficiently small. In fact, there is a trade off between small error and tracking capability of the filter. The first is achieved with a small step size, while the last with a large one, within its bounds already mentioned. Taking into consideration the concrete problem of estimating the self-interference channel, there is the necessity of reducing the estimation error. For that reason, a small step size should be used. Small step sizes have problems tracking small variations of the channel. Therefore, the most suitable is to use time varying step size, which can be initially large to reduce the convergence time and can be made small after that, in order to minimize the estimation error. In section 4.3.5, these LMS filter properties are addressed with more detail.

4.3.4 Recursive Least Squares Cancellation

The previously presented LMS adaptive filtering suffers from two main problems: poor convergence for ill-conditioned systems and noise sensitivity [98]. The poor convergence happens when the correlation matrix $\mathbf{\Sigma}_{\tilde{\mathbf{t}},\tilde{\mathbf{t}}}$ is ill-conditioned, i.e., when there is a large eigenvalue spread. Also, the LMS filter experiences a performance deterioration due to enhancement of the noise, since the observation vector is $\mathbf{r}(n)$, instead of $\mathbf{f}(n)$, introducing additional noise terms that need to be filtered at the relay. For those reasons, a more sophisticated numerical optimization algorithm for the estimation of the MSE is here applied, aiming for better levels of self-interference suppression.

Thus, the recursive least squares algorithm (RLS) is adapted to the problem of full-duplex relaying. Consider a less noise sensitive approximation of the MSE, given by

$$\widehat{MSE}_{RLS}(n, \mathbf{A}(z)) = \sum_{k=1}^{n} \lambda^{n-k} \big(\mathbf{f}(k) - \sum_{l=0}^{L_A} \mathbf{A}[l]\tilde{\mathbf{t}}(k-l)\big)^H \big(\mathbf{f}(k) - \sum_{l=0}^{L_A} \mathbf{A}[l]\tilde{\mathbf{t}}(k-l)\big), \tag{4.39}$$

where $0 < \lambda \leq 1$ is the forgetting factor of the algorithm, which regulates the filter dependency on previous observations. The RLS is derived by exploiting the second derivative of the MSE as a newton type algorithm. Therefore, taking the first and second derivatives of the expression in (4.39) (see appendix A.3) it is obtained

$$\begin{aligned} \frac{\partial}{\partial \mathbf{A}_\star} \widehat{MSE}_{RLS}(n, \mathbf{A}(z)) &= \frac{\partial}{\partial \mathbf{A}_\star} \big(\sum_{k=1}^{n} \lambda^{n-k} (\mathbf{f}(k) - \sum_{l=0}^{L_A} \mathbf{A}[l]\tilde{\mathbf{t}}(k-l))\big)^H \big(\sum_{l=1}^{n} \lambda^{n-l} (\mathbf{f}(l) - \sum_{l=0}^{L_A} \mathbf{A}[l]\tilde{\mathbf{t}}(k-l))\big) \\ &= -2\hat{\mathbf{\Sigma}}^{RLS}_{\tilde{\mathbf{t}},\mathbf{f}}(n) + 2\hat{\mathbf{\Sigma}}^{RLS}_{\tilde{\mathbf{t}},\tilde{\mathbf{t}}}(n)\mathbf{A}_{\star,n}, \end{aligned} \tag{4.40}$$

$$\begin{aligned} \frac{\partial^2}{\partial {\mathbf{A}_\star}^2} \widehat{MSE}_{RLS}(n, \mathbf{A}(z)) &= \frac{\partial^2}{\partial {\mathbf{A}_\star}^2} \sum_{k=1}^{n} \lambda^{n-k} \big(\mathbf{f}(k) - \sum_{l=0}^{L_A} \mathbf{A}[l]\tilde{\mathbf{t}}(k-l)\big) \\ &= 2\hat{\mathbf{\Sigma}}^{RLS}_{\tilde{\mathbf{t}},\tilde{\mathbf{t}}}(n), \end{aligned} \tag{4.41}$$

where $\hat{\mathbf{\Sigma}}^{RLS}_{\tilde{\mathbf{t}},\mathbf{f}}(n) = \sum_{k=1}^{n} \lambda^{n-k} \mathbf{f}(k) \otimes \tilde{\mathbf{T}}^H(k), \in \mathbb{C}^{(L_A+1)M_T \times M_R}$ and $\hat{\mathbf{\Sigma}}^{RLS}_{\tilde{\mathbf{t}},\tilde{\mathbf{t}}}(n) = \sum_{k=1}^{n} \lambda^{n-k} \bar{\mathbf{t}}(k) \otimes \bar{\mathbf{t}}^H(k), \in$

$\mathbb{C}^{(L_A+1)M_T\times(L_A+1)M_T}$, and $\mathbf{A}_{\star,n}$ contains the vertical vector concatenation of the feedback filter coefficients, as previously defined for the LMS filter, all for time instant n. Now, applying the newton method to update the filter coefficients, it is possible to obtain the basic form of the RLS algorithm as

$$\begin{aligned}\hat{\mathbf{A}}_{\star,n} &= \hat{\mathbf{A}}_{\star,n-1} - \frac{\mu}{2}\Big[\frac{\partial^2}{\partial \mathbf{A}_\star^2}\widehat{MSE}_{RLS}(n,\hat{\mathbf{A}}_\star(n-1))\Big]^{-1}\frac{\partial}{\partial \mathbf{A}_\star}\widehat{MSE}_{RLS}(n,\hat{\mathbf{A}}_\star(n-1)) \\ &= \hat{\mathbf{A}}_{\star,n-1} + \mu\big[\hat{\mathbf{\Sigma}}^{RLS}_{\tilde{\mathbf{t}},\tilde{\mathbf{t}}}(n)\big]^{-1}\Big(\hat{\mathbf{\Sigma}}^{RLS}_{\tilde{\mathbf{t}},\mathbf{f}}(n) - \hat{\mathbf{\Sigma}}^{RLS}_{\tilde{\mathbf{t}},\tilde{\mathbf{t}}}(n)\hat{\mathbf{A}}_{\star,n-1}\Big),\end{aligned} \tag{4.42}$$

with the RLS correlation matrices being also updated at each iteration by taking $\hat{\mathbf{\Sigma}}^{RLS}_{\tilde{\mathbf{t}},\tilde{\mathbf{t}}}(n) = \lambda\hat{\mathbf{\Sigma}}^{RLS}_{\tilde{\mathbf{t}},\tilde{\mathbf{t}}}(n-1) + \bar{\mathbf{t}}(n)\otimes\bar{\mathbf{t}}^H(n)$ and $\hat{\mathbf{\Sigma}}^{RLS}_{\tilde{\mathbf{t}},\mathbf{f}}(n) = \hat{\mathbf{\Sigma}}^{RLS}_{\tilde{\mathbf{t}},\mathbf{f}}(n-1) + \mathbf{f}(n)\otimes\tilde{\mathbf{T}}^H(n)$.

The filter update expression in (4.42) is usually not employed when applying this filter, since the inversion of a $((L_A+1)M_T)\times((L_A+1)M_T)$ matrix is required. Therefore, the filter expression can be further improved in terms of computational efficiency, resorting to the Woodbury identity [94, Chap. 3.2.2]. Defining $\bar{\mathbf{P}}(n) = \big[\hat{\mathbf{\Sigma}}^{RLS}_{\tilde{\mathbf{t}},\tilde{\mathbf{t}}}(n)\big]^{-1}$ and $\mathbf{R}_{\tilde{\mathbf{t}}}(n) = \bar{\mathbf{t}}(n)\otimes\bar{\mathbf{t}}^H(n)$, it is possible to derive the update rule for this matrix as

$$\begin{aligned}\bar{\mathbf{P}}(n+1) =& \big[\lambda\hat{\mathbf{\Sigma}}^{RLS}_{\tilde{\mathbf{t}},\tilde{\mathbf{t}}}(n-1) + \bar{\mathbf{t}}(n)\otimes\bar{\mathbf{t}}^H(n)\big]^{-1} \\ =& \frac{1}{\lambda}\big[\bar{\mathbf{P}}^{-1}(n) + \frac{1}{\lambda}\mathbf{R}_{\tilde{\mathbf{t}}}(n)\big]^{-1} \\ =& \frac{1}{\lambda}\Big(\bar{\mathbf{P}}(n) - \frac{\bar{\mathbf{P}}(n)\mathbf{R}_{\tilde{\mathbf{t}}}(n)\bar{\mathbf{P}}(n)}{\lambda + \bar{\mathbf{t}}^H(n)\bar{\mathbf{P}}(n)\bar{\mathbf{t}}(n)}\Big),\end{aligned} \tag{4.43}$$

Finally, the RLS algorithm for the proposed in-band full-duplex relay station, taking again into consideration that the observed vector is $\mathbf{r}(n)$ (already discussed in section 4.3.3), is characterized by the following 3-step update rule

$$\begin{aligned}\mathbf{k}(n) &= \frac{\bar{\mathbf{P}}(n)\bar{\mathbf{t}}(n)}{\lambda + \bar{\mathbf{t}}^H(n)\bar{\mathbf{P}}(n)\bar{\mathbf{t}}(n)}\,, \\ \hat{\mathbf{A}}_{\star,n} &= \hat{\mathbf{A}}_{\star,n-1} + \mu\mathbf{k}(n)\big(\mathbf{r}(n) - \sum_{l=0}^{L_A}\hat{\mathbf{A}}[l](n-1)\tilde{\mathbf{t}}(n-l)\big)^H, \\ \bar{\mathbf{P}}(n+1) &= \frac{1}{\lambda}\Big(\bar{\mathbf{P}}(n+1) - \mathbf{k}(n)\bar{\mathbf{t}}^H(n)\bar{\mathbf{P}}(n)\Big),\end{aligned} \tag{4.44}$$

where vector $\mathbf{k}(n)$ is the update direction of the filter [98]. The recursive algorithm is initialized with $\hat{\mathbf{A}}_{\star,0}$, and with $\bar{\mathbf{P}}(0) = \eta\mathbf{I}$ that may be seen as an uncertainty of the initial filter guess. Moreover the computational costs of the RLS is of the order $\mathcal{O}(((L_A+1)M_T)^2)$.

Brief Analysis of the RLS

Similar to what was done for the LMS, a brief overview of the RLS properties, focusing mainly on its convergence rate and on the influence of the forgetting factor, is here illustrated. Firstly, consider the case where there is no forgetting factor ($\lambda = 1$), i.e., all observed data is treated equally. The RLS filter expression may also be obtained as, similarly to equation (4.28) , $\hat{\mathbf{A}}_{\star,n} = \big[\hat{\mathbf{\Sigma}}^{RLS}_{\tilde{\mathbf{t}},\tilde{\mathbf{t}}}(n)\big]^{-1}\hat{\mathbf{\Sigma}}^{RLS}_{\tilde{\mathbf{t}},\mathbf{q}}(n) = \big[\frac{1}{n}\hat{\mathbf{\Sigma}}^{RLS}_{\tilde{\mathbf{t}},\tilde{\mathbf{t}}}(n)\big]^{-1}\frac{1}{n}\hat{\mathbf{\Sigma}}^{RLS}_{\tilde{\mathbf{t}},\mathbf{q}}(n)$ for an analysis purpose [98]. Under the law of large numbers, the RMS cor-

relation matrices converge in fact to the Weiner solution in (4.28). As performed for the LMS filter, the error matrix may be written as follows (see appendix A.4)

$$\tilde{\mathbf{A}}_{\star,n} = \hat{\mathbf{A}}_{\star,n} - \mathbf{A}_{\star,Opt.} = \left[\hat{\mathbf{\Sigma}}^{RLS}_{\tilde{\mathbf{t}},\tilde{\mathbf{t}}}(n)\right]^{-1}\hat{\mathbf{\Sigma}}^{RLS}_{\tilde{\mathbf{t}},\mathbf{q}}(n) - \mathbf{A}_{\star,Opt.} = \left[\frac{1}{n}\hat{\mathbf{\Sigma}}^{RLS}_{\tilde{\mathbf{t}},\tilde{\mathbf{t}}}(n)\right]^{-1}\frac{1}{n}\sum_{k=1}^{n}\tilde{\mathbf{f}}(k)\otimes\tilde{\mathbf{T}}^{H}(k). \tag{4.45}$$

Equation (4.45) leads then to the covariance of the parameter error (see appendix A.5)

$$\mathbf{Q}(n) = \mathbb{E}\{\tilde{\mathbf{A}}_{\star,n}\tilde{\mathbf{A}}^{H}_{\star,n}\} = \frac{1}{n}\mathbb{E}\Big\{\sum_{k=1}^{n}\sum_{l=1}^{n}\tilde{\mathbf{f}}^{H}(k)\tilde{\mathbf{f}}(l)\Big\}\mathbf{\Sigma}^{-1}_{\tilde{\mathbf{t}},\tilde{\mathbf{t}}}, \tag{4.46}$$

Thus, the error present in the RLS estimation, for $\lambda = 1$, goes to zero as n grows large, which shows that the filter converges to the optimal solution after some iterations. However, when considering $\lambda = 1$, the RLS filter looses the tracking properties since it converges always to the mean value.

For the case where $0 < \lambda < 1$, by introducing the parameter λ^{n-k} in expression (4.45) and performing the same manipulations, the filter coefficients error is obtained

$$\tilde{\mathbf{A}}_{\star,n} = \Big[(1-\lambda)\hat{\mathbf{\Sigma}}^{RLS}_{\tilde{\mathbf{t}},\tilde{\mathbf{t}}}(n)\Big]^{-1}(1-\lambda)\sum_{k=1}^{n}\lambda^{n-k}\tilde{\mathbf{f}}(k)\otimes\tilde{\mathbf{T}}^{H}(k), \tag{4.47}$$

and for a large n and a λ close to 1, it is possible to show that [98]

$$\tilde{\mathbf{A}}_{\star,n} \approx \hat{\mathbf{\Sigma}}^{-1}_{\tilde{\mathbf{t}},\tilde{\mathbf{t}}}(1-\lambda)\sum_{k=1}^{n}\lambda^{n-k}\tilde{\mathbf{f}}(k)\otimes\tilde{\mathbf{T}}^{H}(k), \tag{4.48}$$

which applying the same procedure in (4.46) leads to

$$\mathbf{Q}(n) = \mathbb{E}\Big\{\sum_{k=1}^{n}\sum_{l=1}^{n}\tilde{\mathbf{A}}_{\star,n}\tilde{\mathbf{A}}^{H}_{\star,n}\Big\} = (1-\lambda)\mathbb{E}\Big\{\sum_{k=1}^{n}\sum_{l=1}^{n}\tilde{\mathbf{f}}^{H}(k)\tilde{\mathbf{f}}(l)\Big\}\mathbf{\Sigma}^{-1}_{\tilde{\mathbf{t}},\tilde{\mathbf{t}}}. \tag{4.49}$$

This expression demonstrates that the error of the filter does not converge to zero, for any number of taken iterations, since it considers the presence of the forgetting factor that acts as a weight for the previous observations. This factor allows the filter to be able to track time variations, as the LMS does. Therefore, it is intuitive that there also exists a trade-off between tracking capabilities and convergence to the optimal value. As λ goes to one, the filter parameter error tends to zero, although yielding a poor capability of tracking time variations of the self-interference channel. As λ gets close to zero, the filter becomes capable of following faster channel time variations, at a cost of a larger estimation error.

4.3.5 Performance of Feedback Algorithms

This section evaluates the performance of the derived methods that cope with the problem of self-interference in an in-band full-duplex relay station, mainly with the errors associated to the estimation of the loopback self-interference channel matrix. The convergence time, the BER and the signal-to-interference-plus-noise ratio (SINR) for different channel parameters are evaluated.

System Parameters

Consider an uncoded MIMO-OFDM system, where $N_S = 2$ source antennas transmit a 16-QAM or 64-QAM modulated OFDM stream of data with a block of N_{sub} subcarriers and a cyclic prefix of $N_{cp} = L_{SR}$ (as described in section 3.3), to a destination also with $N_D = 2$ antennas. The relay is considered symmetric and composed by $M_R = 3$ receive antennas and $M_T = 3$ transmit antennas. Further, the channels are assumed to be all of the same order, i.e., $L_{SR} = L_{RD} = L_{LI}$. The matrices $\mathbf{H_{SR}}(z)$ and $\mathbf{H_{RD}}(z)$ are drawn from complex Gaussian distributions, with entries taken from $\mathcal{CN}(0,1)$, while each self-interference matrix channel tap has distribution $\mathbf{H_{LI}}[k] \sim \mathcal{CN}(0, \sigma_{LI}^2\mathbf{I})$, for $k = 0, \cdots, L_{LI}$, where, similarly to section 4.2.3, σ_{LI}^2 accounts for the residual power of the self-interference channel, after propagation and analog-circuit first stage of mitigation. The filter order is set to be $L = L_A = L_{LI}$, so that a perfect estimation of the self-interference channel can be achieved. The transmitted source and relay signals have normalized power, i.e., $\mathbb{E}\{\mathbf{x}^H(n)\mathbf{x}(n)\} = 1$ and $\mathbb{E}\{\tilde{\mathbf{t}}^H(n)\tilde{\mathbf{t}}(n)\} = 1$. Moreover, consider relay transmit signal noise, which is also considered as $\mathcal{E}_{\mathbf{t}}(n) \sim \mathcal{CN}\big(\mathbf{0}, \sigma_{\mathbf{t}}^2\big)$.

Convergence Time

The evaluation of the two algorithms' convergence time, i.e., the number of iterations required from an initial starting point, $\hat{\mathbf{A}}_{\star,0} = \mathbf{0}$ (and $\bar{\mathbf{P}}(1) = \mathbf{I}$ for the RLS), to reach a certain point where the filter parameters satisfy an error metric (EM) [44] is evaluated. This metric takes into consideration the estimation of the self-interference matrix and the real self-interference channel matrix, and it is given by equation

$$EM = \frac{\| \hat{\mathbf{A}}_{\star,n} - \mathbf{H_{LI},\star} \|_F^2}{\| \mathbf{H_{LI},\star} \|_F^2}, \tag{4.50}$$

where $\mathbf{H_{LI},\star} = \big[\mathbf{H_{LI}}[0], \cdots, \mathbf{H_{LI}}[L_A]\big]^T$ is the concatenation of the frequency-selective self-interference channel, similar to that done for the filter parameters matrix $\hat{\mathbf{A}}_{\star,n}$.

LMS: Considering the LMS filter convergence properties, 1000 realizations of the self-interference channel are simulated, for a interference power set to $\sigma_{LI}^2 = 1$, with an update rule described in equation (4.32). The simulation uses 16384 samples, which corresponds to two OFDM symbols with a block of $N_{sub} = 2^{13}$ subcarriers. Also, the SNR, defined as $\frac{P_{\mathbf{x}}}{P_{\mathbf{n_R}}}$, is set to 15 dB, while the transmit relay noise is made negligible by taking $\sigma_{\mathbf{t}}^2 = 10^{-5}$. In order to improve the channel estimation, and as stated in section 4.3.3, a varying step size is introduced, heuristically obtained, and given by the following expression

$$\mu(n) \begin{cases} 0.005, & 1 \leq n < N/4, \\ 0.001, & N/4 \leq n < N/2, \\ 0.0005, & N/2 \leq n < 3N/4, \\ 0.0001, & 3N/4 \leq n \leq N. \end{cases}$$

Fig. 4.5 depicts one case of the LMS filter parameters convergence for the scenario described above and for $L = 1$, where it is possible to observe the convergence of the filter coefficient $\hat{\mathbf{A}}_{1,1}[0]$ real and

imaginary part in 4.5(a) and the filter coefficient $\hat{\mathbf{A}}_{1,1}[1]$ real and imaginary part in 4.5(b). The different

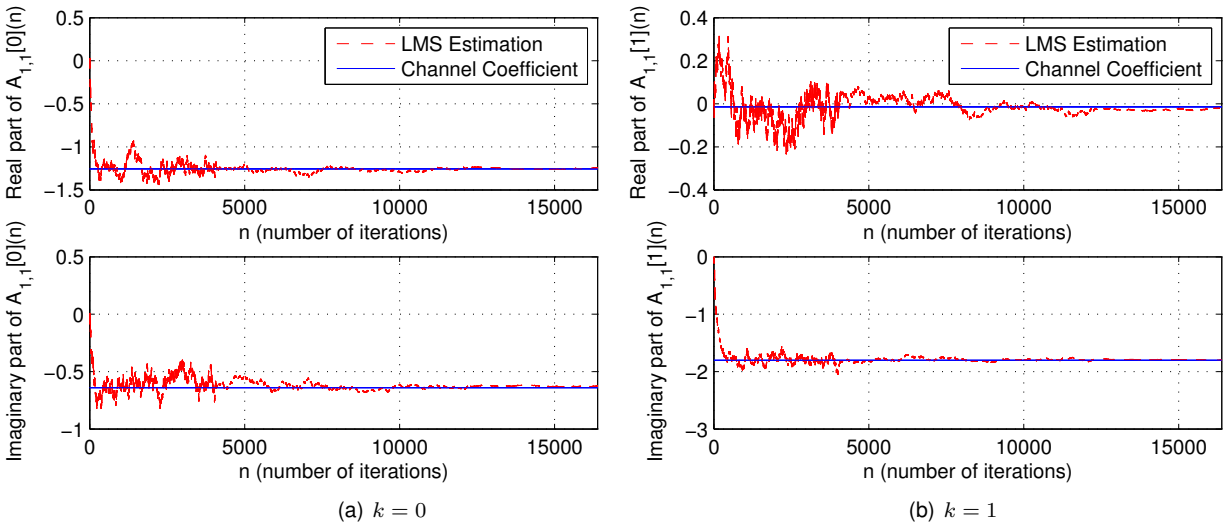

(a) $k = 0$ (b) $k = 1$

Figure 4.5: LMS estimation of the self-interference matrix coefficients $\hat{\mathbf{A}}_{1,1}[k]$ with 16-QAM.

effects of the varying $\mu(n)$ may be observed in the figures, which help the algorithm to converge faster and achieve a small error. On the one hand, when setting a high μ, the filter quickly converges to the channel parameters, yielding a large error. On the other end, setting a small μ outputs a small estimation error, however, causing the filter to converge slower. Nevertheless, the asymptotic estimation error is never zero as predicted in the theoretical filter analysis. For this simulation one obtains an $EM = -35$ dB for the steady state stage of the filter (evaluated in the last iteration taken). The convergence time is also analyzed, again defined as the number of iterations taken from the initialization point, set to $\tilde{\mathbf{A}}_{\star,n} = \mathbf{0}$, to reach a point where the error metric is required to be $EM \leq -30$ dB. The frequency-selective effect on the filter convergence time is evaluated, by considering different channel orders, in this case with $L \in \{1, 3\}$. Fig. 4.6 displays the convergence time distributions in a histogram format with overlaying Kernel distributions (using MATLAB $histfit(\cdot)$ function). As depicted in both figures, the

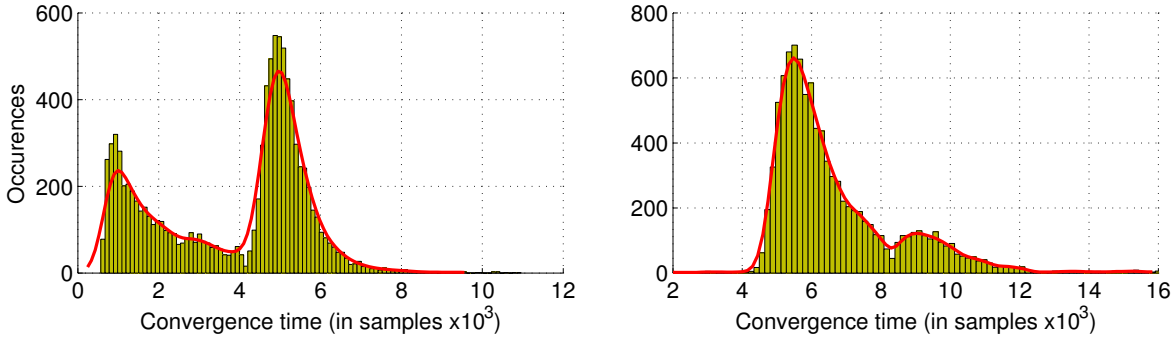

(a) $L = 1$ (b) $L = 3$

Figure 4.6: Convergence time distribution for the LMS estimation of the self-interference matrix with order L with 16-QAM.

convergence time is dependent on the number of channel taps, i.e., the channel order. The simplest

frequency-selective channel with just one past tap is considered and a case with a severe level of ISI with three taps. Both figures show that the convergence time is less than the block length considered for the simulation. Also, the distribution takes an asymmetric shape due to the introduction of a time varying step size. The step size changes at iteration 4069 and iteration at 8192, which creates clusters where the filter may converge. In Fig. 4.6(a), the filter converges for some iterations with step size $\mu = 0.005$ and before iteration 4069. However, when a channel realization takes more than 4069 samples to converge, the algorithm changes the step size to $\mu = 0.001$, forcing the filter to converge immediately. In Fig. 4.6(b), the same effect happens, however for $L = 3$, which introduces more ISI, forcing the filter to converge slower. In this case, most iterations converge for $\mu = 0.001$ and for less that 8192 samples. Nevertheless, some realizations take more than 8192, where the algorithm changes again the step size to $\mu = 0.0005$, in order to force the filter convergence. Furthermore, the Kernel distribution allows an non-parametric estimation of the density function, and for that reason is used to model the aforementioned asymmetric effect. For $L = 1$ it is ensured that the channel estimation parameters converge for less than 8192, while for $L = 3$ the LMS filter never takes more than about 1200 to converge, under the defined parameters. Both values are in most of the cases affordable when compared to typical OFDM transmission lengths. Finally, when converged, the LMS self-interference cancellation method allows a reliable communication link to be established through the relay, even for a severe frequency selective channel.

RLS: In order to evaluate the RLS filter properties, consider a 2^{13} block length, 1000 self-interference channel realizations, $L = 1$, $\mu = 1$ (usual values employed for the RLS [99]) and a forgetting factor $\lambda = 1$. A convergence snapshot of the RLS filter parameters is shown in Fig. 4.7 for the filter coefficient $\hat{\mathbf{A}}_{1,1}[0]$ real and imaginary part and for the filter coefficient $\hat{\mathbf{A}}_{1,1}[1]$ real and imaginary part. The convergence

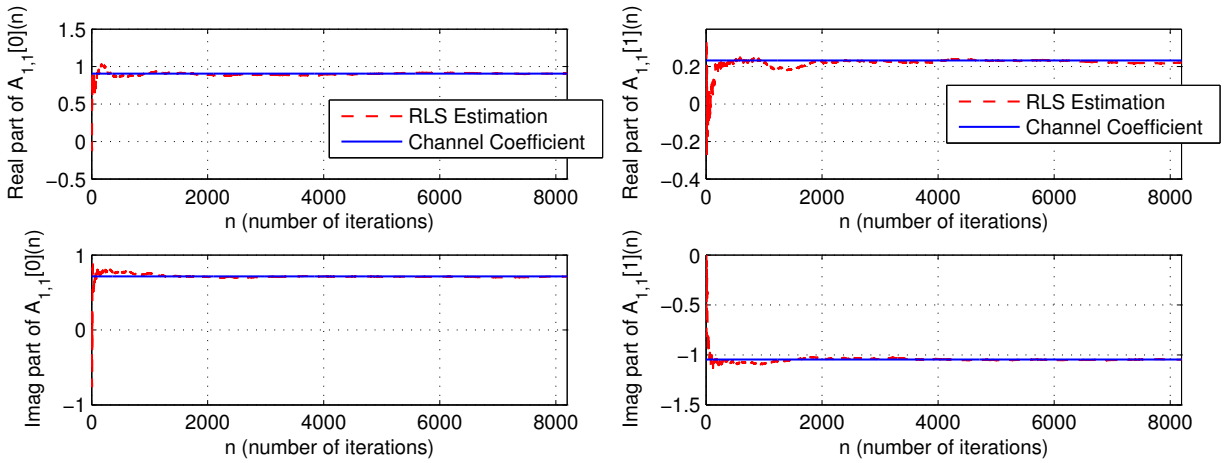

(a) $k = 0$ (b) $k = 1$

Figure 4.7: RLS estimation of the self-interference matrix coefficients $\hat{\mathbf{A}}_{1,1}[k]$ with 16-QAM.

for this filter is virtually instantaneous, taking about 1500 symbols, which corresponds to a fourth of a typical OFDM sequence with a 2^{13} block. Also, the error metric for the steady state filter values is about $EM = -42$ dB, which provides a 7 dB gain over the simulation carried out for the LMS filter. The analysis of the RLS filter convergence is complemented with the histogram of the distribution of

the convergence time. The error metric is again considered as $EM < -30$, also for $L = 1$ and $L = 3$ order self-interference channel, as Fig. 4.8 depicts. In addition, a lognormal distribution is overlaid on the histograms. This distribution correctly models the convergence time, since it approximates a sum of independent and identical distributions that take positive values. The figure shows that the convergence mean time is about 1007 samples for $L = 1$, while for $L = 3$ it takes around 2896. The difference between the mentioned values is explained with the same argument used for the LMS. When considering a higher order for the self-interference channel, there is more ISI present at the relay, which forces the filter to take more iterations to estimate that interference effect. Nevertheless, both values are less than the considered OFDM symbol length, and are considered negligible among OFDM typical transmission lengths.

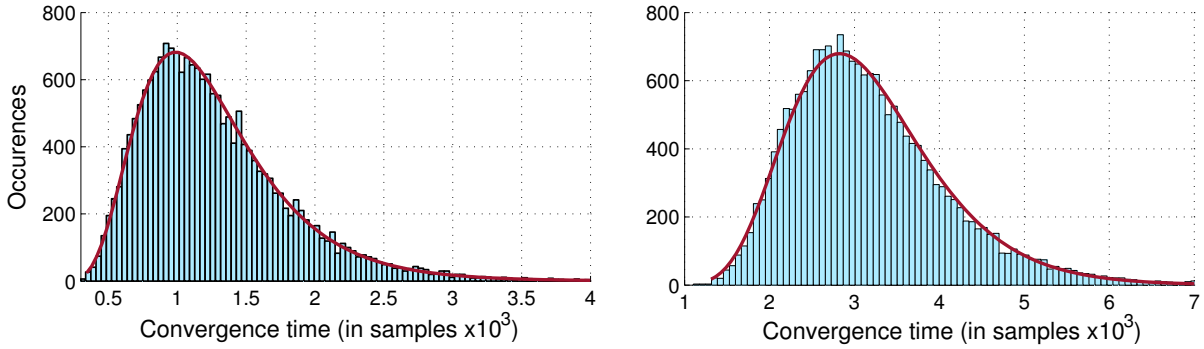

(a) $L = 1$ (b) $L = 3$

Figure 4.8: Convergence time distribution for the RLS estimation of the self-interference channel matrix with order L with 16-QAM.

The RLS filter convergence time is significantly less when compared to the LMS filter convergence time, even if both are acceptable in OFDM transmissions. By taking a better approximation and also by exploiting the second derivative of the MSE expression for the full-duplex relay station, the RLS filter performance drastically improves when compared to the LMS.

BER and SINR Curves

The SINR and the BER of the proposed LMS and RLS filters are evaluated for the considered parameters above and for different values of interference power σ_{LI}^2. Both are also compared with an equivalent HD system, with the case of NI (no filtering scenario, i.e., $\mathbf{A}_\star = \mathbf{0}$), and with the conventional TDC, i.e., with typical estimation errors. In the case of the conventional TDC, the self-interference channel estimation error power is typically considered as $\mathcal{E}_{\mathbf{H_{LI}}}[k](n) \sim \mathcal{CN}(0, \sigma_{\mathbf{H}}^2 \cdot \sigma_{LI}^2)$, where $\sigma_{\mathbf{H}}^2 = 10^{-3}$, as in [34]. The relay hardware imperfections, which are responsible for the transmit signal noise at the relay, are evaluated with $\sigma_{\mathbf{t}}^2 = 10^{-5}$ and $\sigma_{\mathbf{t}}^2 = 10^{-3}$. This parameter affects both TDC, LMS and RLS filters, therefore, it is worth studying its effect in the system performance. Furthermore, it is assumed a 64-QAM modulation of the symbols before the OFDM transmission, Rayleigh fading frequency-selective channels with two taps, i.e., $L = L_{LI} = L_{SR} = L_{RD} = 1$, and also with the filter order of $L_A = L = 1$. The LMS step size $\mu(n)$ is the one considered before, while the RLS step size and forgetting factor λ are

equal to one. The relay is subject to a Gaussian distributed noise, $\mathbf{n_R}(n) \sim \mathcal{CN}(0, \sigma^2_{\mathbf{n_R}})$, with normalized power $\sigma^2_{\mathbf{n_R}} = -15$ dB. Finally, the results were obtained with Monte-Carlo simulation of 2000 OFDM transmitted symbols with length 2^{13} samples.

Fig. 4.9 shows the SINR curves in dB, defined as

$$\text{SINR} = \frac{\| \mathbf{x}(n) \|^2}{\| \mathbf{i}(n) \|^2 + \| \mathbf{n_R}(n) \|^2},$$

where the remaining interference component is given by $\mathbf{i}(n) = \mathbf{f}(n) + \mathbf{z}(n)$, after the cancellation methods analyzed for the four considered cases, when the LMS and RLS algorithm have converged, as shown in the last section. There, it is possible to observe the large gain provided by the LMS and also by the RLS cancellation in terms of SINR, showing that these methods are not affected by erroneous channel estimation, as in the TDC case. The error in the estimated self-interference matrix does not allow the relay to efficiently mitigate the self-interference component when performing conventional TDC. However, by employing these adaptive techniques one can reduce the residual error in this estimation, which is translated to the SINR curve. Moreover, the relay transmit signal error, i.e., $\mathcal{E}_\mathbf{t}(n)$, only slightly affects the SINR in the LMS and RLS for high self-interference power, where the preponderant factor begins to be this error. For the conventional TDC, the factor that chiefly limits its performance is, in this case, the channel estimation errors.

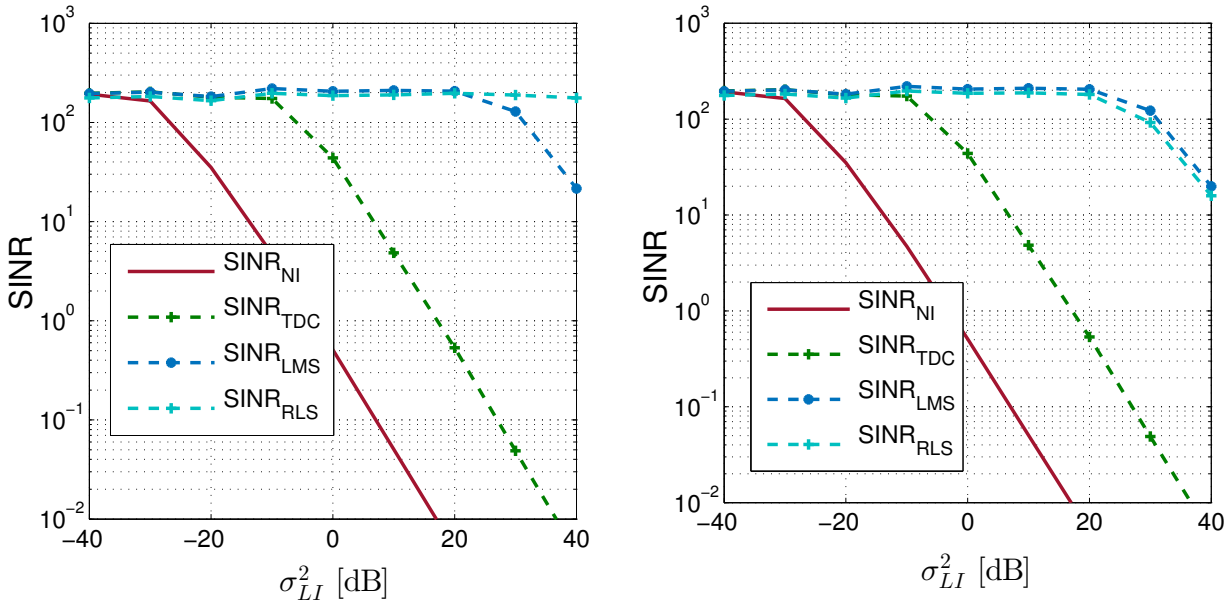

(a) $\sigma^2_{\mathbf{H}} = 10^{-3}, \sigma^2_{\mathbf{t}} = 10^{-5}$.

(b) $\sigma^2_{\mathbf{H}} = 10^{-3}, \sigma^2_{\mathbf{t}} = 10^{-3}$.

Figure 4.9: Impact on the SINR of the self-interference power for the RLS, LMS, TDC and NI methods, for different values of $\sigma^2_{\mathbf{H}}$ and $\sigma^2_{\mathbf{t}}$.

The provided SINR gain in Fig. 4.9 eventually translates into a BER curve gain, as shown in Fig. 4.10. The relay uses a zero forcing (ZF) detector to decode the information from the source, as in section 3.2.3. Firstly, a negligible relay transmit signal error is simulated, with $\sigma^2_{\mathbf{t}} = 10^{-5}$, in order to compare the channels estimation errors effect in both methods under analysis. Thus, in Fig. 4.10(a) it is

possible to observe the LMS and RLS estimation of the self-interference shown in the previous section translated to a BER curve as function of the self-interference channel power. Using these two methods, an approximately 40 dB resilience in terms of self-interference is achieved, i.e., the relay supports 40 more dB of self-interference power at its input. However, when considering higher power relay transmit errors, as in Fig. 4.10(b) for $\sigma_{\mathbf{t}}^2 = 10^{-3}$, the performance of the LMS and the RLS algorithms deteriorates significantly. In fact, the 40 dB of gain shown before are reduced to 30 dB, revealing a great importance in the errors in the relay transmit signal. Nevertheless, these methods still provide a gain of 10 dB when compared to conventional TDC, in which performance is still limited by the errors in the estimation of the self-interference channel.

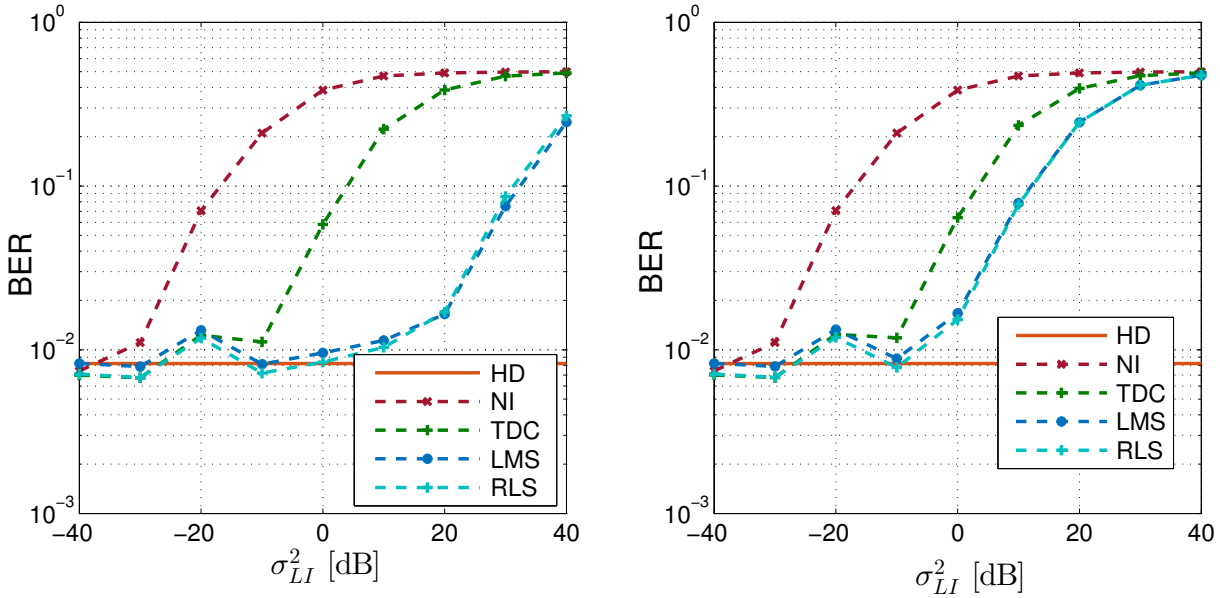

(a) $\sigma_{\mathbf{H}}^2 = 10^{-3}, \sigma_{\mathbf{t}}^2 = 10^{-5}$

(b) $\sigma_{\mathbf{H}}^2 = 10^{-3}, \sigma_{\mathbf{t}}^2 = 10^{-3}$

Figure 4.10: BER comparison of the proposed RLS and LMS algorithms, TDC and NI, for a 64-QAM OFDM ZF detector, for different values of $\sigma_{\mathbf{H}}^2$ and $\sigma_{\mathbf{t}}^2$.

It is worth mentioning that the LMS and RLS filters are capable of tracking time variations of the self-interference matrix, although this aspect has not been explored in the performed analysis. Thus, there is no need to estimate the channel in a certain interval of time, as the conventional TDC requires.

4.4 Concluding Considerations

This chapter has studied techniques that are capable of canceling the undesirable effect of the self-interference present at a relay operating in full-duplex mode. Initially, a theoretical relay system is prosed, that describes the problem of full-duplex relaying, highlighting the presence of a loopback self-interference channel and the problem of having channel estimation errors and transmit signal discrepancies. For that system, spatial suppression filtering is introduced as a technique able to reduce the power of the residual self-interference component by means of MIMO filters. First, NSP is presented, which

creates a null-space in order to transmit the relay signal without interfering with the receive signal. Then, a MIMO filter based on the MMSE criterion is derived, which accounts simultaneously for the thermal noise and self-interference power, while preserving the relay desired signal. After that, feedback filtering is studied, where adaptive filtering techniques are resorted in order to improve the level of residual self-interference cancellation. LMS and RLS adaptive filters are shown to have a good performance in MIMO-OFDM frequency-selective transmissions, while the latter converges much more rapidly. Table 4.1 summarizes the proposed self-interference mitigation techniques gain in dB, when compared with the case of NI in terms of BER.

Technique	**Gain**
Natural Isolation	Reference (0 dB)
NSP	-20 dB
MMSE	-25 dB
LMS	-30 to -40 dB
RLS	-30 to -40 dB
Perfect Cancellation	$-\infty$ dB

Table 4.1: Gain of the proposed self-interference techniques when compared to the NI case (in dB) in terms of BER performance.

Chapter 5

Massive MIMO Full-Duplex Relaying for Independent Multipairs

(This work was partially done in collaboration with Francisco Rosário and published in [10])

Alongside the developments in in-band full-duplex communication, plenty of research has recently been conducted on the capabilities of multiple-input multiple-output (MIMO) systems and its extension to very large arrays. The idea in future networks is to use a large number of antennas at the access points, aiming to serve more users with better connections. To do so, it is necessary to combine various signal processing techniques, such as channel modeling and estimation, precoding and detection algorithms, which should be efficient in terms of both complexity and performance. Massive MIMO techniques may also provide some benefits when applied to full-duplex relaying. Its main advantage lies on the orthogonal properties of large scale channels, which helps in the mitigation of the self-interference inherent in these systems. Furthermore, it allows linear detectors to perform close to optimal ones, thus reducing the system complexity. For those reasons, this chapter proposes a massive MIMO relay station with in-band full-duplex transmissions, designed to serve independent multipairs. The effects of massive MIMO at the relay are evaluated, as well as the end-to-end (e2e) performance of the system. Moreover, an optimal power allocation scheme that guarantees each link necessary rate is introduced.

5.1 System Model

The system model described here is similar to that studied in Chapter 4, although with some slightly modifications. First, it is considered that K user pairs establish a wireless connection through a relay station, which operates in in-band full-duplex mode, i.e., sharing the same time-frequency resources. For that purpose, each user is equipped with a single antenna, while the relay is assumed to be equipped with M_R receiving antennas and M_T transmitting antennas. The number of antennas at the relay are assumed to be of a large dimension and, under the massive MIMO assumptions, are considered to be much larger than the served communications pairs, i.e., $K << M_R, M_T$. Again, the nonexistence of a

direct link between the sources and destinations is assumed, thus, the links are established only through the relay station. A detailed system representation is depicted in figure 5.1, with the filters to be defined.

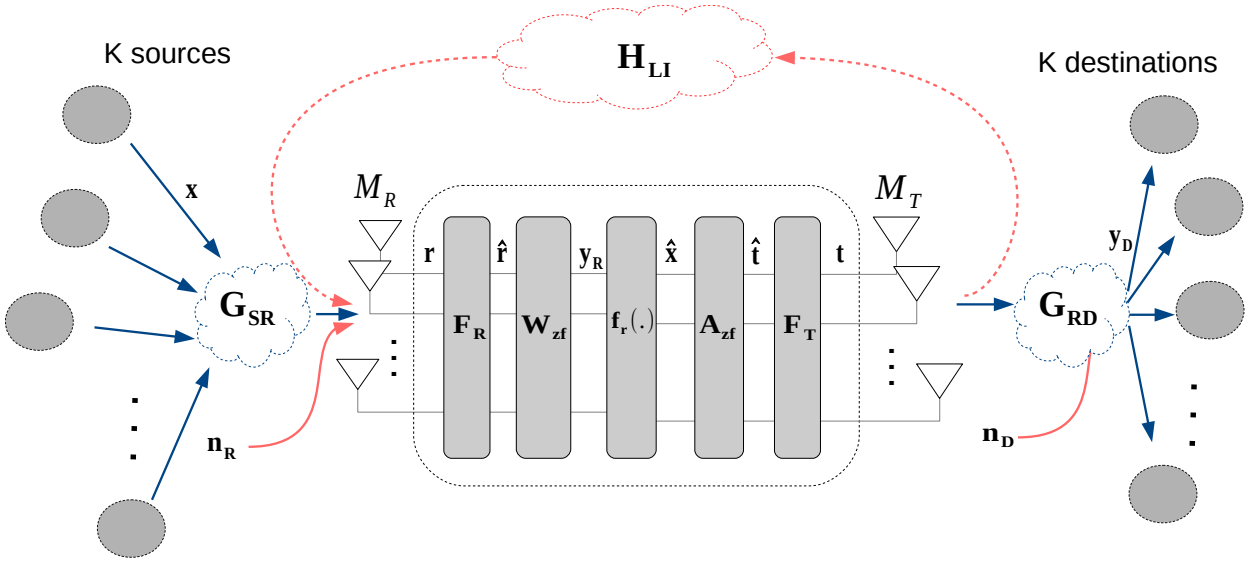

Figure 5.1: Massive MIMO full-duplex relay system with the filtering process detailed.

5.1.1 Channel Model

The desired system information, i.e., the data that flows from one end to the other of the two-hop relay scenario, is carried by the vectors containing the transmitted symbols from the sources to the relay and the symbols from the relay to the destinations, denoted by $\mathbf{x} \in \mathbb{C}^{K\times 1}$ and $\mathbf{t} \in \mathbb{C}^{M_T\times 1}$, respectively. These vectors are the result of a M-QAM mapping of the data bits, normalized and uncorrelated, such that $\mathbb{E}\{\mathbf{x}\mathbf{x}^H\} = \mathbf{I}$ and $\mathbb{E}\{\mathbf{t}^H\mathbf{t}\} = 1$. Therefore, under these normalizations the power transmitted by each source is independent of K and the total transmitted power at the relay dissociated from the number of the relay transmit antennas, M_T, such that the performance evaluation depends neither on the number of pairs nor on the number of transmit antennas at the relay station. Consequently, the received vectors at the relay and at the destinations are given by (5.1) and (5.2), respectively.

$$\mathbf{r} = \mathbf{G_{SR}}\mathbf{D}_{p_S}^{1/2}\mathbf{x} + \sqrt{p_R}\mathbf{H_{LI}}\mathbf{t} + \mathbf{n_R}. \tag{5.1}$$

$$\mathbf{y_D} = \sqrt{p_R}\mathbf{G_{RD}}\mathbf{t} + \mathbf{n_D}. \tag{5.2}$$

The transmitted symbols carried by vector $\mathbf{x}$, go through a MIMO channel from the sources to the relay denoted by $\mathbf{G_{SR}} \in \mathbb{C}^{M_R\times K}$, whereas the symbols from the relay to the destinations go through $\mathbf{G_{RD}} \in \mathbb{C}^{K\times M_T}$. A different model for the fading effects is now considered, in the form of $\mathbf{G_{SR}} = \mathbf{H_{SR}}\mathbf{D_{SR}}^{1/2}$ and $\mathbf{G_{RD}} = \mathbf{D_{RD}}^{1/2}\mathbf{H_{RD}}$, where $\mathbf{D_{SR}}$ and $\mathbf{D_{RD}}$ are diagonal matrices with entries $\beta_{\text{SR},k}$ and $\beta_{\text{RD},k}$ taken from a log-normal distribution, which account for large-scale channel fading, not considered in the previous chapter. The fast-fading channel components are present in $\mathbf{H_{SR}}$ and $\mathbf{H_{RD}}$, both with independent entries taken from a Rayleigh distribution with unitary power $\mathcal{CN}(0,1)$. The self-interference

channel is again represented by matrix $\mathbf{H_{LI}}$, with distribution given by $\mathcal{CN}(0, \sigma_{LI}^2)$, not having a large scale fading effect, and where σ_{LI}^2 naturally accounts for the residual loopback self-interference power after the suppression already imposed in both the propagation and analog-circuit cancellation domains. The vectors $\mathbf{n_R} \sim \mathcal{CN}(0, \sigma_{\mathbf{n_R}}^2)$ and $\mathbf{n_D} \sim \mathcal{CN}(0, \sigma_{\mathbf{n}_d}^2)$ take into consideration the additive white Gaussian noise at the relay and destinations, respectively. Finally, the diagonal matrix $\mathbf{D}_{p_S}$ with entries $p_{S,k}$ regulates each source transmit power, while p_R denotes the relay's average transmit power. In this formulation, large-scale fading effects based on the distance from users to the relay are being considered and, thus, there is a need for each terminal and the relay to transmit with different powers. Therefore, the residual interference will then depend strongly on p_R.

5.1.2 Channel Estimation

In order to efficiently apply detection, precoding and self-interference mitigation techniques to allow the establishment of reliable communication links through the relay, consider the use of traditional channel estimations of the involved channel matrices, $\tilde{\mathbf{H}}_{\mathbf{SR}}$, $\tilde{\mathbf{H}}_{\mathbf{LI}}$ and $\tilde{\mathbf{H}}_{\mathbf{RD}}$ of the true channel matrices, $\mathbf{H_{SR}}$, $\mathbf{H_{LI}}$ and $\mathbf{H_{RD}}$. Applying any of the estimation algorithms proposed in the literature [15], an error in the channel small-scale fading effect matrices is assumed and modeled as in the previous chapter:

$$\mathcal{E}_{\mathbf{H_{SR}}}, \mathcal{E}_{\mathbf{H_{RD}}}, \mathcal{E}_{\mathbf{H_{LI}}} \sim \mathcal{CN}(0, \sigma_{\mathbf{H}}^2)$$

The difference between the estimates of this component and the true channel values are

$$\begin{aligned} \mathbf{H_{SR}} &= \tilde{\mathbf{H}}_{\mathbf{SR}} + \mathcal{E}_{\mathbf{H_{SR}}}; \\ \mathbf{H_{LI}} &= \tilde{\mathbf{H}}_{\mathbf{LI}} + \mathcal{E}_{\mathbf{H_{LI}}}; \\ \mathbf{H_{RD}} &= \tilde{\mathbf{H}}_{\mathbf{RD}} + \mathcal{E}_{\mathbf{H_{RD}}}. \end{aligned} \tag{5.3}$$

The presence of errors in the matrices estimations are only assumed in the small-scale fading channel components, whereas the large-scale fading matrices are perfectly known at the relay station. The impact of any hardware imperfection and impairments at the relay, already discussed, are modeled by means of an additive error component in the transmitted vector [34], which outputs $\mathbf{t} = \tilde{\mathbf{t}} + \mathcal{E}_{\mathbf{t}}$, where $\tilde{\mathbf{t}}$ is the vector to be transmitted after baseband filtering and where all elements of $\mathcal{E}_{\mathbf{t}} \sim \mathcal{CN}(0, \sigma_{\mathbf{t}}^2)$ are assumed to be uncorrelated with $\tilde{\mathbf{t}}$. It is worth mentioning that the covariance of the self-interference term $\sqrt{p_R}\mathbf{H_{LI}t}$ in (5.1) is here controlled by the parameters p_R, σ_{LI}^2, $\sigma_{\mathbf{t}}^2$ and $\sigma_{\mathbf{H}}^2$, while in Chapter 4 it is considered that this effect is only affected by σ_{LI}^2, $\sigma_{\mathbf{t}}^2$ and $\sigma_{\mathbf{H}}^2$, since there uniform power distribution is assumed.

5.1.3 Detection and Precoding for Massive MIMO

The design of the detection and precoding of the considered two-hop transmission link it is firstly done for an equivalent received signal $\hat{\mathbf{r}}$, whose self-interference component has been minimized by any of the relaying protocol independent mitigation schemes. Hence, this system takes into account a transmission

channel where massive array dimensions are always assumed, i.e., $K << M_R$. Under this assumption, linear processing techniques are proven to perform close to optimal [31]. Therefore, aiming to simplify the relaying operation, the usage of a zero forcing (ZF) filtering for both detection and beamforming is considered [100]. Using the estimation of $\mathbf{G_{SR}}$, denoted by $\tilde{\mathbf{G}}_{\mathbf{SR}} = \tilde{\mathbf{H}}_{\mathbf{SR}}\mathbf{D}_{\mathbf{SR}}^{\mathbf{1/2}}$, the estimated symbols after ZF filtering with $\mathbf{W_{zf}}$, are given by

$$\hat{\mathbf{x}} = \mathrm{Q}(\mathbf{W_{zf}}\hat{\mathbf{r}}) = \mathrm{Q}\big((\tilde{\mathbf{G}}_{\mathbf{SR}}^H\tilde{\mathbf{G}}_{\mathbf{SR}})^{-1}\tilde{\mathbf{G}}_{\mathbf{SR}}^H\hat{\mathbf{r}}\big), \tag{5.4}$$

where $\mathrm{Q}(\cdot)$ is a symbol-wise quantizer to the M-ary considered constellation set. Upon detection based on $\hat{\mathbf{x}}$, the estimated symbols are forwarded to the destinations $\mathbf{y_D}$, that are assumed to have very limited processing capabilities. Thus, a ZF precoder filter, $\mathbf{A_{zf}}$, is employed, as in

$$\hat{\mathbf{t}} = \mathbf{A_{zf}}\hat{\mathbf{x}} = \alpha_{\mathsf{zf}}\tilde{\mathbf{G}}_{\mathbf{RD}}^H(\tilde{\mathbf{G}}_{\mathbf{RD}}\tilde{\mathbf{G}}_{\mathbf{RD}}^H)^{-1}\hat{\mathbf{x}}, \tag{5.5}$$

where $\tilde{\mathbf{G}}_{\mathbf{RD}} = \mathbf{D}_{\mathbf{RD}}^{\mathbf{1/2}}\tilde{\mathbf{H}}_{\mathbf{RD}}$ is the estimation of the true $\mathbf{G_{RD}}$ and, $\alpha_{\mathsf{zf}} = \left(\mathbb{E}\{\mathsf{Tr}\{(\tilde{\mathbf{G}}_{\mathbf{RD}}\tilde{\mathbf{G}}_{\mathbf{RD}}^H)^{-1}\}\}\right)^{-\frac{1}{2}}$ is a scalar chosen to normalize the power of $\hat{\mathbf{t}}$, i.e., $\mathbb{E}(\hat{\mathbf{t}}^H\hat{\mathbf{t}}) = 1$. From $\tilde{\mathbf{G}}_{\mathbf{RD}}$, α_{zf} is computed considering that $\mathbf{t} = \alpha_{\mathsf{zf}}\tilde{\mathbf{G}}_{\mathbf{RD}}^H(\tilde{\mathbf{G}}_{\mathbf{RD}}\tilde{\mathbf{G}}_{\mathbf{RD}}^H)^{-1}\hat{\mathbf{x}} = \alpha_{\mathsf{zf}}\mathbf{P}\hat{\mathbf{x}}$, and the fact that $\hat{\mathbf{x}}$ is zero-mean with covariance matrix $\mathbf{C} = \mathbb{E}\{\hat{\mathbf{x}}\hat{\mathbf{x}}^H\} = \mathbf{I}$, it follows from [94] that

$$\mathbb{E}\{\mathbf{t}^H\mathbf{t}\} = \alpha_{\mathsf{zf}}^2\mathbb{E}\{(\mathbf{P}\hat{\mathbf{x}})^H(\mathbf{P}\hat{\mathbf{x}})\} = \alpha_{\mathsf{zf}}^2\mathsf{Tr}\{\mathbf{P}\mathbf{C}\mathbf{P}^H\} = 1. \tag{5.6}$$

$$\mathsf{Tr}\{(\tilde{\mathbf{G}}_{\mathbf{RD}}\tilde{\mathbf{G}}_{\mathbf{RD}}^H)^{-1}) = \mathsf{Tr}\{(\mathbf{D}_{\mathbf{RD}}\tilde{\mathbf{H}}_{\mathbf{RD}}\tilde{\mathbf{H}}_{\mathbf{RD}}^H)^{-1}\}. \tag{5.7}$$

Now noting that $\mathbf{T} \triangleq \tilde{\mathbf{H}}_{\mathbf{RD}}\tilde{\mathbf{H}}_{\mathbf{RD}}^H$ is a central Wishart matrix, where the columns of $\tilde{\mathbf{H}}_{\mathbf{RD}} \in \mathbb{C}^{K\times M_T}$ are zero-mean complex Gaussian vectors with covariance matrix $(1+\sigma_{\mathbf{H}}^2)\mathbf{I}$, it comes from [101] that

$$\mathbb{E}\{(\mathsf{Tr}\{\mathbf{D}_{\mathbf{RD}}\mathbf{T}\})^{-1}\} = \frac{\sum_{k=1}^{K}\left(\beta_{\mathsf{RD,k}}(1+\sigma_{\mathbf{H}}^2)\right)^{-1}}{M_T-K}. \tag{5.8}$$

Merging the results of (5.6), (5.7) and (5.8), the normalization factor α_{zf} is given by

$$\alpha_{\mathsf{zf}} = \sqrt{\frac{(M_T-K)}{\sum_{k=1}^{K}\left(\beta_{\mathsf{RD},k}(1+\sigma_{\mathbf{H}}^2)\right)^{-1}}}. \tag{5.9}$$

5.2 Self-Interference Mitigation

The problem of combating the effect of self-interference is considered by means of a filtering process, already discussed for small dimension matrices, and presented here for the considered system in Fig. 5.1 with large dimensions. Also by finding the optimal relay and sources transmit power for certain conditions, it is possible to reduce the effect of this undesired consequence of in-band full-duplex relaying. Note that the self-interference at the relay is directly related to its transmit power, therefore, special attention should be given to this parameter.

5.2.1 Linear Filtering

After setting the relay detection and precoding method, the self-interference mitigation problem needs to be evaluated. Under the model given by (5.1), the goal of the relay is to minimize the self-interference term $\sqrt{p_R}\mathbf{H_{LI}t}$, while preserving the signal desired component $\mathbf{G_{SR}}\mathbf{D}_{p_S}^{1/2}\mathbf{x}$ and taking into account the covariance of the noise vector $\mathbf{R}_{\mathbf{n_R}}$ at the relay. Thus, the minimum mean square error (MMSE) linear filter described in section 4.2.2 is considered, where a linear pre-filter $\mathbf{F_R}$ and post-filter $\mathbf{F_T}$ are considered, such that $\tilde{\mathbf{t}} = \mathbf{F_T}\hat{\mathbf{t}}$ and $\hat{\mathbf{r}} = \mathbf{F_R}\mathbf{r}$. The filter expressions for this setup are deduced based on section 4.2.2, and described by

$$\begin{aligned} &\mathbf{F_T} = \mathbf{I}; \\ &\mathbf{F_R} = \tilde{\mathbf{G}}_{\mathbf{SR}}\mathbf{D}_{p_S}\tilde{\mathbf{G}}_{\mathbf{SR}}^H(\tilde{\mathbf{G}}_{\mathbf{SR}}\mathbf{D}_{p_S}\tilde{\mathbf{G}}_{\mathbf{SR}}^H + p_R\tilde{\mathbf{H}}_{\mathbf{LI}}\mathbf{R_t}\tilde{\mathbf{H}}_{\mathbf{LI}}^H + \mathbf{R}_{\mathbf{n_R}})^{-1}, \end{aligned} \tag{5.10}$$

where $\mathbf{R_t} = \mathbf{F_T}\mathbf{A}_{\text{zf}}\mathbf{R}_{\hat{\mathbf{x}}}\mathbf{A}_{\text{zf}}^H{\mathbf{F_T}}^H + \sigma_{\mathbf{t}}^2\mathbf{I}$.

The null-space projection filter, analyzed in section 4.2.1, is not considered for this system since the process of beam selection is in general difficult for large dimensions. On the contrary, (5.10) is a closed-form expression containing the channel estimates and covariance matrices of transmitted vectors and noise, that are assumed to be known.

For the considered mode,l and for a given set of parameters, a trade-off in the e2e BER is expected. On the one hand, a lower transmit power at the relay p_R reduces the self-interference effect and diminishes any impact of the estimation errors and system impairments; on the other hand, a higher p_R leads to an improvement in the signal-to-noise ratio (SNR) levels at the destinations and hence a lower bit error rate (BER) in the forward link channel. Thus, for a fixed source transmit power, an optimal choice for p_R that minimizes the e2e BER can be predicted.

5.2.2 Optimal Power Allocation

The level of interference suffered by the relay station depends critically on its transmit power and self-interference channel power, as seen before, and directly perturbs the e2e and rate performance of the relaying process. Therefore, it is desirable to find the optimal power that meets the requirements of the system. In this case, consider that each individual link requires a minimum rate. These rates may be found using a similar procedure to that in [42]. Thus, the expression for the transmission rate between each source and destination pair is limited by the weakest of the two paths that establish the same link, i.e., one of the channels that are used for communication limit the flow of information between the pairs. This may be formulated as follows

$$R_k = \min\{R_{\text{SR},k}, R_{\text{RD},k}\}, \tag{5.11}$$

where $R_{\text{SR},k}$ and $R_{\text{RD},k}$ denote the achievable rates between the sources and the relay and between the relay and the destinations, respectively. Firstly, in order to derive the achievable rate R_k, the received

signal at the relay before detection is considered, which is given by equation (5.12)

$$y_{r,k} = \sqrt{p_{S,k}}(\mathbf{W_{zf}F_R})_k^T \mathbf{g_{SR}}_k x_k + \sum_{j \neq k}^{K} \sqrt{p_{S,j}}(\mathbf{W_{zf}F_R})_k^T \mathbf{g_{SR}}_j x_j + \sqrt{p_R}(\mathbf{W_{zf}F_R})_k^T \mathbf{H_{LI}t} + (\mathbf{W_{zf}F_R})_k^T \mathbf{n_R}, \tag{5.12}$$

where $\mathbf{g_{SR}}_k$ denotes the k^{th} column of channel matrix from the destination to the relay including large-scale fading effects, $\mathbf{G_{SR}}$. Consequently, the received signal at each destination link before detection is given as follows

$$y_{d,k} = \sqrt{p_R}\mathbf{g_{RD}}_k^T (\mathbf{F_T A_{zf}})_k \hat{x}_k + \sqrt{p_R} \sum_{j \neq k}^{K} \mathbf{g_{RD}}_k^T (\mathbf{F_T A_{zf}})_j \hat{x}_j + n_{d,k}. \tag{5.13}$$

where, similarly, $\mathbf{g_{SR}}_k$ denotes the k^{th} column of channel matrix $\mathbf{G_{RD}}$. The expressions in equation (5.12) and (5.13) may be seen as a known mean gain times the desired signal (first term in both equations) plus an uncorrelated effective noise term that includes channel impairment effects, interpair and self-interference, and Gaussian noise (following terms). A valid technique commonly used in large MIMO systems [102] is to approximate the effective noise term, the sum of the latter mentioned terms, by a Gaussian noise component, resorting to the properties of the central limit theorem. By doing so, the problem of computing the rates becomes simpler, while it is proven that this method gives good approximations. Therefore, in order to compute each link rate, firstly the signal-to-interference-plus-noise ratio (SINR), represented by γ, is evaluated at the relay and at the destinations. Equation (5.14) shows the SINR at the relay station

$$\gamma_{\mathsf{SR},k} = \frac{p_{S,k}\mathsf{MV}_{\mathsf{SR},k}}{p_{S,k}\mathsf{V}_{\mathsf{SR},k} + \sum_{j \neq k}^{K} p_{S,j}\mathsf{MP}_{\mathsf{SR},(k,j)} + p_R\mathsf{LI}_{\mathsf{SR},k} + \mathsf{AN}_{\mathsf{SR},k}}, \tag{5.14}$$

where the constants are given by the channel distributions, as $\mathsf{MV}_{\mathsf{SR},k} = |\mathbb{E}\{(\mathbf{W_{zf}F_R})_k^T \mathbf{g_{SR}}_k\}|^2$, $\mathsf{V}_{\mathsf{SR},k} = \mathbb{V}\mathrm{ar}\{(\mathbf{W_{zf}F_R})_k^T \mathbf{g_{SR}}_k\}$, $\mathsf{MP}_{\mathsf{SR},(k,j)} = \mathbb{E}\{|(\mathbf{W_{zf}F_R})_k^T \mathbf{g_{SR}}_j|^2\}$, $\mathsf{LI}_{\mathsf{SR},k} = \mathbb{E}\{\| \mathbf{w_{zf}}_k^T \mathbf{F_R H_{LI} F_T A_{zf}} \|^2\}$ and $\mathsf{AN}_{\mathsf{SR},k} = \sigma_{n_R}^2 \mathbb{E}\{\| (\mathbf{W_{zf}F_R})_k \|^2\}$. Similarly, equation (5.15) shows the SINR at the destinations

$$\gamma_{\mathsf{RD},k} = \frac{p_R\mathsf{MV}_{\mathsf{RD},k}}{p_R\mathsf{V}_{\mathsf{RD},k} + p_R\mathsf{MP}_{\mathsf{RD},k} + \mathsf{AN}_{\mathsf{RD},k}}, \tag{5.15}$$

where $\mathsf{MV}_{\mathsf{RD},k} = |\mathbb{E}\{\mathbf{g_{RD}}_k^T (\mathbf{F_T A_{zf}})_k\}|^2$, $\mathsf{V}_{\mathsf{RD},k} = \mathbb{V}\mathrm{ar}\{\mathbf{g_{RD}}_k^T (\mathbf{F_T A_{zf}})_k\}$, $\mathsf{MP}_{\mathsf{RD},k} = \sum_{j \neq k}^{K} \mathbb{E}\{|\mathbf{g_{RD}}_k^T (\mathbf{F_T A_{zf}})_j|^2\}$ and $\mathsf{AN}_{\mathsf{RD},k} = \sigma_{n_D}^2$. Thus, the rate for each channel can be easily given by

$$\begin{aligned} R_{\mathsf{SR},k} &= \log_2(1 + \gamma_{\mathsf{SR},k}), \\ R_{\mathsf{RD},k} &= \log_2(1 + \gamma_{\mathsf{RD},k}), \end{aligned} \tag{5.16}$$

assuming the in-band full-duplex transmission to drop the $\frac{1}{2}$ constant in each expression.

The goal is then to find the system power allocation, i.e., compute the required power transmitted by both sources and relay, such that the desired rate for each communication pair k is guaranteed. Further-

more, due to capacity limits of amplifiers, peak power constraints are taken into account. Considering green communications, the target is that the overall power consumption is minimized, such that the system uses the minimum amount of energy to work, thus, saving energy at the relay, but essentially saving the battery of the sources, which are assumed to have mobility. In other words, the problem target can be seen as: minimize the system energy efficiency (EE), defined as

$$\mathsf{EE} = \frac{\sum_{k=1}^{K} R_k}{(p_R + \sum_{k=1}^{K} p_{S,k})}, \tag{5.17}$$

ensuring the necessary system rate, while using the minimum necessary amount of energy. Formally, this can be written as an optimization problem in its canonical form, as in (5.18)

$$\begin{aligned} \underset{p_R, p_{\mathsf{S},1} \cdots p_{S,K}}{\text{min.}} \quad & \sum_{k=1}^{K} p_{S,k} + p_R, \\ \text{s.t.} \quad & R_k \geq R_{0,k},\ k = 1, \ldots, K; \\ & 0 \leq p_{S,k} \leq p_{S_{0,k}},\ k = 1, \ldots, K; \\ & 0 \leq p_R \leq p_{R_0}, \end{aligned} \tag{5.18}$$

where $R_{0,k}$ and $p_{S_{0,k}}$ are the required rate and peak power for pair k, respectively, p_{R_0} is the relay station peak power, and where $R_k = \min\{\log_2(1 + \gamma_{\mathsf{SR},k}), \log_2(1 + \gamma_{\mathsf{RD},k})\}$.

Solving the problem in (5.18) involves the derivation of the channel statistics, present in the above SINR expressions. These channel statistics would be easy to compute if the self-interference was not present, thus, not being necessary to employ the MMSE filtering stage. However, the usage of this filtering stage makes the problem highly difficult, since it involves inversion of Wishmart matrices. In terms of the optimization itself, the cost function in (5.18) is convex, nonetheless, the rate constrain involves the mentioned MMSE filter expression, clearly non linear with respect to the optimization variables, making the overall problem non-convex.

For these reasons, an algorithm to solve the optimization problem is proposed, giving an approximation to optimal power allocation. The algorithm is designed to be simple and computationally efficient. The main idea is to assume that the channel coefficients are constant, for some instances of the problem, say i, which gives then a linear reformulation of the optimization problem, noting that $\min\{a, b\} \geq x <=> a \geq x, b \geq x$. This reformulation is given by

$$\begin{aligned} \underset{p_{R,i}, p_{S,1,i} \cdots p_{S,K,i}}{\text{min.}} \quad & \sum_{k=1}^{K} p_{S,k,i} + p_{R,i}, \\ \text{s.t.} \quad & p_{S,k,i}\mathsf{MV}_{\mathsf{SR},k} \geq (2^{R_{0,k}} - 1) \cdot \Big(p_{S,k,i}\mathsf{V}_{\mathsf{SR},k} + \sum_{j \neq k}^{K} p_{\mathsf{S},j,i}\mathsf{MP}_{\mathsf{SR},(k,j)} + p_{\mathsf{R},i}\mathsf{LI}_{\mathsf{SR},k} + \mathsf{AN}_{\mathsf{SR},k} \Big), \\ & p_{R,i}\mathsf{MV}_{\mathsf{RD},k} \geq (2^{R_{0,k}} - 1) \cdot \Big(p_{R,i}\mathsf{V}_{\mathsf{RD},k} + p_{R,i}\mathsf{MP}_{\mathsf{RD},k} + \mathsf{AN}_{\mathsf{RD},k} \Big), \\ & 0 \leq p_{S,k,i} \leq p_{S_{0,k}}, k = 1, \ldots, K; \\ & 0 \leq p_{R,i} \leq p_{R_0}. \end{aligned} \tag{5.19}$$

Thus, by iteratively solving this linear program, the algorithm is capable of converging and obtaining the

desired close solution to the optimal power allocation. At each iteration, the algorithm firstly estimates the involved channel matrices, so that the statistics coefficients in (5.14) and (5.15) are computed for a fixed transmit power at the sources and at the relay. This procedure is performed iteratively to average out the channel effects. Then, the optimization problem specified in (5.19) is solved with a linear programming solver [103]. The process is repeated again until the total number of iterations is reached. Moreover, this value is defined to ensure that a steady power vector is obtained, and which is empirically assumed to be close to the optimal solution when the algorithm converges (always in this case). The proposed algorithm is summarized in 2.

Algorithm 2 Minimum Required Power Allocation to Multipair Relaying

Input: Channel observations, $\tilde{\mathbf{G}}_{\mathbf{SR}}$, $\tilde{\mathbf{G}}_{\mathbf{RD}}$, $\tilde{\mathbf{H}}_{\mathbf{LI}}$. Number of iterations of the algorithm, L. Number of iterations to average channel effects, N_{it}.

Output: Power at sources and relay, $p_R, p_{S,1}...p_{S,K}$.

1. Initialization: Set $i = 1$; initialize powers $p_{S,k,1} = p_{S_{0,k}}$ and $p_{R,0} = p_{R_0}$; define L as the total number of iterations and set N_{it} as the number of channel realizations per iteration.

2. Iteration i:

1) Compute channel statistics:

for N_{it} **do**

i) Obtain $\tilde{\mathbf{G}}_{\mathbf{SR}}$, $\tilde{\mathbf{G}}_{\mathbf{RD}}$, $\tilde{\mathbf{H}}_{\mathbf{LI}}$, $\mathbf{W}_{\mathbf{zf}}$ and $\mathbf{A}_{\mathbf{zf}}$;

ii) Compute filter $\mathbf{F}_{\mathbf{R}}$ with $p_{S,k,i}$ and $p_{R,i}$;

iii) Compute instantaneous rate coefficients for all k pairs: $\mathrm{MV}_{\mathrm{SR},k}$, $\mathrm{V}_{\mathrm{SR},k}$, $\mathrm{MP}_{\mathrm{SR},(k,j)}$, $\mathrm{LI}_{\mathrm{SR},k}$ and $\mathrm{AN}_{\mathrm{SR},k}$ (as in (5.14)) $\mathrm{MV}_{\mathrm{RD},k}$, $\mathrm{V}_{\mathrm{RD},k}$, $\mathrm{MP}_{\mathrm{RD},k}$ and $\mathrm{AN}_{\mathrm{RD},k}$ (as in (5.15))

end for

2) Average to obtain channel statistics.

3) Solve the linear program (5.19) with the coefficients found in step 2) to obtain the new $p_{S,k,i}$ and $p_{R,i}$.

4) Set $p_{S,k,i+1} = p_{S,k,i}$ and $p_{R,i+1} = p_{R,i}$.

3. Check: If $i = L$ end algorithm, else set $i = i + 1$.

5.3 System Performance Evaluation

This section compares the performance of the proposed filters with special emphasis on the e2e link reliability and on the efficiency of the proposed power allocation algorithm. Assumed a symmetric system with the same number of users K on both sides with one antenna each and $M = M_T = M_R$ antennas at the relay. Transmission and reception at the relay are conducted in the same time-slot and frequency band, and an arbitrary processing delay $d \geq 1$ is assumed, so that at time instant n on has that $\hat{\mathbf{x}}(n) = f_r(\mathbf{x}(n-d))$. Both interference cancellation filters are given by (5.10). Without loss of generality, it is considered that $\sigma_{LI}^2 = 1$. In the previous chapter, this value was not considered fixed, since it was assumed that the total amount of self-interference was controlled by it. In a different fashion, this chapter considers different powers at the relay and, thus, the level of self-interference power present at the relay is controlled mainly by p_R. Moreover, the SNR at the relay with large-scale fading effects is here defined

as

$$\mathrm{SNR_R} = \frac{\sum_{k=1}^{K} \beta_{\mathrm{SR},k} p_{S,k}}{\sigma^2_{\mathbf{n_R}}}. \tag{5.20}$$

5.3.1 BER Performance for Different Relay Transmit Powers

Firstly, the performance of the system in terms of BER at both the relay station and destinations, considering only small scale fading, i.e., $\mathbf{D_{SR}}^{1/2} = \mathbf{D_{RD}}^{1/2} = \mathbf{I}$, is evaluated. This comes without loss of generality, as it is assumed that the relay knows exactly the channels large-scale coefficients. Thus, for a given $\mathrm{SNR_R}$ and fixed uniform transmitted power $p_{S,k} = 1$, for all k, different allocated powers at the relay p_R are evaluated, also for an increasing number of antennas M at the relay. Similar to that done is Chapter 4, however, here the transmit power at the relay is the variable, instead of the self-interference power. For simulation purposes, the results are compared against natural isolation (NI) (in this case when $\mathbf{F_R} = \mathbf{F_T} = \mathbf{I}$, ignoring the self-interference effect) and against a half-duplex (HD) equivalent system. Setting the variance in the errors to the typical values in these systems, i.e., $\sigma^2_{\mathbf{t}} = \sigma^2_{\mathbf{H}} = 10^{-3}$, the curves of BER for different values of relay power p_R are depicted in Fig. 5.2, for $M = 16$ and $M = 64$ antennas, five users pairs ($K = 5$), a $\mathrm{SNR_R}$ value of 8 dB and using uncoded 16-QAM modulation. It can be seen that for a large and increasing number of antennas the system using the MMSE filter becomes more robust to the self-interference effect, exhibiting a BER performance slightly closer to HD, for higher values of power p_R, when compared to NI. However, this gain is only marginal for the antenna set considered. Also, it is possible to conclude that the proposed system attains a gain of approximately 20 dB when compared with NI. This value is similar to what was shown for a small number of antennas, in Fig. 4.3, only for high levels of interference.For low levels of interference, the suppression attained by employing more antennas is considerable.

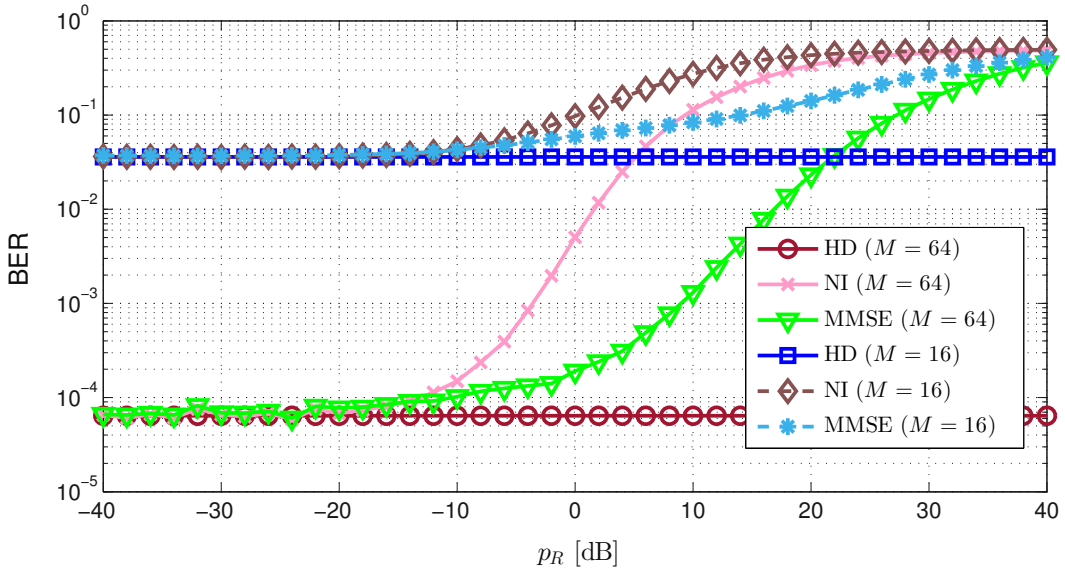

Figure 5.2: BER performance at the relay for different numbers of antennas N, $K = 5$ pairs, $\mathrm{SNR_R} = 8$ dB and 16-QAM.

The e2e BER in terms of the allocated power p_{R} is also studied using the same setup as before. For this purpose, the variance of the noise at the destinations, $\sigma^2_{\mathbf{n}_d}$, is set to two different typical values. The results are shown in Fig. 5.3. It is possible to confirm that for a given configuration there is an optimal choice for the power at the relay that minimizes the e2e BER, i.e., there is an optimal point where the trade off between transmitting with a low relay transmit power, which decreases the self-interference effect at the relay, and employing high transmit power, which increased the SNR at the destinations with a cost of enhancing the self-interference effect at the relay station. Moreover, it is concluded that a larger number of antennas attains the minimum BER with less power, i.e., the optimal transmit power at the relay that minimizes the e2e BER is achieved for less power when the number of antennas is increased. Also the value of the BER is naturally lower for this case. These effects were already expected from the properties of massive MIMO transmissions, since the orthogonal properties of large dimension systems provide an extra gain in terms of system diversity and in terms of self-interference mitigation.

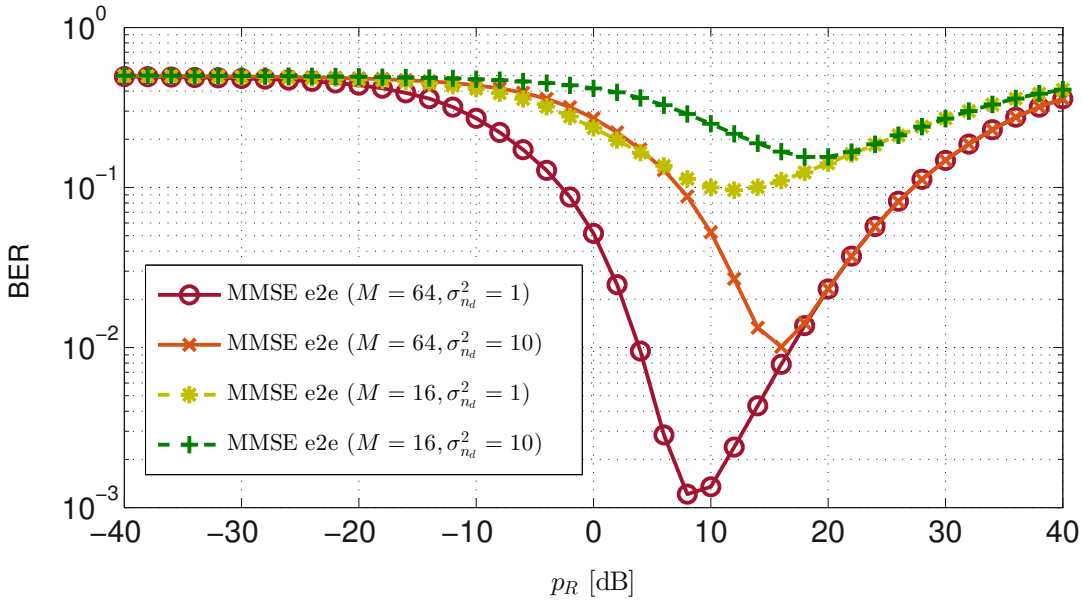

Figure 5.3: End-to-end BER performance for different M and $\sigma^2_{\mathbf{n}_d}$, $K = 5$ pairs, $\mathrm{SNR}_{\mathrm{R}} = 8$ dB and 16-QAM.

5.3.2 End-to-end Sum Rate

The e2e sum rate for the previous system setup, using the expression (5.11) is depicted in Fig. 5.4. This is interesting to evaluate since the formulation of the optimization problem in section 5.2.2 depends directly on these expressions. For a certain range of low relay power, the weakest channel is the one from the relay to the destinations, which is limited by the destinations SNR. For high relay powers, the weakest channel is the one from the sources to the relay, caused by the self-interference problem. These mentioned effects may be observed in the figure, where there is an optimal choice for p_R that maximizes the rate per user, i.e., the point where the rate of both channels from the source to the relay (R_{SR}) and

from the relay to the destinations (R_{RD}) achieve the same value. As it would be expected, the maximum achievable rate per user is higher for a higher number of employed antennas at the relay, and also requires a higher relay transmit power. This fact may be inconsistent with what has been stated before, however, it can be explained considering that the orthogonal effect of massive MIMO brings some gain in terms of canceling the self-interference at the relay. Therefore, with the increase in the number of antennas, the relay station can employ higher powers in order to achieve higher rates, as seen in Fig. 5.4, hence the self-interference resilience also increases with the number of antennas.

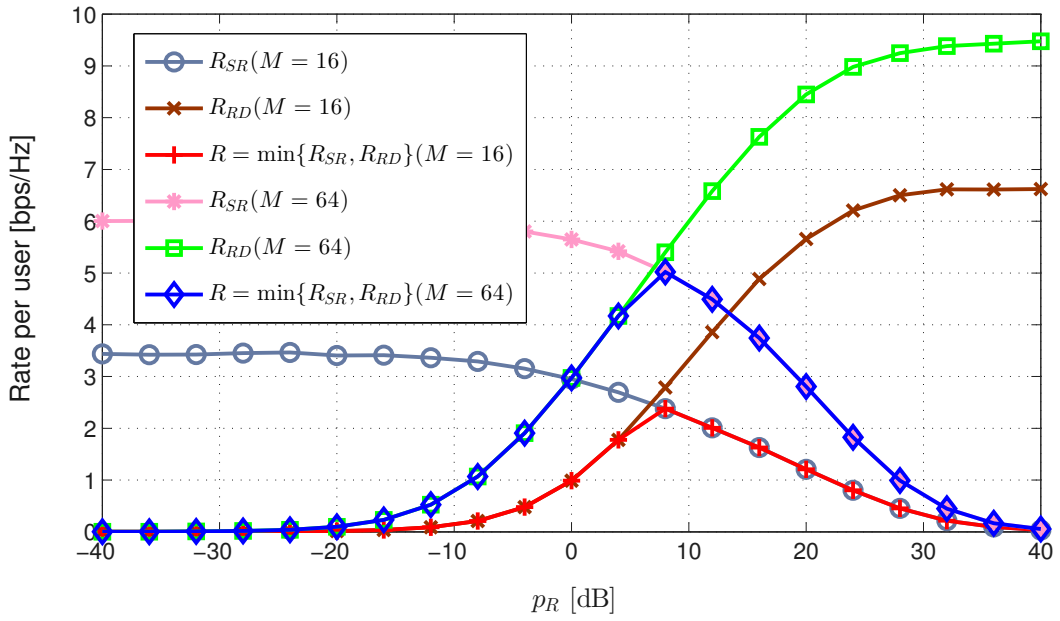

Figure 5.4: Achievable rate per user, for different numbers of antennas M, variance at destinations $\sigma^2_{\mathbf{n}_d} = 1$, $K = 5$ users, and $SNR_R = 8$ dB.

5.3.3 Optimal Power Allocation Algorithm

Finally, the results of the proposed optimization algorithm in section 5.2.2 are evaluated. The objective of this optimization is to find a close-to-optimal power allocation (OPA) that meets the rate constraints of each communication pair and minimizes the overall power of the system. For this evaluation, large-scale fading effects are taken into consideration, more precisely by considering the large-scale gains $\beta_{\text{SR},k}$ and $\beta_{\text{RD},k}$ to be independent variables generated from a log-normal distribution, as proposed in [31, 104], with mean value $m = 1$ and standard deviation $\sigma = 6$ dB. Additionally, the normalized peak power of the sources and relay are set to typical values in practical systems as $p_{S_{0,k}} = 3$ dB and $p_{R_0} = 10$ dB, respectively. In addition, the algorithm iterative parameters are empirically defined as $N_{it} = 10^3$ and $L = 5$, in order to ensure that the channel estimations are sufficiently good and that the algorithm converges to a steady state value, even though it is only guaranteed to be a local minimum of the problem due to the non-convexity of the same. Fig. 5.5 shows the evolution of the powers for source 1 and 2, and the relay power, for six iterations, where the convergence to a local solution is achieved

for the considered algorithm parameters, and for a scenario where $M = 128$, where the variance at destinations is $\sigma^2_{\mathbf{n}_d} = 16$, $K = 10$ users, SNR$_R = 8$ dB, and where the require sum rate of the pairs is 10 Bits/s/Hz.

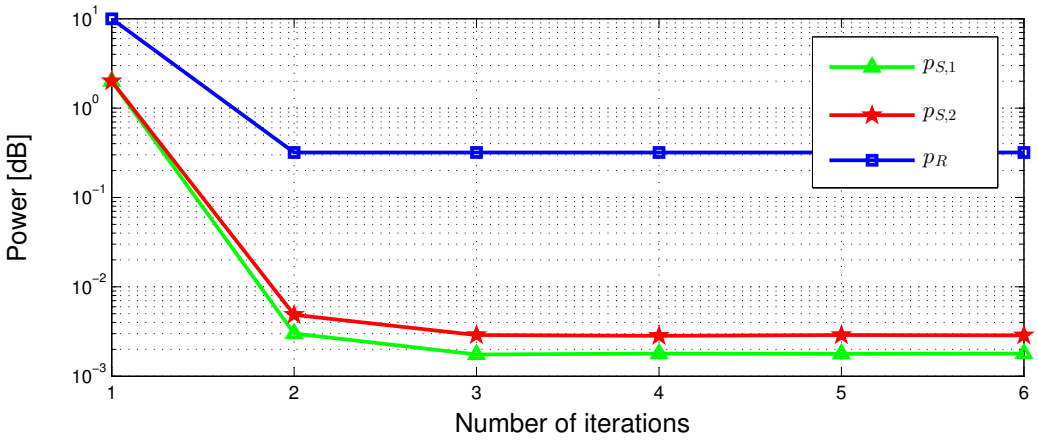

Figure 5.5: Convergence of the powers in algorithm 2 for two sources and for the relay.

The performance of algorithm 2 is determined in terms of the system EE possible to achieve. The target is to have the EE as high as possible, i.e., to use less energy in order to attain the same rate. To that end, the optimal power allocation algorithm is evaluated with different flavors. Firstly, consider the case where the self-interference effects are not taken into account (OPA-NI), and, therefore, the algorithm is applied without considering the filters $\mathbf{F_R}$ and $\mathbf{F_T}$ to reduce the interference effect. This case makes the problem convex, since the non-linearities in $\mathbf{F_R}$ and $\mathbf{F_T}$ are no longer present, so there is no need to an iterative process and a global solution is obtained. The case where the MMSE filter is used (OPA-MMSE) as proposed in 5.2.2 is obviously considered. The algorithm performance is also evaluated when an optimal uniform power allocation (OUPA) is required to serve all users k, which simply corresponds to consider $p_{S,k} = p_S$, for all k, in equation (5.18). Fig. 5.6 depicts the curves of average EE, for different values of desired e2e sum rate, characterized as $\sum_{k=1}^{K} R_{0,k}$. The individual required rates necessary by each user, $R_{0,k}$, are taken from a discrete uniform distribution. This distribution may take values from the set given by

$$R_{0,k} \sim Uniform\Big\{[0.9, 0.95, 1, 1.05, 1.1] \cdot \frac{\sum_{k=1}^{K} R_{0,k}}{K}\Big\},$$

i.e., the rates required by each user have equal probably of being the average rate, or having 5% or 10% variation when compared to it. Thus, it can be ensured that the total rate is always that which is pretended. Moreover, the rates are considered from a discrete distribution, since usually they are associated with communications services, which require minimum discrete rates to ensure a certain quality of service. As may be seen, for the same desired sum rate, the EE of OPA-MMSE is improved significantly when compared to OUPA, while guaranteeing that no link is in outage, i.e., $R_k \geq R_{0,k}$ for all k. Furthermore, since the MMSE filter effectively reduces the self-interference effect, a lower amount of energy is used to achieve the same sum rate when compared with OPA-NI, an effect that becomes

more significant for higher rates.

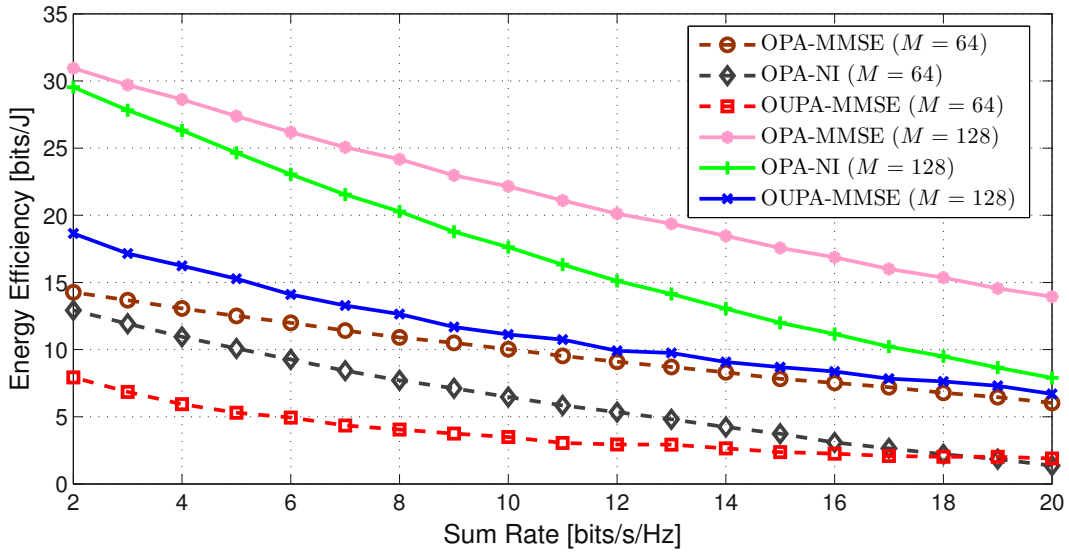

Figure 5.6: Energy efficiency for different power allocation schemes, filters and number of antennas M, for $\sigma^2_{\mathbf{n}_d} = 1$, $K = 10$ pairs, and for $\text{SNR}_\text{R} = 16$ dB.

5.4 Final Considerations

This chapter proposes a full-duplex relay that takes advantage of the orthogonal properties of massive MIMO transmissions, in order to further suppress self-interference. In this case, a relay that applies two stages of filtering is proposed. Firstly, inner ZF filters are used so that both detection and beamforming are performed at the relay. Secondly, an outer MMSE self-interference suppression filter is used, while preserving the e2e channel. The performance of the system was assessed via simulation in terms of BER at the relay and at the destinations, where the effectiveness of the MMSE filter was confirmed for large dimension matrices and the low complexity, high performance capabilities of linear processing in this scenario. The derivation of the e2e achievable rate of the studied system was then provided and a low complexity iterative algorithm to find the optimal power allocation set was proposed, that takes into consideration large-scale fading effects, peak power constraints and the rate requirements for each individual pair. Finally, the optimization problem results were evaluated in terms of EE, and the system employing MMSE filtering outperformed both NI and OUPA, specially for high sum rates.

Chapter 6

Physical Layer Network Coding for Full-Duplex Bidirectional Relaying

(The work in this chapter will be submitted in [12] and in [13])

The exchange of information in a two-way relay network has recently gained plenty of interest in academia, mostly due to the search for new multi-user protocols in future wireless networks. Initially, users in a two-hop network would exchange information through a relay using four time slots (or channel resources). Recently, the advances in network coding have reduced the number of used time slots to three, and even to two, when considering the physical properties of the wireless medium and the properties of network codes. Thus, this chapter incorporates physical layer network coding (PLNC) within the framework of in-band full-duplex, with the objective of asymptotically using only one time slot to exchange data between two terminals via a relay station.

6.1 System Model

This chapter adopts a relay system similar to the previous ones, however, in this case the terminals transmit and receive in in-band full-duplex mode. The previous models study the full-duplex one-way relay channel, where only the relay itself operates in full-duplex mode and only one directional communication link is established. Here, the full-duplex two-way relay channel (FD-TWRC) is assumed, i.e., a system where the relay and both terminals operate using in-band full-duplex transmissions, thus, extending the self-interference problem to all the considered terminals.

Therefore, assume that a terminal $\mathcal{A}$ and a terminal $\mathcal{B}$, both with one receive and one transmit antenna, want to exchange information, which is only possible via a relay station $\mathcal{R}$, since the pathloss between them does not make possible direct link communication. As mentioned before, the exchange of information is done in only one time slot, using the same frequency band, implying that each terminal and the relay transmit simultaneously within the same channel resources. Thus, contrary to a typical PLNC scheme, the multiple access channel (MAC) phase and the broadcast channel (BC) phase, i.e., the phases when the terminals transmit data to the relay and when the relay sends the data back,

respectively, are merged. Consequently, consider that each terminal transmits data streams using single antenna, $x_A(n)$ and $x_B(n)$, respectively, to the relay, which is assumed to have $M_R \geq 1$ antennas to receive and $M_T \geq 1$ antennas to transmit. The relay receives a signal composed of the terminals' messages after their respective channel effects and a component of self-inflicted interference, since it is also broadcasting information for the terminals in $\mathbf{x_R}(n)$ at the same time, as in

$$\mathbf{y_R}(n) = \sqrt{p_A}\mathbf{h_{AR}}x_A(n) + \sqrt{p_B}\mathbf{h_{BR}}x_B(n) + \sqrt{p_R}k_R\mathbf{H_{RR}}\mathbf{x_R}(n) + \mathbf{n_R}(n), \tag{6.1}$$

where $\mathbf{h_{AR}} \in \mathbb{C}^{M_R \times 1}$ and $\mathbf{h_{BR}} \in \mathbb{C}^{M_R \times 1}$ are the channel vectors from the terminal $\mathcal{A}$ and $\mathcal{B}$ to the relay $\mathcal{R}$, $\mathbf{H_{RR}}\mathbb{C}^{M_R \times M_T}$ is the self-interference channel matrix, and $\mathbf{n_R}(n)$ accounts for the additive noise effect at the relay. The powers used for transmitting at terminal $\mathcal{A}$, $\mathcal{B}$ and relay $\mathcal{R}$ are given by p_A, p_B and p_R, respectively. The constant k_R accounts for the residual self-interference present after applying the studied mitigation schemes in chapter 4, as explained in the next section. At the same time, the terminals receive the signal from the relay and are affected by the self-interference inherent in full-duplex communications, yielding the following expressions

$$\begin{aligned} y_A(n) &= \sqrt{p_R}\mathbf{h_{RA}}\mathbf{x_R}(n) + \sqrt{p_A}k_A h_{AA}x_A(n) + n_A(n), \\ y_B(n) &= \sqrt{p_R}\mathbf{h_{RB}}\mathbf{x_R}(n) + \sqrt{p_B}k_B h_{BB}x_B(n) + n_B(n), \end{aligned} \tag{6.2}$$

where again $\mathbf{h_{RA}} \in \mathbb{C}^{1 \times M_T}$ and $\mathbf{h_{RB}} \in \mathbb{C}^{1 \times M_T}$ represent the channel vector from the relay to each terminal, h_{AA} and h_{BB} account for the self-interference at the terminals, and $n_A(n)$ and $n_B(n)$ are the terminals' noise component. Again, the terms k_A and k_B take into consideration the (always present) residual self-interference at the terminals, which is a consequence of imperfect filtering, already discussed. Note that channel reciprocity is not assumed, i.e., the channel from a terminal to the relay is considered to be different from the channel from the relay to the terminal, since the number of transmit and receive antennas at the relay are not necessarily equal. Fig. 6.1 illustrates the described FD-TWRC. Finally, the terminals and the relay employ a network coding scheme to carry information while dealing with the self-interference, which is proposed in the following sections.

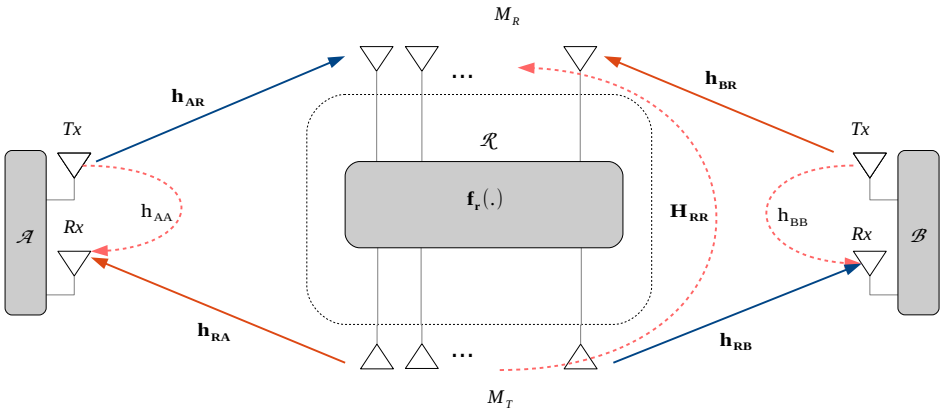

Figure 6.1: Two-way relay channel under full-duplex transmission (FD-TWRC).

6.2 Mitigation of the Self-Interference

The self-interference present at the TWRC has to be mitigated at all the three existing nodes in the considered system. In Chapter 4, the performance of mitigation schemes that can cancel the effect of the linear terms of the self-interference present at a relay station was studied. These can also be applied to end nodes with different antennas to transmit and receive. However, the analyzed methods are not able to effectively eliminate the interference component due to the presence of errors in the estimation of the self-interference channel matrix and in the baseband received signal. To simplify, this chapter takes the mitigation performance into consideration by the gain terms k_R, k_A and k_B, which account for the residual remaining component of the self-interference channel, when compared to the actual level of self-interference at the terminals and at the relay. Therefore, they represent a relative mitigation gain with respect to the case where no filtering process is applied, presented before as natural isolation (NI).

Considering that the terminals only employ one antenna to transmit and one antenna to receive (two antenna design), feedback adaptive cancellation schemes can be used to reduce the undesired effect of the interference component, as in section 4.3. Therefore, it is assumed here that for the relay $\mathcal{R}$, the remaining interference component is given by

$$\begin{aligned}
&\mathbf{H_{RR}x_R}(n) - \widehat{\mathbf{H_{RR}x_R}}(n) \\
&= \left(\tilde{\mathbf{H}}_{\mathbf{RR}} + \mathcal{E}_{\mathbf{H_{RR}}}\right)\left(\tilde{\mathbf{x}}_{\mathbf{R}}(n) + \mathcal{E}_{\mathbf{x_R}}(n)\right) - \widehat{\mathbf{H_{RR}x_R}}(n) \\
&\triangleq k_R \mathbf{H_{RR}x_R}(n),
\end{aligned} \tag{6.3}$$

where, as in section 4.3, $\tilde{\mathbf{H}}_{\mathbf{RR}}$ and $\mathcal{E}_{\mathbf{H_{RR}}}$ represent the estimation of the self-interference channel matrix and the estimation error associated to it, respectively. The estimated transmitted signal at the relay is $\tilde{\mathbf{x}}_{\mathbf{R}}(n)$, while $\mathcal{E}_{\mathbf{x_R}}(n)$ represents the estimation error to its true value. The term $\widehat{\mathbf{H_{RR}x_R}}(n)$ accounts for the estimation of the whole interference component using time-domain and adaptive cancellation methods. Similarly, the same is considered for terminal $\mathcal{A}$ and terminal $\mathcal{B}$, as follows

$$\begin{aligned}
h_{AA}x_A(n) - \widehat{h_{AA}x_A}(n) &\triangleq k_A h_{AA}x_A(n), \\
h_{BB}x_B(n) - \widehat{h_{BB}x_B}(n) &\triangleq k_B h_{BB}x_B(n),
\end{aligned} \tag{6.4}$$

where $\widehat{h_{AA}x_A}(n)$ and $\widehat{h_{BB}x_B}(n)$ are the estimations of the self-interference components at terminal $\mathcal{A}$ and $\mathcal{B}$, respectively. Thus, accordingly to the results in table 4.1, assuming a steady state operation of the methods there proposed, table 6.1 summarizes the typical values of the parameters k_A, k_B and k_R.

	(k_A, k_B, k_R)
Natural isolation	Reference (0 dB)
Conventional time-domain cancellation	-20 dB
Recursive least squares cancellation	-30 to -40 dB
Perfect cancellation	$-\infty$ dB

Table 6.1: Gain of the feedback self-interference cancellation methods when compared to the NI case, in dB (i.e., using $20\log_{10}(\cdot)$).

6.3 Denoise-and-Forward with QPSK

In order to enable each terminal to decode the information coming from its corresponding pair, the system must employ a proper network code that separates the desired information. Thus, the most simple and popular network coding scheme is first described in this section, the objective of which is to make an introduction to this complex and recent topic. The following section focuses on the state-of-the-art protocol and proposes a novel technique, and combines it with the use of massive arrays. The problem of self-interference is addressed separately, since its mitigation scheme is designed in such a way that it does not change the relay protocol. For that reason, the self-interference residual component may be considered together with the thermal noise, which form the effective noise.

This network coding protocol is known as denoise-and-forward (DeF), and is here adapted from [66] to the full-duplex operation with multiple antennas. The main idea is that the relay only needs to forward a function of the jointly received codewords back to the terminals. Firstly, the relay removes the noise present in the jointly received signal (both thermal and residual self-interference noise components) and maps it to a joint codeword, upon which it performs "some function". This function is known at the terminals and at the relay, and is associated with operations over the Galois Field GF(Q), where the transmitted codewords belong to (the Galois field is always assumed to be the integers $\mathbb{Z}_Q$).

Therefore, terminal $\mathcal{A}$ and $\mathcal{B}$ generate a modulated signal $x = \mathcal{M}(S)$, where the mapper is considered as $\mathcal{M} : \mathbb{Z}_Q \to \mathcal{D}_Q$, and creates a one-to-one mapping from the source codewords $S \in \mathbb{Z}_Q = \{0, 1, \ldots, Q-1\}$ to the constellation alphabet of cardinality Q. Assuming a 4-ary alphabet and a quadrature-phase-shift keying (QPSK) constellation, the elements from the finite field $\mathbb{Z}_4 = \{0, 1, 2, 3\}$ are mapped into a normalized QPSK constellation by meas of some $\mathcal{M}$ mapping. During the protocol, the relay receives the superimposed signals from the terminals as in equation (6.1). The first step of this protocol is to perform a joint maximum likelihood (ML) detection of the transmitted codewords (the protocol name comes from the joint detection procedure), S_A and S_B, as

$$(\hat{S}_A, \hat{S}_B) = \underset{(s_1,s_2)\in\mathbb{Z}_Q^2}{\text{argmin}} \quad \| \mathbf{y_R}(n) - \left(\mathbf{h_{AR}}\mathcal{M}(s_1) + \mathbf{h_{BR}}\mathcal{M}(s_2)\right) \|^2 . \tag{6.5}$$

After that, the relay aims at transmitting a network coded data, S_R, back to the terminals, from the estimates $(\hat{S}_A, \hat{S}_B)$, such that the terminals can then decode the codeword from their correspondent pair. Therefore, the function used to generate the relay coded message is $\mathcal{C} : \mathbb{Z}_Q^2 \to \mathbb{Z}_Q,\ S_R = \mathcal{C}(\hat{S}_A, \hat{S}_B)$, which is then mapped into a constellation with the relay mapper $\mathcal{M}_R$. The relay then transmits $x_R[n+d] = \mathcal{M}_R(S_R)$, where d represents the necessary delay for the full-duplex operation.

Finally, the terminals receive a signal containing the data sent by the relay, as in equation (6.2). Each terminal then preforms a ML estimation of the message from the other pair, based on the used network function, as follows

$$\begin{aligned} \hat{S}'_B &= \underset{s\in\mathbb{Z}_Q}{\text{argmin}} \| \mathbf{y_A}(n) - \mathbf{h_{RA}}\mathcal{M}_R(\mathcal{C}(S_A, s)) \|^2, \\ \hat{S}'_A &= \underset{s\in\mathbb{Z}_Q}{\text{argmin}} \| \mathbf{y_B}(n) - \mathbf{h_{RB}}\mathcal{M}_R(\mathcal{C}(S_B, s)) \|^2, \end{aligned} \tag{6.6}$$

where it is assumed that the relay has successfully jointly decoded the terminals codewords, i.e., $\mathcal{C}(\hat{S}_A, \hat{S}_B) = \mathcal{C}(S_A, S_B)$.

6.3.1 Coding Schemes

In order to allow a proper exchange of information, the system should employ a suitable network coding function and used constellations, i.e., a denoising map that is capable of decoding the terminal's information. This denoising map depends directly on the chosen function properties, that have to allow each terminal to correctly extract their desired information, from both the received and its own codeword. For that to happen, there must exist a function $\mathcal{C}$, that operates over the codewords finite field, and that satisfies the following properties, known as the *exclusive law* [66]

$$\begin{aligned} &\mathcal{C}(s_1, s_2) \neq \mathcal{C}(s_1', s_2) \text{ for any } s_1 \neq s_1' \in \mathbb{Z}_Q \text{ and } s_2 \in \mathbb{Z}_Q, \\ &\mathcal{C}(s_1, s_2) \neq \mathcal{C}(s_1, s_2') \text{ for any } s_1 \in \mathbb{Z}_Q \text{ and } s_2 \neq s_2' \in \mathbb{Z}_Q. \end{aligned} \tag{6.7}$$

There must also be a relay mapper, $\mathcal{M}_R$ with the same cardinality of the generated network codeword, S_R. Consider two feasible and practical coding schemes, commonly used in coded networks for their known simplicity and easy implementation. The first is the popular code based on the bit-wise exclusive-or (XOR) operation, i.e.

$$\mathcal{C}: \ \mathbb{Z}_Q^2 \to \mathbb{Z}_Q, \ \mathcal{C}(S_1, S_2) = S_1 \oplus S_2, \tag{6.8}$$

where $\oplus$ represents the bit-wise XOR function (exemplified in the following section). Another possibility is to consider the modulo-Q addition over the reals

$$\mathcal{C}: \ \mathbb{Z}_Q^2 \to \mathbb{Z}_Q, \ \mathcal{C}(S_1, S_2) = [S_1 + S_2] \text{mod } Q, \tag{6.9}$$

i.e., in this case over a finite Galois field GF(Q), of cardinality Q (in this case $\mathbb{Z}_Q$). In the following section the best coding function and mapping scheme is evaluated for the FD-TWRC.

6.3.2 Optimized Constellation Mapping

There are several possibilities to map the codewords from the terminals and from the relay, before each transmission. In this section, only practical per-symbol PLNC is considered rather than the theoretical schemes of per-message PLNC, proposed mainly in information theory works [71], which exploit unpractical infinite size channel correction codes. Instead, a simple QPSK modulation for $\mathcal{M}$ and for $\mathcal{M}_\mathcal{R}$ is assumed, which when spatial diversity is available at the relay can be optimal in terms of maximizing the square distances between received symbols [66], thus, minimizing the error probability. This QPSK mapping at the relay station, $\mathcal{M}_\mathcal{R}$, may be also jointly optimized with the network function in the sense that it can slightly reduce the error probability. In this two-way communication scenario, the probability that each terminal decodes the correct message is related to the following three events:

1. Uplink error: Due to the noise and self-interference present at the relay, the ML decoded symbol

may be wrong, i.e., the joint decoded messages $\mathcal{C}(\hat{S}_1, \hat{S}_2) \neq \mathcal{C}(S_1, S_2)$. Note that due to the *exclusive law*, if one message is wrong, the relay message will also be wrong, for example, if $\hat{S}_1 \neq S_1$ and $\hat{S}_2 = S_2$, $\mathcal{C}(\hat{S}_1, \hat{S}_2) \neq \mathcal{C}(S_1, S_2)$. However, if $\hat{S}_1 \neq S_1$ and $\hat{S}_2 \neq S_2$, it may be the case that $\mathcal{C}(\hat{S}_1, \hat{S}_2) = \mathcal{C}(S_1, S_2)$;

2. Downlink error: Each terminal may detect a message different form $\mathcal{M}_R\big(\mathcal{C}(S_1, S_2)\big)$ due to the existence of self-interference and thermal noise, and as result of the *exclusive law*, the terminals are not able to decode the correct message from their pair;

3. Bit-error: The component of the error which is associated to the number of flipped bits in each constellation symbol and that directly depends on the used mapping scheme.

Using a QPSK modulation (4-ary modulation) at both terminals and relay, it is possible to have three different $\mathcal{M}_{R,4}$ mapping strategies for the two considered network functions, since there are two alternatives in this constellation for the symbols: they can be adjacent or diagonally opposite. Also considering the symmetry of the constellation, there are $\binom{4}{2}/2 = 3$ possibilities. The possible different mapping at the relay for the two considered network functions are shown in table 6.2.

	$\mathcal{C}(S_1, S_2) = S_1 \oplus S_2$				$\mathcal{C}(S_1, S_2) = [S_1 + S_2] \text{mod} Q$			
Pair message (S_A, S_B)	(0,0) (1,1) (2,2) (3,3)	(0,1) (1,0) (2,3) (3,2)	(0,2) (1,3) (2,0) (3,1)	(0,3) (1,2) (2,1) (3,0)	(0,0) (1,3) (2,2) (3,1)	(0,1) (1,0) (2,3) (3,2)	(0,2) (1,1) (2,0) (3,3)	(0,3) (1,2) (2,1) (3,0)
Code $S_R = \mathcal{C}(S_A, S_B)$	0	1	2	3	0	1	2	3
Mapping $\mathcal{M}_{R,4}$: 1)	$+1+j$	$+1-j$	$-1+j$	$-1-j$	$+1+j$	$+1-j$	$-1+j$	$-1-j$
2)	$+1+j$	$-1-j$	$+1-j$	$-1+j$	$+1+j$	$-1-j$	$+1-j$	$-1+j$
3)	$+1+j$	$+1-j$	$-1-j$	$-1+j$	$+1+j$	$+1-j$	$-1-j$	$-1+j$

Table 6.2: QPSK possible mapping schemes for the considered network codes.

The analysis of the above mappings and network function that optimizes the bit error rate (BER) is based on the framework developed in [65]. Also, it is only analyzed the BER performance for the terminal $\mathcal{A}$, which is similar to terminal $\mathcal{B}$. Thus, the average bit error probability is then given by

$$P_{BER,\mathcal{A}} = P(\hat{S}_2' \neq S_2) = \sum_{S_1 \in \mathbb{Z}_Q} P(S_1) \Big[\sum_{S_2 \in \mathbb{Z}_Q} P(S_2) \times \sum_{\tilde{S}_2 \neq S_2} P(\mathcal{M}_{R,Q}(\mathcal{C}(S_1, S_2)) \rightarrow \mathcal{M}_{R,Q}(\mathcal{C}(S_1, \tilde{S}_2))) \times \frac{d_H(B_Q(S_2), B_Q(\tilde{S}_2))}{\log_2 Q} \Big] \tag{6.10}$$

where $P(S_1) = P(S_2) = 1/Q$ are the probabilities of choosing a symbol, and $P(\mathcal{M}_{R,Q}(\mathcal{C}(S_1, S_2)) \rightarrow \mathcal{M}_{R,Q}(\mathcal{C}(S_1, \tilde{S}_2))$ is the pairwise probability of decoding a message S_2 from $\mathcal{B}$ as $\tilde{S}_2$, when terminal's $\mathcal{A}$ message is S_1. The $B_Q : \mathbb{Z}_Q \rightarrow \mathbb{Z}_2^{\log_2 Q}$ function defines the mapping of a codeword into a binary word, which is considered simply as direct conversion to binary with the most significant bit at the left-hand side. Finally, the function $d_H : \mathbb{Z}_2^{2\log_2 Q} \rightarrow \mathbb{Z}$ gives the Hamming distance between two binary words [79]. Following the same procedure done in [65] and defining $X = \mathcal{M}_{R,Q}(\mathcal{C}(S_1, S_2))$ and $\tilde{X} =$

$\mathcal{M}_{R,Q}(\mathcal{C}(S_1, \tilde{S}_2))$, the expression in equation (6.10) may be rewritten in the following way

$$\begin{aligned} P_{BER,\mathcal{A}} = P(\hat{S}_2' \neq S_2) &= \sum_{S_1 \in \mathbb{Z}_Q} P(S_1) \Big[\frac{1}{Q \log_2 Q} \sum_{X \in \mathcal{D}_Q} \sum_{\tilde{X} \neq X \in \mathcal{D}_Q} P(X \to \tilde{X}) \\ &\times d_H(B_Q(x:\ \mathcal{M}_{R,Q}(\mathcal{C}(S_1, x)) = X), B_Q(x:\ \mathcal{M}_{R,Q}(\mathcal{C}(S_1, x)) = \tilde{X})) \Big] \\ &= \frac{1}{Q \log_2 Q} \sum_{X \in \mathcal{D}_Q} \sum_{\tilde{X} \neq X \in \mathcal{D}_Q} P(X \to \tilde{X}) \times \\ &\underbrace{\Big[\sum_{S_1 \in \mathbb{Z}_Q} P(S_1) \times d_H(B_Q(x:\ \mathcal{M}_{R,Q}(\mathcal{C}(S_1, x)) = X), B_Q(x:\ \mathcal{M}_{R,Q}(\mathcal{C}(S_1, x)) = \tilde{X})) \Big]}_{\triangleq N_B(X \to \tilde{X})} \\ &= \frac{1}{Q \log_2 Q} \sum_{X \in \mathcal{D}_Q} \sum_{\tilde{X} \neq X \in \mathcal{D}_Q} P(X \to \tilde{X}) N_B(X \to \tilde{X}). \end{aligned} \tag{6.11}$$

The term $N_B(X \to \tilde{X})$ represents the average on bit errors when terminal $\mathcal{A}$ detects a symbol $\tilde{X}$, given that it was supposed to receive X. The probability of a terminal to detect $\tilde{X}$ knowing X is the correct symbol, $P(X \to \tilde{X})$, may also be decomposed into $P(X \to \tilde{X}) = P(X \to X_R)P(X_R \to \tilde{X})$, where $P(X \to X_R)$ is the probability of decoding X_R knowing that X is the correct symbol to broadcast, and $P(X_R \to \tilde{X})$ is the probability of decoding $\tilde{X}$ where the transmitted symbol was X_R. Therefore, the main objective is to minimize the following expression, by selecting a proper different mapping scheme and a network function:

$$P_{BER,\mathcal{A}} = P(\hat{S}_2' \neq S_2) = \frac{1}{Q \log_2 Q} \sum_{X \in \mathcal{D}_Q} \sum_{\tilde{X} \neq X \in \mathcal{D}_Q} P(X \to X_R)P(X_R \to \tilde{X})N_B(X \to \tilde{X}). \tag{6.12}$$

The analytical computation of (6.12) is possible by evaluating the *a priori* probability of the different combinations of errors for the different mappings and network functions. To this end, it is necessary to evaluate the $2 \cdot Q!$ (for the QPSK it amounts to $2 \cdot 4! = 48$) error component of each probability distribution. Additionally, it is necessary to assume a normal distribution for the effective noise, which encompasses a thermal and a self-interference component. Therefore, based on this analysis, the simulation of the BER curves for the system described is presented for the two considered network coding function, so that it is possible to numerically evaluate the performance of the system for different levels of both interference and thermal noise.

Comparison of the Network Coding Schemes

Consider the system introduced in section 6.1 with $M_R = 4$ receive antennas and $M_T = 1$ transmit antennas. The channels' coefficients are generated from a complex normal distribution, $\mathbf{h_{AR}}$, $\mathbf{h_{BR}}$, $\mathbf{h_{RR}} \sim \mathcal{CN}(0, \mathbf{I})$, and h_{RA}, h_{RB}, h_{AA}, $h_{BB} \sim \mathcal{CN}(0, 1)$. It is considered that the system employs feedback cancellation techniques to mitigate the self-interference, where $k_R = k_A = k_B = -20$ dB. The thermal noise normalized power is -10 dB and assumed to be the same in the terminals and in the relay antennas. Fig. 6.2 depicts the BER for two different mappings and network functions, where uniform power allocation is assumed at the relay and at the terminals, i.e., $\mathsf{P} = p_A = p_B = p_R$.

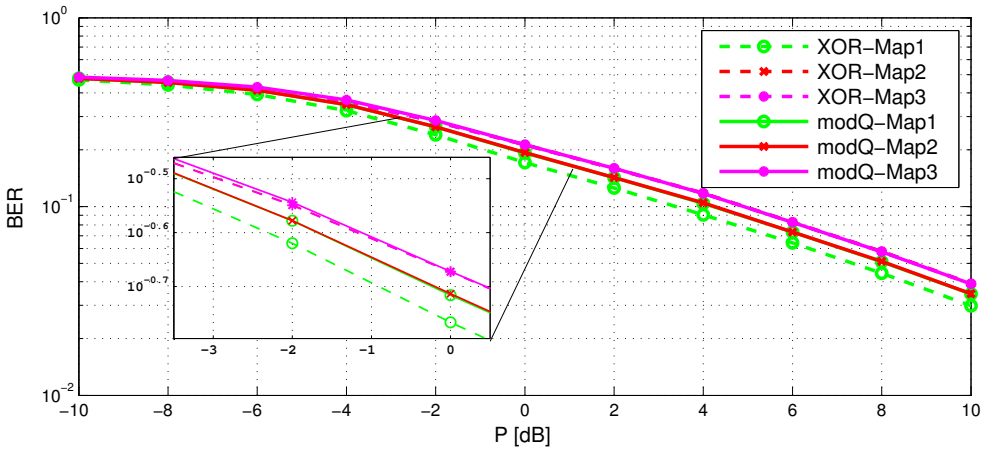

Figure 6.2: BER performance of the different possible mapping schemes and considered network functions for the FD-TWRC, with $\sigma^2_{\mathbf{n}} = -10$ dB and $k_R = k_A = k_B = -20$ dB, with $M_R = 4$.

It is possible to observe that the best combination of mapping and network function is to use the map number 1) in table 6.2 with the XOR function. This fact may be explained if the symmetry present in the denoising scheme is considered. Since map 1) corresponds to Grey mapping, the value taken by $N_B(X \to \tilde{X})$ is minimized by the Hamming distances between codewords. Also the XOR function symmetry between codewords present in table 6.2, reduces the joint error components $P(X \to X_R)$ and $P(X_R \to \tilde{X})$, since if a codeword is detected with an error at the relay, it is probable that it will be mistaken with its neighbor constellation point, which is also a neighbor in the finite field. Thus, when it is sent back to the terminals, there is a higher probability of recovering the original codeword, by having two consecutive errors. However, by changing the mapping in the XOR function, this symmetry probability no longer holds, and for that reason the two remaining BER curves become the worst. On the other hand, the first two mappings, $\mathcal{M}_R$, joined with the $[\cdot]\text{mod}Q$ function attain the same performance. In this case, the two maps have different distributions in terms of joint $P(X \to X_R)$ and $P(X_R \to \tilde{X})$ probabilities conjugated with $N_B(X \to \tilde{X})$. For map 2) there are a larger number of constellation points that, when flipped, are close to the correspondent finite field codeword. However, the term $N_B(X \to \tilde{X})$ takes lower values in the case of map 1), which compensates for the overall probability of error. Nevertheless, the difference between the considered curves is small (but significant, ≈ 2 dB), indicating that both network functions may be employed in such systems without significant BER performance degradation.

6.4 Compute-and-Forward with Lattice Coding

Besides its simplicity, the DeF PLNC scheme achieves good performance both in terms of BER and rate gain. However, its design is very basic, which gives the idea that a better scheme may be employed to increase the system capacity. Thus, the recent developed theory of the protocol termed compute-and-forward (CF) is studied for the case of bidirectional relaying in this section [105, 106]. Furthermore, the use of massive MIMO is proposed and studied for the first time in such scenario.

As mentioned in chapter 2, the concept is that the relay forwards a function of the superimposed

received symbols. However, in opposition to DeF, the network function is directly employed in the transmitted constellation, i.e., there is an isomorphism between the properties of the wireless medium and the mapped codewords with the properties given in (6.7). The main idea consists of the fact that any sum of two transmitted symbols is itself a symbol, or is physically related to one. In practice, this isomorphism is done by resorting to nested lattice codes, which are introduced as follows.

6.4.1 Nested Lattice Coding

As briefly introduced in Chapter 3, a lattice is a n-dimensional discrete set of points in $\mathbb{R}^n$ represented by $\Lambda = \{\mathbf{x} = \mathbf{M}\mathbf{z},\ \mathbf{z} \in \mathbb{Z}\}$, where $\mathbf{M}$ is called the generator matrix of the lattice. The most important property of lattices is linearity, which guarantees that any integer combination of points of one lattice is a point of the same lattice, i.e., $a\mathbf{x} + b\mathbf{y} \in \Lambda$, for $\mathbf{x}, \mathbf{y} \in \Lambda$ and $a, b \in \mathbb{Z}$. Associated with any lattice is the lattice quantizer Q_Λ, that maps a real n-dimensional vector $\mathbf{x}$ to the nearest point in Λ in terms of euclidean distances, i.e., $\mathrm{Q}_\Lambda(\mathbf{x}) = \text{argmin}_{\lambda\in\Lambda} \parallel \mathbf{x} - \lambda \parallel$. The region that quantizes to a lattice point is called the Voronoi region. The fundamental Voronoi region of a lattice, $\mathcal{V}_\Lambda$, corresponds to the Voronoi region of the zero vector, i.e., $\mathcal{V}_\Lambda = \{\mathbf{x} :\ \mathrm{Q}_\Lambda(\mathbf{x}) = \mathbf{0}\}$. Also, the operation denoted usually by mod_Λ returns the quantization error with respect to Λ, given by $\mathbf{x} \in \mathbb{R}^n :\ [\mathbf{x}]\text{mod}_\Lambda = \mathbf{x} - \mathrm{Q}_\Lambda(\mathbf{x})$. These properties as well as the ones that follow next are thoroughly described in [107, 108]. Thus, it is possible to define a nested lattice code as being the set of all points of a fine lattice, Λ_F, that falls within the fundamental Voronoi region of a coarse lattice, Λ_C, as

$$\mathcal{L} = \Lambda_\mathsf{F} \cap \mathcal{V}_{\Lambda_\mathsf{C}}, \in \mathbb{R}^n = \{\lambda = [\lambda_\mathsf{F}]\text{mod}_{\Lambda_\mathsf{C}}, \lambda_\mathsf{F} \in \Lambda_\mathsf{F}\}. \tag{6.13}$$

These nested lattice codes are used in this context because they achieve the capacity of the additive white Gaussian noise (AWGN) channel [69] and obtain high rates in the case of multiple access channels [57]. To do so, these codes are generated from low-density parity-check codes (LDPC) over finite fields, by applying the methods designated in literature as *construction A* or *construction D*, in order to design a fine lattice with larger dimensions [71]. In the context of this work, only a nested lattice code known *a priori* is assumed, and with simple properties, which facilitates the process of simulation and analysis.

To that end, consider that terminal $\mathcal{A}$ and $\mathcal{B}$ want to exchange messages, or codewords, S_A and S_B, respectively, assumed to belong to a prime finite field, $\mathbb{F}_Q^n$ (with Q prime). Initially, each terminal maps its message to the same nested lattice constellation. The mapping process is done by means of a function $\phi(\cdot)$, that translates the isomorphism between codewords and constellation points, and is defined as

$$\begin{aligned} \phi : \mathbb{F}_Q^n \rightarrow \mathcal{L} = \Lambda_\mathsf{F} \cap \mathcal{V}_{\Lambda_\mathsf{C}} (\in \mathbb{R}^n), \\ S_A, S_B \rightarrow \mathbf{x_A}, \mathbf{x_B}. \end{aligned} \tag{6.14}$$

Moreover, the sequence of messages mapped to lattice points, present in $x_A(n)$ and $x_B(n)$, are considered to have normalized power, i.e., $\frac{1}{n} \parallel \mathbf{x_A} \parallel^2 \leq \frac{1}{n} \parallel \mathbf{x_B} \parallel^2 \leq 1$. As previously described, the relay and the terminals experience complex channels. Thus, to adapt the transmit sequences to this kind of channel, a two dimensional orthogonal lattice ($n = 2$) is considered, which "lives" in the complex plane,

i.e., there is a simple conversion from $\mathbb{R}^2$ to $\mathbb{C}$. This lattice is known in the literature as Gaussian lattice, proposed in [71], and is defined as

$$\Lambda_G = \{x \in \mathbb{C} : x = c_R \cdot z_1 + j c_I \cdot z_2;\ z = (z_1, z_2) \in \mathbb{Z}^2 \text{ and } c_1, c_2 \in \mathbb{R}\}. \tag{6.15}$$

In order to define the nested lattice code, the fine lattice, $\Lambda_\mathsf{F} \in \Lambda_G$, is first considered to be generated with parameters $c_R = 2$ and $c_I = 3$, while the coarse lattice, by the definition in equation (6.13), is consequently given by $\Lambda_\mathsf{C} = Q \cdot \lambda_\mathsf{F}, \in \Lambda_G$, i.e., it has parameters $c_R = 6$ and $c_I = 9$. Thus, it is possible to obtain a nested lattice codebook in the complex field $\mathbb{C}$, denoted as $\mathcal{L}_G$, where the function that gives the isomorphism between codewords and constellation points, ϕ, is easily obtained in [71]. Therefore, the use of this nested lattice code is assumed, for codebook with length $Q = 3$ and dimension $n = 2$, where codewords $\mathbb{Z}_3^2 = \{(0,0), (0,1), (1,0), (1,1), (1,2), (2,1), (2,2)\}$ are mapped into the points $\{0+0j, 0+3j, 2+0j, 2+3j, 2-3j, -2+3j, -2-3j\}$, respectively, by means of ϕ. Fig 6.3 depicts the used nested lattice code with the codewords near to their corresponding constellation point (the mapping is the same for each box). Although the codebook length is small, it is possible to easily change the considered lattice so that Q can take higher values. Finally, the considered protocol for bidirectional relaying in an in-band full-duplex system that uses the described nested lattice to carry the desired information by each source is following described.

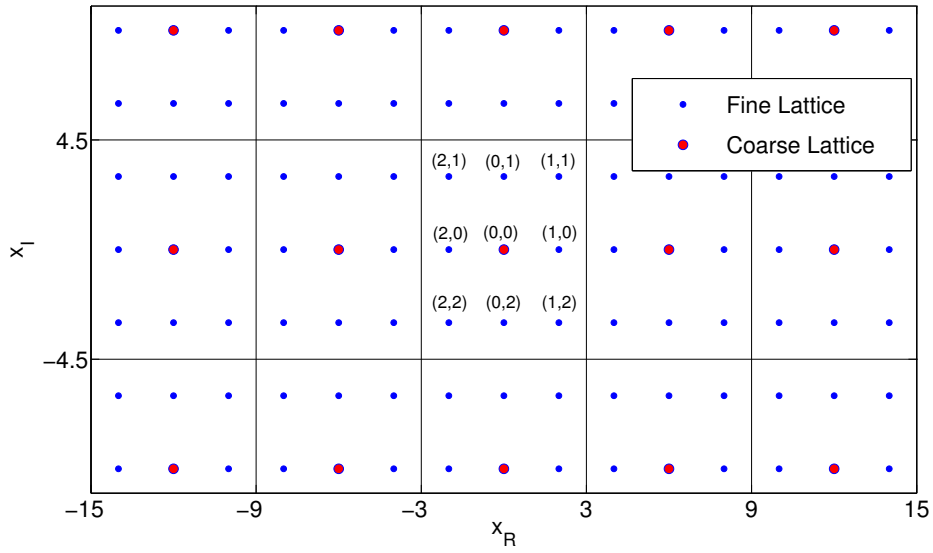

Figure 6.3: The used Gaussian nested lattice code with mapping function $\mathbb{Z}_{Q=3}^2 \to \mathbb{C}:\ x = \phi(S)$.

6.4.2 Relaying Protocol for the TWRC

In the first stage of communication, the relay receives a combination of the terminals' messages, i.e. $x_A = \phi(S_A)$ and $x_B = \phi(S_B)$, plus self-interference and thermal noise, as in equation (6.1). For the CF protocol assume first that $M_T = M_R = 1$. The relay aims to detect an integer linear combination of the transmitted terminal symbols. These symbols should reach the terminal changed only by real

coefficients, i.e., the protocol is only designed to tolerate a scaling in the lattice points and can not handle any phase rotation of the lattice structure. To combat this problem, it is assumed that each terminal has the knowledge of their correspondent channel, so that they can employ a transmit gain in order to cancel the complex effect of it. This gain should be normalized in order not to change the terminals' transmit power. Therefore, having each terminal transmitting with unit power, (6.1) can be rewritten for this case as

$$\begin{aligned} y_R(n) &= h_{AR}\Big(\frac{h_{AR}^*}{< h_{AR} >}x_A(n)\Big) + h_{BR}\Big(\frac{h_{BR}^*}{< h_{BR} >}x_B(n)\Big) + \tilde{n}(n), \\ &= g_{AR}\cdot\phi(S_A) + g_{BR}\cdot\phi(S_B) + \tilde{n}(n), \end{aligned} \tag{6.16}$$

where the $< \cdot >$ represents the norm of a complex number, $\tilde{n}(n)$ accounts for the equivalent Gaussian noise (since the thermal noise is assumed to be Gaussian, as well as the residual self-interference), and $g_{AR} = \left(\frac{h_{AR}h_{AR}^*}{<h_{AR}>}\right)$ and $g_{BR} = \left(\frac{h_{BR}h_{BR}^*}{<h_{BR}>}\right)$ are the equivalent real channel gains. Also, $p_A = p_B = p_R = 1$ is assumed. As already stated, the target of the relay is to recover an integer linear combination of the original transmitted symbols and map it back to a nested lattice code point, in the form of

$$v = [a_A \cdot x_A + a_B \cdot x_B]\text{mod}_{\Lambda_C}, \tag{6.17}$$

where $x_A, x_B \in \mathcal{L}_G$, belong to the nested lattice code, and $a_A, a_B \in \mathbb{Z}$ are freely selected by the relay to quantize the equivalent real channel coefficients, which form the so-called lattice network code. The latter tries to approximate the channel output to a point in the nested lattice constellation, i.e., it tries to interpret the effect of a real channel by means of linear integer combinations. To this end, the relay employs the following steps, as detailed in [67]:

Processing Stage at the Relay for each $y_R(n)$:

1) Scale the received relay signal, using the MMSE scaling factor: $\tilde{y}_R = \alpha \cdot y_R$;
2) Quantize $\tilde{y}_R$ to the closest fine lattice point: $\text{Q}_{\Lambda_F}(\tilde{y}_R)$;
3) Perform modulo operation with respect to the coarse lattice to obtain back a point in the nested lattice code: $x_R = [\text{Q}_{\Lambda_F}(\tilde{y}_R)]\text{mod}_{\Lambda_C}$.

The first step consists of scaling the received signal, in a way that is possible to reduce the error when approximating the real equivalent channel by an integer one. Consider that $\mathbf{a} = [a_A, a_B]$ is the network code that tries to approximate the channel vector $\mathbf{g} = [g_{AR}, g_{BR}]$. The estimated signal at the relay depends on the scaling factor α and on the chosen network code $\mathbf{a}$. This signal may be written in the following formulation:

$$\begin{aligned} x_R &= [\text{Q}_{\Lambda_F}(\tilde{y}_R)]\text{mod}_{\Lambda_C} \\ &= [\text{Q}_{\Lambda_F}([\alpha \cdot y_R]\text{mod}_{\Lambda_C})]\text{mod}_{\Lambda_C} \\ &= \text{Q}_{\Lambda_F}([\alpha \cdot (g_{AR} \cdot x_A + g_{BR} \cdot x_B + \tilde{n})]\text{mod}_{\Lambda_C}) \\ &= \text{Q}_{\Lambda_F}([a_A \cdot x_A + a_B \cdot x_B + (\alpha \cdot g_{AR} - a_A) \cdot x_A + (\alpha \cdot g_{BR} - a_B) \cdot x_B + \alpha \cdot \tilde{n}]\text{mod}_{\Lambda_C}) \\ &= \text{Q}_{\Lambda_F}([v]\text{mod}_{\Lambda_C} + [(\alpha \cdot g_{AR} - a_A) \cdot x_A + (\alpha \cdot g_{BR} - a_B) \cdot x_B + \alpha \cdot \tilde{n}]\text{mod}_{\Lambda_C}), \end{aligned} \tag{6.18}$$

where v is the desired relay signal. The first step comes from the fact that the quantization operation of a point to a lattice is interchangeable with the modulo function over the same lattice, while the remaining steps are straightforward expression substitutions [107]. Thus, the relay effective noise is

$$\| (\alpha \cdot g_{AR} - a_A) \cdot x_A + (\alpha \cdot g_{BR} - a_B) \cdot x_B + \alpha \cdot \tilde{n} \|^2 = (\alpha \cdot g_{AR} - a_A)^2 + (\alpha \cdot g_{BR} - a_B)^2 + \alpha^2 \sigma_{\tilde{n}}^2,$$

where independently generated symbols and a total noise-plus-interference power level of $\sigma_{\tilde{n}}^2$ is assumed. The minimum mean square error (MMSE) scaling factor is consequently obtained such that the equivalent noise power is minimized with respect to α, given $\mathbf{a} \neq \mathbf{0}$ in such a way that equation (6.7) is satisfied. As shown in [67], it is possible to obtain

$$\alpha = \frac{\gamma \cdot \mathbf{g}\mathbf{a}^H}{1 + \gamma \cdot \mathbf{g}\mathbf{g}^H}, \tag{6.19}$$

where γ represents the signal-to-interference-plus-noise ratio (SINR) and is computed at the relay as $\gamma = \frac{g_{AR}^2 + g_{BR}^2}{k_R + \sigma_{\mathbf{n}}^2}$. The choice of the optimal network code is also derived based on (6.18), by means of maximizing the total amount of information flow, which is equivalent to minimizing the equivalent noise power with respect to $\mathbf{a}$. As demonstrated by Feng *et al.* [71], this corresponds to minimize the term $\mathbf{a}\mathbf{M}\mathbf{a}^H$, where matrix $\mathbf{M}$ is given by

$$\mathbf{M} = \gamma \cdot \mathbf{I} - \frac{\gamma^2}{\gamma \cdot \mathbf{g}\mathbf{g}^H + 1} \cdot \mathbf{g}^H \mathbf{g}.$$

In order to do so, observing that $\mathbf{M}$ is an Hermitian and positive-definite matrix, one may perform a Cholesky decomposition, i.e., $\mathbf{M} = \mathbf{L}\mathbf{L}^H$, where $\mathbf{L}$ is a lower triangular matrix, to reformulate it as

$$\mathbf{a_{Feng}} = \underset{\mathbf{a} \neq \mathbf{0}}{\arg\min.} \quad \| \mathbf{a}\mathbf{L} \|, \tag{6.20}$$

solved using the Fincke-Pohst algorithm for finding the solution (similar to a Sphere Decoder)[108].

After processing the received information, the relay sends back to the terminals $x_R(n)$. Upon reception of this signal, after passing through a wireless channel as in (6.2), each terminal employs the following steps to extract the desired information from the received lattice point and from its own message:

Processing Stage at Terminal $\mathcal{A}$ (similar for $\mathcal{B}$):

1) Decode the relay transmitted signal, taking into consideration the complex channel effect, using the ML detector for the nested lattice code: $\hat{x}_R = \arg\min_{\lambda \in \Lambda_F \cap \mathcal{V}_{\Lambda_C}} \| y_A - h_{RA}\lambda \|$;
2) Map the received information back to the finite field:
First component $u_1 = \phi^{-1}(\mathcal{R}\{\hat{x}_R\}) = [q_A S_{A,1} + q_B S_{B,1}] \text{mod}_Q$ and
second component $u_2 = \phi^{-1}(\mathcal{I}\{\hat{x}_R\}) = [q_A S_{A,2} + q_B S_{B,2}] \text{mod}_Q$ (where the coefficients q_A, q_B are naturally given by $q_A = [a_A] \text{mod}_Q$ and $q_B = [a_B] \text{mod}_Q$);
3) Subtract own information: $w_{A,1} = [u_1 - q_A S_{A,1}] \text{mod}_Q = q_B S_{B,1}$ and
$w_{A,2} = [u_2 - q_A S_{A,2}] \text{mod}_Q = q_B S_{B,2}$;
4) Remove channel integer effect over the finite field, q_B, to obtain $\hat{S}_B = (\hat{S}_{B,1}; \hat{S}_{B,2})$.

where $\mathcal{R}\{\cdot\}$ and $\mathcal{I}\{\cdot\}$ take the real and imaginary part of a complex number. respectively.

The process described above allows each terminal to extract the desired information from the linear combination of the transmitted signals and the knowledge of the network code. However, the information theoretic deduction of the optimal network code, in (6.20), does not take into consideration practical details for the TWRC. Note that the correct recovering of the messages dependents on the integer coefficients q_A, q_B, which reflect the channel effect in the finite field. Therefore, none of them should be zero in order to ensure that no message is lost during the terminal's decoding process. As proposed by Mejri in [105], by not allowing q_A, q_B to be equal to zero, the performance of CF improves drastically. This is done by changing the problem in (6.20), to include the aforementioned constraint

$$\mathbf{a_{Mejri}} = \underset{q_A=[a_A]\text{mod}_Q\neq 0, q_B=[a_B]\text{mod}_Q\neq 0}{\text{arg min.}} \| \mathbf{aL} \| . \tag{6.21}$$

The following simulation work uses a brute force approach for finding both optimal network code for problem 6.20 and 6.21, since only few iterations are need for the considered parameter.

Performance with Estimation Errors

The symbol error rate (SER) of the considered bidirectional relaying CF protocol is evaluated, for a single antenna system. It is noted that for the isomorphism between constellation points and codewords, there is the need to have a *prime* finite field, thus, a comparison is not made with the DeF in terms of BER. This point is actually one of the main drawbacks of this protocol, which were initially developed in the information theory abstraction and still lacks some implementation details. Nevertheless, the performance of the CF scheme is compared with an equivalent direct machine-to-machine (m2m) transmission, i.e., direct communication between the two terminals with ML detection for the same nested lattice constellation. Additionally, the above presented network codes and the effect of errors in the estimations of the channels are compared, since the CF proposed protocol directly depends on it. To that end, assume symmetry for the channel coefficients, i.e., $h_A = h_{AR} = h_{RA}$ and $h_B = h_{BR} = h_{RB}$, and also that each channel coefficient has Rayleigh fading distribution with unitary normalized power. Furthermore, it is considered that each terminal and the relay only have access to erroneous estimations of the channel, modeled with an additive perturbation $\mathcal{E}_{h_A}, \mathcal{E}_{h_B}$, both drawn from $\mathcal{CN}(0, \sigma_h^2)$, so that $\hat{h}_A = h_A + \mathcal{E}_{h_A}$ and $\hat{h}_B = h_B + \mathcal{E}_{h_B}$. Fig. 6.4 depicts the SER curves for the considered protocol in such scenario and for different values of self-interference and thermal noise power. Considering that $k = k_R = k_A = k_B$ and that $\mathbf{n_R}$, n_A and n_B have entries generated from a complex Gaussian distribution with normalized power σ^2, the total interference-plus-noise power at each antenna is defined as $\sigma_{eq}^2 = k + \sigma^2$. It can be observed that the network code proposed by Feng (blue curve) stalls for high values of noise power, since for network codes that are multiple of the finite field size is not possible to recover the desired messages. By introducing the correction proposed by Mejri, the performance of the protocol is drastically improved when there are no estimation errors (green curve). This curve actually has the same diversity of a direct m2m transmission with the ML detector (black curve), i.e., the terminals exchanging directly data without using the relay, which may be regarded as the asymptotic target for any network

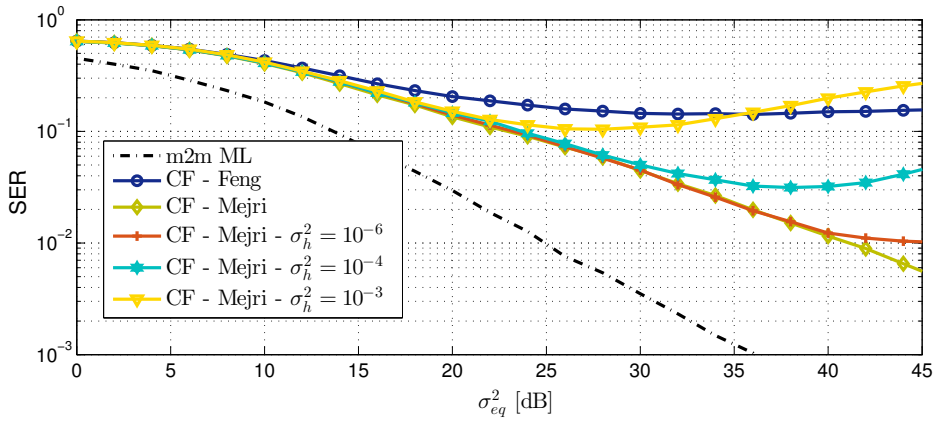

Figure 6.4: SER performance of the bidirectional CF protocol for different values of σ^2_{eq} and for different powers of the channel estimation errors σ^2_h.

scheme. Moreover, the shift between these two curves is caused mainly by the error at the relay from the erroneous approximation of a real channel by a integer one. When introducing estimation errors, the remaining SER curves start to initially tend to a floor stage and then tilt up towards higher values of SER. Since the protocol requires perfect channel state information (CSI), this unknown error component is not taken into consideration by the network code and, as expected, the system performance rapidly deteriorates when the errors in the channel estimations get large, which increases for high values of SINR due to the MMSE scaling coefficient α.

6.4.3 The Effect of Massive MIMO

The presented CF PLNC scheme for the TWRC can in fact be improved by employing massive antenna arrays at the relay station. For this reason, a PLNC system similar to the one above is proposed, however, each terminal now has N_T transmit and receive antennas. The relay uses several M_R antennas to receive, considered much larger than N_T, and has $M_T = N_T$ antennas to transmit the information back to the terminals. Fig. 6.5 shows the considered relaying system for $N_T = 2$. The following described scheme involves three major techniques that, to the best of our knowledge, are put together for the first time: full-duplex, PLNC with CF, and massive MIMO.

Assume that each terminal independently generates several streams of data, $S_{A,i}, S_{B,i} \in \mathbb{Z}_3^2$, for each antenna $i = 1, \cdots, N_T$, which are then mapped accordingly to the considered nested lattice code as in (6.14), to form $\mathbf{x_A}, \mathbf{x_B} \in \mathbb{C}^{N_T \times 1} (\in \mathcal{L}_G^{N_T \times 1})$. These symbols reach the relay and add up in the following manner

$$\begin{aligned} \mathbf{y_R}(n) &= \mathbf{H_{AR}}\mathbf{x_A}(n) + \mathbf{H_{BR}}\mathbf{x_B}(n) + k_R\mathbf{H_{RR}}\mathbf{x_R}(n) + \mathbf{n_R}(n) \\ &= \mathbf{H_{AR}}\mathbf{x_A}(n) + \mathbf{H_{BR}}\mathbf{x_B}(n) + \tilde{\mathbf{n}}_\mathbf{R}(n), \end{aligned} \tag{6.22}$$

where $\mathbf{H_{AR}} \in \mathbb{C}^{M_R \times N_T}$ and $\mathbf{H_{BR}} \in \mathbb{C}^{M_R \times N_T}$, $\mathbf{H_{RR}} \in \mathbb{C}^{M_R \times M_T}$, and where $\tilde{\mathbf{n}}_\mathbf{R}(n) \in \mathbb{C}^{M_R \times 1}$ accounts for both residual self-interference and thermal noise term. The idea is to explore the orthogonality between large dimension matrices to extract an independent combination of each transmitted stream.

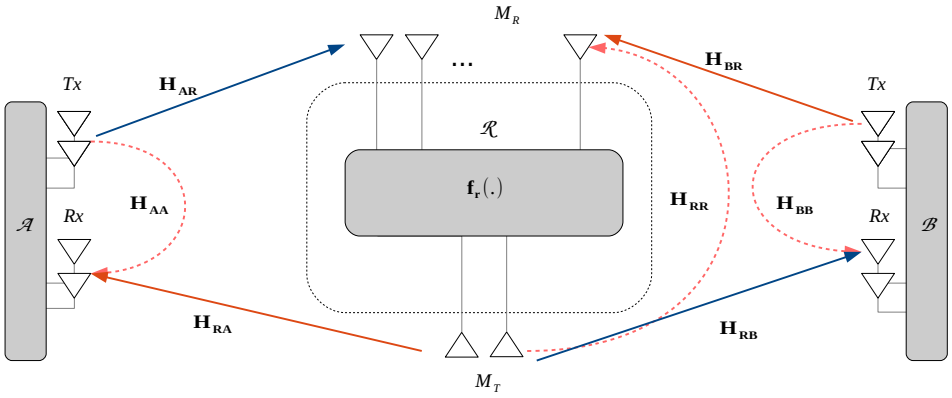

Figure 6.5: Massive MIMO two-way relay channel with full-duplex operation, for $N_T = 2$.

Thus, the relay wants to obtain an independent linear combination of each antennas stream of transmitted data, now reformulated as

$$\Big[\mathbf{D_A x_A}(n) + \mathbf{D_B x_B}(n)\Big] \text{mod}_{\Lambda_C}, \tag{6.23}$$

where $\mathbf{D_A}, \mathbf{D_B} \in \mathbb{Z}^{N_T \times N_T}$ are diagonal matrices with integer entries forming the network code.

As previously mentioned, the nature of space-time communications distort the received signal, both in terms of inter-pair interference (IPI), but also in terms of a rotation in the received constellation. For these reasons, in order to recover the information as in (6.23), one relies on the massive MIMO orthogonality property to ensure a good performance of the linear detection filters. Therefore, instead of employing a transmit gain, it is proposed that the relay first processes the received signal with zero forcing (ZF) filters such that the interference is removed. Equation (6.24) shows the procedure, where it is performed and added the output of a ZF filter for channel $\mathbf{H_{AR}}$ and channel $\mathbf{H_{BR}}$,

$$\begin{aligned}
\mathbf{y_P}(n) =& \mathbf{H_{AR}}^{\dagger}\mathbf{y_R}(n) + \mathbf{H_{BR}}^{\dagger}\mathbf{y_R}(n) \\
=& (\mathbf{H}_{\mathbf{AR}}^{H}\mathbf{H_{AR}})^{-1}\mathbf{H}_{\mathbf{AR}}^{H}\mathbf{y_R}(n) + (\mathbf{H}_{\mathbf{BR}}^{H}\mathbf{H_{BR}})^{-1}\mathbf{H}_{\mathbf{BR}}^{H}\mathbf{y_R}(n) \\
=& \big(\mathbf{H_{AR}}^{\dagger}\mathbf{H_{AR}}\mathbf{x_A}(n) + \mathbf{H_{BR}}^{\dagger}\mathbf{H_{BR}}\mathbf{x_B}(n)\big) \\
&+ \big(\mathbf{H_{BR}}^{\dagger}\mathbf{H_{AR}}\mathbf{x_A}(n) + \mathbf{H_{AR}}^{\dagger}\mathbf{H_{BR}}\mathbf{x_B}(n)\big) + \big(\mathbf{H_{BR}}^{\dagger} + \mathbf{H_{AR}}^{\dagger}\big)\tilde{\mathbf{n}}_{\mathbf{R}}(n) \\
=& \underbrace{\mathbf{D_A x_A}(n) + \mathbf{D_B x_B}(n)}_{\text{desired component}} + \underbrace{\tilde{\mathbf{n}}_{\mathbf{R}}^{\star}(n)}_{\text{equivalent total noise}}
\end{aligned} \tag{6.24}$$

where $\mathbf{y_P}(n) \in \mathbb{C}^{N_T \times 1}$ is the signal that is given to the CF protocol. Thus, by employing this technique with perfect CSI, it is possible to actually obtain a perfect sum of the terminals transmitted message, i.e., having an unitary network code ($\mathbf{D_A} = \mathbf{D_B} = \mathbf{I}$). However, the total amount of interference and noise are the main obstacle to this procedure. The equivalent total noise in (6.24) is split in several terms for analysis purposes:

1. Cross terms interference from the proposed protocol in (6.24): $\big(\mathbf{H_{BR}}^{\dagger}\mathbf{H_{AR}}\mathbf{x_A}(n) + \mathbf{H_{AR}}^{\dagger}\mathbf{H_{BR}}\mathbf{x_B}(n)\big)$;
2. Self-interference noise term: $\big(\mathbf{H_{BR}}^{\dagger} + \mathbf{H_{AR}}^{\dagger}\big)k_R\mathbf{H_{RR}}\mathbf{x_R}(n)$;

3. Thermal noise term: $(\mathbf{H_{BR}}^{\dagger} + \mathbf{H_{AR}}^{\dagger})\mathbf{n_R}(n)$;

One may initially think that the interference and noise terms may be the impossible to overcome in the proposed system. Nonetheless, the massive MIMO properties ensure that independent and randomly generated infinite dimension matrices are orthogonal. Therefore, the first term of interference becomes then

$$\mathbf{H_{BR}}^{\dagger}\mathbf{H_{AR}} \to \mathbf{0}, \mathbf{H_{AR}}^{\dagger}\mathbf{H_{BR}} \to \mathbf{0}, \text{ as } M_R \to \infty \tag{6.25}$$

which in practice does not pose any problem for large M_R antennas [31, 47]. The second term, self-interference, is treated with proper techniques that are translated into k_R, and is also mitigated with the orthogonality property between $(\mathbf{H_{BR}}^{\dagger} + \mathbf{H_{AR}}^{\dagger})$ and $\mathbf{H_{RR}}$. Finally, the thermal noise term is also reduced with the same principle, which is the one that guarantees a close to optimal performance with a ZF detector when using massive MIMO transmissions [46]. Thus, the CF protocol stages described in 6.4.2, in this case considering a unitary code, are adapted to massive MIMO relaying, in order to process each received stream of data, $y_{P,i}(n) = x_{A,i}(n) + x_{B,i}(n) + \tilde{n}_{R,eq,i}(n)$, for each transmit antenna $i = 1, \cdots, N_T$, and each terminal received symbol

$$\mathbf{y_A}(n) = \mathbf{H_{RA}}\mathbf{x_R}(n) + \tilde{\mathbf{n}}_{\mathbf{A}}(n), \ \mathbf{y_B}(n) = \mathbf{H_{RB}}\mathbf{x_R}(n) + \tilde{\mathbf{n}}_{\mathbf{B}}(n), \tag{6.26}$$

where $\mathbf{H_{RA}} \in \mathbb{C}^{N_T \times M_T}$ and $\mathbf{H_{RB}} \in \mathbb{C}^{N_T \times M_T}$, and where $\tilde{\mathbf{n}}_{\mathbf{A}}, \tilde{\mathbf{n}}_{\mathbf{B}} \in \mathbb{C}^{N_T \times 1}$ take into consideration the residual self-interference and thermal noise components, in the same previous fashion. Finally, the protocol is summarized as the following procedure:

Procedure 3 PLNC Scheme for Massive MIMO Relaying

Processing stage at the relay for each $\mathbf{y_R}(n)$:

1) Zero forcing process of the received signal: $\mathbf{y_P}(n) = \mathbf{H_{AR}}^{\dagger}\mathbf{y_R}(n) + \mathbf{H_{BR}}^{\dagger}\mathbf{y_R}(n)$;

for $i = 1, \cdots, N_T$ **do**

2) Scale the processed relay signal, using the MMSE scaling factor $y_{P,i}$: $\tilde{y}_{P,i} = \alpha_i \cdot y_{P,i}$;

3) Quantize $\tilde{y}_{P,i}$ to the closest fine lattice point: $\mathrm{Q}_{\Lambda_\mathsf{F}}(\tilde{y}_{P,i})$;

4) Perform modulo operation with respect to the coarse lattice to obtain back a point of the nested lattice code: $x_{R,i} = [\mathrm{Q}_{\Lambda_\mathsf{F}}(\tilde{y}_{P,i})] \mathrm{mod}_{\Lambda_\mathsf{C}}$:

end for

5) Transmit the signal $\mathbf{x_R}(n) = [x_{R,1}, \cdots, x_{R,N_T}]$;

Processing stage at terminal $\mathcal{A}$ **(similar for** $\mathcal{B}$**)**:

1) Decode the relay transmitted signal using the ML detector for the nested lattice code: $\hat{\mathbf{x}}_\mathbf{R} = \arg\min_{\lambda \in (\Lambda_\mathsf{F} \cap \mathcal{V}_{\Lambda_\mathsf{C}})^{N_T}} \parallel \mathbf{y_A} - \mathbf{H_{RA}}\lambda \parallel$;

for $i = 1, \cdots, N_T$ **do**

2) Map the received information back to the finite field: $u_{1,i} = \phi^{-1}(\mathcal{R}\{\hat{x}_{R,i}\}) = [S_{A,1,i} + S_{B,1,i}] \mathrm{mod} Q$ and $u_{2,i} = \phi^{-1}(\mathcal{I}\{\hat{x}_{R,i}\}) = [S_{A,2,i} + S_{B,2,i}] \mathrm{mod} Q$ (where here $q_A = 1, q_B = 1$);

3) Subtract own information to obtain: $\hat{S}_{B,1,i} = [u_{1,i} - S_{A,1,i}] \mathrm{mod} Q$ and $\hat{S}_{B,2,i} = [u_{2,i} - S_{A,2,i}] \mathrm{mod} Q$;

end for

4) Obtain $\hat{S}_{B,i} = (\hat{S}_{B,1,i}; \hat{S}_{B,2,i})$ for $i = 1, \cdots, N_T$.

SER for Different Numbers of Receiving Antennas

The proposed PLNC scheme for massive MIMO full-duplex relaying relies on the orthogonal properties between all involved channel matrices, which are represented in equation (6.25). For this reason, it is interesting to evaluate the effect of having a finite number of receive antennas at the relay, instead of the asymptotic and theoretical case of having infinite antennas. To that end, consider that each channel has entries generated from a Rayleigh fading distribution, i.e., $\mathbf{H_{AR}}, \mathbf{H_{BR}}, \mathbf{H_{RA}}, \mathbf{H_{RB}}, \mathbf{H_{RR}}$ entries are generated from distribution $\mathcal{CN}(0,1)$. The average SER at both terminals is depicted in Fig. 6.6, for different number of antennas: the SER is depicted against the equivalent noise power, which considers a fixed self-interference mitigation gain (as in section 6.2) and varying thermal noise, i.e., for the relay assume that $\tilde{\mathbf{n}}_{\mathbf{R}}(n) \sim \mathcal{CN}(0, \sigma_{eq}^2\ \mathbf{I}_{\mathbf{M_T \times M_T}})$ and that each terminal has $\tilde{\mathbf{n}}_{\mathbf{A}}(n), \tilde{\mathbf{n}}_{\mathbf{B}}(n) \sim \mathcal{CN}(0, \sigma_{eq}^2\ \mathbf{I}_{\mathbf{N_T \times N_T}})$.

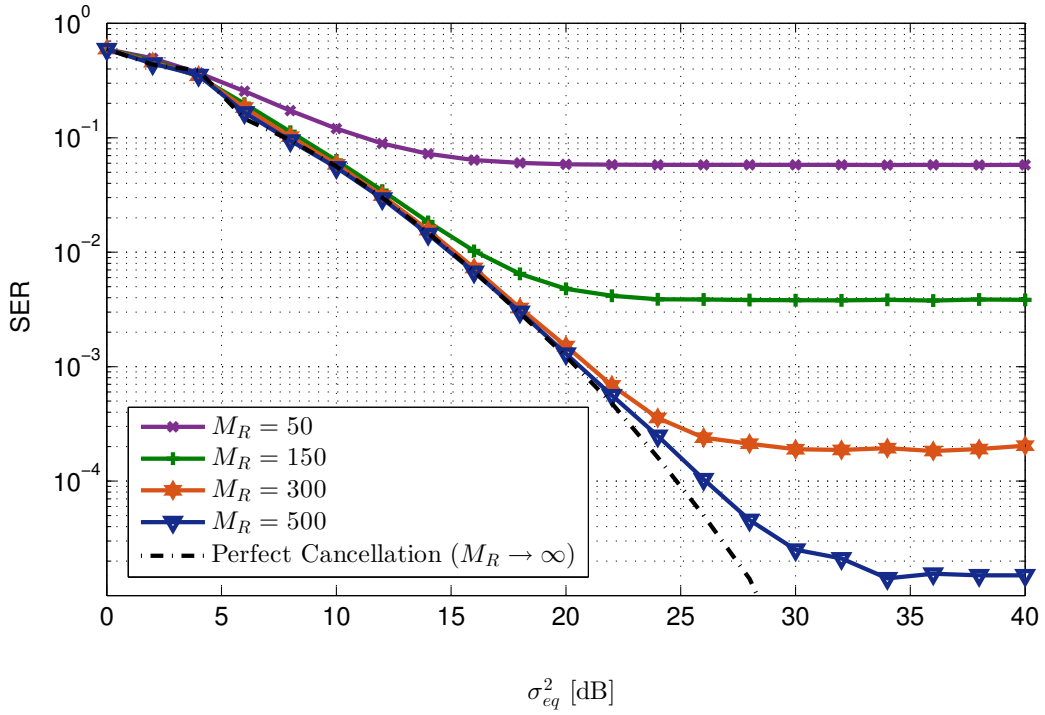

Figure 6.6: SER performance of the bidirectional CF massive MIMO protocol for different numbers of relay receiving antennas M_R and different interference and noise power levels σ_{eq}^2.

The asymptotic effect mentioned above becomes clear in Fig. 6.6. For a low number of antennas, the orthogonal properties of large dimension arrays do not hold. For that reason, for the considered number M_R of antennas at the relay, the SER curves stall at an error floor that decreases with M_R and is caused by the three aforementioned interference components that are not canceled by the properties of employing massive arrays. Nevertheless, when a larger number of antennas is considered, for example $M_T = 500$, the effect of imperfect cancellation starts to be negligible, as the matrices orthogonal property is valid for a large range of σ_{eq}^2. Thus, the noise floor in this case appears for acceptable values of SER, and the curve tends to the asymptotic case of perfect interference cancellation, i.e., $M_R = \infty$ (in this case simulated with $M_R = 1000$ and by subtracting the interference terms from the relay received signal).

Channel Estimation Errors Effect in the SER

Another interesting aspect is to evaluate how imperfect CSI may deteriorate the protocol performance. To that end, consider the above described system, however, assume that the relay only has access to erroneous estimations of the channel matrices, i.e., each entry of the channel matrices is known at the relay apart from some error component. Thus, it is assumed for all channel matrices that $\mathbf{H} = \tilde{\mathbf{H}} + \mathcal{E}_{\mathbf{H}}$, where the error component is generated from a complex Gaussian distribution as $\mathcal{CN}(0, \sigma^2_{\mathbf{H}})$, and where $\sigma^2_{\mathbf{H}}$ accounts for the estimation error power. Fig. 6.7 depicts the average SER performance for different values of equivalent noise, different numbers of antennas and different estimation errors power. The

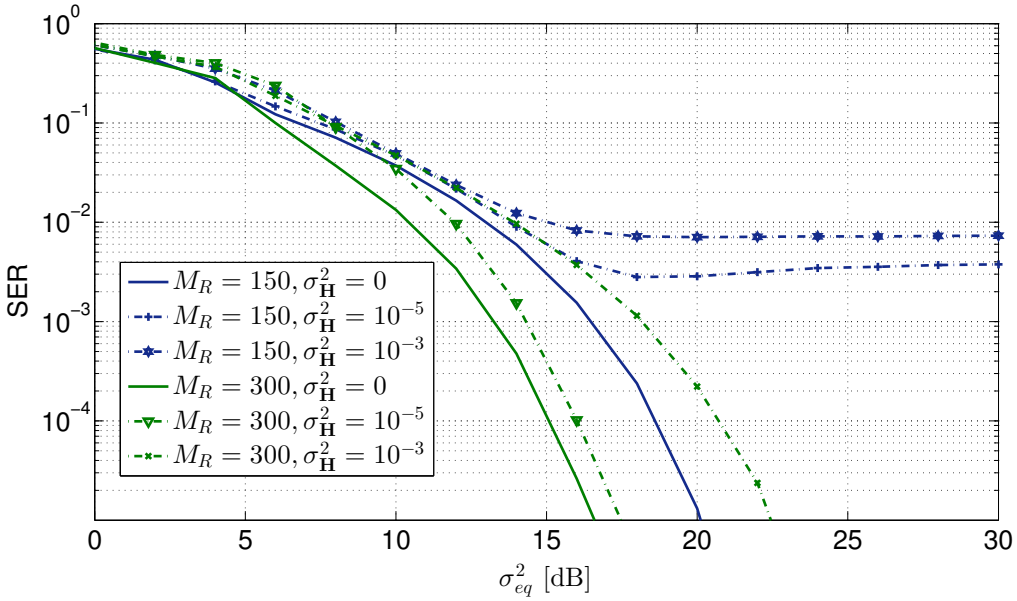

Figure 6.7: SER curves of the CF massive MIMO protocol for different numbers of relay receiving antennas M_R, different interference power levels σ^2_{eq} and different channel estimation errors power $\sigma^2_{\mathbf{H}}$.

estimation errors in the channel matrices are still a major draw back in the CF protocol for massive MIMO. For $M_R = 150$ antennas (blue curves), when the relay does not know the channel matrices exactly, the SER curves for $\sigma^2_{\mathbf{H}} = 10^{-5}$ and for $\sigma^2_{\mathbf{H}} = 10^{-3}$ tend error floor. This is mainly caused by the error propagation at the ZF filtering stage, that limits the performance in the presence of imperfect channel estimations, since $\mathbf{D_A} = \mathbf{D_B} = \mathbf{I}$ is no longer obtained, i.e., a unitary network code is never achieved. In this case, the network code becomes a complex number, introducing a phase rotation in the lattice constellation that cannot be handled by the CF scheme. The interference terms enumerated earlier are not affected by these errors, since the orthogonality between large matrices is blind to their content, if randomly distributed. Also, when a larger number of antennas is considered, as the green curves show for $M_R = 300$ and for the same estimation errors power, the error floor disappears for the depicted SER values. This effect is also explained by the orthogonal property between large dimension arrays, which can reduce the propagation of the errors to the ZF filtering. However, these SER curves will eventually stall at a error floor for lower values of SER. When increasing the number of antennas M_R, the SER stalling value decreases to a point that is targeted in wireless communications likes ($\approx 10^{-3}$).

6.5 Bidirectional Rate Analysis

This section derives the instantaneous and average bidirectional sum rate for the specific case where in the system model defined in Fig. 6.1, $N_T = 1$, $M_T = 1$, and for any M_R, i.e., a single-input multiple-output (SIMO) scenario. This analysis assumes that CF and DeF protocols achieve the same highest rate, thus, it presents only an upper bound for the proposed system capacity. Nevertheless, this approach provides good results for scenarios such as these [75, 105]. Also, there is global channel state information (GCSI) at the relay, i.e., the relay has perfect knowledge of all channels. The final goal is to optimize this sum rate, that involves solving a non-concave problem, similarly to that done in section 5.2.2.

6.5.1 Instantaneous Rate

Firstly, the instantaneous SINR (denoted again by γ) at all elements of the system is obtained. Considering the relay model in equation (6.1) and assuming that $M_T = 1$, it is possible to show that

$$\gamma_{\mathcal{R}} = \frac{\mathbb{E}\{p_A x_A^*(n)\mathbf{h}_{\mathbf{AR}}^H \mathbf{h}_{\mathbf{AR}} x_A(n)\} + \mathbb{E}\{p_B x_B^*(n)\mathbf{h}_{\mathbf{BR}}^H \mathbf{h}_{\mathbf{BR}} x_B(n)\}}{\mathbb{E}\{k_R^2 p_R x_R^*(n)\mathbf{h}_{\mathbf{RR}}^H \mathbf{h}_{\mathbf{RR}} x_R(n)\} + \mathbb{E}\{\mathbf{n}_{\mathbf{R}}^H(n)\mathbf{n}_{\mathbf{R}}(n)\}}$$

$$= \frac{p_A \mathbf{h}_{\mathbf{AR}}^* \mathbf{h}_{\mathbf{AR}} \mathbb{E}\{x_A^*(n)x_A(n)\} + p_B \mathbf{h}_{\mathbf{BR}}^H \mathbf{h}_{\mathbf{BR}} \mathbb{E}\{x_B^*(n)x_B(n)\}}{k_R^2 p_R \mathbf{h}_{\mathbf{RR}}^* \mathbf{h}_{\mathbf{RR}} \mathbb{E}\{x_R^*(n)x_R(n)\} + \mathbb{E}\{\mathbf{n}_{\mathbf{R}}^H(n)\mathbf{n}_{\mathbf{R}}(n)\}} = \frac{p_A \mathbf{h}_{\mathbf{AR}}^H \mathbf{h}_{\mathbf{AR}} + p_B \mathbf{h}_{\mathbf{BR}}^H \mathbf{h}_{\mathbf{BR}}}{k_R^2 p_R \mathbf{h}_{\mathbf{RR}}^H \mathbf{h}_{\mathbf{RR}} + \sigma_{\mathbf{n_R}}^2}, \quad (6.27)$$

where the relay knows exactly the channel vectors, and where the transmitted vectors are normalized, i.e., a normalized constellation to transmit is used, thus, $\mathbb{E}\{x_A^*(n)x_A(n)\} = \mathbb{E}\{x_B^*(n)x_B(n)\} = \mathbb{E}\{x_R^*(n)x_R(n)\} = 1$. The noise power is $\sigma_{\mathbf{n_R}}^2$. Furthermore, each terminal's individual contribution to the relay SINR is consequently given by

$$\gamma_{\mathcal{R},\mathcal{A}} = \frac{p_A \mathbf{h}_{\mathbf{AR}}^H \mathbf{h}_{\mathbf{AR}}}{k_R^2 p_R \mathbf{h}_{\mathbf{RR}}^H \mathbf{h}_{\mathbf{RR}} + \sigma_{\mathbf{n_R}}^2}, \ \gamma_{\mathcal{R},\mathcal{B}} = \frac{p_B \mathbf{h}_{\mathbf{BR}}^H \mathbf{h}_{\mathbf{BR}}}{k_R^2 p_R \mathbf{h}_{\mathbf{RR}}^H \mathbf{h}_{\mathbf{RR}} + \sigma_{\mathbf{n_R}}^2}. \quad (6.28)$$

To compute the SINR at the terminals, consider the same procedure as above. Taking into consideration (6.2), it is possible to write the following expressions

$$\begin{aligned} \gamma_{\mathcal{A}} &= \frac{\mathbb{E}\{p_R x_R^*(n) h_{RA}^* h_{RA} x_R(n)\}}{\mathbb{E}\{k_A^2 p_A x_A^*(n) h_{AA}{}^* h_{AA} x_A(n)\} + \mathbb{E}\{n_A^*(n) n_A(n)\}} = \frac{p_R h_{RA}^* h_{RA}}{k_A^2 p_A h_{AA}^* h_{AA} + \sigma_{n_A}^2}, \\ \gamma_{\mathcal{B}} &= \frac{\mathbb{E}\{p_R x_R^*(n) h_{RB}^* h_{RB} x_R(n)\}}{\mathbb{E}\{k_B^2 p_B x_B^*(n) h_{BB}^* h_{BB} x_B(n)\} + \mathbb{E}\{n_B^*(n) n_B(n)\}} = \frac{p_R h_{RB}^* h_{RB}}{k_B^2 p_B h_{BB}^* h_{BB} + \sigma_{n_B}^2}. \end{aligned} \quad (6.29)$$

Then, based on the SINR computed expressions, the rates for each path of the FD-TWRC are derived. Firstly, consider the transmission of information from terminal $\mathcal{A}$ and $\mathcal{B}$ to the relay. Since the protocols under consideration employ a non-linear mechanism of detection that depends on both received signals, the sum rate at the relay is defined by the contributions from both terminals, as in the equation

$$R_{\mathcal{R}}^{total} = \log_2(1 + \gamma_{\mathcal{R}}) = \log_2\left(1 + \frac{p_A \mathbf{h}_{\mathbf{AR}}^H \mathbf{h}_{\mathbf{AR}} + p_B \mathbf{h}_{\mathbf{BR}}^H \mathbf{h}_{\mathbf{BR}}}{k_R^2 p_R \mathbf{h}_{\mathbf{RR}}^H \mathbf{h}_{\mathbf{RR}} + \sigma_{\mathbf{n_R}}^2}\right). \quad (6.30)$$

In order to evaluate each terminal's contribution to the rate at the relay, it is necessary to separate the SINR components from $\mathcal{A}$ and $\mathcal{B}$. Thus, the contribution to the rate in 6.30 from $\mathcal{A}$ and from $\mathcal{B}$ is given

by equations (6.31) and (6.32), respectively.

$$R_{\mathcal{A},\mathcal{R}} = \log_2(1+\gamma_{\mathcal{R},\mathcal{A}}) = \log_2\Big(1+\frac{p_A \mathbf{h}_{\mathbf{AR}}^H \mathbf{h}_{\mathbf{AR}}}{k_R^2 p_R \mathbf{h}_{\mathbf{RR}}^H \mathbf{h}_{\mathbf{RR}} + \sigma^2_{\mathbf{n_R}}}\Big). \tag{6.31}$$

$$R_{\mathcal{B},\mathcal{R}} = \log_2(1+\gamma_{\mathcal{R},\mathcal{B}}) = \log_2\Big(1+\frac{p_B \mathbf{h}_{\mathbf{BR}}^H \mathbf{h}_{\mathbf{BR}}}{k_R^2 p_R \mathbf{h}_{\mathbf{RR}}^H \mathbf{h}_{\mathbf{RR}} + \sigma^2_{\mathbf{n_R}}}\Big). \tag{6.32}$$

Similarly, considering the information that follows from the relay to the terminals, the instantaneous rate at terminal $\mathcal{A}$ and terminal $\mathcal{B}$, is derived as

$$\begin{aligned} R_{\mathcal{R},\mathcal{A}} &= \log_2(1+\gamma_{\mathcal{A}}) = \log_2\Big(1+\frac{p_R h_{RA}^* h_{RA}}{k_A^2 p_A h_{AA}^* h_{AA} + \sigma^2_{n_A}}\Big), \\ R_{\mathcal{R},\mathcal{B}} &= \log_2(1+\gamma_{\mathcal{B}}) = \log_2\Big(1+\frac{p_R h_{RB}^* h_{RB}}{k_B^2 p_B h_{BB}^* h_{BB} + \sigma^2_{n_B}}\Big). \end{aligned} \tag{6.33}$$

To compute the bidirectional rates between the two terminals, i.e., the amount of information flowing from $\mathcal{A}$ to $\mathcal{B}$, and vice-versa, assume that the flow of information is always limited by the worst of the two channels. As demonstrated in [31, 64] and in most literature, the communication rate between the terminals is necessarily limited by the smaller of the two rates: the rate between each terminal and the relay or the rate between the relay and each terminal. Therefore, the rate of the stream of information that follows from terminal $\mathcal{A}$ to terminal $\mathcal{B}$ is given by

$$R_{\mathcal{A},\mathcal{B}} = \min\{R_{\mathcal{A},\mathcal{R}}, R_{\mathcal{R},\mathcal{B}}\} = \min\{\log_2(1+\gamma_{\mathcal{R},\mathcal{A}}), \log_2(1+\gamma_{\mathcal{B}})\} = \log_2(1+\min\{\gamma_{\mathcal{R},\mathcal{A}}, \gamma_{\mathcal{B}}\}). \tag{6.34}$$

where the last step comes from the fact that $\log_2(1+x)$ is an injective and monotonically increasing function for $x \in \mathbb{R}^+$. For the stream of information from $\mathcal{B}$ to $\mathcal{A}$ it is likewise obtained

$$R_{\mathcal{B},\mathcal{A}} = \min\{R_{\mathcal{B},\mathcal{R}}, R_{\mathcal{R},\mathcal{A}}\} = \min\{\log_2(1+\gamma_{\mathcal{R},\mathcal{B}}), \log_2(1+\gamma_{\mathcal{A}})\} = \log_2(1+\min\{\gamma_{\mathcal{R},\mathcal{B}}, \gamma_{\mathcal{A}}\}). \tag{6.35}$$

Finally, the total rate of the system (the bidirectional sum rate) is computed by adding the two bidirectional rates above, as expressed in equation (6.36)

$$\begin{aligned} R_\Sigma &= R_{\mathcal{A},\mathcal{B}} + R_{\mathcal{B},\mathcal{A}} \\ &= \log_2(1+\min\{\gamma_{\mathcal{R},\mathcal{A}}, \gamma_{\mathcal{B}}\}) + \log_2(1+\min\{\gamma_{\mathcal{R},\mathcal{B}}, \gamma_{\mathcal{A}}\}) \\ &= \log_2\Big(1+\min\Big\{\frac{p_A \mathbf{h}_{\mathbf{AR}}^H \mathbf{h}_{\mathbf{AR}}}{k_R^2 p_R \mathbf{h}_{\mathbf{RR}}^H \mathbf{h}_{\mathbf{RR}} + \sigma^2_{\mathbf{n_R}}}, \frac{p_R h_{RB}^* h_{RB}}{k_B^2 p_B h_{BB}^* h_{BB} + \sigma^2_{n_B}}\Big\}\Big) + \\ &+ \log_2\Big(1+\min\Big\{\frac{p_B \mathbf{h}_{\mathbf{BR}}^H \mathbf{h}_{\mathbf{BR}}}{k_R^2 p_R \mathbf{h}_{\mathbf{RR}}^H \mathbf{h}_{\mathbf{RR}} + \sigma^2_{\mathbf{n_R}}}, \frac{p_R h_{RA}^* h_{RA}}{k_A^2 p_A h_{AA}^* h_{AA} + \sigma^2_{n_A}}\Big\}\Big). \end{aligned} \tag{6.36}$$

6.5.2 Ergodic Rate

Besides the instantaneous sum rate, the ergodic rate for the system presented above is evaluated. Therefore, consider that the channel distribution is known at the relay and that all channels' coefficients are realizations of a Rayleigh distribution with zero mean and unitary normalized variance, i.e., the channel elements are drawn from $\mathcal{CN}(0,1)$, as has been assumed for simulation purposes. Thus, taking

into account (6.34) and (6.35), the ergodic rate for each stream of data is stated as follows

$$\begin{aligned}\tilde{R}_{\mathcal{A},\mathcal{B}} = \min\{\tilde{R}_{\mathcal{A},\mathcal{R}}, \tilde{R}_{\mathcal{R},\mathcal{B}}\} &= \min\{\log_2(1+\mathbb{E}\{\gamma_{\mathcal{R},\mathcal{A}}\}), \log_2(1+\mathbb{E}\{\gamma_{\mathcal{B}}\})\} = \log_2(1+\min\{\hat{\gamma}_{\mathcal{R},\mathcal{A}}, \hat{\gamma}_{\mathcal{B}}\}) \\ &= \log_2\Big(1+\min\Big\{\frac{p_A M_R}{k_R^2 M_R p_R + \sigma^2_{\mathbf{n_R}}}, \frac{p_R}{k_B^2 p_B + \sigma^2_{n_B}}\Big\}\Big),\end{aligned} \tag{6.37}$$

$$\begin{aligned}\tilde{R}_{\mathcal{B},\mathcal{A}} = \min\{\tilde{R}_{\mathcal{B},\mathcal{R}}, \tilde{R}_{\mathcal{R},\mathcal{A}}\} &= \min\{\log_2(1+\mathbb{E}\{\gamma_{\mathcal{R},\mathcal{B}}\}), \log_2(1+\mathbb{E}\{\gamma_{\mathcal{A}}\})\} = \log_2(1+\min\{\hat{\gamma}_{\mathcal{R},\mathcal{B}}, \hat{\gamma}_{\mathcal{A}}\}) \\ &= \log_2\Big(1+\min\Big\{\frac{p_B M_R}{k_R^2 M_R p_R + \sigma^2_{\mathbf{n_R}}}, \frac{p_R}{k_A^2 p_A + \sigma^2_{n_B}}\Big\}\Big),\end{aligned} \tag{6.38}$$

where the average of the channels are $\mathbb{E}\{\mathbf{h}_{\mathbf{AR}}^H \mathbf{h}_{\mathbf{AR}}\} = \mathbb{E}\{\mathbf{h}_{\mathbf{BR}}^H \mathbf{h}_{\mathbf{BR}}\} = \mathbb{E}\{\mathbf{h}_{\mathbf{RR}}^H \mathbf{h}_{\mathbf{RR}}\} = M_R$ and $\mathbb{E}\{h_{RA}^* h_{RA}\} = \mathbb{E}\{h_{RB}^* h_{RB}\} = \mathbb{E}\{h_{AA}^* h_{AA}\} = \mathbb{E}\{h_{BB}^* h_{BB}\} = 1$. Finally, the ergodic sum rate for the system under consideration is simply given by $\tilde{R}_\Sigma = \tilde{R}_{\mathcal{A},\mathcal{B}} + \tilde{R}_{\mathcal{B},\mathcal{A}}$, as above.

6.6 Power Allocation Scheme

The power allocation for similar systems to the one under consideration may take several different flavors, depending naturally on each system goal. For instance, one may employ uniform power in all elements, i.e., having $p_A = p_B = p_R$ and then find a power level where the sum rate is instantaneous, or on average, above a certain threshold. Also, assuming different transmit powers, a desired rate for the flow of information may be set, while enhancing the system energy efficiency, as done in section 5.2.2. The approach employed in this section is to assume a greedy position, i.e., try to achieve the maximum bidirectional sum rate of the system, under power constraints only due to amplifiers' limitations.

6.6.1 Sum Rate Maximization

The maximum sum rate would be achieved with peak powers in a scenario without self-interference. However, this effect at the relay and at the terminals makes the problem of allocating powers non-trivial. Therefore, assuming that the peak power of the terminal $\mathcal{A}$ is $P_{A,max}$, of the terminal $\mathcal{B}$ is $P_{B,max}$ and of the relay is $P_{R,max}$, writing a formulation of such problem in a canonical form, for the instantaneous and ergodic case, yields

$$\begin{aligned} \underset{p_R,p_A,p_B}{\text{max.}} \quad & R_\Sigma \text{ (or } \tilde{R}_\Sigma) \\ \text{s.t.} \quad & 0 < p_A \leq P_{A,max};\ 0 < p_B \leq P_{B,max};\ 0 < p_R \leq P_{R,max}; \end{aligned} \tag{6.39}$$

which can be then expanded to

$$\begin{aligned} \underset{p_R,p_A,p_B}{\text{max.}} \quad & \log_2\Big(1+\min\Big\{\frac{p_A C_{AR}}{p_R C_{RR} + \sigma^2_{\mathbf{n_R}}}, \frac{p_R C_{RB}}{p_B C_{BB} + \sigma^2_{n_B}}\Big\}\Big) + \log_2\Big(1+\min\Big\{\frac{p_B C_{BR}}{p_R C_{RR} + \sigma^2_{\mathbf{n_R}}}, \frac{p_R C_{RA}}{p_A C_{AA} + \sigma^2_{n_A}}\Big\}\Big) \\ \text{s.t.} \quad & 0 < p_A \leq P_{A,max};\ 0 < p_B \leq P_{B,max};\ 0 < p_R \leq P_{R,max}; \end{aligned} \tag{6.40}$$

where it is defined that $C_{AR} = \mathbf{h}_{\mathbf{AR}}^H \mathbf{h}_{\mathbf{AR}}$, $C_{BR} = \mathbf{h}_{\mathbf{BR}}^H \mathbf{h}_{\mathbf{BR}}$, $C_{RR} = k_R^2 \mathbf{h}_{\mathbf{RR}}^H \mathbf{h}_{\mathbf{RR}}$, $C_{RA} = h_{AR}^* h_{RA}$, $C_{RB} = h_{RB}^* h_{RB}$, $C_{AA} = k_A^2 h_{AA}^* h_{AA}$ and $C_{BB} = k_B^2 h_{BB}^* h_{BB}$, for the instantaneous coefficients. For the ergodic case $C_{AR} = C_{BR} = M_R$, $C_{RR} = k_R^2 M_R$, $C_{RA} = C_{RB} = 1$, $C_{AA} = k_A^2$ and $C_{BB} = k_B^2$.

6.6.2 Fair Sum Rate Maximization

As optimization problem (6.40) is formulated, the transmit powers of each terminal and relay cannot be zero, however, one terminal may get a transmit power very close to zero, which would destroy the exchange of information. In that case, the sum rate would be maximized, nevertheless, only one link would be active, which is not desirable in the definition of the TWRC and as the problem has been presented. For that reason, the optimization problem in (6.39) is reformulated to avoid this case, by only adding one extra constraint that forces a linear relation between transmit powers at the terminals. Thus, equation (6.41) reformulates the problem to ensure the two flows of information, as follows

$$\begin{aligned} \underset{p_R, p_A, p_B}{\text{max.}} \quad & R_\Sigma \text{ (or } \tilde{R}_\Sigma) \\ \text{s.t.} \quad & 0 < p_A \leq P_{A,max}; 0 < p_B \leq P_{B,max}; 0 < p_R \leq P_{R,max}; \\ & (1-\varrho) p_B \leq p_A \leq (1+\varrho) p_B; \end{aligned} \tag{6.41}$$

where the utility function is the same as in section 6.6.1, and where ϱ is a constant set *a priori* to control the power imbalance at the terminals, from now on referred to as unbalance factor.

6.6.3 Proposed Solution

Before starting to solve any of the problems stated in (6.40) or (6.41), note that both problems are clearly non-concave, since their utility function, which is given by function $r(p_A, p_B, p_R)$, as

$$\begin{aligned} r(p_A, p_B, p_R) : \mathbb{R}_+^3 \to \mathbb{R} : r(p_A, p_B, p_R) = & \log_2 \left(1 + \min\left\{ \frac{p_A C_{AR}}{p_R C_{RR} + \sigma_{\mathbf{n_R}}^2}, \frac{p_R C_{RB}}{p_B C_{BB} + \sigma_{n_B}^2} \right\}\right) + \\ & + \log_2 \left(1 + \min\left\{ \frac{p_B C_{BR}}{p_R C_{RR} + \sigma_{\mathbf{n_R}}^2}, \frac{p_R C_{RA}}{p_A C_{AA} + \sigma_{n_A}^2} \right\}\right), \end{aligned} \tag{6.42}$$

is not a concave function (necessary to make a maximization problem concave [109]). The constraints of both formulations are linear functions of the optimization variables and do not pose any problem. Therefore, the idea is to reach a solution for problem (6.40) based on an algorithm, which can then be used to solve problem (6.41), only by adding the unbalance factor.

To do so, start by introducing two epigraph variables, s and t, as in

$$\begin{aligned} \underset{p_R, p_A, p_B, s, t}{\text{max.}} \quad & \log_2(1+s) + \log_2(1+t), \\ \text{s.t.} \quad & 0 < p_A \leq P_{A,max};\ 0 < p_B \leq P_{B,max};\ 0 < p_R \leq P_{R,max}; \\ & (s \cdot p_R) C_{RR} + s \cdot \sigma_{\mathbf{n_R}}^2 \leq p_A C_{AR};\ (s \cdot p_B) C_{BB} + s \cdot \sigma_{n_B}^2 \leq p_R C_{RB}; \\ & (t \cdot p_R) C_{RR} + t \cdot \sigma_{\mathbf{n_R}}^2 \leq\ p_B C_{BR};\ (t \cdot p_A) C_{AA} + t \cdot \sigma_{n_A}^2 \leq p_R C_{RA}, \end{aligned} \tag{6.43}$$

that replace the minimum terms in the utility function [110], where it is noted again that $\min\{a,b\} \geq x <=> a \geq x, b \geq x$, after performing some basic manipulations. This reformulation in (6.43) shows a concave utility function, in this case a sum of two concave functions (since $\log(1+x)$ is concave for $x > -1, x \in \mathbb{R}$). Nevertheless, it only transfers the difficulty of solving (6.43) to the constraints in the last two lines of (6.43), in this case in the form of bilinear terms. Thus, isolating those bilinear terms, a new reformulation is then obtained

$$\begin{aligned}
\underset{p_R,p_A,p_B,s,t,z_1,z_2,z_3,z_4}{\text{max.}} \quad & \log_2(1+s) + \log_2(1+t), \\
\text{s.t.} \quad & 0 < p_A \leq P_{A,max};\ 0 < p_B \leq P_{B,max};\ 0 < p_R \leq P_{R,max}; \\
& z_1 C_{RR} + s \cdot \sigma^2_{\mathbf{n_R}} \leq p_A C_{AR};\ z_2 C_{BB} + s \cdot \sigma^2_{n_B} \leq p_R C_{RB}; \\
& z_3 C_{RR} + t \cdot \sigma^2_{\mathbf{n_R}} \leq\ p_B C_{BR};\ z_4 C_{AA} + t \cdot \sigma^2_{n_A} \leq p_R C_{RA}; \\
& z_1 = s \cdot p_R;\ z_2 = s \cdot p_B;\ z_3 = t \cdot p_R;\ z_4 = t \cdot p_A.
\end{aligned} \tag{6.44}$$

which is based on a linear utility function, nine optimization variables, seven linear constraints and four non-linear constraints. So far, this formulations of the problem remained all non-concave. However, this last formulation was drawn in order to construct an algorithm to find the solution. To that end, it is necessary to employ a convex/concave relaxation method, which approaches this non-concave problem by concave means, making it possible to find an approximation of the optimal solution in feasible time.

Piecewise MacCormick Relaxation

Thus, finding a solution to problem (6.44), requires one to treat the bilinear terms present in the problem constraints. These bilinear terms transform the feasible region of this problem into a non-concave set, where finding the optimal solution may be infeasible. However, it is possible to effectively draw tight linear bounds to the bilinear terms and, thus, obtain an approximation to the global solution for the non-concave problem by employing gradient-based solvers. Among these techniques, MacCormick relaxation [111] is one of the best methods known to deal with such problems. The main idea is that, for some instances of the utility function domain, the regions described by non-linear constraints may be linear hyperplanes [112], which can be treated separately to transform the non-concave problem into an equivalent concave optimization problem. Basically, it is possible to approximate a non-concave optimization problem into several concave ones.

For this reason, consider the use of Piecewise MacCormick envelopes (or partitions of the feasible region of the problem) in order to replace the bilinear constraints by tight hyperplanes that locally create a convex hull over these non-linear terms. Thus, consider the general case of a bilinear constraint in an optimization problem over a subset of the problem feasible region [113], formulated as

$$\begin{aligned}
\underset{x,y,z}{\text{max.}} \quad & f(x,y,z), \\
\text{s.t.} \quad & z = xy, \\
& (x^L, y^L, z^L) \leq (x,y,z) \leq (x^U, y^U, z^U).
\end{aligned} \tag{6.45}$$

The MacCormick relaxation aims to lower bound the bilinear terms with a convex function and to upper bound it with a concave function, both in a form of linear constraints, as

$$\begin{aligned} \underset{x,y,z}{\text{max.}} \quad & f(x,y,z), \\ \text{s.t.} \quad & z \geq x^L y + y^L x - x^L y^L, \\ & z \geq x^U y + y^U x - x^U y^U, \\ & z \leq x^U y + y^L x - x^U y^L, \\ & z \leq x^L y + y^U x - x^L y^U, \\ & (x^L, y^L, z^L) \leq (x, y, z) \leq (x^U, y^U, z^U), \end{aligned} \tag{6.46}$$

which transforms it in a concave problem, making it possible to obtain a solution by using convex/concave solvers. Moreover, the error of this solution when compared with the optimal one is dependent on the tightness of the used bounds, which is naturally related to the number of envelopes created for the problem domain, i.e., the used partitions of the problem feasible region.

Therefore, the same procedure is applied to each bilinear term present in (6.44). The feasible region of the problem is decomposed in hypercubes, i.e., $(P^L_{A,i}, P^L_{B,j}, P^L_{R,k}) \leq (p_A, p_B, p_R) \leq (P^U_{A,i}, P^U_{B,j}, P^U_{R,k})$, for $(i,j,k) = (1,1,1), \cdots, (N_{part,A}, N_{part,B}, N_{part,R})$, where $N_{part,A}$, $N_{part,B}$ and $N_{part,R}$ represent the number of partitions per variable. Since the partitions used in the Piecewise MacCormick relaxation requires a closed set, a minimum value for each power is introduced (close to zero as desired). Thus, it is considered that $P^L_{A,1} = P_{A,min}$, $P^L_{B,1} = P_{B,min}$, $P^L_{R,1} = P_{R,min}$, and that $P^U_{A,N_{part,A}} = P_{A,max}$, $P^U_{B,N_{part,B}} = P_{B,max}$, $P^U_{R,_{part,B}} = P_{R,max}$. Also, assume that the partitions cover all the space where the three powers belong, i.e., $P^L_{A,i} = P^U_{A,i-1}$, $P^L_{B,j} = P^U_{B,j-1}$ and $P^L_{R,k} = P^U_{R,k-1}$. Finally, it is possible to obtain a concave approximation of the problem in (6.44), for subset partition (i,j,k), as follows

$$\begin{aligned} \underset{p_R,p_A,p_B,s,t,z_1,z_2,z_3,z_4}{\text{max.}} \quad & \log_2(1+s) + \log_2(1+t), \\ \text{s.t.} \quad & (P^L_{A,i}, P^L_{B,j}, P^L_{R,k}) \leq (p_A, p_B, p_R) \leq (P^U_{A,i}, P^U_{B,j}, P^U_{R,k}); \\ & z_1 \cdot C_{RR} + s \cdot \sigma^2_{\mathbf{n_R}} \leq p_A C_{AR};\ z_2 \cdot C_{BB} + s \cdot \sigma^2_{n_B} \leq p_R C_{RB}; \\ & z_3 \cdot C_{RR} + t \cdot \sigma^2_{\mathbf{n_R}} \leq\ p_B C_{BR};\ z_4 \cdot C_{AA} + t \cdot \sigma^2_{n_A} \leq p_R C_{RA}; \\ & z_1 \geq p_R \cdot S_{\min} + s \cdot P^L_{R,k} - S_{\min} \cdot P^L_{R,k};\ z_1 \geq p_R \cdot S_{\max} + s \cdot P^U_{R,k} - S_{\max} \cdot P^U_{R,k}; \\ & z_1 \leq p_R \cdot S_{\min} + s \cdot P^U_{R,k} - S_{\min} \cdot P^U_{R,k};\ z_1 \leq p_R \cdot S_{\max} + s \cdot P^L_{R,k} - S_{\max} \cdot P^L_{R,k}; \\ & z_2 \geq p_B \cdot S_{\min} + s \cdot P^L_{B,j} - S_{\min} \cdot P^L_{B,j};\ z_2 \geq p_B \cdot S_{\max} + s \cdot P^U_{B,j} - S_{\max} \cdot P^U_{B,j}; \\ & z_2 \leq p_B \cdot S_{\min} + s \cdot P^U_{B,j} - S_{\min} \cdot P^U_{B,j};\ z_2 \leq p_B \cdot S_{\max} + s \cdot P^L_{B,j} - S_{\max} \cdot P^L_{B,j}; \\ & z_3 \geq p_R \cdot T_{\min} + t \cdot P^L_{R,k} - T_{\min} \cdot P^L_{R,k};\ z_3 \geq p_R \cdot T_{\max} + t \cdot P^U_{R,k} - T_{\max} \cdot P^U_{R,k}; \\ & z_3 \leq p_R \cdot T_{\min} + t \cdot P^U_{R,k} - T_{\min} \cdot P^U_{R,k};\ z_3 \leq p_R \cdot T_{\max} + t \cdot P^L_{R,k} - T_{\max} \cdot P^L_{R,k}; \\ & z_4 \geq p_A \cdot T_{\min} + t \cdot P^L_{A,i} - T_{\min} \cdot P^L_{A,i};\ z_4 \geq p_A \cdot T_{\max} + t \cdot P^U_{A,i} - T_{\max} \cdot P^U_{A,i}; \\ & z_4 \leq p_A \cdot T_{\min} + t \cdot P^U_{A,i} - T_{\min} \cdot P^U_{A,i};\ z_4 \leq p_A \cdot T_{\max} + t \cdot P^L_{A,i} - T_{\max} \cdot P^L_{A,i}; \end{aligned} \tag{6.47}$$

where it is assumed that the epigraph variables s and t take values from the interval $[S_{\min}, S_{\max}]$ and $[T_{\min}, T_{\max}]$, respectively. Further, these bound values used for the MacCormick relaxation method may be computed regarding that s and t represent SINR values, at the relay or at the terminals, for a certain range of the transmit powers. Thus, they are computed as

$$S_{\max} = \min\Big\{\frac{P_{A,i}^{U}C_{AR}}{P_{R,k}^{L}C_{RR}+\sigma_{n_R}^2}, \frac{P_{R,k}^{U}C_{RB}}{P_{B,j}^{L}C_{BB}+\sigma_{n_B}^2}\Big\},\ S_{\min} = \min\Big\{\frac{P_{A,i}^{L}C_{AR}}{P_{R,k}^{U}C_{RR}+\sigma_{\mathbf{n_R}}^2}, \frac{P_{R,k}^{L}C_{RB}}{P_{B,j}^{U}C_{BB}+\sigma_{n_B}^2}\Big\};$$

$$T_{\max} = \min\Big\{\frac{P_{B,j}^{U}C_{BR}}{P_{R,k}^{L}C_{RR}+\sigma_{n_R}^2}, \frac{P_{R,k}^{U}C_{RA}}{P_{A,i}^{L}C_{AA}+\sigma_{n_A}^2}\Big\},\ T_{\min} = \min\Big\{\frac{P_{B,j}^{L}C_{BR}}{P_{R,k}^{U}C_{RR}+\sigma_{\mathbf{n_R}}^2}, \frac{P_{R,k}^{L}C_{RA}}{P_{A,i}^{U}C_{AA}+\sigma_{n_A}^2}\Big\}.$$

Refinement of the Solution

The solution obtained via Piecewise MacCormick relaxation is only an approximation to the sum rate non-concave optimization problem. This solution may indeed contain a large error when compared with the optimal solution, depending on the number of space partitions, as mentioned. On the other hand, a large number of space partitions increases the algorithm complexity exponentially. Thus, it may be necessary to refine the powers after the MacCormick relaxation stage is performed. The refinement of the solution is then carried out by approximating the utility function in (6.42) with a concave upper bound function, for the space partition where the obtained MacCormick solution lies.

The idea is to use the well known relation, $\log(x) \leq x - 1$, twice such that a concave upper bound is obtained. This idea is shown for the general case of a quotient of variables as follows

$$\frac{x}{y} = \frac{x_k}{y_k}\cdot\frac{x/x_k}{y/y_k} \geq \frac{x_k}{y_k}\Big(\log\big(\frac{x}{x_k}\big) - \log\big(\frac{y}{y_k}\big) + 1\Big) \geq \frac{x_k}{y_k}\Big(\log\big(\frac{x}{x_k}\big) - \frac{y}{y_k} + 2\Big)$$

where x_k and y_k are introduced constants that are further used in an iterative process, in order to successively obtain better approximations. Therefore, this procedure is applied to each SINR term present in the utility function that has the form of a quotient of variables, and that are the argument of the $\min\{\cdot\}$ functions in (6.42). By doing so, it is possible to obtain

$$\frac{p_A C_{AR}}{p_R C_{RR}+\sigma_{\mathbf{n_R}}^2} \geq g_1(p_A,p_B,p_R) = \frac{p_{A,k}C_{AR}}{p_{R,k}C_{RR}+\sigma_{\mathbf{n_R}}^2}\Big(\log_2\Big(\frac{p_A C_{AR}}{p_{A,k}C_{AR}}\Big) - \frac{p_R C_{RR}+\sigma_{\mathbf{n_R}}^2}{p_{R,k}C_{RR}+\sigma_{\mathbf{n_R}}^2} + 2\Big) \quad (6.48)$$

$$\frac{p_R C_{RB}}{p_B C_{BB}+\sigma_{\mathbf{n_B}}^2} \geq g_2(p_A,p_B,p_R) = \frac{p_{R,k}C_{RB}}{p_{B,k}C_{BB}+\sigma_{\mathbf{n_B}}^2}\Big(\log_2\Big(\frac{p_R C_{RB}}{p_{R,k}C_{RB}}\Big) - \frac{p_B C_{BB}+\sigma_{\mathbf{n_B}}^2}{p_{B,k}C_{BB}+\sigma_{\mathbf{n_B}}^2} + 2\Big) \quad (6.49)$$

$$\frac{p_B C_{BR}}{p_R C_{RR}+\sigma_{\mathbf{n_R}}^2} \geq f_1(p_A,p_B,p_R) = \frac{p_{B,k}C_{BR}}{p_{R,k}C_{RR}+\sigma_{\mathbf{n_R}}^2}\Big(\log_2\Big(\frac{p_B C_{BR}}{p_{B,k}C_{BR}}\Big) - \frac{p_R C_{RR}+\sigma_{\mathbf{n_R}}^2}{p_{R,k}C_{RR}+\sigma_{\mathbf{n_R}}^2} + 2\Big) \quad (6.50)$$

$$\frac{p_R C_{RA}}{p_A C_{AA}+\sigma_{\mathbf{n_A}}^2} \geq f_2(p_A,p_B,p_R) = \frac{p_{R,k}C_{RA}}{p_{A,k}C_{AA}+\sigma_{\mathbf{n_A}}^2}\Big(\log_2\Big(\frac{p_R C_{RA}}{p_{R,k}C_{RA}}\Big) - \frac{p_A C_{AA}+\sigma_{\mathbf{n_A}}^2}{p_{A,k}C_{AA}+\sigma_{\mathbf{n_A}}^2} + 2\Big) \quad (6.51)$$

where g_1, g_2, f_1 and f_2 are all linear functions, and where the constants $p_{A,k}, p_{B,k}$ and $p_{R,k}$ are introduced such that an iterative process can be applied to the refinement method as well. Furthermore, these successive approximations guarantee a strict refinement of the solution, i.e., a process that always gets closer to the optimal solution, since these functions form an upper bound to the problem utility function,

thus, always having a negative gradient.

Therefore, a refinement stage is introduced, aiming to solve, at each iteration k, the following problem

$$\begin{aligned} \underset{p_R,p_A,p_B}{\text{max.}} \ & \log_2\left(1+\min\{g_1,g_2\}\right)+\log_2\left(1+\min\{f_1,f_2\}\right), \\ \text{s.t. } & P_{A,min}<p_A\leq P_{A,max};\ P_{B,min}<p_B\leq P_{B,max};\ P_{R,min}<p_R\leq P_{R,max}, \end{aligned} \tag{6.52}$$

where here the utility function of this problem is concave, since it is the sum of a composition of concave monotonically increasing functions with linear ones. The constraints are also linear, making the problem concave and, thus, solvable with gradient-based methods [109]. Finally, the algorithm proposed to find an approximation to the optimal powers that maximize the bidirectional sum rate, based on Piecewise MacCormick relaxation and followed by an iterative solution refinement is stated in algorithm 4.

Algorithm 4 Close to Optimal Powers for Sum Rate Maximization

Input: Channel coefficients, C_{AR}, C_{BR}, C_{RR}, C_{RA}, C_{RB}, C_{AA}, and C_{BB} (instantaneous or ergodic); Peak power for each element, $P_{A,max}$, $P_{B,max}$, and $P_{R,max}$;

Output: Close to optimal powers, p_A^*, p_B^* and p_R^*;

1. Initialization: Set the number of partitions per variable, $N_{part,A}$, $N_{part,B}$, $N_{part,R}$; Set the partitions sizes of each variable; Initialize power bounds, $P_{A,1}^L$, $P_{B,1}^L$, $P_{R,1}^L$, $P_{A,1}^U$, $P_{B,1}^U$, $P_{R,1}^U$; Set the number of iterations for refinement N_{ref} and stopping criteria η.

2. Piecewise MacCormick Iterations: for $(i,j,k)=(1,1,1),\cdots,(N_{part,A},N_{part,B},N_{part,R})$**:**

Solve Optimization problem in (6.47):

i) Power range: $P_{A,i}^L$, $P_{B,j}^L$, $P_{R,k}^L$, $P_{A,i}^U$, $P_{B,j}^U$, $P_{R,k}^U$;

ii) Use convex/concave optimization tools [103];

iii) Store obtained powers, $p_{A,i}$, $p_{B,j}$ and $p_{R,k}$.

3. Evaluation: Revisit all obtained powers and pick ($\hat{p}_A$, $\hat{p}_B$, $\hat{p}_R$) that maximizes R_Σ and correspondent space partition ($\hat{P}_A^L$, $\hat{P}_B^L$, $\hat{P}_R^L$,$\hat{P}_A^U$, $\hat{P}_B^U$, $\hat{P}_R^U$);

4. Refinement: Refine the obtained powers to get (p_A^*,p_B^*,p_R^*):

Initiate power constants: $p_{A,0}=\hat{p}_A$, $p_{B,0}=\hat{p}_B$ and $p_{R,0}=\hat{p}_R$;

Power range: $(P_{A,min},P_{B,min},P_{R,min})=(\hat{P}_A^L,\hat{P}_B^L,\hat{P}_R^L)$, $(P_{A,max},P_{B,max},P_{R,max})=(\hat{P}_A^U,\hat{P}_B^U,\hat{P}_R^U)$;

for $k=1,\cdots,N_{ref}$ **do**

i) Solve optimization problem in (6.52) for the chosen space partition [103];

ii) Update power constants: $p_{A,k+1}=p_{A,k}$, $p_{B,k+1}=p_{B,k}$ and $p_{R,k+1}=p_{R,k}$;

iii) Stopping criteria: if $\|\,(p_{A,k+1},p_{B,k+1},p_{R,k+1})-(p_{A,k},p_{B,k},p_{R,k})\,\|^2\ /\ \|\,(p_{A,k},p_{B,k},p_{R,k})\,\|^2\leq\eta$;

end for

5. Terminate: After all iterations are completed or reached the stopping criteria: $p_A^*=p_{A,end}$, $p_B^*=p_{B,end}$ and $p_R^*=p_{R,end}$.

Note that the fair sum rate optimization can be solved with algorithm 4 by only adding the linear extra constraint, as in (6.41), in each optimization stage (in optimization problem (6.47) and (6.52)).

6.7 Numerical Results of the Proposed Algorithm

This section evaluates the performance of the sum rate maximization algorithm, previously proposed. For simulation proposes, it is considered that the relay has $M_R=4$ receive antennas and $M_T=1$

transmit antennas. As previously stated, it is assumed that all channels vectors are generated from a complex normal distribution, i.e., $\mathbf{h_{AR}}$, $\mathbf{h_{BR}}$, $\mathbf{h_{RR}}$ entries take values from $\mathcal{CN}(0,1)$, while the channel gains h_{RA}, h_{RB}, h_{AA}, h_{BB} are drawn from $\mathcal{CN}(0,1)$. Also, it is assumed that the thermal noise at each antenna of the system has normalized power of -10 dB, i.e., $\sigma^2_{n_A} = \sigma^2_{n_B} = -10$ dB and that $\sigma^2_{n_R} = -4$ dB. The power range for the terminals is considered to be $[-20, 10]$ dB, while the relay normalized power can take values from $[0, 30]$ dB, i.e., $P_{A,min} = P_{B,min} = -20$ dB, $P_{A,max} = P_{B,max} = 10$ dB and $P_{R,min} = 0$ dB, $P_{R,max} = 30$ dB. These normalized power ranges reflect that done in practical systems, where the relay can transmit with much larger power since it is fixed and connected to a power supply, while the terminals only have access to batteries with limited capacity. Moreover, these ranges may be larger when compared to practical scenarios in order to broadly understand the algorithm performance.

Utility Function Analysis

In order to understand the complexity of the optimization problem proposed in (6.40), its utility function is depicted in Fig. 6.8 after 10^3 channel realizations (approximation of the ergodic case), for two fixed p_R values and varying p_A and p_B values. The residual self-interference is set to $k_A = k_B = k_R = -20$ dB.

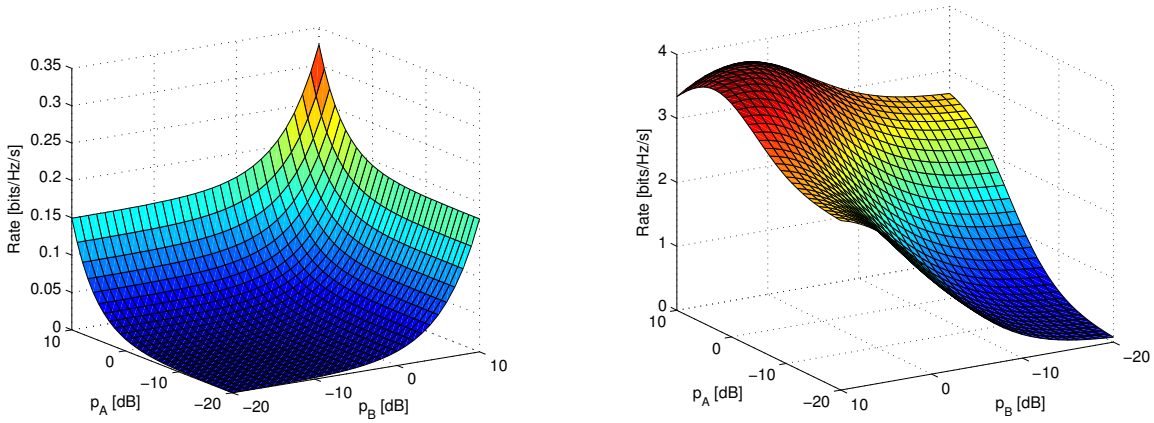

(a) $p_R = 30$ dB.

(b) $p_R = 5$ dB.

Figure 6.8: Utility function of the optimization problem for fixed relay transmit power p_R.

As may be observed in 6.8(a), the figure shows that when the relay is transmitting with its maximum power, the terminals should also employ their peak powers in order to maximize the system sum rate. However, in this case the relay suffers major system degradation due to the self-interference component, that also increases with p_R, and for that reason the sum rate takes very low values. Notwithstanding, Fig. 6.8(b) shows that when the relay transmits with a power inferior to the terminal's peak powers, the sum rate may take higher values, which is desirable. Thus, the power allocation at the terminals and at the relay is clearly not obvious, and so proposed algorithm is expected to find both terminals and relay transmit power that maximizes the sum rate.

Before evaluating the output of the proposed algorithm, it is interesting to define the following reference cases for comparison and analysis purposes:

Perfect Self-Interference Cancellation

The case of perfect self-interference cancellation (P-SIC) is the upper bound to the sum rate considered in this problem, since the effect of interference is not considered. It is then possible to employ the maximum power at each terminal and at the relay. This yields a sum rate that is given by

$$R_{\Sigma,\text{P-SIC}} = \log_2\left(1+\min\left\{\frac{P_{A,max}C_{AR}}{\sigma^2_{\mathbf{n_R}}},\frac{P_{R,max}C_{RB}}{\sigma^2_{n_B}}\right\}\right)+\log_2\left(1+\min\left\{\frac{P_{B,max}C_{BR}}{\sigma^2_{\mathbf{n_R}}},\frac{P_{R,max}C_{RA}}{\sigma^2_{n_A}}\right\}\right). \tag{6.53}$$

Half-Duplex

The case of half-duplex (HD) defines the threshold above which it the use of full-duplex mode is worthy as it achieves a gain in the system sum rate, which may be also computed with the maximum powers. However, it is necessary to use two channel resources, which drops the achievable rate to

$$R_{\Sigma,\text{HD}} = \frac{1}{2}\log_2\left(1+\min\left\{\frac{P_{A,max}C_{AR}}{\sigma^2_{\mathbf{n_R}}},\frac{P_{R,max}C_{RB}}{\sigma^2_{n_B}}\right\}\right)+\frac{1}{2}\log_2\left(1+\min\left\{\frac{P_{B,max}C_{BR}}{\sigma^2_{\mathbf{n_R}}},\frac{P_{R,max}C_{RA}}{\sigma^2_{n_A}}\right\}\right). \tag{6.54}$$

Peak Power Transmission

It is also interesting to compare the proposed algorithm with two cases where the maximum available power is used. The first is maximum power (MP) and consists of using the maximum available power of each terminal and of the relay, yielding

$$\begin{aligned} R_{\Sigma,\text{MP}} =& \log_2\left(1+\min\left\{\frac{P_{A,max}C_{AR}}{P_{R,max}C_{RR}+\sigma^2_{\mathbf{n_R}}},\frac{P_{R,max}C_{RB}}{P_{B,max}C_{BB}+\sigma^2_{n_B}}\right\}\right)+ \\ &+\log_2\left(1+\min\left\{\frac{P_{B,max}C_{BR}}{P_{R,max}C_{RR}+\sigma^2_{\mathbf{n_R}}},\frac{P_{A,max}C_{RA}}{P_{A,max}C_{AA}+\sigma^2_{n_A}}\right\}\right). \end{aligned} \tag{6.55}$$

The other case is to assume uniform distribution of power (UP), i.e., the terminals and relay employed the same power to transmit, as $P_{max} = \min\{P_{A,max}, P_{B,max}, P_{R,max}\}$. Since it is considered a lower and equal peak power for the terminals, $P_{max} = P_{A,max}$. The rate is then given by

$$\begin{aligned} R_{\Sigma,\text{UP}} =& \log_2\left(1+\min\left\{\frac{P_{max}C_{AR}}{P_{max}C_{RR}+\sigma^2_{\mathbf{n_R}}},\frac{P_{max}C_{RB}}{P_{max}C_{BB}+\sigma^2_{n_B}}\right\}\right)+ \\ &+\log_2\left(1+\min\left\{\frac{P_{max}C_{BR}}{P_{max}C_{RR}+\sigma^2_{\mathbf{n_R}}},\frac{P_{max}C_{RA}}{P_{max}C_{AA}+\sigma^2_{n_A}}\right\}\right). \end{aligned} \tag{6.56}$$

6.7.1 Different Number of Space Partitions and Refinement Iterations

Evaluating firstly the effect of the algorithm parameters, i.e., how the number of space partitions and the number of refinement iterations affect the performance of the algorithm, consider the ergodic sum rate optimization (with utility function as in 6.5.2). Fig. 6.9 shows the sum rate for the ergodic channel and for different $N_{part} = N_{part,A} = N_{part,B} = N_{part,R}$ and N_{ref} (without stopping criteria), and also for varying levels of interference. It is evaluated the case when the solution refinement is used with

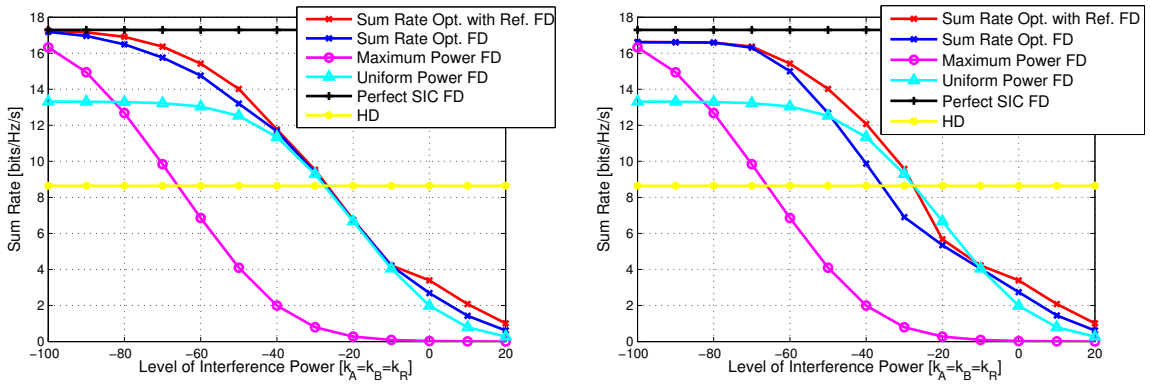

(a) $N_{part} = 3$, $N_{ref} = 200$.

(b) $N_{part} = 2$, $N_{ref} = 1000$.

Figure 6.9: Impact of the number of space partitions N_{part} and the number of refinement iterations N_{ref} on the proposed algorithm, for the ergodic case.

MacCormick relaxation (red lines) and also when the algorithm is performed without refinement (dark blue lines). As may be observed, the best solution which attains higher sum rates depends directly on the parameters under evaluation. In 6.9(a), the curve for $N_{part} = 3$ and $N_{ref} = 200$ demonstrates that it is possible to obtain a sum rate above the reference schemes, considering interference effects, which indicates the good performance of the algorithm. In fact, it does not prove that a close to the optimal solution is obtained, however, it may be assumed so when comparing both curves in the figure. The P-SIC and HD curves are obviously independent of the self-interference power. The target is to have a sum rate between the two, i.e., having a real rate gain by using full-duplex transmissions when compared with the half-duplex transmission. Since a considerable number of space partitions are taken, the refinement method only introduces a small but significant gain in terms of sum rate, especially for low and high power levels of interference. Moreover, there is the need to solve $3^3 + 200 = 227$ linear programs, which is computationally feasible. In contrast, Fig 6.9(b) only employs two partitions per variable, which shows that it is necessary to use a higher number of iterations in the refinement algorithm to obtain a sum rate which is better than the previously mentioned reference schemes for some levels of interference. Nevertheless, solving $3^2 + 1000 = 1009$ linear programs does not improve the algorithm performance, hence the critical aspect of the proposed algorithm resides in choosing an appropriate number of partitions.

6.7.2 Sum Rate Performance with and without Fair Constraint

Another interesting aspect is to evaluate the instantaneous sum rate, i.e., the power allocation for a channel realization, also for the cases where the fair rate constraint is and is not considered. It is expected that when introducing it, the algorithm performance will decrease, however, the bidirectional exchange of information will be guaranteed.

Fig. 6.10(a) shows the sum rate curves for $N_{part,A} = N_{part,B} = N_{part,R} = 3$, $N_{ref} = 200$, with a stopping criteria $\eta = 10^{-6}$ and an aggressive unbalance factor of $\varrho = 0.05$. Also the channel under consideration is defined by $\mathbf{h_{AR}} = [1.0 - j1.2, 2.2 + j0.4, -0.2 - j2.4, -0.3 - j0.4]^T$, $\mathbf{h_{BR}} = [0.7 -$

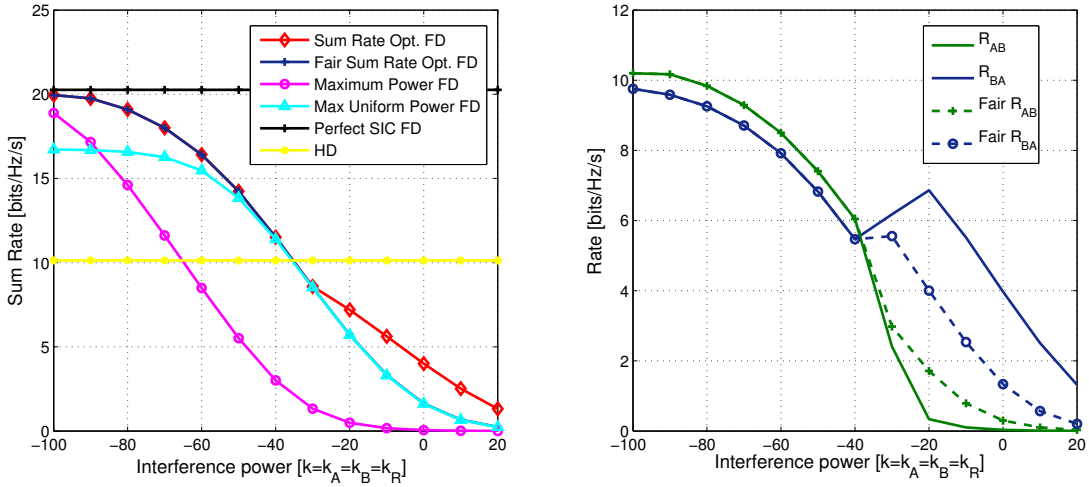

(a) Sum rate with and without fair rate constraint.

(b) Bidirectional rates with and without fair rate constraint (both with refinement).

Figure 6.10: Impact evaluation of the fair sum rate constraint for one channel realization on the proposed algorithm.

$j0.5, 1.5 + j1.6, -1.2 - j0.9, 1.0 + j0.4]^T$, $\mathbf{h_{RR}} = [0.8 - j0.7, 0.9 + j0.3, -0.5 - j1.1, 1.5 + j0.1]^T$, and by $h_{RA} = 3.1 + j1.7$, $h_{RB} = -1.1 + j0.2$, $h_{AA} = 2.4 - j1.7$, $h_{BB} = -2.2 + j0.4$.

Firstly, observe the fair sum rate is under the curve where this constraint is not considered. However, this only happens for high levels of interference power. For low levels of interference, the fair sum rate and the sum rate achieved by the proposed algorithm match perfectly. This effect is also illustrated in Fig. 6.10(b) where the two bidirectional rates are plotted for different levels of interference. As may be observed, when the interference power is higher than -40 dB, the best scheme is to turn one of the terminals almost off and transmit at full power with the other. The mentioned effect unbalances the flow of information, which is not desirable in such a scenario. Thus, by introducing the fair rate constraint there is a trade-off between maximizing the sum rate and having the the terminals transmitting with similar powers and rates.

Fig. 6.11 illustrates the power distribution for different levels of interference, where it is possible to understand the mentioned effect. In Fig. 6.11(b), the power employed at each terminal is always very similar and close to the peak power for low levels of interference, while in Fig. 6.11(a) for high interference power one of the terminals transmits close to the minimum power and the other close to the maximum. In both cases the transmitted relay power is the variable which reflects mostly the effect of self-interference in terms of sum rate.

In fact, the in-band full-duplex mode should only be employed if its rate is higher than the half-duplex counterpart (yellow line). For this channel, this occurs for levels of interference smaller than approximately -40 dB where, as Fig. 6.10(a) shows, the optimal power allocation is virtually the same considering and not considering the fair sum rate constraint. Moreover, this numerical analysis shows also that the only optimization variable should be the relay power, p_R, while the transmit terminal power should always be $p_A = p_B = P_{A,max} = P_{B,max}$, saving computation time in the algorithm. Finally, it is

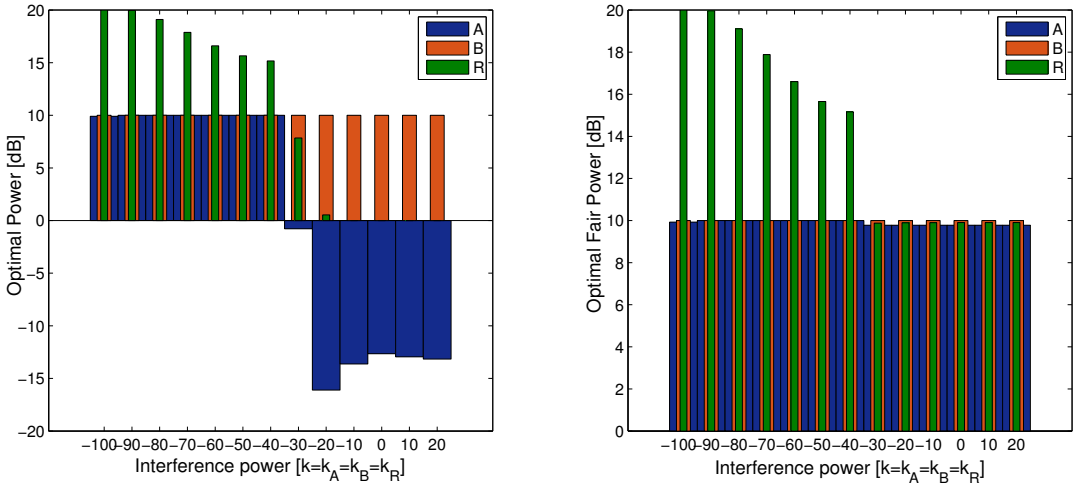

(a) Power allocation without fair rate constraint.

(b) Power allocation with fair rate constraint.

Figure 6.11: Allocated powers for one channel realization of the proposed algorithm.

worth referring to the fact that the power allocation gain is clear when it is compared with MP and UP.

6.8 Concluding Remarks

This chapter proposes an in-band full-duplex system that uses the properties of PLNC to improve the used resources in a bidirectional exchange of information between two terminals through a relay station. Firstly, a basic PLNC scheme was introduced, the DeF protocol, that uses a QPSK constellation along with well-known network code functions. The possibility of establishing a reliable communication was shown with it, despite this scheme's simplicity. Furthermore, the best network function and constellation mapping was derived and numerically evaluated. Then, state-of-the-art CF protocol for the complex fast fading channel is proposed with transmission precoding. However, since the protocol relies on the channel estimations, its performance deteriorates in the presence of imperfect CSI. Massive MIMO transmissions were introduced into the system and it was shown how the orthogonality between large matrices helps reduce the protocol inherent interference, but also the effect of the self-interference. The latter effect was verified with SER curves, where the errors in the channel estimations may be mitigated with large dimension transmissions.

Finally, an optimization problem was presented that assumes only peak power constraints in the relay and in the terminals and tries to maximize the bidirectional sum rate of the system. This problem was shown to be non-concave, and thus, an iterative algorithm based on Piecewise MacCormick relaxation with a refinement stage was derived. The algorithm was shown to achieve a good performance in terms of sum rate. Moreover, the numerical analysis performed demonstrates that for low levels of interference, the terminals should transmit with their maximum power, while only the relay power should be considered for optimization.

Chapter 7

Conclusions

The work presented in the previous chapters evaluates the possibility of in-band full-duplex transmissions for future multi-hop networks. To begin with, a full-duplex relaying system is characterized and different methods for canceling the problem of self-interference are examined. Then, the use of massive arrays at the relay station is incorporated, so that an extra level of mitigation is obtained. Finally, bidirectional communication is taken into account by exploring the recent advances in physical layer network coding (PLNC). The following section summarizes the statements already made within the document. In addition, some research paths for possible future work are suggested.

7.1 Overall Considerations

The forthcoming change of paradigm along with the predicted exponential growth of data flowing through our wireless networks is driving the search for disruptive technologies capable of corresponding with these new demands. Among them and with great potential, lies in-band full-duplex communications, which will double the spectral efficiency of current transmissions and will facilitate management of the available spectrum. However, self-inflicted interference poses a great challenge to the deployment of this technology. If not properly dealt with, this so-called self-interference may create unbearable signal-to-interference-plus noise ratios (SINR) for allowing the establishment of reliable communication links. Thus, this thesis starts by reviewing the literature on in-band full-duplex systems and basic concepts of multiple-input multiple-output (MIMO) wireless communications, which allows it to study and propose new techniques and systems where the performance of full-duplex transmissions can be enhanced. The contribution of this work is summarized in the following paragraphs.

In first place, an in-band full-duplex relay station was formally and fully described, special focus was given to the system impairments that cause residual self-interference. In order to mitigate this effect, spatial suppression filters were studied, that take advantage of the extra degrees of freedom brought by MIMO transmissions. The bit error rate (BER) for two different types of these filters, null-space projection (NSP) and minimum mean square error (MMSE), was evaluated and where it was possible to observe a self-interference resilience of approximately 20 dB. However, spatial suppression suffers from distortion

when shaping the transmitted and desired signal. For that reason, adaptive feedback cancellation filters were proposed. Namely, a least mean square (LMS) and a recursive least squares (RLS) filter were derived for MIMO frequency-selective channels and under OFDM transmissions. Both techniques' performance was measured in terms of BER plots that demonstrate the possibility of obtaining levels up to 40 dB of self-interference resilience, depending on the system impairments that pose the main obstacle for these filters.

Secondly, and considering the methods derived for canceling self-interference, the use of a massive array at the relay station was explored. The orthogonal properties between large dimension matrices can in fact contribute to cancellation of the residual part of this undesirable effect. Therefore, a system with MMSE filtering was proposed combined with zero forcing (ZF) detection and precoding filters. The BER was assessed at the relay and at the final destinations, showing a gain in interference resilience when using several antennas and revealing an optimal relay transmit power. Consequently, an algorithm to find the optimal power allocation scheme that minimizes the system energy efficiency (EE) under a minimum link quality was derived.

Finally, bidirectional relaying was brought together with in-band full-duplex transmissions, in the hope of reducing the number of employed resources in a two-way relay channel (TWRC) to the same as machine-to-machine communication (m2m). To that end, techniques from PLNC were studied and adapted to the previous systems. Two protocols were considered for this purpose, namely, denoise-and-forward (DeF) and compute-and-forward (CF), where it was possible to evaluate the performance of both schemes in terms of BER or symbol error rate (SER). Furthermore, the integration of large antennas is proposed for the CF protocol and the performance degradation of the scheme was assessed for different numbers of antennas and for channel estimation errors. Additionally, the achievable sum rate of this system was derived and an optimization algorithm proposed in order to find the optimal transmit powers that maximize it.

7.2 Future Research Work

Due to the nature of this thesis, there are many possible research paths that directly follow the work developed and presented. This section succinctly enumerates some research that would complement this work. The first to mention is the possibility of combining spatial suppression and feedback adaptive cancellation filters, so that higher levels of self-interference mitigation could be achieved. This requires carefully choosing each filter's relative position and understanding their mutual effect. Another meaningful result is to assume more realistic channel estimations when considering large arrays of antennas. In fact, this is one of the major problems of large dimension channel matrices, which is neglected in this work by simply assuming the same procedure for the small number of antennas case. Finally, the next step in research is to generalize the bidirectional full-duplex relaying for the TWRC to the case of multiple-way relay channel, exploring more advanced CF techniques with higher dimension lattices proposed in [67].

Bibliography

[1] Andrea Goldsmith. *Wireless Communications*. Cambridge, 1^{st} edition, 2004. ISBN:978-0521837163.

[2] Afif Osseiran, Federico Boccardi, Volker Braun, Katsutoshi Kusume, Patrick Marsch, Michal Maternia, Olav Queseth, Malte Schellmann, Hans Schotten, Hidekazu Taoka, Hugo Tullberg, Mikko A. Uusitalo, Bogdan Timus, and Mikael Fallgren. "Scenerios for 5G Mobile and Wireless Communications". *IEEE Communications Magazine*, 52(5):26–35, May 2014.

[3] "The 5G Infrastructure Public Private Partnership". Web platform: *http://5g-ppp.eu* [June 2015].

[4] "5th Generation Non-Orthogonal Waveforms for Asynchronous Signalling". Web platform: *http://www.5gnow.eu* [June 2015].

[5] "Mobile and Wireless Communications Enablers for Twenty-Twenty (2020) Information Society". Web platform: *https://www.metis2020.com* [June 2015].

[6] Gerhard Wunder, Peter Jung, Martin Kasparick, Thorsten Wild, Frank Schaich, Yejian Chen, Stephan ten Brink, Ivan Gaspar, Nicola Michailow, Andreas Festag, Luciano Mendes, Nicolas Cassiau, Dimitri Kténas Marcin Dryjanski, Slawomir Pietrzyk, Bertalan Eged, Peter Vago, and Frank Wiedmann. "5GNOW: Non-Orthogonal, Assynchronous Waveforms for Future Mobile Applications". *IEEE Communications Magazine*, 52(2):97–105, February 2014.

[7] A. Osseiran, V. Braun, T. Hidekazu, P. Marsch, H. Schotten, H. Tullberg, M.A. Uusitalo, and M. Schellman. "The Foundation of the Mobile and Wireless Communications System for 2020 and Beyond: Challenges, Enablers and Technology Solutions". In *IEEE* 77^{th} *Vehicular Technology Conference (VTC Spring)*, pages 1–5, June 2013.

[8] Federico Boccardi, Robert W. Heath Jr., Angel Lozano, Thomas L. Marzetta, and Petar Popovski. "Five Disruptive Technology Directions for 5G". *IEEE Communications Magazine*, 52(5):74–80, May 2014.

[9] Steven Hong, Joel Brand, Jung Il Choi, Mayank Jain, Jeff Mehlman, Sachin Katti, and Philip Levis. "Applications of Self-Interference Cancelation in 5G and Beyond". *IEEE Communications Magazine*, 52(2):114–121, February 2014.

[10] João S. Lemos, Francisco Rosário, Francisco A. Monteiro, João Xavier, and António Rodrigues. "Massive MIMO Full-Duplex Relaying with Optimal Power Allocation for Independent Multipairs". In *IEEE 16^{th} Workshop on Signal Processing Advances in Wireless Communications (SPAWC)*, pages 306–310, July 2015. [Online]. Available: http://arxiv.org/abs/1504.06746.

[11] João S. Lemos, Francisco A. Monteiro, Ivo Sousa, and António Rodrigues. "Full-Duplex Relaying in MIMO-OFDM Frequency-Selective Channels with Optimal Adaptive Filtering". *Accepted in the IEEE 3^{rd} Global Conference on Signal and Information Processing (GlobalSIP)*, Dec 2015. [Online]. Available: http://arxiv.org/abs/1505.00850.

[12] João S. Lemos, Francisco A. Monteiro, João Xavier, and António Rodrigues. "Sum Rate Maximization for Full-Duplex Bidirectional Relaying with Physical Layer Network Coding". *In preparation for submission*, 2015.

[13] João S. Lemos, Francisco A. Monteiro, and António Rodrigues. "On the Massive MIMO Effect in Practical Physical Layer Network Coding Systems". *In preparation for submission*, 2015.

[14] A. Sabharwal, P. Schniter, Dongning Guo, D.W. Bliss, S. Rangarajan, and R. Wichman. "In-Band Full-Duplex Wireless: Challenges and Opportunities". *IEEE Journal on Selected Areas in Communications*, 32(9):1637–1652, September 2014.

[15] Melissa Duarte, Chris Dick, and Ashutosh Sabharwal. "Experiment-Driven Characterization of Full-Duplex Wireless Systems". *IEEE Transactions on Wireless Communications*, 11(2):4296–4307, July 2012.

[16] Zhongshan Zhang, Xiaomeng Chai, Keping Long, A.V. Vasilakos, and L. Hanzo. "Full Duplex Techniques for 5G Networks: Self-Interference Cancellation, Protocol Design, and Relay Selection". *IEEE Communications Magazine*, 53(5):128–137, May 2015.

[17] Mikko Valkama. Full-Duplex Radio Communications. Presentation, April 2013. Tampere University of Technology. [Online]. Available: http://www.cs.tut.fi/ieee_spcas/Seminar%20photos/Mikko.pdf (December 2014).

[18] M. Duarte and A. Sabharwal. "Full-Duplex Wireless Communications Using Off-the-Shelf Radios: Feasibility and First Results". In *Conference Record of the 44^{th} Asilomar Conference on Signals, Systems and Computers (ASILOMAR)*, pages 1558–1562, Nov 2010.

[19] E. Everett, A. Sahai, and A. Sabharwal. "Passive Self-Interference Suppression for Full-Duplex Infrastructure Nodes". *IEEE Transactions on Wireless Communications*, 13(2):680–694, February 2014.

[20] Achaleshwar Sahai, Gaurav Patel, and Ashutosh Sabharwal. "Pushing the Limits of Full-Duplex: Design and Real-time Implementation". *Arxiv preprint arXiv:1107.0607*, June 2011.

[21] Ehsan Aryafar, Mohammad Amir Khojastepour, Karthikeyan Sundaresan, Sampath Rangarajan, and Mung Chiang. "MIDU: Enabling MIMO Full Duplex". In *Proceedings of the 18^{th} Annual*

International Conference on Mobile Computing and Networking, Mobicom '12, pages 257–268, 2012.

[22] E. Everett, M. Duarte, C. Dick, and A. Sabharwal. "Empowering Full-Duplex Wireless Communication by Exploiting Directional Diversity". In *Conference Record of the 45th Asilomar Conference on Signals, Systems and Computers (ASILOMAR)*, pages 2002–2006, Nov 2011.

[23] Jung Il Choi, Mayank Jain, Kannan Srinivasan, Phil Levis, and Sachin Katti. "Achieving Single Channel, Full Duplex Wireless Communication". In *Proceedings of the 16^{th} Annual International Conference on Mobile Computing and Networking*, MobiCom '10, pages 1–12, 2010.

[24] Dinesh Bharadia, Emily McMilin, and Sachin Katti. "Full Duplex Radios". In *Proceedings of the ACM 2013 Conference on SIGCOMM*, SIGCOMM '13, pages 375–386. ACM, 2013.

[25] Michael E. Knox. "Single Antenna Full Duplex Communications using a Common Carrier". *In the IEEE 13th Annual Wireless and Microwave Technology Conference*, pages 1–6, April 2012.

[26] Peter Lindberg and Erik Öjefors. "A Bandwidth Enhancement Technique for Mobile Handset Antennas Using Wavetraps". *IEEE Transactions on Antennas and Propagation*, 54(8):2226–2233, August 2006.

[27] Dan Sievenpiper, Lijun Zhang, Romulo F. Jimenez Broas, Nicholas G. Alexopolous, and Eli Yablonovitch. "High-Impedance Electromagnetic Surfaces with a Forbidden Frequency Band". *IEEE Transactions on Microwave Theory and Techniques*, 47(11):2059–2074, November 1999.

[28] Ki-Jin Kim and Kyu-Ho Park. "The High Isolation Dual-Band Inverted F Antenna Diversity System with the Small N-Section Resonators on the Ground Plane". *Asia-Pacific Microwave Conference (APMC)*, pages 195–198, September 2011.

[29] M. Heino, D. Korpi, T. Huusari, E. Antonio-Rodriguez, S. Venkatasubramanian, T. Riihonen, L. Anttila, C. Icheln, K. Haneda, R. Wichman, and M. Valkama. "Recent Advances in Antenna Design and Interference Cancellation Algorithms for In-Band Full Duplex Relays". *IEEE Communications Magazine*, 53(5):91–101, May 2015.

[30] Ioannis Krikidis and Himal A. Suraweera. "Full-Duplex Cooperative Diversity with Alamouti Space-Time Code". *IEEE Wireless Communication Letters*, 2(5):519–522, October 2013.

[31] Hien Quoc Ngo, Himal A. Suraweera, Michail Matthaiou, and Erik G. Larsson. "Multipair Full-Duplex Relaying with Massive Arrays and Linear Processing". *IEEE Journal on Selected Areas in Communications*, 32(9):1721–1737, September 2014.

[32] Taneli Riihonen, Stefan Werner, and Risto Wichman. "Optimized Gain Control for Single-Frequency Relaying with Loop Interference". *IEEE Transactions on Wireless Communications*, 8(6):2801–2806, April 2009.

[33] Himal A. Suraweera, Ioannis Krikidis, Gan Zheng, Chau Yuen, and Peter J. Smith. "Low-Complexity End-to-End Performance Optimization in MIMO Full-Duplex Relay System". *IEEE Transactions on Wireless Communications*, 13(2):913 – 926, February 2014.

[34] Taneli Riihonen, Stefan Werner, and Risto Wichman. "Mitigation of Loopback Self-Interference in Full-Duplex MIMO Relays". *IEEE Transactions on Signal Processing*, 59(12):5983 – 5993, December 2011.

[35] Melissa Duarte. *Full-duplex Wireless: Design, Implementation and Characterization.* PhD thesis, Rice University, 2012.

[36] Mayank Jain, Jung Il Choi, Taemin Kim, Dinesh Bharadia, Siddharth Seth, Kannan Srinivasan, Philip Levis, Sachin Katti, and Prasun Sinha. "Practical, Real-time, Full Duplex Wireless". In *Proceedings of the* 17^{th} *Annual International Conference on Mobile Computing and Networking*, MobiCom '11, pages 301–312, 2011.

[37] T. Riihonen, S. Werner, and R. Wichman. "Comparison of Full-Duplex and Half-Duplex Modes with a Fixed Amplify-and-Forward Relay". In *IEEE Wireless Communications and Networking Conference (WCNC 2009)*, pages 1–5, April 2009.

[38] Taneli Riihonen, Stefan Werner, and Risto Wichman. "Optimized Gain Control for Single-Frequency Relaying with Loop Interference". *IEEE Transactions on Wireless Communications*, 8(6):2801–2806, June 2009.

[39] Taneli Riihonen, Stefan Werner, and Risto Wichman. "Spatial Loop Interference Suppression in Full-Duplex MIMO Relays". In *Conference Record of the* 43^{th} *Asilomar Conference on Signals, Systems and Computers (ASILOMAR)*, pages 1508–1512, Nov 2009.

[40] Panagiota Lioliou, Mats Viberg, Mikael Coldrey, and Fredrik Athley. "Self-Interference Suppression in Full-Duplex MIMO Relays". In *Conference Record of the 44*th *Asilomar Conference on Signals, Systems and Computers (ASILOMAR)*, pages 658–662, Nov 2010.

[41] Taneli Riihonen, Stefan Werner, and Risto Wichman. "Hybrid Full-Duplex/Half-Duplex Relaying with Transmit Power Adaptation ". *IEEE Transactions on Wireless Communications*, 10(9):2059–2074, November 2011.

[42] Taneli Riihonen, Stefan Werner, and Risto Wichman. "Transmit Power Optimization for Multi-antenna Decode-and-Forward Relays with Loopback Self-Interference from Full-Duplex Operation". *Conference Record of the* 45^{th} *Asilomar Conference on Signals, Systems and Computers (ASILOMAR)*, pages 1408–1412, 2011.

[43] T. Riihonen, M. Vehkapera, and R. Wichman. "Large-System Analysis of Rate Regions in Bidirectional Full-Fuplex MIMO Link: Suppression versus Cancellation". In 47^{th} *Annual Conference on Information Sciences and Systems (CISS)*, pages 1–6, March 2013.

[44] Emilio Antonio-Rodriguez., Roberto Lopez-Valcarce, Taneli Riihonen, Stefan Werner, and Risto Wichman. "Adaptive Self-Interference Cancellation in Wideband Full-Duplex Decode-and-Forward MIMO Relays". *IEEE* 14^{th} *Workshop on Signal Processing Advances in Wireless Communications (SPAWC)*, pages 370–374, June 2013.

[45] Dani Korpi, Sathya Venkatasubramanian, Taneli Riihonen, Lauri Anttila, Strasdosky Otewa, Clemens Icheln, Katsuyuki Haneda, Sergei Tretyakov, Miko Valkama, and Risto Wichman. "Advanced Self-Interference Cancellation and Multiantenna Techniques for Full-Duplex Radios". *Conference Record of the* 47^{th} *Asilomar Conference on Signals, Systems and Computers (ASILOMAR)*, pages 3–8, November 2013.

[46] Fredrik Rusek, Daniel Persson, Buon Kiong Lau, Erik G. Larsson, Thomas L. Marzetta, Ove Edfors, Fredrik Tufvesson, Post Print, Fredrik Rusek, Daniel Persson, Buon Kiong Lau, Erik G. Larsson, Thomas L. Marzetta, Fredrik Rusek, Daniel Persson, Buon Kiong Lau, Erik G. Larsson, Thomas L. Marzetta, Ove Edfors, and Fredrik Tufvesson. "Scaling up MIMO: Opportunities and Challenges with Very Large Arrays". *IEEE Signal Processing Magazine*, 30(1):40–60, January 2013.

[47] U. Madhow, D.R. Brown, S. Dasgupta, and R. Mudumbai. "Distributed Massive MIMO: Algorithms, Architectures and Concept Systems". In *Information Theory and Applications Workshop (ITA), 2014*, pages 1–7, February 2014.

[48] H.A. Suraweera, Hien Quoc Ngo, T.Q. Duong, Chau Yuen, and E.G. Larsson. "Multi-Pair Amplify-and-Forward Relaying with Very Large Antenna Arrays". In *IEEE International Conference on Communications (ICC)*, pages 4635–4640, June 2013.

[49] Hongyu Cui, Lingyang Song, and Bingli Jiao. "Multi-Pair Two-Way Amplify-and-Forward Relaying with Very Large Number of Relay Antennas". *IEEE Transactions on Wireless Communications*, 13(5):2636–2645, May 2014.

[50] Tuyet Van Thi Le and Yun Hee Kim. "Power and Spectral Efficiency of Multi-Pair Massive Antenna Relaying Systems With Zero-Forcing Relay Beamforming". *IEEE Communications Letters*, 19(2):243–246, February 2015.

[51] Bei Yin, M. Wu, C. Studer, J.R. Cavallaro, and J. Lilleberg. "Full-Duplex in Large-Scale Wireless Systems". In *Conference Record of the Asilomar Conference on Signals, Systems and Computers (ASILOMAR)*, pages 1623–1627, Nov 2013.

[52] Wei Zhang, Xiaoli Ma, Brian Gestner, and David V. Anderson. "Designing Low-Complexity Equalizers for Wireless Systems". In 45^{th} *Annual Conference on Information Sciences and Systems (CISS)*, pages 1–6, March 2011.

[53] R. Ahlswede, Ning Cai, S.-Y.R. Li, and R.W. Yeung. "Network Information Flow". *IEEE Transactions on Information Theory*, 46(4):1204–1216, July 2000.

[54] Shengli Zhang, Soung Chang Liew, and Patrick P. Lam. "Hot Topic: Physical-Layer Network Coding". In *Proceedings of the* 12^{th} *Annual International Conference on Mobile Computing and Networking*, MobiCom '06, pages 358–365, 2006.

[55] P. Popovski and H. Yomo. "The Anti-Packets Can Increase the Achievable Throughput of a Wireless Multi-Hop Network". In *IEEE International Conference on Communications (ICC)*, volume 9, pages 3885–3890, June 2006.

[56] B. Nazer and M. Gastpar. "Computing over Multiple-Access Channels with Connections to Wireless Network Coding". In *IEEE International Symposium on Information Theory*, pages 1354–1358, July 2006.

[57] Bobak Nazer and Michael Gastpar. "Reliable Physical Layer Network Coding". *Proceedings of the IEEE*, 99(3):438 – 460, March 2011.

[58] Petar Popovski and Toshiaki Koike-Akino. "Coded Bidirectional Relaying in Wireless Networks". In *New Directions in Wireless Communications Research*, pages 291–316. Springer US, 2009.

[59] Sachin Katti, Shyamnath Gollakota, and Dina Katabi. "Embracing Wireless Interference: Analog Network Coding". In *Proceedings of the 2007 Conference on Applications, Technologies, Architectures, and Protocols for Computer Communications*, SIGCOMM '07, pages 397–408, 2007.

[60] Shiqiang Wang, Qingyang Song, Xingwei Wang, and A. Jamalipour. "Rate and Power Adaptation for Analog Network Coding". *IEEE Transactions on Vehicular Technology*, 60(5):2302–2313, June 2011.

[61] Binyue Liu and Ning Cai. "Analog Network Coding in the Generalized High-SNR Regime". In *IEEE International Symposium on Information Theory Proceedings (ISIT)*, pages 74–78, July 2011.

[62] Raymond H.Y. Louie, Yonghui Li, and B. Vucetic. "Practical Physical Layer Network Coding for Two-Way Relay Channels: Performance Analysis and Comparison". *IEEE Transactions on Wireless Communications*, 9(2):764–777, February 2010.

[63] M.P. Wilson, K. Narayanan, H.D. Pfister, and A. Sprintson. "Joint Physical Layer Coding and Network Coding for Bidirectional Relaying". *IEEE Transactions on Information Theory*, 56(11):5641–5654, November 2010.

[64] R.F. Wyrembelski, T.J. Oechtering, and H. Boche. "Decode-and-Forward Strategies for Bidirectional Relaying". In *IEEE* 19^{th} *International Symposium on Personal, Indoor and Mobile Radio Communications (PIMRC)*, pages 1–6, Sept 2008.

[65] R.Y. Chang, Sian-Jheng Lin, and Wei-Ho Chung. "Symbol and Bit Mapping Optimization for Physical-Layer Network Coding with Pulse Amplitude Modulation". *IEEE Transactions on Wireless Communications*, 12(8):3956–3967, August 2013.

[66] T. Koike-Akino, P. Popovski, and Vahid Tarokh. "Optimized Constellations for Two-Way Wireless Relaying with Physical Network Coding". *IEEE Journal on Selected Areas in Communications*, 27(5):773–787, June 2009.

[67] B. Nazer and M. Gastpar. "Compute-and-Forward: Harnessing Interference with Structured Codes". In *IEEE International Symposium on Information Theory, 2008. ISIT 2008*, pages 772–776, July 2008.

[68] Bobak Nazer and Michael Gastpar. "Compute-and-Forward: Harnessing Interference Through Structured Codes". *IEEE Transactions on Information Theory*, 57(10):6463 – 6486, October 2011.

[69] U. Erez and R. Zamir. "Achieving 1/2 log (1+SNR) on the AWGN Channel with Lattice Encoding and Decoding". *IEEE Transactions on Information Theory*, 50(10):2293–2314, September 2004.

[70] O. Ordentlich, Jiening Zhan, U. Erez, M. Gastpar, and B. Nazer. "Practical Code Design for Compute-and-Forward". In *2011 IEEE International Symposium on Information Theory Proceedings (ISIT).*, pages 1876–1880, July 2011.

[71] Chen Feng, D. Silva, and F.R. Kschischang. "An Algebraic Approach to Physical-Layer Network Coding". In *2010 IEEE International Symposium on Information Theory Proceedings (ISIT)*, pages 1017–1021, June 2010.

[72] Jiening Zhan, B. Nazer, M. Gastpar, and U. Erez. "MIMO Compute-and-Forward". In *IEEE International Symposium on Information Theory (ISIT)*, pages 2848–2852, June 2009.

[73] Bobak Nazer. "Successive Compute-and-Forward". In *Proceedings of the International Zurich Seminar on Communications*, pages 103–106, 2012.

[74] Gan Zheng. "Joint Beamforming Optimization and Power Control for Full-Duplex MIMO Two-Way Relay Channel". *IEEE Transactions on Signal Processing*, 63(3):555–566, December 2015.

[75] S. Tedik and G.K. Kurt. "Practical Full Duplex Physical Layer Network Coding". In *IEEE* 79^{th} *Vehicular Technology Conference (VTC Spring)*, pages 1–4, May 2014.

[76] John G. Proakis and Masoud Salehi. *Digital Communications*. McGraw-Hill, 5^{th} edition, 2008. ISBN:978-007295716.

[77] David Tse and Pramod Viswanath. *Fundamentals of Wireless Communications*. Cambridge, 1^{st} edition, 2005. ISBN:978-0521845274.

[78] Lin Bai and Jinho Choi. *Low Complexity MIMO Detection*. Springer, 1^{st} edition, 2012. ISBN:978-1441985828.

[79] Upamanyu Madhow. *Fundamentals of Digital Communications*. Cambridge, 1^{st} edition, 2008. ISBN:978-0521874144.

[80] F. A. Monteiro, I. J. Wassell, and N. Souto. *"MIMO Detection Methods"*. In MIMO Processing for 4G and Beyond: Fundamentals and Evolution, M. M. da Silva and F. A. Monteiro, Eds., CRC Press / Taylor & Francis Group, Florida, USA, 2014, ch. 2. Chapter 2, ISBN:978-1466598072.

[81] Tim Brown, Elisabeth De Carvalho, and Persefoni Kyritsi. *Pratical Guide to the MIMO Radio Channel*. Wiley, 1^{st} edition, 2005. ISBN:978-0470994498.

[82] P. W. Wolniansky, G. J. Foschini, G. D. Golden, and R. A. Valenzuela. "V-BLAST: An Architecture for Realizing Very High Data Rates Over the Rich-Scattering Wireless Channel". *In the IEEE International Symposium on Signals, Systems, and Electronics*, pages 295 – 300, September 1998.

[83] Yue Shang and Xiang-Gen Xia. "An Improved Fast Recursive Algorithm for V-BLAST with Optimal Ordered Detections". In *IEEE International Conference on Communications (ICC)*, pages 756–760, May 2008.

[84] Francisco A. T. B. N. Monteiro. *Lattices in MIMO Spatial Multiplexing: Detection and Geometry*. PhD thesis, Fitzwilliam College, University of Cambridge, 2012.

[85] Huan Yao and Gregory W. Wornell. "Lattice-Reduction-Aided Detectors for MIMO Communication Systems". In *IEEE Global Telecommunications Conference (GLOBECOM)*, volume 1, pages 424–428 vol.1, Nov 2002.

[86] Xiaoli Ma and Wei Zhang. "Performance Analysis for MIMO Systems with Lattice-Reduction Aided Linear Equalization". *IEEE Transactions on Communication*, 56(2):308–318, February 2008.

[87] Joaquin Jaldén and Björn Ottersten. "On the Complexity of Sphere Decoding in Digital Communications". *IEEE Transactions on Signal Processing*, 53(4):1474 – 1484, April 2005.

[88] Mahmoud Taherzadeh, Amin Mobasher, and Amir K. Khandani. "LLL Reduction Achieves the Receive Diversity in MIMO Decoding". *IEEE Transactions on Information Theory*, 53(12):4801 – 4805, December 2007.

[89] Jerry R. Hampton. *Introduction to MIMO Communications*. Cambridge University Press, 1^{st} edition, 2013. ISBN:978-1107337527.

[90] N. Souto and F. A. Monteiro. *"MIMO optimized for OFDM"*. In MIMO Processing for 4G and Beyond: Fundamentals and Evolution, M. M. da Silva and F. A. Monteiro, Eds., CRC Press / Taylor & Francis Group, Florida, USA, 2014, ch. 4. ISBN:978-1466598072.

[91] Paulo S. R. Diniz, Eduardo A. B. da Silva, and Sergio L. Netto. *Digital Signal Processing: System Analysis And Design*. Cambridge University Press, 2^{nd} edition, 2010. ISBN:978-0511784644.

[92] Zheng Zhang, Tolga Duman, and Erozan M. Kurtas. "Achievable Information Rates and Coding For Mimo Systems over ISI Channels and Frequency-Selective Fading Channels". *IEEE Transactions on Communications*, 52(10):1698–1710, November 2004.

[93] P. Almers, F. Tufvesson, and A. F. Molisch. "Keyhole Effect in MIMO Wireless Channels: Measurements and Theory". *IEEE Transactions on Wireless Communications*, 5(12):3596–3604, December 2006.

[94] Kaare Brandt Petersen and Michael Syskind Pedersen. *The Matrix Cookbook*. 2012. [Online]. Available: http://www.imm.dtu.dk/pubdb/views/edoc_download.php/3274/pdf/imm3274.pdf (March 2015).

[95] Jeongwook Seo and Jong-Ho Paik. "A Full-Duplex MIMO Relay with an MMSE Filter and a Modified Alamouti Encoder against Spatial Loop Interference in Wireless Multihop Networks". *International Journal of Software Engineering and its Applications*, 6(3):17–26, July 2012.

[96] Are Hjorungnes and David Gesbert. "Complex-Valued Matrix Differentiation: Techniques and Key Results". *IEEE Transaction on Signal Processing*, 55(6):2740–2746, June 2007.

[97] E. Eleftheriou and D.D. Falconer. "Tracking Properties and Steady-State Performance of RLS Adaptive Filter Algorithms". *IEEE Transactions on Acoustic, Speech, Signal Processing*, 34(5):1097–1110, October 1986.

[98] Simon O. Haykin. *Adaptive Filter Theory*. Prentice Hall, 5^{th} edition, 2013. ISBN:978-0132671453.

[99] Paulo S.R. Diniz. *Adaptive Filtering Algorithms and Practical Implementation*. Springer, 4^{th} edition, 2012. ISBN:978-1461441052.

[100] Hong Yang and Thomas L Marzetta. "Performance of Conjugate and Zero-Forcing Beamforming in Large-Scale Antenna Systems". *IEEE Journal on Selected Areas in Communications*, (31):172–179, February 2013.

[101] Antonio M. Tulino and Sergio Verdú. "Random Matrix Theory and Wireless Communications". *Foundations and Trends in Communications and Information Theory*, 1(1):1–182, June 2004.

[102] Babak Hassibi and Bertrand Hochwald. "How Much Training is Needed in Multiple-Antenna Wireless Links?". *IEEE Transaction on Information Theory*, 49(4):951–963, April 2003.

[103] Michael Grant and Stephen Boyd. CVX: Matlab Software for Disciplined Convex Programming, version 2.1. `http://cvxr.com/cvx`, March 2014.

[104] Wan Choi and Jeffrey G Andrews. "The Capacity Gain from Intercell Scheduling in Multi-Antenna Systems". *IEEE Transaction on Wireless Communications*, 7(2):714–725, February 2008.

[105] A. Mejri and G. Rekaya-Ben Othman. "Bidirectional Relaying via Network Coding: Design Algorithm and Performance Evaluation". In *20^{th} International Conference on Telecommunications (ICT)*, pages 1–5, May 2013.

[106] A. Mejri and G. Rekaya-Ben Othman. "Efficient Decoding Algorithms for the Compute-and-Forward Strategy". *IEEE Transactions on Communications*, PP(99):1–1, May 2015.

[107] Ram Zamir. *Lattice Coding for Signals and Networks*. Cambridge University Press, 1^{st} edition, 2014. ISBN: 978-1139045520.

[108] E. Agrell, T. Eriksson, A. Vardy, and K. Zeger. "Closest Point Search in Lattices". *IEEE Transactions on Information Theory*, 48(8):2201–2214, Aug 2002.

[109] Stephen Boyd and Lieven Vandenberghe. *Convex Optimization*. Cambridge University Press, 1^{st} edition, 2004. ISBN:978-0521833783.

[110] Igor Griva, Stephen G. Nash, and Ariela Sofer. *Linear and Nonlinear Optimization*. Society for Industrial and Applied Mathematics, 2^{nd} edition, 2009. ISBN:978-0898717730.

[111] Garth P. McCormick. "Computability of Global Solutions to Factorable Nonconvex Programs: Part I — Convex Underestimating Problems". *Mathematical Programming*, 10(1):147–175, 1976.

[112] Leo Liberti and Constantinos C. Pantelides. "An Exact Reformulation Algorithm for Large Nonconvex NLPs Involving Bilinear Terms". *Journal of Global Optimization*, 36(2):161–189, 2006.

[113] Scott Kolodziej, Pedro M. Castro, and Ignacio E. Grossmann. "Global Optimization of Bilinear Programs with a Multiparametric Disaggregation Technique". *Journal of Global Optimization*, 57(4):1039–1063, 2013.

Appendix A

Analysis of the Feedback Cancellation Algorithms

A.1 LMS Estimation Mean Error

The mean error of the LMS filter is derived based on the average theory assuming the use of a small step size μ [98]. Defining the vector $\tilde{\mathbf{f}}(n) = \mathbf{f}_{Opt.}(n) - \mathbf{r}(n) = \sum_{l=0}^{L_A} \mathbf{A}_{Opt.}[k]\tilde{\mathbf{t}}(n-l) - \mathbf{r}(n)$ and the MSE optimal solution for the feedback filter parameters $\mathbf{A}_{\star,Opt.}$ is as in (4.28) (usually called the Wiener solution), it comes

$$
\begin{aligned}
\tilde{\mathbf{A}}_{\star,n} = \hat{\mathbf{A}}_{\star,n} - \mathbf{A}_{\star,Opt.} = \ & \hat{\mathbf{A}}_{\star,n-1} - \mathbf{A}_{\star,Opt.} + \mu\big(\mathbf{r}(n) - \mathbf{f}_{Opt.}(n) + \mathbf{f}_{Opt.}(n) - \mathbf{A}_{\star}^{T} \odot \tilde{\mathbf{T}}(n)\big) \otimes \tilde{\mathbf{T}}^{H}(n) \\
&= \tilde{\mathbf{A}}_{\star,n-1} - \mu\tilde{\mathbf{f}}(n) \otimes \tilde{\mathbf{T}}^{H}(n) + \mu\big(\mathbf{f}_{Opt.}(n) - \sum_{l=0}^{L_A} \big(\hat{\mathbf{A}}[l](n) - \hat{\mathbf{A}}_{Opt.}[l](n) + \hat{\mathbf{A}}_{Opt.}[l](n)\big)\tilde{\mathbf{t}}(n-l)\big) \otimes \tilde{\mathbf{T}}^{H}(n) \\
&= \tilde{\mathbf{A}}_{\star,n-1} - \mu\tilde{\mathbf{f}}(n) \otimes \tilde{\mathbf{T}}^{H}(n) + \mu\big(\sum_{l=0}^{L_A} \tilde{\mathbf{A}}[l](n)\tilde{\mathbf{t}}(n-l)\big) \otimes \tilde{\mathbf{T}}^{H}(n) \\
&= \tilde{\mathbf{A}}_{\star,n-1} - \mu\tilde{\mathbf{f}}(n) \otimes \tilde{\mathbf{T}}^{H}(n) + \mu\big(\big[\tilde{\mathbf{A}}_{Opt.}[0]|\cdots|\tilde{\mathbf{A}}_{Opt.}[L_A]\big] \odot \big[\tilde{\mathbf{t}}(k)|\cdots|\tilde{\mathbf{t}}(k-L_A)\big]\big) \otimes \tilde{\mathbf{T}}^{H}(n) \\
&= \big[\mathbf{I} - \mu\bar{\mathbf{t}}(n) \otimes \bar{\mathbf{t}}(n)\big]\tilde{\mathbf{A}}_{\star,n-1} - \mu\tilde{\mathbf{f}}(n) \otimes \tilde{\mathbf{T}}^{H}(n) \\
&\approx \big[\mathbf{I} - \mu\boldsymbol{\Sigma}_{\tilde{\mathbf{t}},\tilde{\mathbf{t}}}\big]\tilde{\mathbf{A}}_{\star,n-1} - \mu\tilde{\mathbf{f}}(n) \otimes \tilde{\mathbf{T}}^{H}(n),
\end{aligned}
\tag{A.1}
$$

where, the approximation taken in the last step comes from the average theory.

A.2 LMS Mean Square Parameter Error

To evaluate the MSE of the filter parameter error, it is necessary to assume that the state matrix $\tilde{\mathbf{A}}_{\star,n-1}$ is uncorrelated with the filter input $\tilde{\mathbf{q}}(n) \otimes \bar{\mathbf{t}}(n)$, for $k = 0, \cdots, L_A$, and that the signal $\tilde{\mathbf{r}}(n)$ and the vector $\bar{\mathbf{t}}(n)$ are mutually independent. The first assumption is highly unrealistic, since the filter error depends

clearly on the previous observed vector, however, it allows to simplify this problem yielding good results [98]. Therefore, defining the mean square error matrix as

$$\mathbf{P}(n) = \mathbb{E}\{\tilde{\mathbf{A}}_{\star,n}\tilde{\mathbf{A}}_{\star,n}^{H}\}, \tag{A.2}$$

considering equation (4.35) and the above assumptions, it is obtained that

$$\mathbf{P}(n) = \big[\mathbf{I} - \mu\boldsymbol{\Sigma}_{\tilde{\mathbf{t}},\tilde{\mathbf{t}}}\big]\mathbf{P}(n-1)\big[\mathbf{I} - \mu\boldsymbol{\Sigma}_{\tilde{\mathbf{t}},\tilde{\mathbf{t}}}\big]^{H} + \mu^2\mathbb{E}\{\tilde{\mathbf{f}}^{H}(n)\tilde{\mathbf{f}}(n)\}\boldsymbol{\Sigma}_{\tilde{\mathbf{t}},\tilde{\mathbf{t}}}, \tag{A.3}$$

which represents a linear time-invariant state space model with $\mathbf{P}(n)$ as state variables. Once again, the above system, that has eigenvalues given by all the combinations of $(1-\mu\lambda_i)\cdot(1-\mu\lambda_j)$, where $\lambda_{i,j}$, for $i,j = 1,\cdots,L_A$ are the eigenvalues of $\boldsymbol{\Sigma}_{\tilde{\mathbf{t}}\tilde{\mathbf{t}}}$, converges to a steady state value i.f.f. $0 < \mu < 2/\lambda_1$. The steady state value of the error, $\mathbf{P}$, is obtained by solving the Lyapunov equation

$$\mathbf{P} = \big[\mathbf{I} - \mu\boldsymbol{\Sigma}_{\tilde{\mathbf{t}},\tilde{\mathbf{t}}}\big]\mathbf{P}\big[\mathbf{I} - \mu\boldsymbol{\Sigma}_{\tilde{\mathbf{t}},\tilde{\mathbf{t}}}\big]^{H} + \mu^2\mathbb{E}\{\tilde{\mathbf{f}}^{H}(n)\tilde{\mathbf{f}}(n)\}\boldsymbol{\Sigma}_{\tilde{\mathbf{t}},\tilde{\mathbf{t}}}. \tag{A.4}$$

To solve the problem, consider the spectral decomposition of $\boldsymbol{\Sigma}_{\tilde{\mathbf{t}},\tilde{\mathbf{t}}} = \mathbf{V}\boldsymbol{\Lambda}\mathbf{V}^{H}$. By multiplying the Lyapunov equation by $\mathbf{V}^{H}$ from the left and $\mathbf{V}$ from the right

$$\begin{aligned}\mathbf{V}^{H}\mathbf{P}\mathbf{V} &= \mathbf{V}^{H}\big[\mathbf{I} - \mu\boldsymbol{\Sigma}_{\tilde{\mathbf{t}},\tilde{\mathbf{t}}}\big]\mathbf{P}\big[\mathbf{I} - \mu\boldsymbol{\Sigma}_{\tilde{\mathbf{t}},\tilde{\mathbf{t}}}\big]^{H}\mathbf{V} + \mu^2\mathbb{E}\{\tilde{\mathbf{f}}(n)\tilde{\mathbf{f}}(n)\}\mathbf{V}^{H}\boldsymbol{\Sigma}_{\tilde{\mathbf{t}},\tilde{\mathbf{t}}}\mathbf{V} \\ &= \big[\mathbf{I} - \mu\boldsymbol{\Lambda}\big]\mathbf{V}^{H}\mathbf{P}\mathbf{V}\big[\mathbf{I} - \mu\boldsymbol{\Lambda}\big]^{H} + \mu^2\mathbb{E}\{\tilde{\mathbf{f}}^{H}(n)\tilde{\mathbf{f}}(n)\}\boldsymbol{\Lambda} \\ &\quad \big[\mathbf{I} - \mu\boldsymbol{\Lambda}\big]\mathbf{Q}\big[\mathbf{I} - \mu\boldsymbol{\Lambda}\big]^{H} + \mu^2\mathbb{E}\{\tilde{\mathbf{f}}^{H}(n)\tilde{\mathbf{f}}(n)\}\boldsymbol{\Lambda},\end{aligned} \tag{A.5}$$

where $\mathbf{Q} = \mathbf{V}^{H}\mathbf{P}\mathbf{V}$ is a diagonal matrix (since $\mathbf{I}, \boldsymbol{\Lambda}$ are diagonal matrices), which entries are given by

$$q_i = (1-\mu\lambda_i)^2 q_i + \mu^2\mathbb{E}\{\tilde{\mathbf{f}}^{H}(n)\tilde{\mathbf{f}}(n)\}\lambda_i,$$

giving the following solution

$$q_i = \frac{\mu^2\mathbb{E}\{\tilde{\mathbf{f}}^{H}(n)\tilde{\mathbf{f}}(n)\}}{2-\mu\lambda_i}, \text{for } i = 1,\cdots,L_A. \tag{A.6}$$

A.3 First Derivative of the RLS MSE Approximation

The derivative of the LMS MSE approximation in equation (4.40) is given by

$$\begin{aligned}
\frac{\partial}{\partial \mathbf{A}_\star}\widehat{MSE}_{RLS}(n,\mathbf{A}(z)) &= \frac{\partial}{\partial \mathbf{A}_\star}\big(\sum_{k=1}^{n}\lambda^{n-k}(\mathbf{f}(k)-\sum_{l=0}^{L_A}\mathbf{A}[l]\tilde{\mathbf{t}}(k-l))\big)^H\big(\sum_{l=1}^{n}\lambda^{n-l}(\mathbf{f}(l)-\sum_{l=0}^{L_A}\mathbf{A}[l]\tilde{\mathbf{t}}(k-l))\big)\\
&= -2\sum_{k=1}^{n}\lambda^{n-k}\big(\mathbf{f}(k)-\mathbf{A}_\star^T\odot\tilde{\mathbf{T}}(k)\big)\otimes\tilde{\mathbf{T}}^H(n)\\
&= -2\sum_{k=1}^{n}\lambda^{n-k}\mathbf{f}(k)\otimes\tilde{\mathbf{T}}^H(k)+2\sum_{k=1}^{n}\lambda^{n-k}\sum_{l=0}^{L_A}\mathbf{A}[l]\tilde{\mathbf{t}}(k-l)\otimes\tilde{\mathbf{T}}^H(k)\\
&= -2\sum_{k=1}^{n}\lambda^{n-k}\mathbf{f}(k)\otimes\tilde{\mathbf{T}}^H(k)+2(\sum_{l=0}^{L_A}\mathbf{A}[l]\sum_{k=1}^{n}\lambda^{n-k}\tilde{\mathbf{t}}(k-l))\otimes\tilde{\mathbf{T}}^H(k)\\
&= -2\hat{\mathbf{\Sigma}}^{RLS}_{\tilde{\mathbf{t}},\mathbf{f}}(n)+2\hat{\mathbf{\Sigma}}^{RLS}_{\tilde{\mathbf{t}},\tilde{\mathbf{t}}}(n)\mathbf{A}_{\star,n},
\end{aligned} \tag{A.7}$$

A.4 RLS Estimation Error

Considering that $\hat{\mathbf{A}}_{\star,n}=\big[\hat{\mathbf{\Sigma}}^{RLS}_{\tilde{\mathbf{t}},\tilde{\mathbf{t}}}(n)\big]^{-1}\hat{\mathbf{\Sigma}}^{RLS}_{\tilde{\mathbf{t}},\mathbf{r}}(n)=\big[\frac{1}{n}\hat{\mathbf{\Sigma}}^{RLS}_{\tilde{\mathbf{t}},\tilde{\mathbf{t}}}(n)\big]^{-1}\frac{1}{n}\hat{\mathbf{\Sigma}}^{RLS}_{\tilde{\mathbf{t}},\mathbf{r}}(n)$, the LMS error matrix may be written as follows

$$\begin{aligned}
\tilde{\mathbf{A}}_{\star,n} &= \hat{\mathbf{A}}_{\star,n}-\mathbf{A}_{\star,Opt.}\\
&= \big[\hat{\mathbf{\Sigma}}^{RLS}_{\tilde{\mathbf{t}},\tilde{\mathbf{t}}}(n)\big]^{-1}\hat{\mathbf{\Sigma}}^{RLS}_{\tilde{\mathbf{t}},\mathbf{r}}(n)-\mathbf{A}_{\star,Opt.}\\
&= \big[\hat{\mathbf{\Sigma}}^{RLS}_{\tilde{\mathbf{t}},\tilde{\mathbf{t}}}(n)\big]^{-1}\sum_{k=1}^{n}\mathbf{r}(k)\otimes\tilde{\mathbf{T}}^H(k)-\mathbf{A}_{\star,Opt.}\\
&= \big[\hat{\mathbf{\Sigma}}^{RLS}_{\tilde{\mathbf{t}},\tilde{\mathbf{t}}}(n)\big]^{-1}\sum_{k=1}^{n}(\mathbf{r}(k)-\mathbf{f}_{Opt.}(k)+\mathbf{f}_{Opt.}(k))\otimes\tilde{\mathbf{T}}^H(k)-\mathbf{A}_{\star,Opt.}\\
&= \big[\hat{\mathbf{\Sigma}}^{RLS}_{\tilde{\mathbf{t}},\tilde{\mathbf{t}}}(n)\big]^{-1}\sum_{k=1}^{n}(\tilde{\mathbf{f}}(k)+\sum_{l=0}^{L_A}\mathbf{A}_{Opt.}[l]\tilde{\mathbf{t}}(k-l))\otimes\tilde{\mathbf{T}}^H(k)-\mathbf{A}_{\star,Opt.}\\
&= \big[\hat{\mathbf{\Sigma}}^{RLS}_{\tilde{\mathbf{t}},\tilde{\mathbf{t}}}(n)\big]^{-1}\sum_{k=1}^{n}\tilde{\mathbf{f}}(k)\otimes\tilde{\mathbf{T}}^H(k)\\
&\quad+\big[\hat{\mathbf{\Sigma}}^{RLS}_{\tilde{\mathbf{t}},\tilde{\mathbf{t}}}(n)\big]^{-1}\sum_{k=1}^{n}\big[\mathbf{A}_{Opt.}[0]|\cdots|\mathbf{A}_{Opt.}[L_A]\big]\odot\big[\tilde{\mathbf{t}}(k)|\cdots|\tilde{\mathbf{t}}(k-L_A)\big]\otimes\tilde{\mathbf{T}}^H(k)-\mathbf{A}_{\star,Opt.}\\
&= \big[\hat{\mathbf{\Sigma}}^{RLS}_{\tilde{\mathbf{t}},\tilde{\mathbf{t}}}(n)\big]^{-1}\sum_{k=1}^{n}\tilde{\mathbf{f}}(k)\otimes\tilde{\mathbf{T}}^H(k)+\big[\hat{\mathbf{\Sigma}}^{RLS}_{\tilde{\mathbf{t}},\tilde{\mathbf{t}}}(n)\big]^{-1}\Big(\sum_{k=1}^{n}\overline{\mathbf{t}}(k)\otimes\overline{\mathbf{t}}^H(k)\Big)\mathbf{A}_{\star,Opt.}-\mathbf{A}_{\star,Opt.}\\
&= \Big[\frac{1}{n}\hat{\mathbf{\Sigma}}^{RLS}_{\tilde{\mathbf{t}},\tilde{\mathbf{t}}}(n)\Big]^{-1}\frac{1}{n}\sum_{k=1}^{n}\tilde{\mathbf{f}}(k)\otimes\tilde{\mathbf{T}}^H(k).
\end{aligned} \tag{A.8}$$

where the MSE optimal solution for the feedback filter parameters is $\mathbf{A}_{\star,Opt.}$ and $\tilde{\mathbf{f}}(n)=\mathbf{f}_{Opt.}(n)-\mathbf{r}(n)=\sum_{l=0}^{L_A}\mathbf{A}_{Opt.}[k]\tilde{\mathbf{t}}(n-l)-\mathbf{r}(n)$.

A.5 RLS Mean Square Parameter Error

The Equation covariance of the parameter error, considering (4.45) may be derived as

$$
\begin{aligned}
\mathbf{Q}(n) &= \mathbb{E}\{\tilde{\mathbf{A}}_{\star,n}\tilde{\mathbf{A}}_{\star,n}^{H}\} \\
&= \mathbb{E}\Big\{\Big[\frac{1}{n}\hat{\mathbf{\Sigma}}_{\tilde{\mathbf{t}},\tilde{\mathbf{t}}}^{RLS}(n)\Big]^{-1}\frac{1}{n^2}\sum_{k=1}^{n}\tilde{\mathbf{f}}(k)\otimes\tilde{\mathbf{T}}^{H}(k)\Big(\sum_{l=1}^{n}\tilde{\mathbf{f}}(l)\otimes\tilde{\mathbf{T}}^{H}(l)\Big)^{H}\Big[\frac{1}{n}\hat{\mathbf{\Sigma}}_{\tilde{\mathbf{t}},\tilde{\mathbf{t}}}^{RLS}(n)\Big]^{-1}\Big\} \\
&\approx \mathbf{\Sigma}_{\tilde{\mathbf{t}},\tilde{\mathbf{t}}}^{-1}\mathbb{E}\Big\{\frac{1}{n^2}\sum_{k=1}^{n}\tilde{\mathbf{f}}(k)\otimes\tilde{\mathbf{T}}^{H}(k)\Big(\sum_{l=1}^{n}\tilde{\mathbf{f}}(l)\otimes\tilde{\mathbf{T}}^{H}(l)\Big)^{H}\Big\}\mathbf{\Sigma}_{\tilde{\mathbf{t}},\tilde{\mathbf{t}}}^{-1} \\
&= \mathbf{\Sigma}_{\tilde{\mathbf{t}},\tilde{\mathbf{t}}}^{-1}\frac{1}{n^2}\mathbb{E}\Big\{\sum_{k=1}^{n}\sum_{l=1}^{n}\overline{\mathbf{t}}(k)\tilde{\mathbf{f}}^{H}(k)\tilde{\mathbf{f}}(l)\overline{\mathbf{t}}^{H}(l)\Big\}\mathbf{\Sigma}_{\tilde{\mathbf{t}},\tilde{\mathbf{t}}}^{-1} \\
&= \mathbb{E}\Big\{\sum_{k=1}^{n}\sum_{l=1}^{n}\tilde{\mathbf{f}}^{H}(k)\tilde{\mathbf{f}}(l)\Big\}\mathbf{\Sigma}_{\tilde{\mathbf{t}},\tilde{\mathbf{t}}}^{-1}\frac{1}{n}\mathbb{E}\Big\{\frac{1}{n}\sum_{k=1}^{n}\sum_{l=1}^{n}\overline{\mathbf{t}}(k)\overline{\mathbf{t}}^{H}(l)\Big\}\mathbf{\Sigma}_{\tilde{\mathbf{t}},\tilde{\mathbf{t}}}^{-1} \\
&= \frac{1}{n}\mathbb{E}\Big\{\sum_{k=1}^{n}\sum_{l=1}^{n}\tilde{\mathbf{f}}^{H}(k)\tilde{\mathbf{f}}(l)\Big\}\mathbf{\Sigma}_{\tilde{\mathbf{t}},\tilde{\mathbf{t}}}^{-1},
\end{aligned}
\tag{A.9}
$$

where it was assumed the same assumptions used for the LMS filter analysis and where the approximation in the first deduction comes from considering that for a large n the expected value of the matrix $\mathbb{E}\big\{\frac{1}{n}\hat{\mathbf{\Sigma}}_{\tilde{\mathbf{t}},\tilde{\mathbf{t}}}^{RLS}(n)\big\}$ is approximately the correlation matrix $\mathbf{\Sigma}_{\tilde{\mathbf{t}},\tilde{\mathbf{t}}}$ [98].